Synthesis of ruthenium complexes having one or more N-heterocyclic carbene ligands supported on hybrid mesostructured silicas and their use in the hydrogenation of carbon dioxide

Mathieu Baffert

N° d'ordre 158-2011 Année 2011

THESE DE L'UNIVERSITE DE LYON

Délivrée par

L'UNIVERSITE CLAUDE BERNARD LYON 1

Ecole Doctorale de Chimie de Lyon (ED 206)

DIPLOME DE DOCTORAT

(arrêté du 7 août 2006)

Spécialité : Chimie

soutenue publiquement le 30.09.11

par

Monsieur Mathieu BAFFERT

TITRE :

Synthèse de complexes du ruthénium avec un ou plusieurs ligands carbènes N-hétérocycliques supportés sur des silices hybrides mésostructurées et leur utilisation dans des réactions d'hydrogénation du dioxide de carbone

Directeur de thèse : Monsieur Christophe COPERET

JURY :

Monsieur	Lionel DELAUDE
Monsieur	Hubert MUTIN
Madame	Anne GIROIR-FENDLER
Monsieur	Atsushi URAKAWA
Monsieur	Christophe COPERET
Madame	Chloé THIEULEUX

N° d'ordre 158-2011 Année 2011

THESE DE L'UNIVERSITE DE LYON

Délivrée par

L'UNIVERSITE CLAUDE BERNARD LYON 1

Ecole Doctorale de Chimie de Lyon (ED 206)

DIPLOME DE DOCTORAT

(arrêté du 7 août 2006)

Spécialité : Chimie

soutenue publiquement le 30.09.11

par

Monsieur Mathieu BAFFERT

TITLE :

Synthesis of ruthenium complexes having one or more N-heterocyclic carbene ligands supported on hybrid mesostructured silicas and their use in the hydrogenation of carbon dioxide

Directeur de thèse : Monsieur Christophe COPERET

JURY :

Monsieur	Lionel DELAUDE
Monsieur	Hubert MUTIN
Madame	Anne GIROIR-FENDLER
Monsieur	Atsushi URAKAWA
Monsieur	Christophe COPERET
Madame	Chloé THIEULEUX

UNIVERSITE CLAUDE BERNARD - LYON 1

Président de l'Université	**M. A. Bonmartin**
Vice-président du Conseil d'Administration	M. le Professeur G. Annat
Vice-président du Conseil des Etudes et de la Vie Universitaire	M. le Professeur D. Simon
Vice-président du Conseil Scientifique	M. le Professeur J-F. Mornex
Secrétaire Général	M. G. Gay

COMPOSANTES SANTE

Faculté de Médecine Lyon Est – Claude Bernard	Directeur : M. le Professeur J. Etienne
Faculté de Médecine et de Maïeutique Lyon Sud – Charles Mérieux	Directeur : M. le Professeur F-N. Gilly
UFR d'Odontologie	Directeur : M. le Professeur D. Bourgeois
Institut des Sciences Pharmaceutiques et Biologiques	Directeur : M. le Professeur F. Locher
Institut des Sciences et Techniques de la Réadaptation	Directeur : M. le Professeur Y. Matillon
Département de formation et Centre de Recherche en Biologie Humaine	Directeur : M. le Professeur P. Farge

COMPOSANTES ET DEPARTEMENTS DE SCIENCES ET TECHNOLOGIE

Faculté des Sciences et Technologies	Directeur : M. le Professeur F. Gieres
Département Biologie	Directeur : M. le Professeur F. Fleury
Département Chimie Biochimie	Directeur : Mme le Professeur H. Parrot
Département GEP	Directeur : M. N. Siauve
Département Informatique	Directeur : M. le Professeur S. Akkouche
Département Mathématiques	Directeur : M. le Professeur A. Goldman
Département Mécanique	Directeur : M. le Professeur H. Ben Hadid
Département Physique	Directeur : Mme S. Fleck
Département Sciences de la Terre	Directeur : Mme le Professeur I. Daniel
UFR Sciences et Techniques des Activités Physiques et Sportives	Directeur : M. C. Collignon
Observatoire de Lyon	Directeur : M. B. Guiderdoni
Ecole Polytechnique Universitaire de Lyon 1	Directeur : M. P. Fournier
Ecole Supérieure de Chimie Physique Electronique	Directeur : M. G. Pignault
Institut Universitaire de Technologie de Lyon 1	Directeur : M. le Professeur C. Coulet
Institut de Science Financière et d'Assurances	Directeur : M. le Professeur J-C. Augros
Institut Universitaire de Formation des Maîtres	Directeur : M. R. Bernard

Abstract

Reducing global carbon dioxide emissions has become one of the top challenges that need to be solved within the next decades, and we therefore need to find multiple approaches. While limiting the emissions at the source by reducing our consumption of fossil resources needs to be the first action, there are alternative solutions that can have a favourable impact. Among them, the utilization of CO_2 as a C_1 building-block has taken a more important place, as CO_2 emissions are becoming a critical environmental issue and European taxes on CO_2 emissions are being more and more significant at the same time. Many homogeneous catalytic systems have been described for the hydrogenation of CO_2 into valuable chemicals, including formic acid, formamides or organic carbonates. Ruthenium and Iridium are the two most effective metals for these reactions, associated with electron-rich ligands such as phosphines, pyridines and more recently N-Heterocyclic Carbenes (NHC). Here, the goal of this PhD was to elaborate supported Ru-NHC catalytic materials based on hybrid organic-inorganic materials having imidazolium units perfectly distributed within a silica matrix. Passivation of these imidazolium materials followed by formation of NHC-carbene and reaction with $[RuCl_2(p\text{-cymene})]_2$ provided these well-defined surface sites of general structures $RuCl_2(NHC)(L)$, where L was para-cymene (p-cymene) or THF depending on the reaction conditions, which could be further replaced by PMe_3. These systems were then tested in the hydrogenation of CO_2 in presence of amine to give formamides. The mono-NHC systems were highly active only in the presence of PMe_3 ligands, but suffered from Ru leaching, evidencing the low stability of the NHC-Ru bond under the reaction conditions. On the other hand, dinuclear bis-NHC Ru systems were also developed, and they displayed much improved activity and stability in the hydrogenation of CO_2 in the presence of PMe_3 compared to the mono-NHC systems. This allowed the use of much higher reaction temperatures (200 °C) and provided heterogeneous catalysts with performances close to those obtained with the best homogeneous catalysts, $Cl_2Ru(dppe)_2$.

Résumé

La réduction de nos émissions globales de dioxyde de carbone est devenue un enjeu majeur qui a besoin d'être résolu dans les prochaines dizaines d'années. Pour cela, il sera nécessaire de développer des approches multiples. Alors que limiter les émissions de CO_2 à la source par réduction de la consommation de ressources fossiles doit rester la priorité, il existe des solutions alternatives qui pourraient avoir également un impact favorable. Parmi elles, l'utilisation du CO_2 comme source de carbone pour l'industrie chimique a pris une plus grande place, alors que les taxes européennes sur les rejets de CO_2 deviennent de plus en plus importantes. Plusieurs catalyseurs homogènes ont été décrits pour l'hydrogénation du CO_2 en produits chimiques tels que l'acide formique, les formamides ou encore les carbonates organiques. Le ruthénium et l'iridium sont les deux métaux les plus performants pour ces types de réactions, en association avec des ligands de type phosphine, pyridine et plus récemment des carbènes N-hétérocycliques (NHC). L'objectif de cette thèse a été de développer des matériaux catalytiques contenant des complexes Ru(NHC), à partir de matériaux hybrides organique-inorganique contenant des fonctions imidazolium parfaitement distribuées dans une matrice de silice. La passivation de surface de ces matériaux, suivie de la formation du NHC et d'une réaction avec $[RuCl_2(p\text{-cymene})]_2$ a permis d'obtenir des espèces de surface bien définies de formule générale $RuCl_2(NHC)(L)$, où L est un ligand para-cymene (p-cymene) ou un ligand THF, selon les conditions de réaction, et peut être remplacé par PMe_3. Ces catalyseurs ont ensuite été testés dans la réaction d'hydrogénation du CO_2 en présence d'amines pour donner des formamides. Les systèmes mono-NHC se sont avérés très actifs en présence de ligands PMe_3, mais la lixiviation du métal a été observée, mettant en évidence la faible stabilité de la liaison Ru-NHC dans les conditions de réaction. Cependant, des systèmes dinucléaires Ru(bis-NHC) ont été développés, et ils ont montré une meilleure activité et stabilité que les systèmes mono-NHC dans l'hydrogénation du CO_2, en présence de PMe_3 comme ligand. Cela a permis d'utiliser des températures de réaction bien plus élevées (200°C) et d'obtenir des catalyseurs hétérogènes avec des performances s'approchant du meilleur catalyseur homogène, $Cl_2Ru(dppe)_2$.

Table of content

List of Abbreviations

BET	Brunauer-Emmett-Teller
DEPT	Distortionless Enhancement by Polarization Transfer
CP	Cross-Polarization
COSY	COrrelation SpectroscopY
GC	Gas chromatography
HPDEC	High Power Decoupling
HSQC	Heteronuclear Single Quantum Correlation
IPCC	International Panel on Climate Change
KHMDS	Potassium hexamethyldisilazide
MAS	Magic Angle Spinning
MCM	Mobil Catalytic Material
Mes	Mesityl
NHC	N-Heterocyclic Carbene
NMR	Nuclear Magnetic Resonance
P123	Pluronic 123
p-cymene	para-cymene
PMO	Periodic Mesoporous Organosilica
PPM	Parts per million
SBA	Santa Barbara
TEOS	Tetra ethyl orthosilicate
THF	Tetrahydrofuran
TMSBr	Trimethylsilylbromide
TOF	Turnover frequency
TON	Turnover Number
XRD	X-Ray Diffraction

Introduction

The objective of this PhD is to develop heterogeneous catalysts having well-dispersed and fully accessible ruthenium N-heterocyclic carbene complexes designed for the hydrogenation of carbon dioxide.

Chapter 1 reviews the different catalytic systems for the utilization of CO_2, then focuses on the N-heterocyclic carbenes and their use in coordination chemistry of transition metals to finally discuss about the different ways to form highly ordered hybrid mesoporous silica and the way of supporting metal complexes on such materials.

Chapter 2 describes the formation of molecularly-defined Ru(NHC) catalytic materials from the already developed propyl-mesityl imidazolium material. These catalysts are then evaluated in the catalytic hydrogenation of CO_2 and in Kharasch reactions.

Chapter 3 introduces new hybrid mesoporous materials bearing amine functionalities and their use in the formation of amide bonds or imidazolium units, including bis-imidazolium units.

Chapter 4 presents the formation of ruthenium bis-NHC complexes of ruthenium and concludes on their catalytic performances compared to the first systems described in chapter 1.

Chapter 5 concludes on this PhD thesis and gives prospects to these projects

Chapter 1

Bibliography

TABLE OF CONTENT

LIST OF FIGURES

LIST OF TABLES

I-1 Introduction

In the last decades, major advances have appeared in the field of catalysis. In homogeneous catalysis, this has been due to the design of better catalytic systems and particularly the development of more and more effective ligands and metal complexes with tuneable electronic and steric environments. Of them, systems based on N-heterocyclic carbenes have become notorious and have led to key improvement steps in the area of alkene metathesis.[1,2] Today, it is clear that the *moto* of homogeneous catalysis is rational design of well-defined single-site catalysts and the improvement of their catalytic performances through structure-reactivity relationship. In parallel, heterogeneous catalysts show complementary advantages with separation, recovery, recycling and regeneration technologies. It is thus obvious that both systems have their specific advantages and that hybrid systems combining the advantages of both worlds could be a way to develop "ideal" catalytic systems based on well-defined heterogeneous catalysts.

Moreover, in the context of sustainable development, the conversion of CO_2 to more valuable products has been proposed, and in the past fourty years several homogeneous catalysts have been developed for the hydrogenation of CO_2. In this PhD, we raised the question on how to generate the corresponding well-defined heterogeneous catalysts.

I-2 Utilization of CO_2

2.1 Introduction

Recent reports of IPCC have linked human activities with global warming,[3] because the increase of carbon dioxide concentration, a green house gas, and the increase of temperatures over the past centuries seem to be related. As global warming has been identified as a major problem for the coming decades, reducing CO_2 emissions is thus one of the top objectives of the European Union, with the hope to make it accepted world wide. While the direct reduction of CO_2 emissions is the priority, there is also a trend to reduce its emission indirectly, by utilizing CO_2 in industrial processes for instance as a fluid for processing, or as a source of carbon for the synthesis of chemicals or fuels. For instance,

this can be illustrated by the process of extraction of caffeine from coffee beans using supercritical CO_2, the synthesis of aspirin from CO_2 or polycarbonate polymers and more recently, the production of biofuels from microalgae.[4]

2.2 Use of carbon dioxide for energy supply

2.2.1 Formic acid as a hydrogen storage molecule

More recently, carbon dioxide has been proposed as a candidate to store hydrogen and therefore as a way to store energy. Indeed, CO_2 can easily incorporate one molecule of dihydrogen when hydrogenated to formic acid, and the reverse reaction, the decomposition of formic acid, can be used to release H_2. Although the first step was already well-known, the catalytic splitting of formic acid was only recently reported by Beller *et al*[5], using $RuCl_2(PPh_3)_3$ as a catalyst. This approach is very interesting, but now depends largely on the availability of dihydrogen from non-carbon sources (renewable).

2.2.2 The methanol economy

The concept of “methanol economy” has been proposed as a solution for the energy problem which has to be solved within the next century. (see Figure 1) Fossil resources will one day disappear, and so will cheap energy sources. As these resources are decreasing, alternatives need to be investigated. The problem is even more difficult to solve if we consider that ideally new sources of energy should be compatible with the existing technologies, and particularly with explosion engines. Following this strategy, methanol could be an interesting candidate to substitute oil. Indeed, methanol is a very good fuel, its toxicity is quite acceptable if we compare it with gasoline or diesel, and it can be easily stored and transported.[6] The industrial process to synthesize methanol is the use of syngas, but a lot of work has been performed in the last decades to synthesize methanol directly from carbon dioxide and dihydrogen. In this concept, the source of energy is dihydrogen, which will have to be produced from renewable energies, for example by electrocatalytic splitting of water with solar energy.

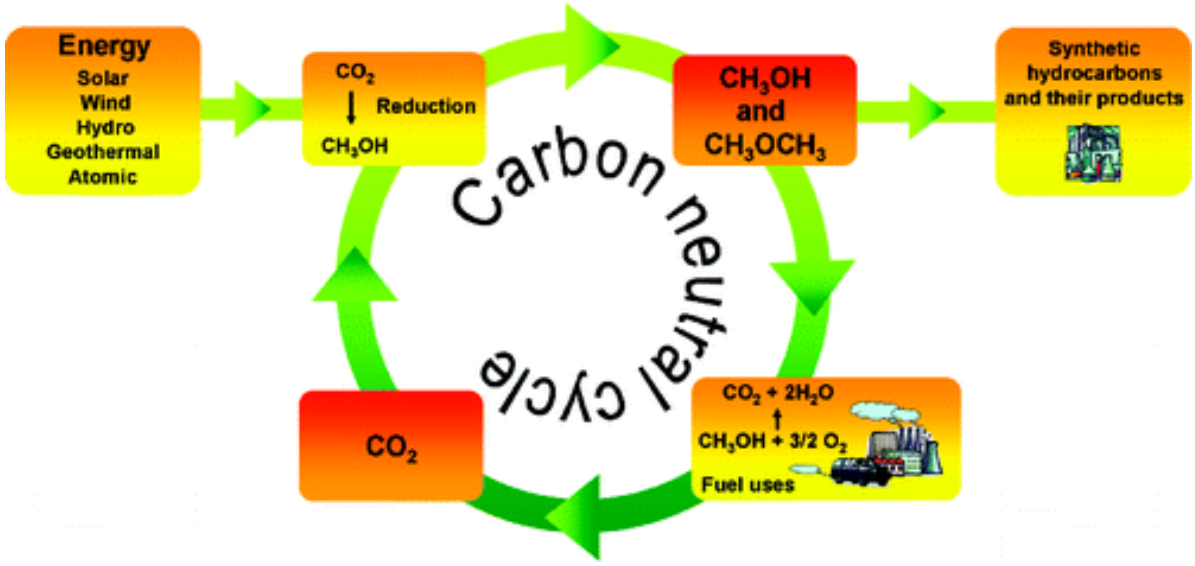

Figure 1. Concept of the methanol economy (*taken from ref.* [6])

2.3 Hydrogenation of CO_2

2.3.1 First discoveries

The utilization of carbon dioxide as a C_1 feedstock has generated a lot of interest since the seventies, but the major challenge to overcome is that CO_2 is in a thermodynamic well, hence a lot of energy is required to convert it into products. One approach consists in the hydrogenation of CO_2 in the presence of noble metal complexes, in particular group VIII metals, such as ruthenium, iridium and rhodium. For instance, the hydrogenation of CO_2 into formamides was discovered by Haynes *et al.* in 1970,[7] which was followed by the discovery of the direct hydrogenation of CO_2 to formic acid.[8] While various systems have been developed in the nineties,[9] there is still a need to develop better catalysts in terms of activity and stability.

2.3.2 Production of formamides

The first breakthrough in this field was obtained by Noyori and Jessop[10-12] using ruthenium trimethylphosphine complexes as catalyst precursors in combination with supercritical carbon dioxide as the active phase to dramatically improve the hydrogenation reaction. For instance, the activities in the hydrogenation of CO_2 to formamides were increased by 100-fold with turnover numbers (TON) and turnover frequencies (TOF) reaching *ca.* 420 000 and 6000 h^{-1}

respectively in the synthesis of DMF. The second major advance was introduced by Baiker *et al.*, with the use of chelating ligands such as diphenylphosphinoethane (dppe). In fact, $RuCl_2(dppe)_2$ is to date the best catalyst for the hydrogenation of CO_2 to formamides, with TON up to 720 000 and TOF reaching 360 000 h^{-1} for the synthesis of DMF.[13] The other major reports for this type of reactions are summarized in Table 1.

2.3.3 Production of formic acid

Keeping the concept of chelating ligands, different systems were also developed for the hydrogenation of CO_2 to formic acid with iridium-based complexes (see **1** and **2** in Figure 2), the best system to date being the iridium P-N-P pincer complex **2**, which displays very important TON (3 500 000) at only 60 bar in a H_2O/KOH mixture.[14] Besides phosphine ligands, Peris *et al.* recently introduced iridium (**3**) and ruthenium (**4**) complexes based on bi-dentate NHC ligands (see Figure 2), which showed promising activities in the direct hydrogenation of CO_2 to formic acid as well as in the transfer hydrogenation of CO_2 with iso-propanol.[15,16] The very high thermal stability of bis-NHC complexes[17,18] is noteworthy, allowing reaction to be carried out at temperatures up to 200°C. The other major reports for this type of reactions are summarized in Table 2.

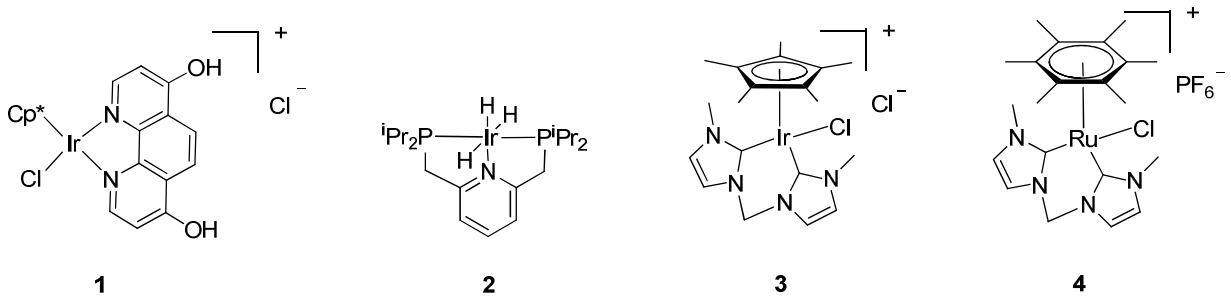

Figure 2. Structure of some chelate complexes active in the hydrogenation of CO_2 to HCOOH

Table 1. Comparison of different catalytic systems for the hydrogenation of CO_2 to formamides

Catalyst precursor	solvent	amine	pH_2/CO_2 (bar)	T (℃)	t (h)	TON	TOF (h^{-1})	Ref.
$RuCl_2(PMe_3)_4$	$scCO_2$	$HNMe_2$	80/130	100	37	370000	10000	[10]
$RuCl_2(dppe)_2$	$scCO_2$	$HNMe_2$	85/130	100	2,05	740000	360000	[13]
$RuCl_2(dppm)_2$	$scCO_2$	$HNMe_2$	85/130	100	0,5	95000	190000	[13]
$RuCl_2(dppp)_2$	$scCO_2$	$HNMe_2$	85/130	100	4,05	10700	2650	[13]
$RuCl_2(dppe)_2$	$scCO_2$	Pyrrolidine	85/na	100	3	126510	42170	[19]

2.3.4 Mechanisms involved in homogeneous catalysts

The hydrogenation of CO_2 to formic acid has been studied in details for ruthenium and rhodium systems.[28-31] These studies agree on the rapid formation of a formate complex by the reaction of CO_2 with a metal hydride complex (insertion), and on a rate-determining step associated with the activation of dihydrogen (already coordinated onto the metal center as a (η^2-H_2) complex) by the metal-oxygen bond, and thus being similar to σ-bond metathesis and corresponding to the heterolytic activation of H_2. Finally, formic acid is formed via the subsequent reductive elimination of the formate with a hydride. This mechanistic scheme is consistent with recent calculations performed on Ru(dmpe)H_2 via ab-initio metadynamics,[30] which allows exploring the free energy potential energy surfaces of complex

Table 2. Comparison of different catalytic systems for the hydrogenation of CO_2 to formic acid

Catalyst precursor	solvent	additives	pH_2/CO_2 (bar)	T (℃)	t (h)	TON	TOF (h^{-1})	Ref.
PdCl2	H_2O	KOH	110/na	160	3	1580	527	[20]
$[RuCl_2(CO)_2]n$	H_2O+iPrOH	NEt_3	81/27	80	0,3	400	1333	[21]
$[Rh(cod)Cl]_2$	dmso	NEt_3 + dppb	20/20	rt	22	1150	52	[22]
$RhCl[P(C_6H_4\text{-}m\text{-}SO_3Na)_3]_3$	H_2O	$NHMe_2$	20/20	rt	12	3439	287	[23]
$RuH_2[P(CH_3)_3]_4$	$scCO_2$	NEt_3 + H2O	85/120	50	1	1400	1400	[11]
$RuCl_2[P(CH_3)_3]_4$	$scCO_2$	NEt_3 + H2O	85/120	50	47	7200	153	[11]
$[RhH(cod)]_4$	dmso	NEt_3 + dppb	40 total	rt	18	2200	122	[24]
Rh(dcpb)(hfacac)	dmso	NEt_3	20/20	25	/	/	1335	[25]
$RuCl(Oac)(PMe_3)_4$	$scCO_2$	NEt_3 + C_6F_5OH	70/120	50	0,3	31667	95000	[12]
$[RuCl_2(bpy)_2(H_2O)_2][O_3SCF_3]_2$	EtOH	NEt_3	30/30	150	8	5000	625	[26]
$[RuCl(C_6Me_6)(DHPT)]Cl$	H_2O	KOH	30/30	120	24	15400	642	[27]
[Cp*IrCl(DHPT)]Cl **(1)**	H_2O	KOH	30/30	120	48	222000	4625	[27]
$[RuCl(bis\text{-}NHC)(C_6Me_6)]PF_6$ **(4)**	H_2O	KOH	30/30	200	75	23000	307	[15]
[Cp*IrCl(bis-NHC)]Cl **(3)**	H_2O	KOH	30/30	200	20	9500	475	[15]
$Ir(PNP)H_3$ **(2)**	H_2O	KOH	30/30	120	48	3500000	73000	[14]

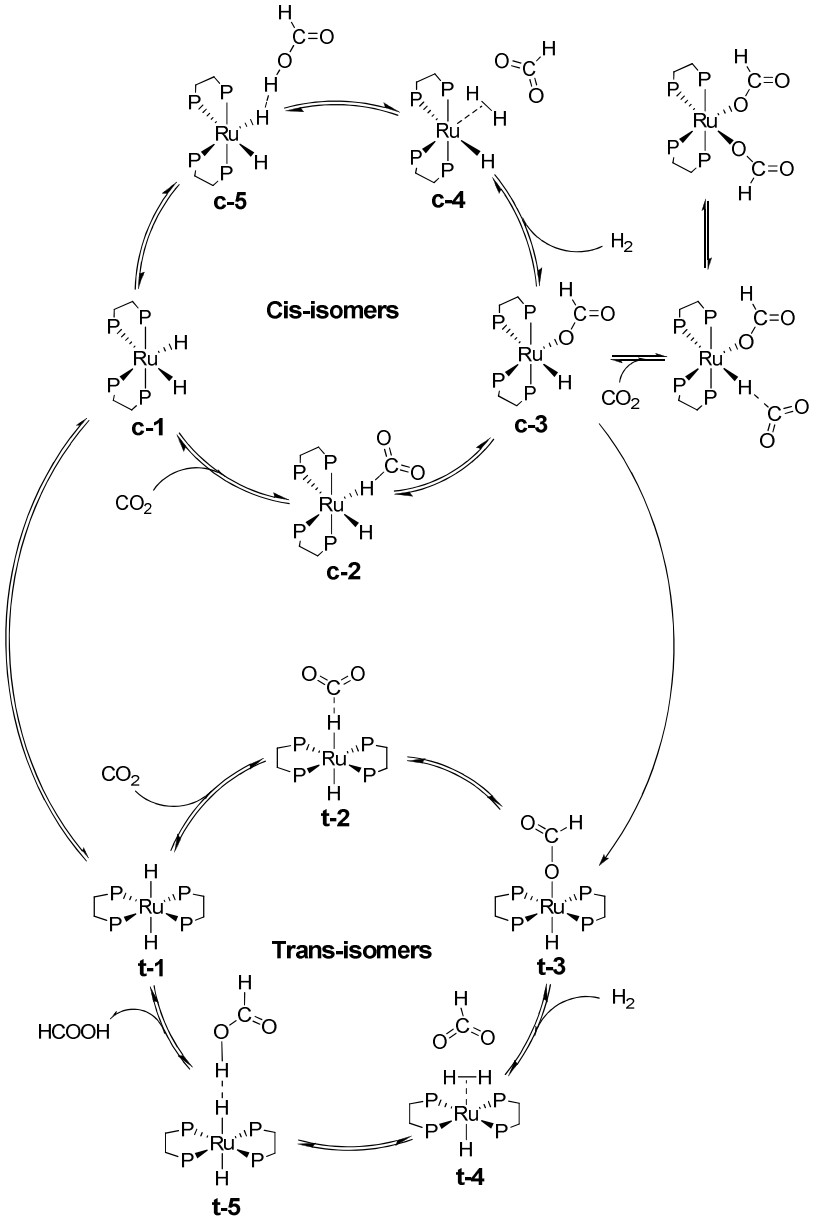

Figure 3. Mechanism of the hydrogenation of CO_2 to formic acid proposed by Baiker et al.

reaction pathways. Here, they showed that CO_2 can easily insert in the ruthenium hydride bond to generate a formate, using the *cis* or the *trans* di-hydride complex (See catalytic cycle in Figure 3). Then, rate determining step corresponds to the approach of H_2 towards the ruthenium centre, which requires the de-coordination of the formate ligand. This step has a particularly low activation barrier of 10 kcal.mol^{-1} for the trans complex, while it is associated with a significantly higher activation energy for the cis-complex (22 kcal.mol^{-1}). This is consistent with experimental results which show, by identifying the active species with high pressure NMR and IR experiments, that only the *trans* route is present. [32]

2.3.5 Production of methanol

The direct hydrogenation of CO_2 into methanol is probably an even more important process, considering that it permits the use of CO_2 and methanol/dimethyl ether as energy vectors. This reaction requires the use of heterogeneous catalysts, typically based on Cu/ZnO, which are used industrially for the synthesis of methanol from CO/H_2 mixtures. [33-39] In fact, it has been shown that addition of CO_2 in the syngas mixture improves the activity of the catalyst[40] up to a certain concentration, above which the reaction rate decreased. This was explained by two competing phenomena: on the one hand, the presence of CO_2 limits coke formation and thus deactivation of the catalyst because of Boudouard reaction ($CO_2 + C \rightarrow 2\ CO$); on the other hand, CO_2 decreases the activity of the catalysts, because it competes with CO on the adsorption sites. While homogeneous systems based on $Ru_3(CO)_{12}$ were claimed to be effective for this reaction,[41] their activity might be related to the formation of particles under the reaction conditions.

2.3.6 The use of immobilized molecular complexes

In contrast to homogeneous systems, conventional heterogeneous catalysts are not efficient for the reduction of CO_2 to formic acid and formamides. Thus, research efforts were directed to generate supported homogeneous catalysts for ease of separation and recovery of catalysts for this application. Baiker *et al.* have developed various supported systems based on the condensation of silylated group VIII metal complexes in a sol-gel process.[42-46] While this strategy provides highly active catalysts, the performances are very low compared to their homogeneous analogues. This is probably due to a problem of accessibility of the metal complex. Another strategy, developed by Zhang *et al.* proposes the coordination of ruthenium species on different amine-functionalized silica materials.[47-49] While this method allows the preparation of broad variety of metal complexes, it displays a major drawback: important metal leaching under reaction conditions.[50] There is therefore still a need to develop new supported catalysts using a much more controlled approach and allowing of the formation of well-defined, tuneable, accessible and stable active sites.

I-3 N-Heterocyclic carbenes

3.1 Generalities

3.1.1 Definition

N-heterocyclic carbenes are a family of heterocycles bearing at least one nitrogen atom and a divalent carbon atom having six valence electrons. Arduengo's carbenes like imidazolylidenes, imidazolinylidenes or triazolylidenes are the most common ones where the carbene is linked to two nitrogens. There are also Bertrand's carbenes in which the carbene is linked to only one nitrogen.

3.1.2 Electronic properties

The singular properties of these carbenes are due to a particular electronic environment. If we consider imidazolium-based carbenes, they have an aromatic system, which make them very stable, but the delocalization is less important than the corresponding imidazolium units. The N-C=C-N π system stabilizes the carbene, and the electronegativity of nitrogen is also an important factor to reduce the electron density on the carbon atom. Due to this electronic stabilization, N-heterocyclic carbenes exist in a singlet state as the most stable configuration

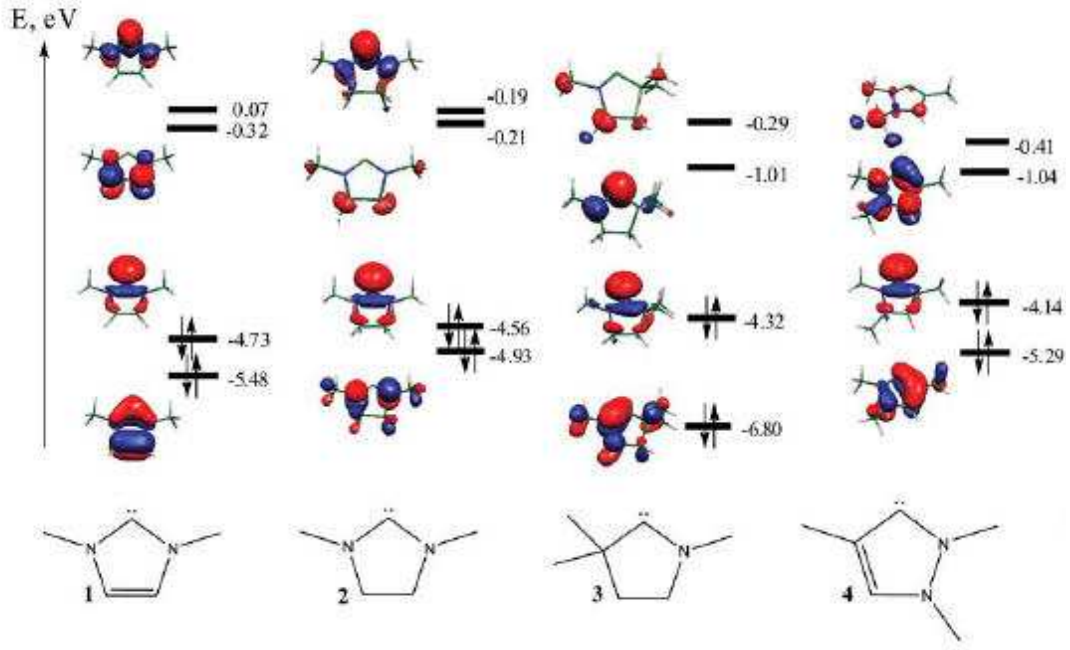

Figure 4. Electron density calculations on different N-heterocyclic carbenes. (*taken from ref. [51]*)

in contrast to non-stabilized carbenes, which are usually found in their triplet state. The electronic properties of the NHC mainly depends on the number of nitrogen present at the ylidene carbon.[51] When the number of nitrogen atom is decreased, the carbene becomes a better σ-donor ligand, but as a drawback, its stability is lower. (See Figure 4)

3.1.3 Isolation

Symmetric imidazolium rings can easily be prepared with a simplified procedure using glyoxal, formaldehyde and a primary amine.[52] The use of additional ammonium acetate can be also employed to form a substituted imidazole ring that can be further transformed to a unsymmetrical imidazolium ring. [53] In 1991, Arduengo and co-workers were the first to isolate a free NHC from an imidazolium salt. The key to stabilise this carbene and avoid its dimerization was the use of bulky substituents on the imidazole ring. For instance, 1,3-di-adamantylimidazol-2-ylidene could be crystallized and characterized by single-crystal X-ray diffraction and NMR spectroscopy. The presence of the carbene was attested by the presence of the peak at 211 ppm in ^{13}C NMR and a partial loss of aromaticity of the imidazole ring, highlighted by the decrease of its chemical shifts in ^{1}H and ^{13}C NMR. Recently, Bertrand *et al.* reported the formation of a free Cyclic Alkyl Amino Carbene (CAAC), bearing only one nitrogen atom in α-position to the carbonic carbon atom. [54]

3.2 Metallo-NHC complexes (M-NHC)

3.2.1 Generalities

The first M-NHC complexes were discovered long before the isolation of the first free carbene. In 1968, Ofele *et al.* reported the reaction between an imidazolium salt and $HCo(CO)_5^-$ yielding to imidazolylidene cobalt pentacarbonyl complex, which could be further transformed to a bis-imidazolylidene cobalt complex.[55] In parallel to this work, Wanzick *et al.* discovered a bis-NHC complex of mercury.[56] Later studies from Ofele and Herrmann showed that NHC and phosphine have important similarities when coordinated to transition metals like Cr, Mo, W, Fe and Ni[57]. These results finally led to study M-NHC complexes of group VIII noble transition metals, Rh and Pd.[58] In 1998, a notable breakthrough occurred with the generation of metathesis catalysts based on NHC-Ru alkylidene complexes.[1]

3.2.2 Ruthenium-based NHC complexes

Since the 1990's and the discovery of imidazolium-based N-Heterocyclic carbenes (NHC),[59] there has been a substantial research effort to develop catalysts based on NHC-metal complexes. NHC are good σ-donor ligands and poorer π-acceptors and they are considered highly electron-donating ligands which can advantageously replace phosphine ligands. A lot of work has been reported in this way for alkene metathesis catalysts.[1,2,60,61] As very electron-rich ligands, carbenes can coordinate to many metal centers, and their reactivity was studied with various ruthenium precursors. Ruthenium p-cymene dichloride complex was found to be an interesting precursor to generate a variety of Ru-NHC complexes for metathesis,[62] ring-opening metathesis polymerisation,[63] atom transfer radical polymerisation[64] and hydrogenation of carbon dioxide[15]. Beside ruthenium cymene complexes, various ruthenium phosphine precursors were used to generate Ru-NHC complexes. In this case, it was shown that the resulting complexes can activate C-C and C-H bond and can therefore generate new species in which C-H or C-C bonds of the carbene ligand have been activated. [65-68]

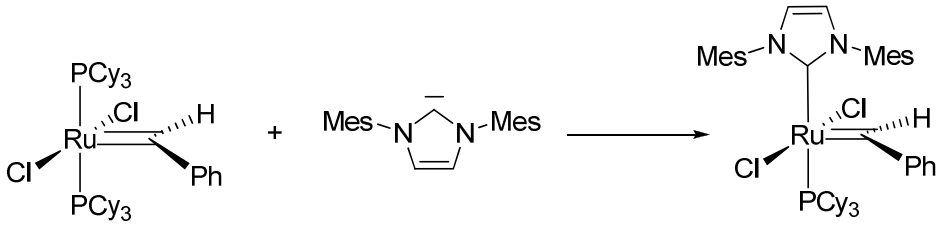

Figure 5. Formation of a NHC-based Ru catalyst for olefin metathesis

3.2.3 Recent advances: chelating bis- and tris-NHC complexes

In some cases, particularly in metal-hydride complexes, M-NHC complexes are very unstable as they can readily undergo reductive elimination to regenerate the imidazolium salt. Thus, it has been proposed to use chelating NHC units in order to prevent this elimination, first by the chelating effect itself, but also because it holds the carbene in a conformation which disfavours reductive elimination.[17] This confers to M-NHC complexes a very high thermal stability, resisting temperatures up to 200°C. For instance, in Pd-catalysts for the Heck reaction,[69,70] complex **5** is a very active catalyst at 140°C but slowly decomposes to Pd black, whereas complex **6** is as active and fully stable in the same reaction conditions. The CNC[†] pincer NHC ligand was used to generate binuclear Rh complex **7** catalytically active in hydroformylation reactions.[71] This ligand was also transposed to Ru, giving complex **8** from $[Ru(COD)Cl_2]_n$ and the dibromo imidazolium, using triethylamine as the base, in ethanol. Complex **8** shows good activity for the oxidation of olefins to aldehydes with no further reoxidation. As described in part 1, the high thermal stability of bis-NHC complexes was also used by Peris *et al.* who described the use of a cationic arene bis-NHC Ru complex **4** for the hydrogenation of CO_2 to formate salts at 200°C, which temperature can not be used with the more classical phoshine ligands.[15]

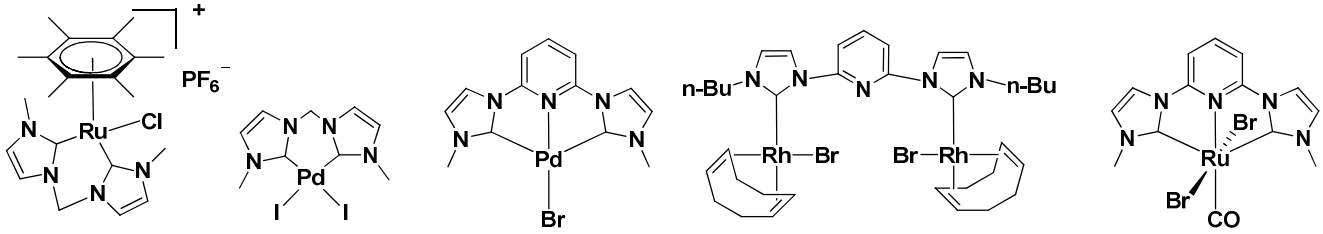

4 5 6 7 8

Figure 6. Structure of some bis-NHC complexes of Ru and Pd.

[†] CNC are tridentate ligands that allow formation of two metal-carbon bonds and one metal-nitrogen bond

I-4 From sol-gel process to nanostructured functionalized materials

4.1 Sol-gel process

4.1.1 Introduction

Historically, metal oxides were prepared by thermal processes, involving high temperatures, typically above 400°C. However, this method allowed very poor control of the morphology of the obtained material. In order to have a better control over the final solid, the sol-gel process was introduced as a mild-condition process for generating a wide range of oxide materials. The initial principle is to perform the oxide synthesis using organic precursors (typically alkoxyde derivatives) in organic solvent with presence of water. The sol-gel process is considered as an inorganic polymerisation of metal alkoxide species and involves two reactions: hydrolysis and condensation.

$$Si(OR)_4 + 2\,H_2O \xrightarrow{\text{Catalyst}} SiO_2 + 4\,ROH \quad (1)$$

Figure 7. Hydrolysis of tetraalkoxy silanes.

In the particular case of silicon, tetraalkoxysilanes of general formula $Si(OR)_4$ (with R = Me, Et, iPr) undergo hydrolysis in the presence of water and a catalyst followed by a condensation process thus yielding SiO_2 (equation (1), see Figure 7). The formation of the final oxide material will take place during four main steps which are first the formation of the sol, then formation of the gel, followed by the aging period and finally the drying.[72] Non-hydrolytic processes also exist, and they involve the condensation of a metal alkoxide with a metallic chloride.[73]

4.1.2 Formation of the sol

When the alkoxide is mixed with water, two main reactions will occur in the solution (see Figure 8), which are the hydrolysis (equation 2) in which a silicon alkoxide bond will react with water to form a silanol and the condensation (equations 3 and 4) during which a silanol will react on another silanol or an alkoxide to generate a Si-O-Si bridge. As the condensation occurs, there is formation of colloidal particles (1-100 nm), whose size and structure will highly depend on the reaction conditions (pH and H_2O/alkoxide ratio mainly).

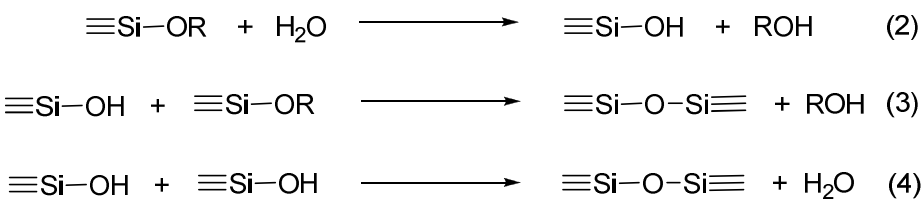

Figure 8. Main reactions involved during the sol-gel process

4.1.3 Formation of the gel

When the sol is formed, the colloidal particles will start to aggregate together through condensation reactions, which will lead to the formation of a three-dimensional network. This is the sol-gel transition, also called gelation period. During this period, there will be a strong contraction of the solid and the viscosity of all the mixture will increase sharply. The gelation is a very important step, as the global structure of the material will be defined during this step, depending mainly on the rates of hydrolysis and condensation reactions.

4.1.4 Aging

The aging period, also called Syneresis, will take place by leaving the solid in solution after the gel formation. The general structure is already formed, but the polycondensation will continue and a long aging will allow increasing the strength of the gel and obtaining more robust materials. This will be of great importance to avoid the structure to collapse during the drying step.

4.1.5 Drying

During the drying of the material, high tensions can appear, in particular in the presence of small pores (smaller than 20 nm), due to the presence of capillary forces. The drying method is thus very important, because the presence of too much tension will lead to a cracking of the material. But this can be avoided by controlling the drying process: a supercritical drying can be used, that will allow to keep completely the structure and form an aerogel with a very high pore volume of around 98%; the second option is to have a monodisperse distribution of pore sizes which will allow to dry the material without any cracking. In other cases, drying at ambient pressure will lead to a partial collapse of the structure and formation of a xerogel.

4.2 Mesostructured materials

4.2.1 Introduction

In the 1990s, the discovery of novel highly structured mesoporous materials having perfectly periodic structuration has open the way to better defined silica-based materials. Of them, MCM-41 and SBA-15 are two different types of highly ordered 2D-hexagonal structured silica. They are prepared via hydrolysis and polycondensation of tetraethyl orthosilicate (TEOS) in the presence of a structure directing agent usually called template. In the case of MCM-41,[74] this template is a quaternary ammonium surfactant giving pore-sizes of 2-3 nm, whereas in the case of SBA-15, a three-block copolymer [poly(ethylene oxide)$_x$–poly(propylene oxide)$_y$–poly(ethylene oxide)$_z$] (PEO-PPO-PEO) is used, which allows to form pore diameters between 5 and 30 nm. [75]

4.2.2 Mechanism

Depending on the experimental conditions, these surfactants arrange through supramolecular interaction into hexagonal, cubic, lamellar or vermicular phases.[76] The arrangement of the micelles during the sol-gel process will create the porous network, because the hydrolysis and polycondensation will only take place in the water-phase. Three different mechanisms were reported to describe the formation of the micellar mesophase: the True Liquid-crystal templating (LCT), the Cooperative Self-Assembly (CSA)[77] and the Hard-

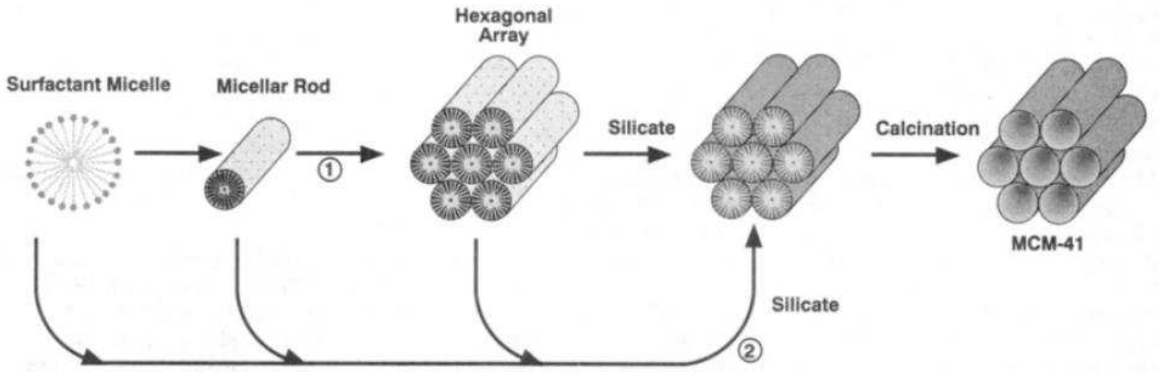

Figure 9. Two mechanistic pathways: 1) liquid crystal phase initiated (LCT), 2) silicate initiated (CSA) (*taken from ref. [73]*)

Sphere Packing (HSP)[78]. As a simplified summary, as this will not be discussed in details, in the LCT mechanism, the assembly which will lead to the structuration is taking place before the condensation; in the CSA mechanism, it takes place during the condensation and in the more recent HSP mechanism, the structuration is formed after condensation.

4.3 Mesostructured hybrid organic-inorganic materials

4.3.1 Post-synthesis treatment

The functionalization of pre-synthesized mesoporous silica is feasible by reaction of the surface silanols with organosilanes that can be chlorosilanes, alkoxysilanes or silazanes. The advantage of this method is that it can be used with a wide range of organic functionalities. The main drawback is that functionalization is not homogeneous, more important on the entry of channels than inside. Moreover, the grafted organosilanes have poor level of condensation, leaving residual uncondensed silanols.[79]

4.3.2 Direct-synthesis

After the discovery of MCM-41, Mann *et al.* prepared the first hybrid organic-inorganic material by co-condensation of organosilane and TEOS.[80] Considering the apolar property of these organic fragments (octyl and phenyl), the organic functionalities are strongly interacting with the apolar part of the surfactant, i.e. the micelle core, and this interaction remains during the condensation process, leading to homogeneously dispersed functionality within the pores of the material in contrast to post-grafting approach.[79] This has led to the preparation of a wide variety of functionalized materials incorporating all sorts of functional groups like alkyl, amine,[81,82] thiol,[83] pyridine,[84] imidazole[84] and many other ones.[85] Nonetheless, the incorporation of organic functionalities can imply important modifications in the micelle network, depending on the affinity of these functionalities with the surfactant. If we consider the aminopropyl group, it will be present as an ammonium in an acidic media, traditionally used for the synthesis of SBA. Thus, as an ionic species, it will not be able to interact with the apolar core of the micelle, and this will lead to problems for the structuration of the material.

Therefore, the incorporation of each functional group within the pores of SBA-type materials

requires a specific approach in which the starting material incorporates rather apolar functionalities that can be further modified. Using this strategy, different materials were developed recently by Corriu's group, incorporating iodopropyl[86] and aminopropyl functionalities.[87] In the case of aminopropyl, a protecting Boc group was used to decrease the polar character of the amine. It is also possible to generate bifunctionnal materials with homogeneous distribution of the two functional groups by choosing the right precursors.[88]

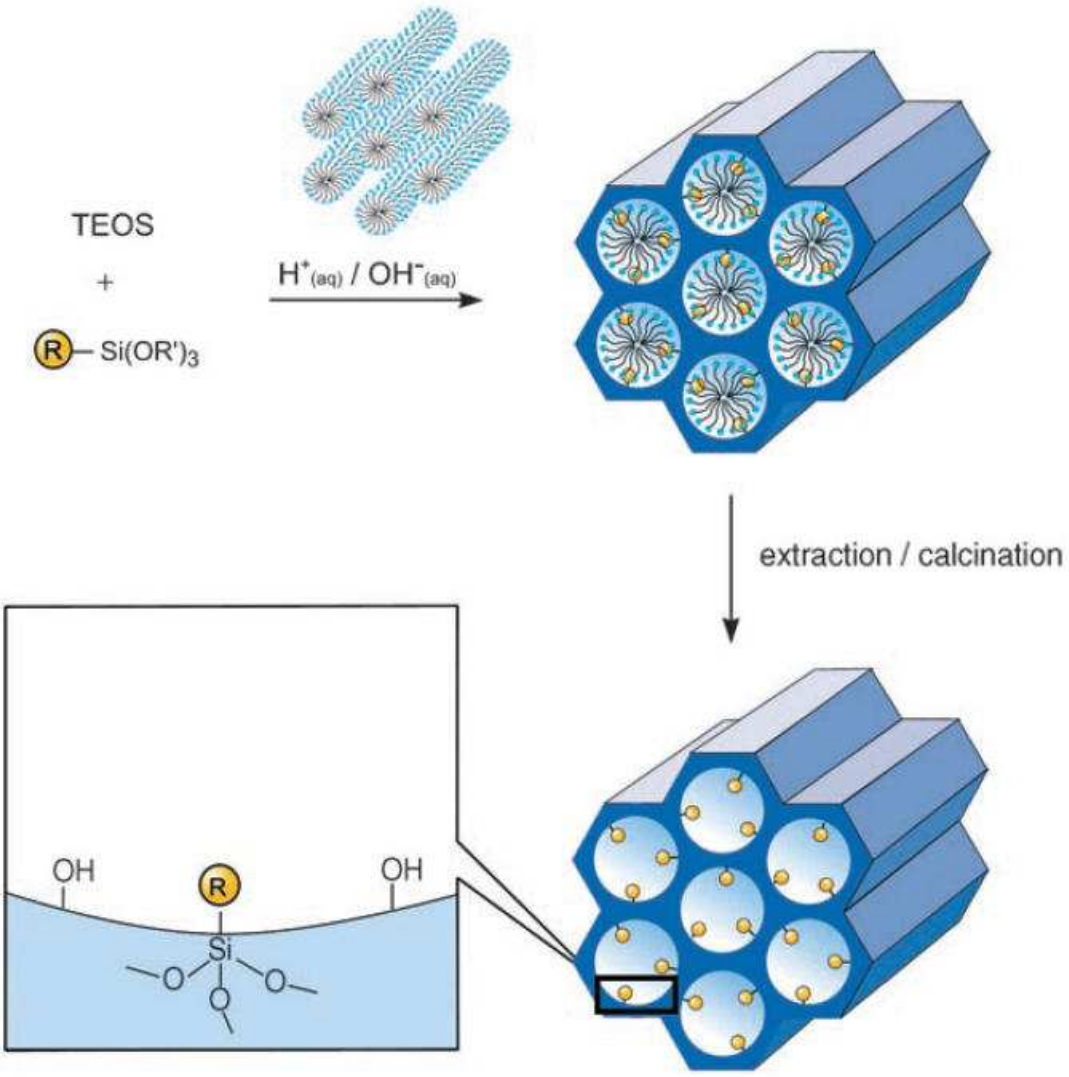

Figure 10. Synthesis of hybrid mesoporous materials by direct-synthesis (*taken from ref. [84]*)

I-5 Well-dispersed organometallic species on silica supports

5.1 Surface organometallic chemistry

The objective of surface organometallic chemistry (SOMC) is to generate well-defined and homogeneously dispersed metallic species on the surface of a support oxide.[89] Typically, organometallic species will react with surface hydroxyl groups, which surface density can be controlled by a thermal treatment.[90] Typically, when Ta(=CH*t*Bu)(CH_2*t*Bu)$_3$ reacts with silica dehydroxylated at 700°C, there is selective formation of a mono-podal species by cleavage of a Ta-C bond by a surface hydroxyl group. When performed on silica dehydroxylated at 500°C, the grafting is non-selective and there is formation of a 1:1 mixture of mono-podal and bi-podal species (see Figure 11). When the same is done with a silica treated at 300°C, only bi-podal species are formed. These results are directly linked to the variation of the density of surface silanols with the dehydroxylation temperature.[91] When treated at 700°C, the surface of silica is mainly composed of isolated silanols, whereas silica treated at lower temperatures have an increasing amount of geminal and vicinal hydroxyl groups.

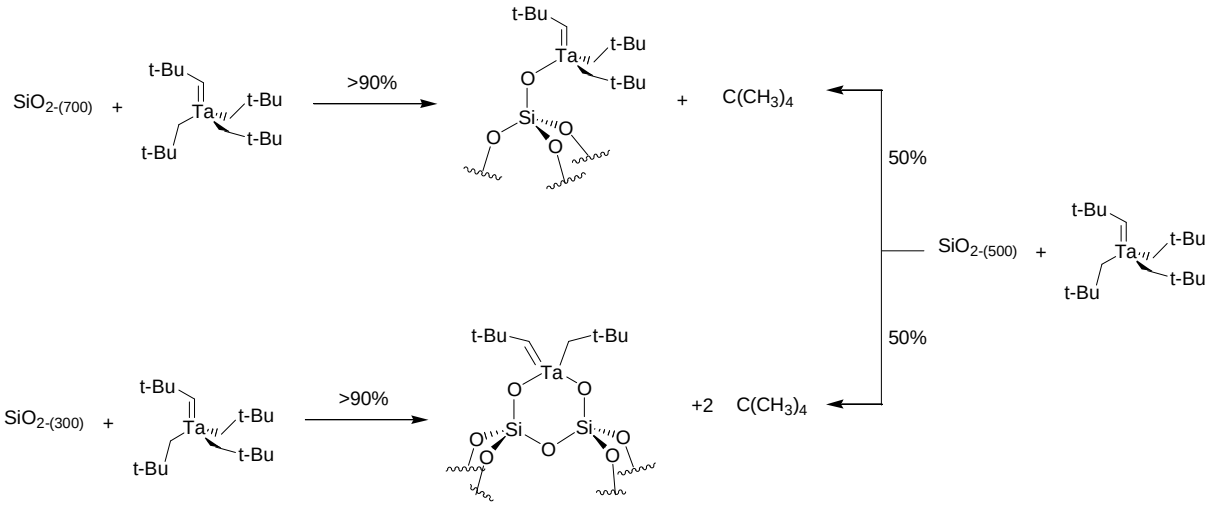

Figure 11. Reaction of Ta(=CH*t*Bu)(CH_2*t*Bu)$_3$ on partially dehydroxylated silica

Silica dehydroxylated at 700°C has the other advantage to present a relatively low silanol density of 0.7/nm². This low density allows to lower interactions between two complexes

through site isolation. This is important for catalysis, because a lot of deactivation processes imply bimolecular processes. Generally, the grafting of organometallic complexes onto silica dehydroxylated at 700°C leads to well-defined mono-podal species. This was particularly studied for homoleptic d^0 complexes of group 4[92] or heteroleptic complexes of molybdenum[93] and tungsten.[94]

5.2 Strategies to immobilize organometallic complexes on mesoporous silica

5.2.1 Post-synthesis grafting

As mentioned previously, it is possible to functionalize highly ordered mesoporous silica by treatment of the surface silanols by organo-silane precursors. This strategy has been widely used for the immobilization of coordination complexes on mesoporous silica. It is usually performed in two step with first the anchoring of a specific ligand bearing a chloro silane or alkoxy silane group and then coordination of the metallic complex. Johnson et al. developed an immobilized catalyst by incorporation of 3-bromopropyl functionalities by grafting the corresponding organosilane within the channels of the material, then it was reacted with the amine-functionalized chiral ligand to incorporate it covalently within the matrix of silica. Finally, after reaction with $PdCl_2$, the phosphine complex is formed within the channels of silica. (See reaction scheme in Figure 12.) As a comparison, the same treatment was done on a non mesostructured material. The heterogeneous catalysts and the corresponding homogeneous complex were tested in the asymmetric allylic amination reaction between cinnamyl acetate and benzylamine. Interestingly, the supported catalysts show a better activity than the homogeneous one, and a different selectivity. Whereas the homogeneous catalyst only formed the straight chain, heterogeneous catalysts showed a more important selectivity for the branched chiral product. Further more, a major difference between the immobilized complex on MCM-41 and on amorphous silica is that the latter produces only 2% of the branched product and with a poor ee (43 %) whereas the former produces 50% of branched products with 99% ee. These results show that the support can have a big influence on catalytic activity of the immobilized complexes.

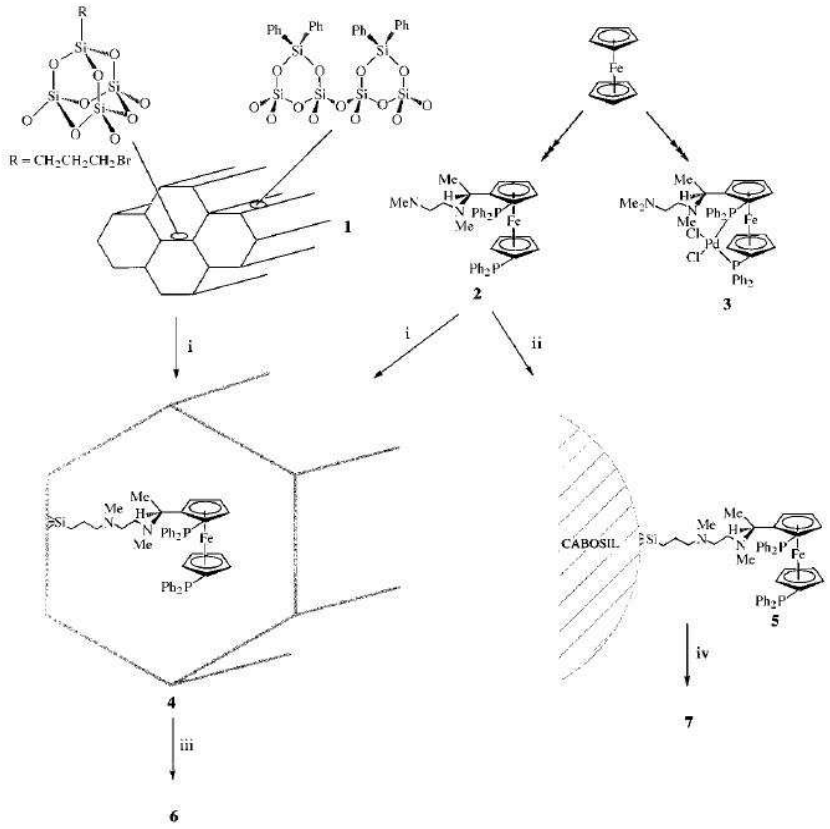

Figure 12. Example of strategy to immobilize a Pd complex on MCM-41, developed by Johnson *et al.* (*taken from ref.* [95])

5.2.2 Direct synthesis

Within the last years, a lot of work has been carried out in our laboratory to develop supported molecular complexes by a direct synthesis route. This research effort led to interesting results because of a strong collaboration with the LCMOS team (Prof. A. Mehdri, C. Reyre and RJP Corriu). This collaboration led to the publication of two articles dealing with the synthesis of highly ordered hybrid mesoporous silica bearing homogeneously distributed imidazolium functionalities with a concentration of around 0.4 mmol/g and their further in situ transformation into iridium[96] and ruthenium[97] NHC-based materials. The general methodology used here was first the preparation of an hybrid organic-inorganic mesostructured material having a reactive functionality (here an halogenated propyl or benzyl group), perfectly distributed within the pores of the mesoporous silica by the direct synthesis method.[86,96] The functionality was then used to anchor the desired ligand by reaction of the halogenated derivative with an excess of mesitylimidazole to form the imidazolium ring (See Figure 13).

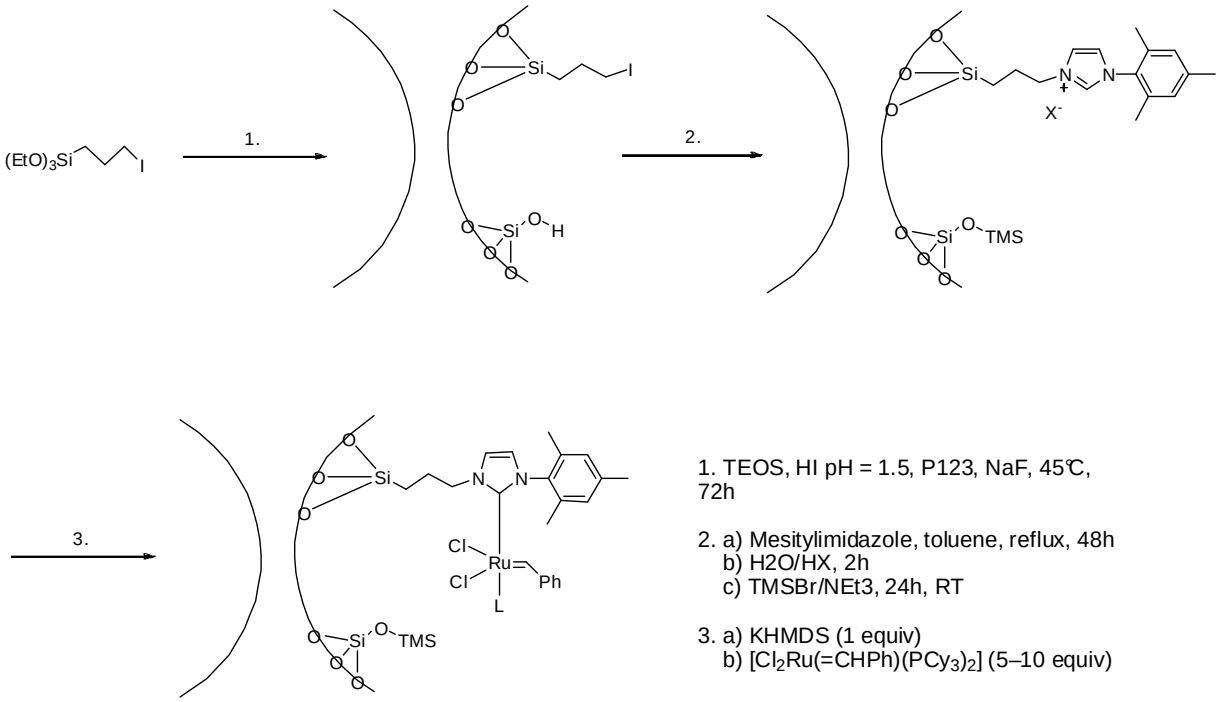

Figure 13. Formation of ordered mesoporous materials bearing homogeneously dispersed Ru-NHC complexes

The metallo-NHC complex was then formed by deprotonation of the imidazolium ring with KHMDS and reaction with the organometallic precursor, but this method is unfortunately not quantitative in the case of ruthenium Grubbs complexes. The other approach was carried out: it implies the use of an intermediate silver carbene and the subsequent transmetallation with the desired molecular complex. This method requires the use of a soluble silver base able to reach the imidazolium functionalities in the channels of the material. Typically, $AgOC(CF_3)_3$ was found to be a very good candidate to perform the formation of the silver carbene[98] and this methodology led to quantitative grafting of Ir[96] and Au[99] complexes. The Ru-NHC catalyst was tested in the metathesis of ethyl oleate, and showed a high activity, stability and it could be easily recycled. The Ir-NHC catalyst was tested in the H/D exchange reaction of acetophenone with methanol(d_4). The heterogeneous catalyst shows comparable activity with the homogeneous one and could be recycled without any metal leaching. The gold catalyst was tested in methanol addition to 1-hexyne.

Recently, another group reported the synthesis of a PMO incorporating imidazolium units within the walls of the hybrid material with a quite high concentration (0.7 mmol/g).[100] This material was obtained by co-condensation of bis(triethoxysilyl)ethane and the bis(triethoxysilyl)imidazolium salt with various ratios (see Figure 14). The imidazolium units were further reacted with $Pd(OAc)_2$ with tBuOK as a base. The material was analyzed by XPS to identify the Pd oxidation states: Pd(0) and Pd(II) species were detected but a clear insight in the nature of Pd species was not obtained. Another material was synthesized with equivalent conditions but with TEOS instead of the ethane-bridged silane. Both catalysts were studied in various Suzuki coupling reactions. The catalyst with ethane-bridges showed an improved catalytic activity compared to the other one and could be recycled 8 times without any significant loss in activity.

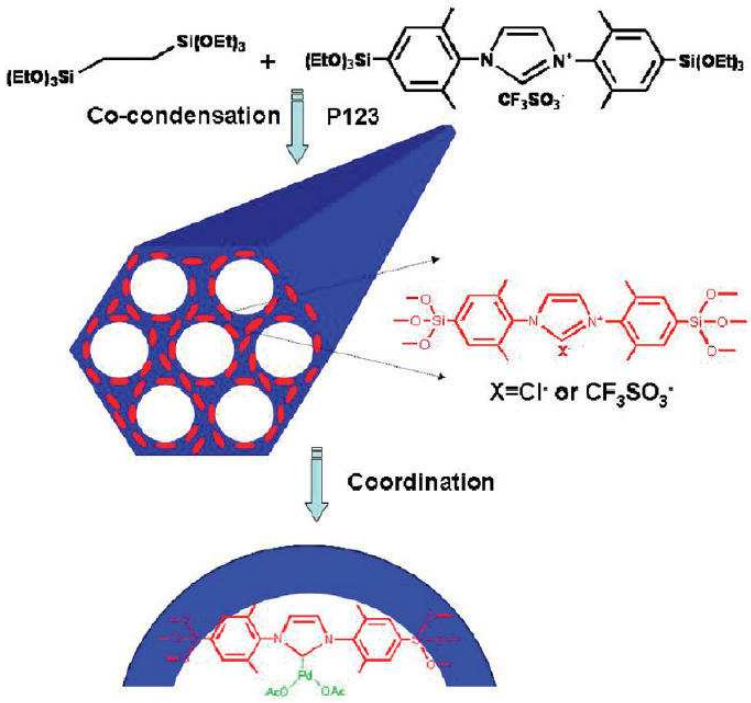

Figure 14. Synthesis of an imidazolium-functionalized PMO and subsequent formation of Pd-NHC units proposed by Yang et al. (*taken from ref.* [99])

I-6 Strategy

6.1 State of the Art

We recently developed imidazolium-functionalized materials and their use to obtain

ruthenium and iridium NHC complexes.[96,97] As described before, Metallo-NHC complexes have proved their high potential for the hydrogenation of CO_2, and we therefore have a big interest in developing ruthenium supported systems for this application. Phosphine complexes are another interesting candidate, so the development of complexes bearing both an NHC ligand and phosphines was found interesting. The formation of Ru-NHC complexes from phosphine Ru-complexes have been described in the literature,[65,66] but it shows a complex reactivity, involving the possibility of C-H activations on the NHC unit. Furthermore, if we directly form a Ru-NHC complex bearing a specific phosphine ligand, the exchange with the targeted phosphine could be difficult. We therefore aim at finding a more convenient Ru-NHC precursor on which we could easily coordinate the desired phosphine ligand.

6.2 Objectives

Many highly efficient homogeneous catalysts have been developed recently for the catalytic hydrogenation of CO_2, which show very high TON greater than 3 million in the formation of formic acid and 700,000 for the formation of DMF. But all attempts to immobilize molecular complexes on silica supports have shown an important loss in activity compared to the homogeneous systems. Yet, highly efficient heterogeneous catalysts are still an interesting goal because they can be used in a continuous flow fixed-bed reactor. Furthermore, dispersion of the molecular complex on the surface of a support could avoid the problem of insolubility of the complex in supercritical CO_2.

Our goal is to combine the advantages of homogeneous and heterogeneous catalysis through the development of ordered mesoporous silica materials bearing molecular ruthenium complexes, homogeneously distributed along the channel pores of the silica matrix.

6.3 Imidazolium-functionalized materials

6.3.1 From already developed materials

Different imidazolium-containing materials were developed in our lab and in the LCMOS, bearing either rigid (benzyl) or flexible (propyl) tethers. We chose to use only flexible tethers, because it might be interesting to have interactions with the surface, for example by using

OH groups as an acidic source for hydrogen transfer. It was proven that a simultaneous two-hydrogen transfer process is very effective for the reduction of CO_2.[101] The first step of the project will therefore be to develop ruthenium-NHC supported species from the already developed imidazolium materials in our lab, starting from an iodopropyl-functionalized material[86] as a first step to validate our methodology, and study the activity of the resulting catalysts in the hydrogenation of CO_2.

6.3.2 A new approach

In a second step, we aimed at developing other imidazolium materials that could be much more concentrated. Indeed, iodopropyl materials are typically synthesized in our lab with a ratio organic functionality/TEOS of 1/30 but the higher limit is 1/19. If we want to reach higher contents like 1/10, one application being the formation of bis-NHC complexes, we need to find another organic functionality that could be transformed to imidazolium units. Recently, Stack et al. described the synthesis of an azidopropyl-functionalized material by direct synthesis, and they could easily synthesize materials with dilutions up to 1/12, because of the strong lipophily of the azidopropyl group.[102] In organic chemistry, the azide group can be easily reduced to amine by the Staudinger reaction,[103] involving reaction of a phosphine to form an iminophosphorane, that can be hydrolyzed to the corresponding primary amine, producing phosphine oxide as the by-product. It should therefore be feasible to form a highly-concentrated amine material by reduction of the azide and to further transform the amino group into imidazolium or imidazole moieties adapting Arduengo's procedures. The reaction of an aminopropyl-functionalized material with glyoxal and formaldehyde in presence of an ammonium salt should lead to the formation of an imidazole ring. If this hypothesis is verified, we could then easily develop unsymmetrical imidazolium salts, by reaction of an halogenated compound with the imidazole ring, or more interestingly, directly from the NH_2 material by replacing the ammonium salt with a primary amine.

6.3.3 Towards bis-imidazolium units

If this approach is feasible, we would be able to form a wide variety of imidazolium units, depending on the amine which is used for the synthesis. If we use a diamine, it should then

be feasible to synthesize bis-imidazolium units. This is of big interest for us, as recent works of Peris et al. showed the high potential of bis-NHC ruthenium complexes in the hydrogenation of CO_2 thanks to their high thermic stability.[15]

6.4 Formation of the Ru-NHC catalytic material

In many recent works involving the formation of ruthenium-NHC complexes, arene derivatives like $[RuCl_2(p\text{-cymene})]_2$ have proved to be good candidates to selectively form the desired Ru-NHC complex. In some cases, they could also be transformed to the desired complex by adding another carbene ligand.[62] We therefore chose to use this precursor which can form various Ru-NHC complexes in a very selective way. Indeed, we need very selective reactions, because Ru-NHC complexes will be formed in situ on the imidazolium material, and if some by-products are formed, they will remain on the silica surface. This should be avoided if we want to develop single-site catalysts. Furthermore, as p-cymene is a rather weak ligand compared to a phosphine ligand, the exchange should be easily achieved. To have a good understanding of our system, we will first study the formation of molecular complexes starting from an imidazolium salt having the same structure as the one we target to develop in on our materials. This preliminary study will be important to optimize the formation of the Ru-NHC bond in homogeneous conditions. We will investigate two approaches, i) the transmetallation with silver carbene, and ii) the deprotonation of the imidazolium and further coordination of the “free” carbene. Depending on the results obtained, the procedures will be implemented to the imidazolium materials.

6.5 Catalytic hydrogenation of CO_2

In order to evaluate the performances of our materials, they will be mainly tested in the hydrogenation of CO_2 to 1-formylpyrrolidine in batch reactors. This reaction is more convenient than the synthesis of DMF, which involves the use of the gaseous dimethylamine.

I-7 References

[1] J. Huang; E. D. Stevens; S. P. Nolan; J. L. Petersen *J. Am. Chem. Soc.* **1999**, *121*, 2674-2678.

[2] M. Scholl; T. M. Trnka; J. P. Morgan; R. H. Grubbs *Tetrahedron Lett.* **1999**, *40*, 2247-2250.

[3] *IPCC, 2007: Climate Change 2007: Synthesis Report. Contribution of Working Groups I, II and III to the Fourth Assessment Report of the Intergovernmental Panel on Climate Change [Core Writing Team, Pachauri, R.K and Reisinger, A. (eds.)]. IPCC, Geneva, Switzerland, 104 pp.*

[4] R. H. Wijffels; M. J. Barbosa *Science*, *329*, 796-799.

[5] B. Loges; A. Boddien; H. Junge; M. Beller *Angew. Chem.-Int. Ed.* **2008**, *47*, 3962-3965.

[6] G. A. Olah; A. Goeppert; G. K. S. Prakash *J. Org. Chem.* **2008**, *74*, 487-498.

[7] P. Haynes; L. H. Slaugh; J. F. Kohnle *Tetrahedron Lett.* **1970**, 365-368.

[8] Y. Inoue; H. Izumida; Y. Sasaki; H. Hashimoto *Chem. Lett.* **1976**, 863-864.

[9] P. G. Jessop; T. Ikariya; R. Noyori *Chem. Rev.* **1995**, *95*, 259-272.

[10] P. G. Jessop; Y. Hsiao; T. Ikariya; R. Noyori *J. Am. Chem. Soc.* **1994**, *116*, 8851-8852.

[11] P. G. Jessop; T. Ikariya; R. Noyori *Nature* **1994**, *368*, 231-233.

[12] P. Munshi; A. D. Main; J. C. Linehan; C. C. Tai; P. G. Jessop *J. Am. Chem. Soc.* **2002**, *124*, 7963-7971.

[13] O. Krocher; R. A. Koppel; A. Baiker *Chem. Commun.* **1997**, 453-454.

[14] R. Tanaka; M. Yamashita; K. Nozaki *J. Am. Chem. Soc.* **2009**, *131*, 14168-14169.

[15] S. Sanz; A. Azua; E. Peris *Dalton Trans.* **2010** *39*, 6339-6343.

[16] S. Sanz; M. Benitez; E. Peris *Organometallics* **2010**, *29*, 275-277.

[17] E. Peris; R. H. Crabtree *Coord. Chem. Rev.* **2004**, *248*, 2239-2246.

[18] J. A. Mata; M. Poyatos; E. Peris *Coord. Chem. Rev.* **2007**, *251*, 841-859.

[19] L. Schmid; A. Canonica; A. Baiker *Appl. Catal. A-Gen.* **2003**, *255*, 23-33.

[20] K. Kudo; N. Sugita; Y. Takezaki *Nihon Kagaku Kaishi* **1977**, 302-309.

[21] D. J. Drury; J. E. Hamlin *Eur. Patent Appl.*, 0 095 321, **1983**.

[22] E. Graf; W. Leitner *J. Chem. Soc. Chem. Commun.* **1992**, 623-624.

[23] F. Gassner; W. Leitner *J. Chem. Soc. Chem. Commun.* **1993**, 1465-1466.

[24] W. Leitner; E. Dinjus; F. Gassner *J. Organomet. Chem.* **1994**, *475*, 257-266.

[25] R. Fornika; H. Gorls; B. Seemann; W. Leitner *J. Chem. Soc. Chem. Commun.* **1995**, 1479-1481.

[26] C. P. Lau; Y. Z. Chen *J. Mol. Catal. A-Chem.* **1995**, *101*, 33-36.

[27] Y. Himeda; N. Onozawa-Komatsuzaki; H. Sugihara; K. Kasuga *J. Photochem. Photobiol. A-Chem.* **2006**, *182*, 306-309.

[28] F. Hutschka; A. Dedieu; M. Eichberger; R. Fornika; W. Leitner *J. Am. Chem. Soc.* **1997**, *119*, 4432-4443.

[29] Y. Musashi; S. Sakaki *J. Am. Chem. Soc.* **2000**, *122*, 3867-3877.

[30] A. Urakawa; M. Iannuzzi; J. Hutter; A. Baiker *Chem.-Eur. J.* **2007**, *13*, 6828-6840.

[31] A. D. Getty; C. C. Tai; J. C. Linehan; P. G. Jessop; M. M. Olmstead; A. L. Rheingold *Organometallics* **2009**, *28*, 5466-5477.

[32] A. Urakawa; F. Jutz; G. Laurenczy; A. Baiker *Chem. Eur. J.* **2007**, *13*, 3886-3899.

[33] M. Bowker; H. Houghton; K. C. Waugh *J. Chem. Soc., Faraday Trans. 1* **1981**, *77*, 3023-3036.

[34] Y. Amenomiya *Applied Cat.* **1987**, *30*, 57-68.

[35] M. Saito; T. Fujitani; M. Takeuchi; T. Watanabe *Appl. Catal. A-Gen.* **1996**, *138*, 311-318.

[36] T. Fujitani; I. Nakamura; T. Uchijima; J. Nakamura *Surf. Sci.* **1997**, *383*, 285-298.

[37] T. Inui; H. Hara; T. Takeguchi; J. B. Kim *Catal. Today* **1997**, *36*, 25-32.

[38] J. Toyir; P. R. de la Piscina; J. L. G. Fierro; N. Homs *Appl. Catal. B-Environ.* **2001**, *29*, 207-215.

[39] F. Arena; K. Barbera; G. Italiano; G. Bonura; L. Spadaro; F. Frusteri *J. Catal.* **2007**, *249*, 185-194.

[40] K. Klier; V. Chatikavanij; R. G. Herman; G. W. Simmons *J. Catal.* **1982**, *74*, 343-360.

[41] K. Tominaga; Y. Sasaki; M. Kawai; T. Watanabe; M. Saito *J. Chem. Soc.-Chem. Commun.* **1993**, 629-631.

[42] O. Krocher; R. A. Koppel; A. Baiker *Chem. Commun.* **1996**, 1497-1498.

[43] O. Krocher; R. A. Koppel; M. Froba; A. Baiker *J. Catal.* **1998**, *178*, 284-298.

[44] O. Krocher; R. A. Koppel; A. Baiker *J. Mol. Catal. A-Chem.* **1999**, *140*, 185-193.

[45] L. Schmid; M. Rohr; A. Baiker *Chem. Commun.* **1999**, 2303-2304.

[46] L. Schmid; O. Krocher; R. A. Koppel; A. Baiker *Microp. Mesop. Mat.* **2000**, *35-6*, 181-193.

[47] Y. P. Zhang; J. H. Fei; Y. M. Yu; X. M. Zheng *Catal. Commun.* **2004**, *5*, 643-646.

[48] Y. P. Zhang; J. H. Fei; Y. M. Yu; X. M. Zheng *Catal. Lett.* **2004**, *93*, 231-234.

[49] Y. M. Yu; J. H. Fei; Y. P. Zhang; X. M. Zheng *Chin. J. Chem.* **2006**, *24*, 840-844.

[50] M. Rohr; M. Gunther; F. Jutz; J. D. Grunwaldt; H. Emerich; W. van Beek; A. Baiker *Appl. Catal. A-Gen.* **2005**, *296*, 238-250.

[51] A. A. Tukov; A. T. Normand; M. S. Nechaev *Dalton Trans.* **2009**, 7015-7028.

[52] A. J. Arduengo, US Patent 5077414, **1991**.

[53] A. A. Gridnev; I. M. Mihaltseva *Synth. Comm.* **1994**, *24*, 1547-1555.

[54] V. Lavallo; Y. Canac; C. Präsang; B. Donnadieu; G. Bertrand *Angew. Chem. Int. Ed.* **2005**, *44*, 5705-5709.

[55] K. Öfele; M. Herberhold *Angew. Chem.* **1970**, *82*, 775-776.

[56] H. W. Wanzlick; H. J. Schönherr *Angew. Chem.* **1968**, *80*, 154-154.

[57] K. Öfele; W. A. Herrmann; D. Mihalios; M. Elison; E. Herdtweck; W. Scherer; J. Mink *J. Organomet. Chem.* **1993**, *459*, 177-184.

[58] W. A. Herrmann; L. J. Gooen; M. Spiegler *J. Organomet. Chem.* **1997**, *547*, 357-366.

[59] A. J. Arduengo; R. L. Harlow; M. Kline *J. Am. Chem. Soc.* **1991**, *113*, 361-363.

[60] T. Weskamp; W. C. Schattenmann; M. Spiegler; W. A. Herrmann *Angew. Chem. Int. Ed.* **1998**, *37*, 2490-2493.

[61] J. S. Kingsbury; J. P. A. Harrity; P. J. Bonitatebus; A. H. Hoveyda *J. Am. Chem. Soc.* **1999**, *121*, 791-799.

[62] L. Jafarpour; J. K. Huang; E. D. Stevens; S. P. Nolan *Organometallics* **1999**, *18*, 3760-3763.

[63] L. Delaude; A. Demonceau; A. F. Noels *Chem. Commun.* **2001**, 986-987.

[64] L. Delaude; S. Delfosse; A. Richel; A. Demonceau; A. F. Noels *Chem. Commun.* **2003**, 1526-1527.

[65] S. Burling; E. Mas-Marza; J. E. V. Valpuesta; M. F. Mahon; M. K. Whittlesey *Organometallics* **2009**, *28*, 6676-6686.

[66] S. Burling; G. Kociok-Kohn; M. F. Mahon; M. K. Whittlesey; J. M. J. Williams *Organometallics* **2005**, *24*, 5868-5878.

[67] K. Abdur-Rashid; T. Fedorkiw; A. J. Lough; R. H. Morris *Organometallics* **2004**, *23*, 86-94.

[68] R. F. R. Jazzar; S. A. Macgregor; M. F. Mahon; S. P. Richards; M. K. Whittlesey *J. Am. Chem. Soc.* **2002**, *124*, 4944-4945.

[69] W. A. Herrmann; C. P. Reisinger; M. Spiegler *J. Organomet. Chem.* **1998**, *557*, 93-96.

[70] E. Peris; J. A. Loch; J. Mata; R. H. Crabtree *Chem. Commun.* **2001**, 201-202.

[71] M. Poyatos; P. Uriz; J. A. Mata; C. Claver; E. Fernandez; E. Peris *Organometallics* **2002**, *22*, 440-444.

[72] L. L. Hench; J. K. West *Chem. Rev.* **1990**, *90*, 33-72.

[73] R. J. P. Corriu; D. Leclercq; P. Lefevre; P. H. Mutin; A. Vioux *J. Mater. Chem.* **1992**, *2*, 673-674.

[74] J. S. Beck; J. C. Vartuli; W. J. Roth; M. E. Leonowicz; C. T. Kresge; K. D. Schmitt; C. T. W. Chu; D. H. Olson; E. W. Sheppard; S. B. McCullen; J. B. Higgins; J. L. Schlenker *J. Am. Chem. Soc.* **1992**, *114*, 10834-10843.

[75] D. Y. Zhao; J. L. Feng; Q. S. Huo; N. Melosh; G. H. Fredrickson; B. F. Chmelka; G. D. Stucky *Science* **1998**, *279*, 548-552.

[76] Q. S. Huo; D. I. Margolese; G. D. Stucky *Chem. Mat.* **1996**, *8*, 1147-1160.

[77] A. Monnier; F. Schuth; Q. Huo; D. Kumar; D. Margolese; R. S. Maxwell; G. D. Stucky; M. Krishnamurty; P. Petroff; A. Firouzi; M. Janicke; B. F. Chmelka *Science* **1993**, *261*, 1299-1303.

[78] J. Tang; X. Zhou; D. Zhao; G. Q. Lu; J. Zou; C. Yu *J. Am. Chem. Soc.* **2007**, *129*, 9044-9048.

[79] M. H. Lim; A. Stein *Chem. Mat.* **1999**, *11*, 3285-3295.

[80] S. L. Burkett; S. D. Sims; S. Mann *Chem. Commun.* **1996**, 1367-1368.

[81] C. E. Fowler; S. L. Burkett; S. Mann *Chem. Commun.* **1997**, 1769-1770.

[82] D. J. Macquarrie; D. B. Jackson; J. E. G. Mdoe; J. H. Clark *New J. Chem.* **1999**, *23*, 539-544.

[83] A. Taguchi; F. Schuth *Microp. Mesop. Mat.* **2005**, *77*, 1-45.

[84] M. C. Burleigh; M. A. Markowitz; M. S. Spector; B. P. Gaber *J. Phys. Chem. B* **2001**, *105*, 9935-9942.

[85] F. Hoffmann; M. Cornelius; J. Morell; M. Froba *Angew. Chem. Int. Ed.* **2006**, *45*, 3216-3251.

[86] J. Alauzun; A. Mehdi; C. Reye; R. Corriu *New J. Chem.* **2007**, *31*, 911-915.

[87] A. Mehdi; C. Reye; S. Brandes; R. Guilard; R. J. P. Corriu *New J. Chem.* **2005**, *29*, 965-968.

[88] R. Mouawia; A. Mehdi; C. Reye; R. J. P. Corriu *J. Mater. Chem.* **2008**, *18*, 4193-4203.

[89] C. Coperet; M. Chabanas; R. Petroff Saint-Arroman; J. M. Basset *Angew. Chem. Int. Ed.* **2003**, *42*, 156-181.

[90] L. Lefort; M. Chabanas; O. Maury; D. Meunier; C. Coperet; J. Thivolle-Cazat; J. M. Basset *J. Organomet. Chem.* **2000**, *593*, 96-100.

[91] B. A. Morrow *Stud. Surf. Sci. Catal.* **1990**, *57*, A161.

[92] R. Petroff Saint-Arroman; J. M. Basset; F. Lefebvre; B. Didillon *Appl. Catal. A-Gen.* **2005**, *290*, 181-190.

[93] F. Blanc; J. Thivolle-Cazat; J. M. Basset; C. Coperet; A. S. Hock; Z. J. Tonzetich; A. Sinha; R. R. Schrock *J. Am. Chem. Soc.* **2007**, *129*, 5779-5779.

[94] B. Rhers; A. Salameh; A. Baudouin; E. A. Quadrelli; M. Taoufik; C. Coperet; F. Lefebvre; J. M. Basset; X. Solans-Monfort; O. Eisenstein; W. W. Lukens; L. P. H. Lopez; A. Sinha; R. R. Schrock *Organometallics* **2006**, *25*, 3554-3557.

[95] B. F. G. Johnson; S. A. Raynor; D. S. Shephard; T. Mashmeyer; J. M. Thomas; G. Sankar; S. Bromley; R. Oldroyd; L. Gladden; M. D. Mantle *Chem. Commun.* **1999**, 1167-1168.

[96] T. K. Maishal; J. Alauzun; J. M. Basset; C. Coperet; R. J. P. Corriu; E. Jeanneau; A. Mehdi; C. Reye; L. Veyre; C. Thieuleux *Angew. Chem. Int. Ed.* **2008**, *47*, 8654-8656.

[97] I. Karame; M. Boualleg; J. M. Camus; T. K. Maishal; J. Alauzun; J. M. Basset; C. Coperet; R. J. P. Corriu; E. Jeanneau; A. Mehdi; C. Reye; L. Veyre; C. Thieuleux *Chem. Eur. J.* **2009**, *15*, 11820-11823.

[98] T. K. Maishal; J. M. Basset; M. Boualleg; C. Coperet; L. Veyre; C. Thieuleux *Dalton Trans.* **2009**, 6956-6959.

[99] M. Bouhrara PhD thesis, C2P2 (CPE-Lyon, CNRS, Université Lyon 1), 2010.

[100] H. Yang; X. Han; G. Li; Z. Ma; Y. Hao *J. Phys. Chem. C* **2010**, *114*, 22221-22229.

[101] P. M. Zimmerman; Z. Y. Zhang; C. B. Musgrave *Inorg. Chem.* **2010**, *49*, 8724-8728.

[102] J. Nakazawa; T. D. P. Stack *J. Am. Chem. Soc.* **2008**, *130*, 14360-14361.

[103] H. Staudinger; E. Hauser *Helv. Chimi. Acta* **1921**, *4*, 861-886.

Chapter 2

Formation of Ru-NHC catalytic materials

and their use in catalysis

TABLE OF CONTENT

LIST OF FIGURES

LIST OF SCHEMES

LIST OF TABLES

LIST OF FIGURES IN APPENDIX

II-1 Introduction

The use of CO_2 as a C_1 building block is one of the possible solutions for CO_2 remediation, a point of particular interest considering that atmospheric concentration of CO_2 is reaching critical values.[1] One approach consists in the conversion of CO_2 back into chemicals and fuels[2] with the hydrogenation of CO_2 for instance. For this particular chemical process, homogeneous catalysts based on noble metals were first discovered in the 1970s,[3,4] but one of the critical advances was the use of trimethylphosphine ruthenium complexes and supercritical CO_2 as a "solvent". Depending on the additives present during the reaction, either formic acid,[5] formamides[6] or formate esters,[7] are produced. Introduction of bidendate chelating ligands led to further improvements for the hydrogenation of CO_2 to formamides.[8] PNP[9] or bis-NHC[10] complexes of ruthenium and iridium were also very effective for the hydrogenation of CO_2 to formic acid. While homogeneous catalytic systems are numerous, there are only few examples of heterogeneous catalysts. Two different strategies have been mainly developed to date: coordination of different metal precursors on aminopropyl-functionnalized materials[10] and the incorporation of silicon-containing ruthenium phosphine complexes during a sol-gel process.[11] While the former approach leads to important metal leaching, the latter suffers from lower catalytic performances compared to its homogeneous analogues, one possible reason being a diffusion problem of the reactants.[12] Considering the advantages of heterogeneous catalysts, there is still a need to develop supported catalysts using a much more controlled approach, which allows a control of the

distribution of active sites and avoids any problem of accessibility of the reactants to these sites. Imidazolium-functionnalized materials were developed, using the synthesis of hybrid materials via a direct synthesis, and used to form the corresponding iridium[14] and ruthenium[13,14] NHC catalytic materials for H/D-exchange and alkene-metathesis reactions. Their very high catalytic performances, typically equal or exceeding those of their homogeneous counterparts, result from the control of the synthesis of the catalytic material at a molecular level. Therefore, the use of this strategy will be described to generate catalytic materials based on Ru-NHC species for the hydrogenation of CO_2 to amides, which display promising catalytic performances. Furthermore, as Ru-NHC complexes are also known to be good catalysts for radical-transfer reactions,[15] the catalysts will further be tested in these reactions.

II-2 Formation of Ru-NHC model molecular complexes

2.1 Reaction of $[RuCl_2(p\text{-cymene})]_2$ with a model imidazolium

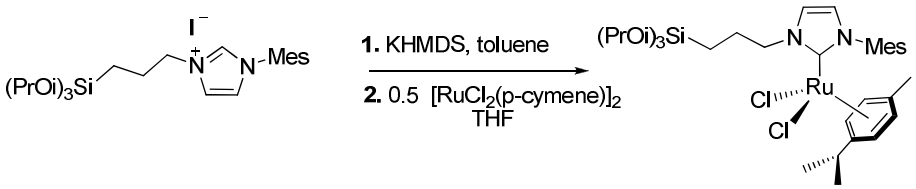

RuCym

The reaction of $[(p\text{-cymene})RuCl_2]_2$ with the deprotonated imidazolium in THF followed by purification by washing with hexane provided a well-defined NHC-Ru complex **RuCym** in 59% yield, whose structure was confirmed by elemental analysis, ^1H (Figure 1), COSY (Figure A2), ^{13}C (Figure 2), DEPT (Figure A1) and ^1H-^{13}C HSQC (Figure A3) NMR experiments. Elemental analysis is overall consistent with the proposed structure, with a maximum relative error of 2% for each element analyzed (Ru, Cl, C, H, N, Si). The full attribution of the ^1H spectrum was confirmed by the use of COSY, DEPT and HSQC experiments. Using DEPT and HSQC, it was possible to differentiate CH and CH_3 from CH_2 signals. This allows the unambiguous attribution of the protons of the propyl chain, as the

integrations are uncertain due to some overlapping signals: signals at 0.9, 2.15 and 4.60 ppm can be attributed to protons h, g and f respectively. From integrations, COSY and comparison with the starting $[RuCl_2(p\text{-cymene})]_2$ and the imidazolium, it is then possible to easily differentiate CH_3 from the mesityl group (ortho position, 6H, 2.01 ppm and para position, 3H, 2.10 ppm), from the isopropoxy group (18H, 1.25 ppm), from the isopropyl of para-cymene (6H, 1.06 ppm) and from the methyl of p-cymene (3H, 1.72 ppm) and CH from the isopropoxy (3H, 4.33 ppm, coupling with the signal at 1.25 ppm) and from the isopropyl of p-cymene (1H, 2.92 ppm, coupling with the signal at 1.06 ppm). Remaining signals are easily assigned from chemical shifts and integrations : the singlet at 6.70 ppm is attributed to the aromatic CH of mesityl, the two doublets at 6.57 and 6.03 ppm to the CH of the imidazolylidene ring **d** and **e** respectively and the two doublets at 4.64 and 5.05 ppm to the aromatic CH of p-cymene **m** and **l** respectively.

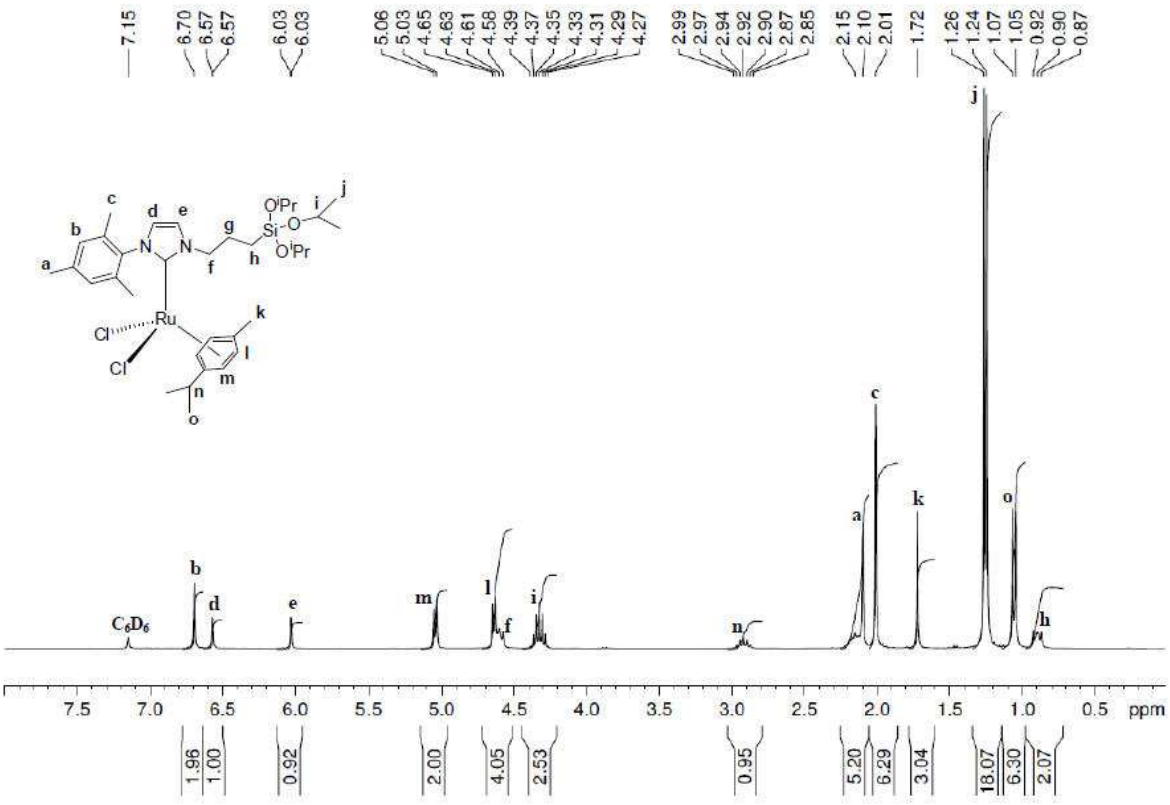

Figure 1. ^{1}H NMR spectrum of complex **RuCym**

Having a full attribution of the ^{1}H spectrum, it is then very easy to attribute the ^{13}C spectrum, by using the ^{1}H-^{13}C HSQC experiment. The attribution of the quaternary carbon atoms is possible by comparison with the starting imidazolium and ruthenium precursor. Most interestingly, the formation of the Ru-NHC bond is attested by the presence of the carbene signal at 172.9 ppm. Overall, elemental analysis, ^{1}H, COSY, ^{13}C, DEPT and HSQC were consistent with this assignment, proving the formation of the complex **RuCym**.

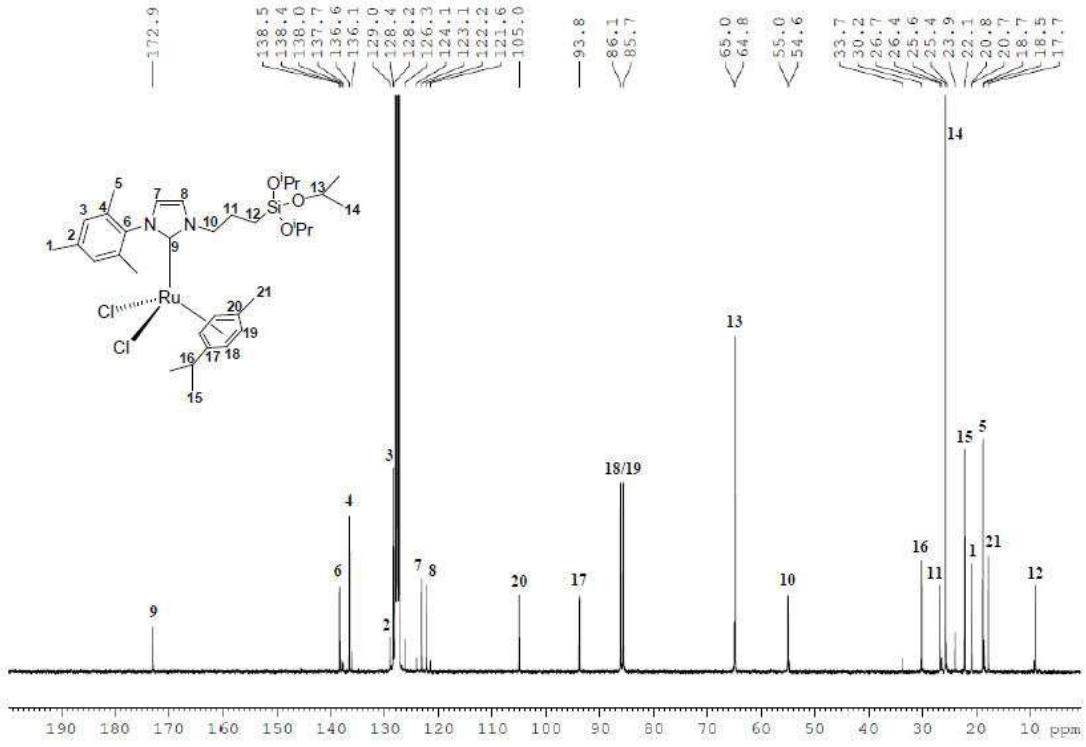

Figure 2. ^{13}C NMR spectrum of complex **RuCym**

2.2 Reaction of $RuCl_2$(NHC)(p-cymene) with PMe_3

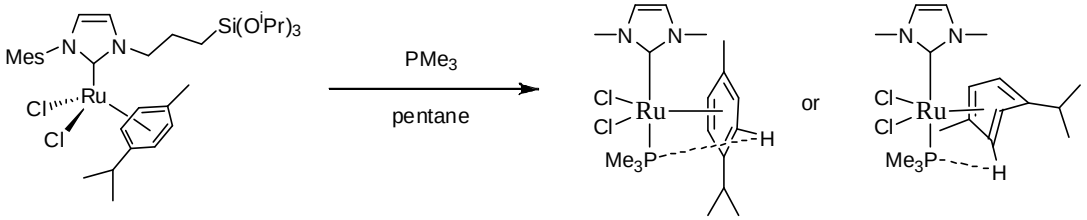

Upon the reaction of **RuCym** with an excess of trimethylphosphine, an intense peak at 4.6 ppm appeared in ^{31}P NMR (see Figure A4), corresponding to PMe_3 coordinated to Ruthenium. Five other minor peaks are also present and can be divided into three sets of peaks having the same intensity and coupling. There is a first signal at 5.1 ppm, very close to

the major one, which may then correspond to an isomer of the major product. The second set of signals corresponds to two singlets of the same intensity at -6.2 and 30.2 ppm. The difference in chemical shifts would suggest that we have two unequivalent positions here, the first one being in cis-position with regards to the NHC and the second one in trans-position with regards to the NHC. The last set of signals consists in two triplets at -10.3 and 9.9 ppm. It would suggest that this complex bears two pairs of PMe_3 which are unequivalent to each other.

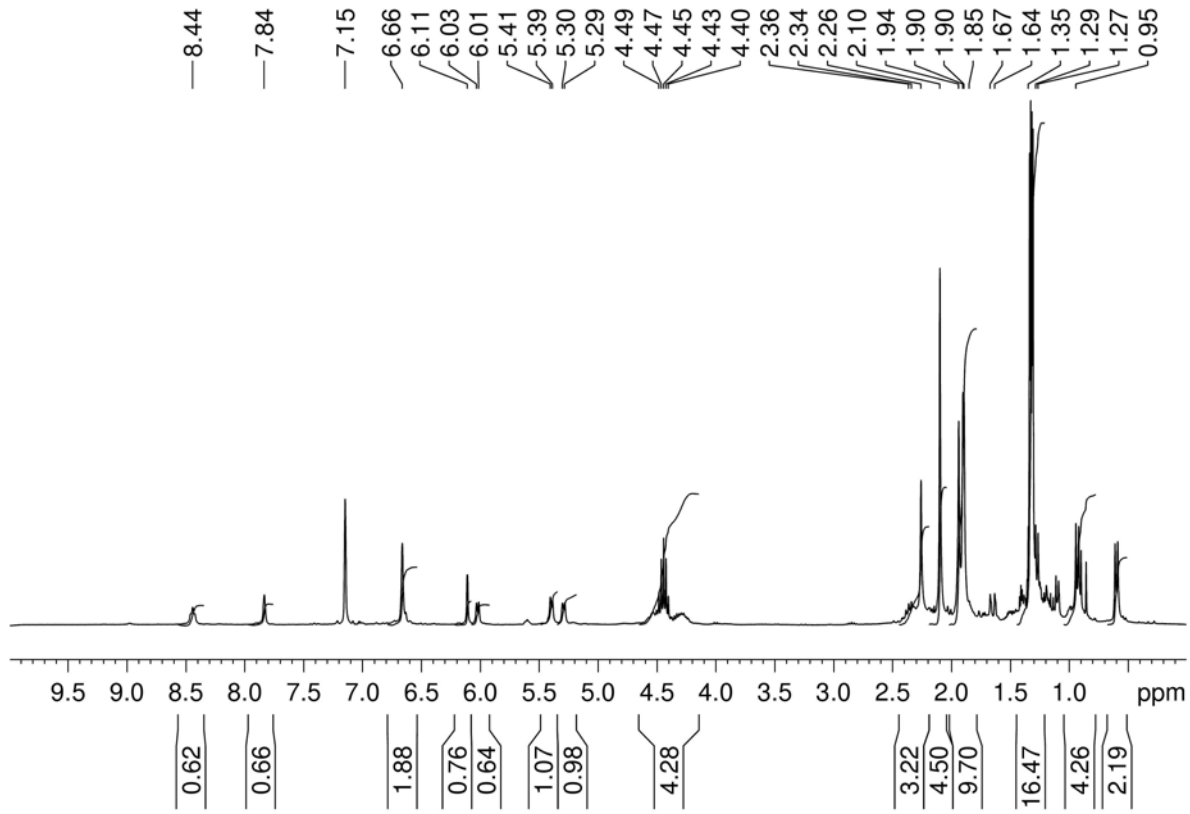

Figure 3. ^{1}H NMR spectrum of complex **RuCymP**

Additional NMR experiments by ^{1}H (Figure 3), COSY (Figure A6) and ^{1}H-^{31}P HSQC (Figure A5) allowed to provide more information on the structure. From ^{1}H NMR, the NHC and the cymene ligand are still bound to Ru. Note in particular that the four protons of the p-cymene ring have become unequivalent, and appear as three doublets at 5.29, 5.39 and 6.02 ppm and a triplet at 8.44 ppm. The attribution of the signal was allowed by the COSY experiment, which shows a clear coupling with the signal at 5.29 ppm. ^{1}H-^{31}P HSQC shows that the

signal at 4.6 ppm in F2 (phosphorus) displays a correlation with the triplet at 8.44 ppm of the cymene ligand, which suggests that these two nuclei are in a close environment. We therefore have a complex which is still bearing both NHC and p-cymene ligands, and which has, in addition, a PMe_3 ligand which shows a correlation with one of the aromatic protons of the p-cymene ligand. However, it is still unclear why the signal at 8.44 ppm in ^1H NMR is a triplet, as we have a coupling phenomenon with only one PMe_3 and one ^1H, which would rather lead to a doublet of doublets. Also, it is difficult to tell whether we have a true $20e^-$ complex (which would be possible if the Ru nuclei use vacant f orbitals) or whether the p-cymene ligand could be in a particular η^4 coordination mode. The first hypothesis is however the most probable, as an η^4-coordination of the p-cymene would lead to a loss of aromaticity, which doesn't seem to happen considering the chemical shifts in ^1H NMR (between 5.3 and 8.4 ppm). NMR alone will not be able to solve the problem, and single crystal X-ray analysis would be necessary to confirm the structure of the complex.

II-3 Grafting of $[RuCl_2(p\text{-cymene})]_2$ on a 1-propyl-3-mesityl-imidazolium functionalized hybrid material.

3.1 Grafting of $[RuCl_2(p\text{-cymene})]_2$ in THF

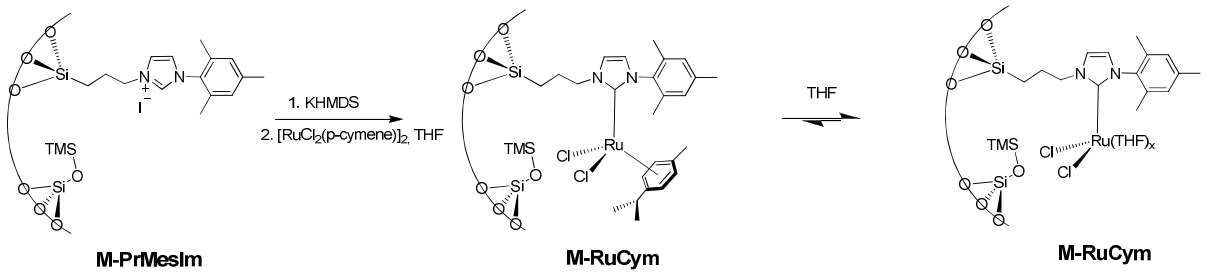

M-PrMesIm **M-RuCym** **M-RuCym**

Using these optimised conditions (0.6 equiv. of the Ru precursor, THF as solvent), the formation of heterogeneous equivalent system **M-RuCym** was studied, using imidazolium-fonctionnalized mesostructured silica prepared via a direct synthesis pathway using a templating route instead of molecular imidazolium compounds. The imidazolium material was obtained by the treatment of a 3-Iodopropyl-functionnalized material with 1-mesitylimidazole and further passivation of the surface with Me_3SiBr as previously reported.[16] Upon a one-pot reaction using 1.2 equiv. of potassium hexamethyldisilazide (KHMDS) and 0.6 equiv.

$[RuCl_2(p\text{-cymene})]_2$ with respect to imidazolium units (the amount of functionalities is determined by nitrogen elemental analysis), the solid turned orange. Elemental analyses on the resulting solid gave ruthenium, nitrogen and chlorine contents of 1.83%$_{wt}$, 0.83%$_{wt}$ and 1.5%$_{wt}$, respectively. In 1g of material, this corresponds to 0.181 mmol Ru, 0.593 mmol N or 0.297 mmol NHC (two nitrogen per NHC) and 0.423 mmol Cl. We therefore have a Cl/Ru ratio of 2.34 and a Ru/NHC ratio of 0.61. These values are consistent with the formation of 60% of Cl_2Ru-NHC surface complexes, leaving 40% of free imidazolium (not coordinated to Ru). The excess of chlorine compared to ruthenium can be explained by the use of HCl during the hydrolysis of the imidazolium material. The ^{29}Si cross-polarization magic-angle-spinning (CPMAS) solid-state NMR spectra confirmed that the Si-C bond remained intact during the various synthetic steps as evidenced by the peak at -68 ppm, corresponding to T_3 sites, as observed in the starting material (See Figure A8).

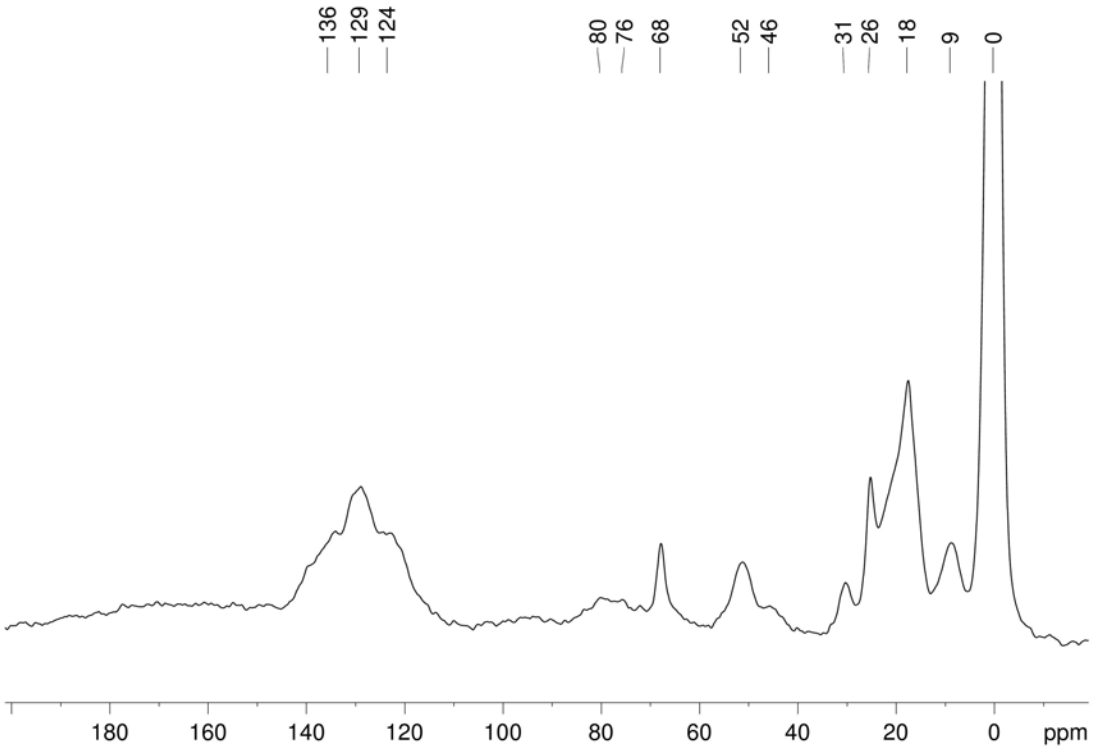

Figure 4. ^{13}C CPMAS NMR spectrum of **M-Ru$_{Cym}$**

The ^{13}C CPMAS solid-state NMR spectrum showed 8 peaks at 0, 9, 18, 26, 31, 68, 80 and 129 ppm (see Figure 4). Beside some of the peaks associated with the organic

fragment of the imidazolium material {surface Me_3Si (0 ppm), the CH_2 in α–position of silicon (9 ppm), the methyl groups of the mesityl and of the isopropyl unit (18 ppm) and the aromatic carbons (129 ppm)}, extra signals appeared: the peak at 80 ppm was unambiguously attributed to the aromatic carbon atoms of the para-cymene ligand coordinated to ruthenium and these at 26 and 68 ppm to THF coordinated to Ru (extended washing and drying under high vacuum did not affect the intensity of these peaks, excluding the presence of physisorbed THF). The weak signals at 31 ppm could be attributed to the isopropyl methyl group of the cymene ligand, but also to THF in a different environment. Note also that additional washings after KHMDS treatment did not influence the grafting (same NMR spectra, same Ru loading). Further analysis of the solvent residue of grafting by GC and GC-MS showed the presence of para-cymene (0.25 equiv per Ru), thus implying its replacement by THF (25% after 3 h of grafting).

3.2 Grafting of $[RuCl_2(p\text{-cymene})]_2$ in toluene

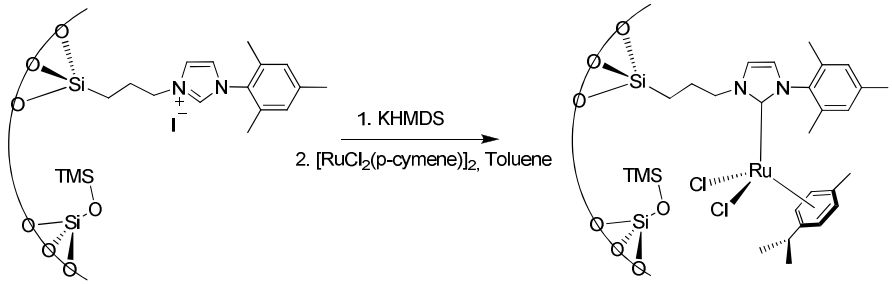

In order to be able to form a single Ru-NHC site at the surface of our materials, the grafting reaction was tested with toluene as a solvent, supposing that toluene and p-cymene should not easily exchange. Apart from the much poorer solubility of $[RuCl_2(p\text{-cymene})]_2$ in toluene than in THF, this experiment was carried out in the exact same conditions as the previous reaction in THF. The solid obtained after reaction, **M-RuCym-Tol**, is darker than the one obtained in THF, but this phenomenon was not due to a higher loading of metal, as confirmed by elemental analysis which gave ruthenium and nitrogen loadings of 1.77% and 0.85% (1.83 and 0.83 when done in THF). As in the case of THF, this corresponds to a grafting ratio of 60%, therefore leaving 40% of unreacted imidazolium. By ^{13}C CPMAS solid-

state NMR, the presence of the p-cymene ligand is confirmed again by the presence of the broad signal at 80 ppm and the sharper one at 30 ppm (both being more intense than in the previous case). The absence of exchange between toluene and p-cymene was confirmed by analysing the solvent residue of grafting by GC and no p-cymene is detected. These results therefore confirm that the grafting reaction in toluene is a convenient way to selectively form a surface Ru(NHC)(p-cymene) complex. This results was surprising to us, as the same reaction performed with the model molecular imidazolium led to a very unselective reaction with several unidentified by-products. This is another example of a very different reactivity between a molecular species and a surface species.

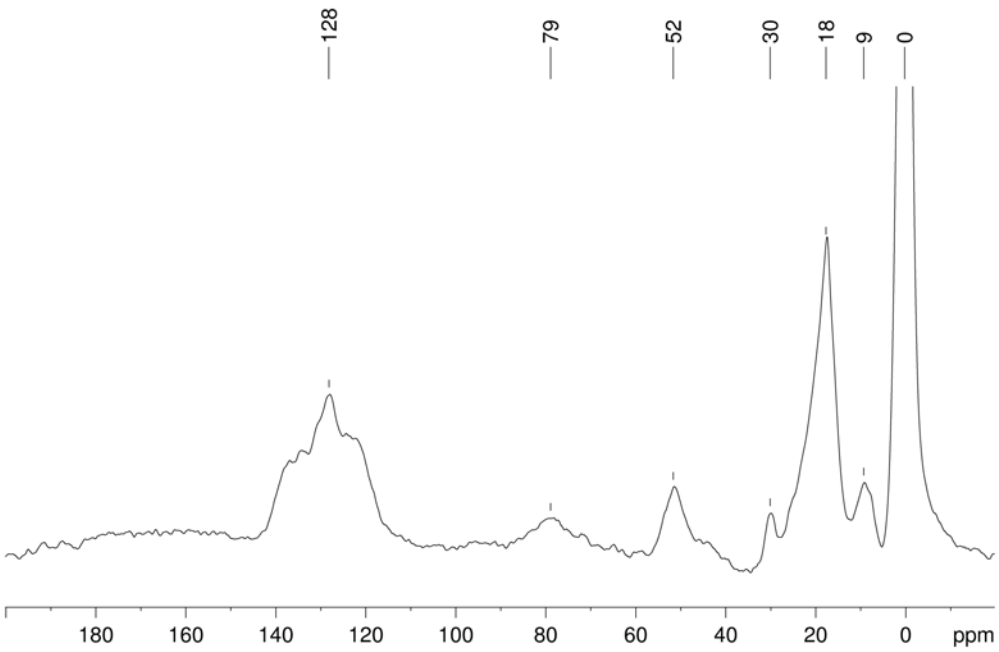

Figure 5. ^{13}C CPMAS spectrum of **M-RuCym-Tol**

3.3 Study of the exchange between p-cymene and THF

Evidence for the exchange reaction between p-cymene and THF led us to further react the material with THF at 40°C for 4 hours. Characterization of this material by ^{13}C CPMAS NMR after drying in high vacuum shows an important decrease of the signals at 31 and 80 ppm, in agreement with the loss of the para-cymene ligand, while two signals at 26 and 68 ppm associated to THF increased in intensity. (see Figure A13) In fact, they

disappear upon treatment of the materials with THF-d^8 due to the absence of proton and thus to inefficient cross-polarisation.(see Figure A14)

3.4 Formation of the Ru-NHC material from a ^{13}C enriched imidazolium in carbenic position

In order to determine whether Ru is coordinated to the NHC system or not, the grafting step was investigated with a ^{13}C-enriched imidazolium material (30% in position 2, natural abundance elsewhere).[†] In this case, a new signal appeared at 173 ppm in CP-MAS solid state NMR, which is similar to that found in the corresponding molecular complex **RuCym** (172.9 ppm), thus fully confirming the formation of Ru-NHC bond (Figure 6). Note however, that in this case, the signal of coordinated THF at 26 and 68 ppm were present, while no signal associated with the para-cymene ligand at 80 ppm was found, in agreement with a more important exchange of the p-cymene with THF. Overall, this clearly shows that **M-RuCym** is a well-defined system containing NHC-$RuCl_2$ fragments stabilized by extra ligands, in particular THF and possibly the surface.

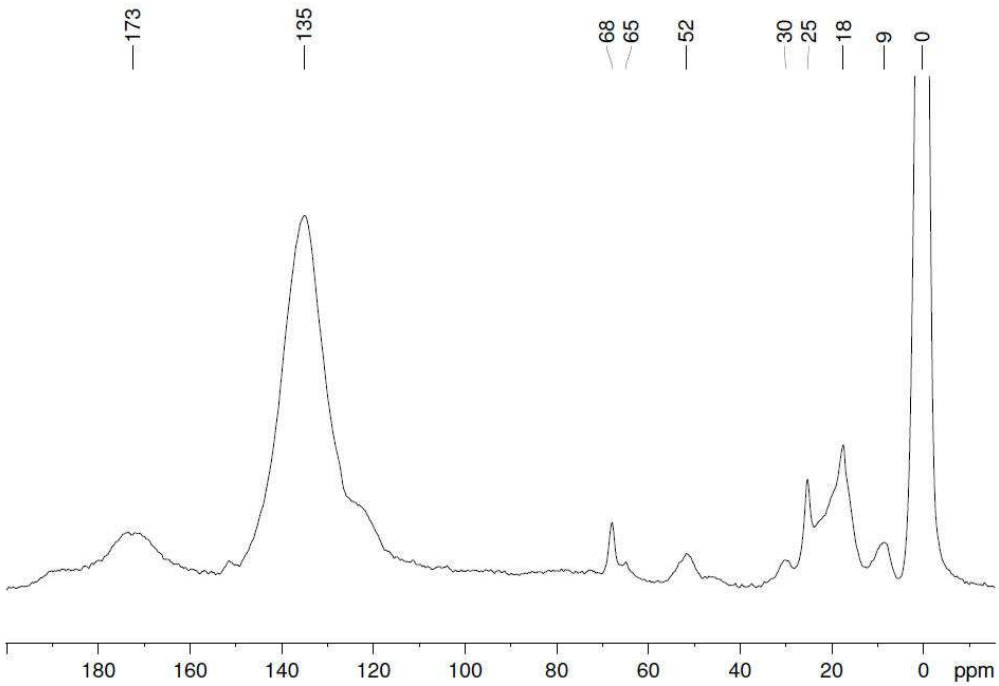

Figure 6. ^{13}C CPMAS NMR spectrum of **M-RuCym***

[†] This product was prepared by T. Maishal

II-4 Reaction of the Ru-NHC-cymene materials with phosphines

4.1 Reaction with trimethylphosphine

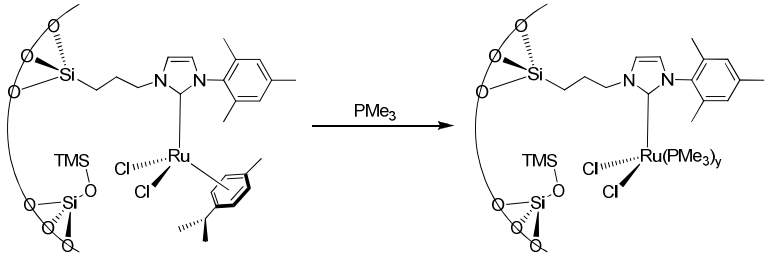

Having obtained well-defined Ru(NHC) surface species, the next objective was to obtain more electron-enriched species for catalytic purposes by replacing labile ligands with phosphine ligands. Therefore, the reactivity of Ru(NHC)(L) species (L being p-cymene or THF) with phosphines was studied. The addition of PMe_3 onto the heterogeneous catalytic materials **M-RuCym** and further removal of the excess of the phosphine under high vacuum for 8h leads to the light yellow material **M-RuPMe$_3$**. While a precise characterisation of **M-RuPMe$_3$** has not been possible so far, ^{31}P MAS NMR showed the presence of two major narrow peaks at 1 and -11 ppm, which are consistent with PMe_3 coordinated to ruthenium (See Figure 7). Additionally, a very weak broad signal at 48 ppm could also be observed, and was attributed to a pentavalent phosphorus, probably resulting from side reaction with the surface leading to a phosphonium or phosphine oxide species.[17] Moreover, the ^{13}C-labelled sample **M-RuP*** displayed a peak at 172 ppm in CPMAS ^{13}C NMR, consistent with a NHC bonded to Ru (see Figure 8). While it is not possible to give an exact structure for the surface complex(es), it is clear that it corresponds to Ru complex(es) bound to one NHC and having PMe_3 ligands. There are different possible surface species that could explain the 31P NMR spectrum. The two peaks could be explained by the presence of two different surface species, which could be isomers (cis or trans) or two species in equilibrium involving the coordination of surface siloxane bridges. Another explanation would be that these two peaks

correspond to two unequivalent phosphorus nuclei on the same ruthenium center (See the possible structures in Scheme 1).

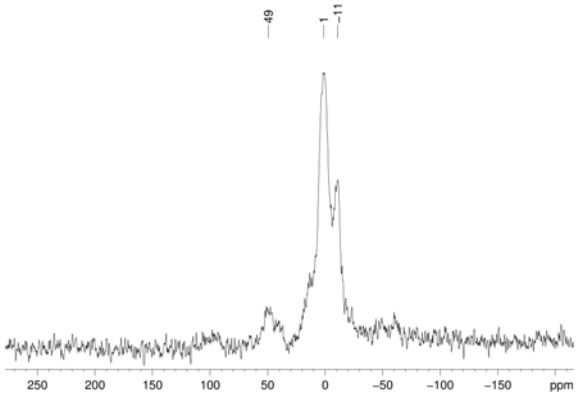

Figure 7. ^{31}P HPDEC NMR spectrum of material **M-RuPMe$_3$**

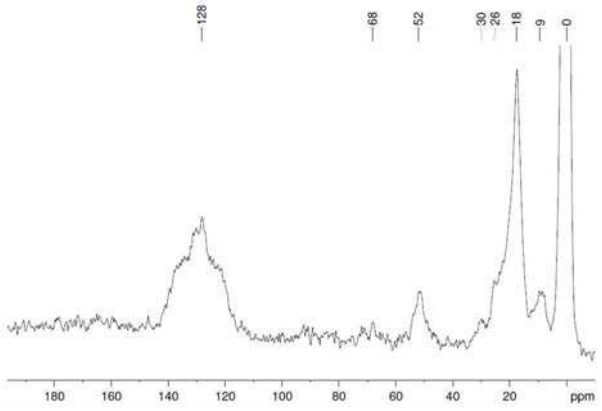

Figure 8. ^{13}C NMR spectrum of material **M-RuPMe$_3$**

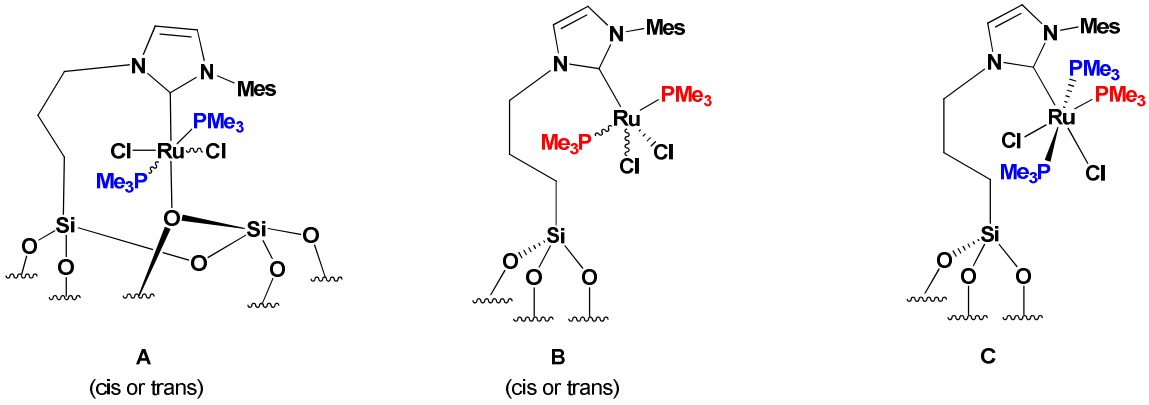

Scheme 1. Hypotheses for the surface species formed in **M-RuPMe$_3$**

4.2 Reaction with diphenylphosphinoethane

The reaction of dppe with material **M-RuCym** in warm THF led to the light yellow **M-Rudppe**. The acquisition of ^{31}P solid-state NMR spectra was difficult, as the signal detected is very low. It was therefore needed to use the faster but non-quantitative CPMAS experiments instead of HPDEC. It shows two main sets of signals (see Figure A12), the first one constituted of two peaks at 64 and 81 ppm corresponding to pentavalent phosphine species showing spinning side bands at 116 and 134 ppm. The second set is constituted of

two peaks at 28 and -17 ppm. The peak at -17 ppm is close to free dppe (-12 ppm) and could correspond either to physisorbed dppe, or to one side of a dppe ligand, which other side is coordinated on ruthenium. The peak at 28 ppm is in the range of coordinated dppe (as a comparison, trans-$RuCl_2(dppe)_2$ shows a single signal at 44.9 ppm). Elemental analysis in Ru and P are respectively 1.02% and 0.20%, which gives a dppe/Ru ratio of only 0.32, meaning that only 32% of the Ru species are bearing a dppe ligand. The case of dppe is therefore more complicated, as the coordination of the phosphine seems to be much more complicated. Indeed, dppe is less electron-rich than PMe_3 and it needs two coordination sites, which might significantly decrease the kinetic of coordination.

II-5 Catalytic performances of the Ru-NHC based materials

5.1 Hydrogenation of CO_2 in presence of pyrrolidine

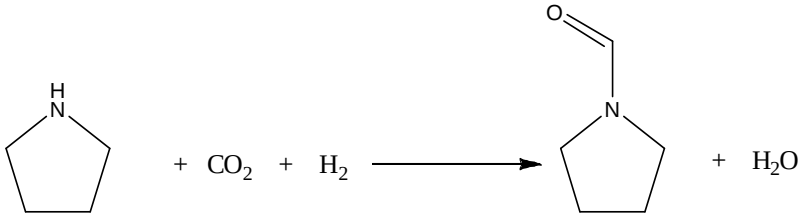

All our catalytic materials were tested in the hydrogenation of carbon dioxide in presence of pyrrolidine, in a stainless steel autoclave at 130 bar and 100°C using a stoichiometric H_2/CO_2 mixture, and their performances were compared under identical conditions with the best homogeneous systems based on Ru, $RuCl_2(dppe)_2$ and $RuCl_2(PMe_3)_4$.[‡] In order to have a precise idea of the specific catalytic activity of each system, it was chosen to work in such conditions that full conversion is not reached.

First, using **M-RuCym** only a low TON of 150 in 5 h could be achieved. However, the introduction of phosphine ligands coordinated to Ru greatly improved the catalytic performances, increasing the TON of 2770 for **M-RuPMe$_3$**. This is to be compared to $RuCl_2(PMe_3)_4$, one of the best homogeneous catalysts, which allow reaching 5300 TON.

[‡] Being limited in terms of equipments, we could not repeat typical experiments of the literature which require higher pressure apparatus (210 bar) and a CO_2 compressor

Table 1. Catalytic hydrogenation of CO_2 in presence of pyrrolidine					
Entry	**Catalyst**	**Substrate/Ru ratio**	**P(bar)**	**t (h)**	**TON**
1	**M-RuCym**	20000	130	5	150
2	$RuCl_2(PMe_3)_4$	20000	130	5	5300
3	**M-RuPMe$_3$**	20000	130	5	2770
4	$RuCl_2(dppe)_2$	20000	130	5	12100
5	**M-Rudppe**	20000	130	5	5110 (15960[a])

a This TON is calculated considering only Ru sites bearing phosphines

These results are quite encouraging since previously developed heterogeneous catalysts displayed performances far below those of homogeneous catalysts (typically one order of magnitude).[12] Introducing bidendate ligands, further improved the catalytic performances to 5110 TON for **M-Rudppe$_{-30}$** , which is a little lower than the corresponding molecular $RuCl_2(dppe)_2$, for which 12100 TON can be reached in 5 h. Note however that the TON of 5110 is calculated based on the total amount of Ru, while only 32% of Ru is coordinated to dppe according to elemental analyses, so that 15960 TON can be achieved by Ru-dppe complex, assuming that the other Ru centers are an order of magnitude less active as shown previously. These results are therefore very encouraging, in particular since higher TON are typically achieved using higher pressures of CO_2, not available during our study.

However, an ICP analysis was performed on the liquid phase of the catalytic reaction at 100℃ with **M-RuPMe$_3$** as catalyst, and around 50% of the metal had leached in the solution. This is not surprising, considering the harsh conditions of reaction: high pressure, high temperature and presence of hydrogen and water. Furthermore, Ru(NHC) complexes are known to be unstable in the presence of hydrogen due to a possible reductive elimination of the NHC with an hydride. In order to have a better stability, the use of the more stable bis-NHC complexes would be an interesting solution.

5.2 Kharasch addition of CCl_4 on styrene.

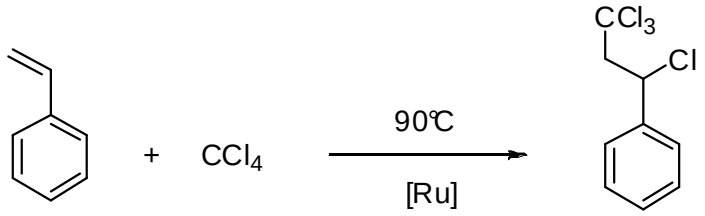

As reported in the literature, Ru(NHC)(p-cymene) complexes can be used to catalyse Kharasch addition reactions.[15] The Ru-NHC catalytic materials were investigated in the Kharasch addition of CCl_4 on styrene. All reactions were performed in toluene at 90℃, by monitoring the conversion and selectivity by GC using undecane as an internal standard. Both **RuCym** and **M-RuCym** were tested. The homogeneous catalyst **RuCym** shows 79% selectivity for the Kharasch product with 66% conversion in 24 hours at 90℃, which is close to the already reported results with bis-mesityl imidazolium (48% selectivity, 70% conversion) and the bis-cyclohexyl imidazolium (62% selectivity, 88% conversion). Yet, it is still below the 3,4-dichloro-1,3-bis-mesityl-imidazolium ligand which gives 97% selectivity and 100% conversion. This typically shows the large influence of substituents at the imidazolium ring in stabilizing the systems. Under the same conditions, **M-RuCym** showed very close performances to **RuCym** with 72% selectivity and 55% conversion at 24 hours. Note here that no metal leaching was observed. Overall, it was shown that it should be in principle possible to develop highly efficient heterogeneous catalysts for the Karasch reaction, provided that a fine tuning of the ligand is investigated.

Table 2. Kharasch addition of CCl_4 on Styrene

entry	catalyst	Substrate/Ru	time (h)	selectivity (%)	conversion (%)
1	M-RuCym	900	24	2,7	56,3
2[(a)]	RuCym	300	9	73	95,7
3	M-RuCym	300	24	71,8	55,4
4	RuCym	300	24	78,8	66,4

a) addition of traces of KHMDS

When increasing the Styrene/Ru ratio to 900, the selectivity drops down to less than 5% to the Kharrasch product and NMR showed the presence of polystyrene. This behaviour was suspected to be originated from traces of unwashed KHMDS from the material that could change the reaction parameters (KHMDS as a strong base could initiate radicals more quickly than ruthenium and therefore add perturbations in the system). It was therefore tried to add some KHMDS in the reaction mixture when doing catalytic tests with the molecular **RuCym** and the results show that KHMDS has indeed an influence on the catalytic tests: we observe no deactivation of the catalyst, which allows 100% conversion after 3 hours. The amount of KHMDS added was not controlled, but this phenomenon might be interesting to study if trying to optimise the reaction conditions.

II-6 Conclusion

The use of imidazolium-functionnalized hybrid mesostructured silica materials for the generation of Ru-NHC materials bearing either para-cymene or phosphine ligands was achieved successfully. The reaction of $[RuCl_2(p\text{-cymene})]_2$ with a deprotonated propyl-mesityl-imidazolium material led to the selective formation of Ru(NHC)(p-cymene) surface complexes with toluene as a solvent. When the reaction was performed in THF, two surface species were formed: Ru(NHC)(p-cymene) as the primary product which is then transformed to $Ru(NHC)(THF)_x$ complexes. These first materials were poorly active in the hydrogenation of CO_2 in presence of pyrrolidine, but they showed interesting performances and stability in the Kharrasch addition of CCl_4 on styrene. These materials were then reacted with phosphine ligands, which dramatically enhanced their activity in the hydrogenation of CO_2. However, the instability of these mono-NHC complexes has been observed, which led us to study a new method of generating diverse imidazolium functionalities at the surface of hybrid mesoporous materials to form more stable Ru-NHC catalytic materials.

II-7 Experimental Section

General procedure. All experiments were carried out using either Schlenck techniques, vacuum line or a glovebox, with freshly distilled, degassed solvents. Passivated imidazolium materials[13] and $[RuCl_2(p\text{-cymene})]_2$[18] were synthesized according to literature procedures. 1-mesityl-3-(3-(triisopropoxysilyl)propyl)-imidazolium iodide was synthesized from 3-iodopropyltriisopropoxylsilane and mesitylimidazole, following literature procedures. Trimethylphosphine was purchased from Strem. KHMDS solution was purchased from Aldrich. ^{1}H and ^{13}C solution spectra were recorded on a Bruker Avance DRX 300 (300MHz). ^{1}H, ^{13}C, ^{31}P and ^{29}Si solid state NMR spectra were recorded on a Bruker Avance 500 (500 MHz) and a Bruker DSX 300 (300 MHz). ^{1}H solid state spectra were recorded using Magic Angle Spinning (MAS) at 10 kHz. ^{13}C solid state spectra were recorded using Cross Polarization with D1 of 2s, p15 of 2 ms, around 30000 scans and MAS at 10 kHz . ^{31}P solid state spectra were recorded with HPDEC direct detection experiments, D1 of 30s and MAS at 10 kHz. ^{29}Si solid state spectra were recorded using both Cross Polarization and MAS at 5 kHz. Elemental analysis were performed at the “Mikroanalytisches Labor Pascher”, Remagen, Germany.

Preparation of (p-cymene)$RuCl_2$[1-mesityl-3-(3-(triisopropoxysilyl)propyl)-imidazol-2-ylidene]Cl_2, RuCym. To a solution of 1-mesityl-3-(3-(triisopropoxysilyl)propyl)-imidazolium iodide (705 mg, 1.26 mmol) in 15 mL of THF was added 2.5 mL of a 0.5 M solution of KHMDS in toluene. After stirring for 30 min, all volatiles were evaporated in vacuo, and the residue extracted with pentane and filtered over a glass filter. After evaporation of the solution to dryness and addition of THF (15 mL) to the residue, $[RuCl_2(p\text{-cymene})]_2$ (350 mg, 0.57 mmol, 0.45 equiv.) was added, and the reaction mixture was stirred for 1 h. After evaporation, the residue was washed with hexane to afford complex **RuCym** (498mg, 59%). ^{1}H NMR (C_6D_6, 300 MHz): 6.70 (s, 2H), 6.57(d, 1H), 6.03 (d,1H), 5.05(d, 2H), 4.64 (d, 2H), 4.60 (m, 2H), 4.33 (m, 3H), 2.92 (m, 1H), 2.15 (m, 2H), 2.10 (s, 3H), 2.01 (s, 6H), 1.72 (s, 3H), 1.25 (d, 18H), 1.06 (d, 6H), 0.90 (m, 2H). $^{13}C\{^{1}H\}$ NMR (C_6D_6, 300 MHz): 172.9, 138.5,

136.6, 129.0, 128.4, 123.1, 122.2, 105.0, 93.8, 86.1, 85.7, 64.8, 55.0, 30.2, 26.7, 25.4, 22.1, 20.7, 18.7, 17.7, 8.9. Elemental Analysis Calculated for $C_{34}H_{55}Cl_2N_2O_3RuSi$ (mol wt 739,87): C, 55.19; H, 7.49; Cl, 9.58; N, 3.79; Ru, 13.66; Si, 3.80. Found: C, 54.03; H, 7.13; Cl, 9.91; N, 4.02; Ru, 14.20; Si, 3.73.

Representative Procedure for the Preparation of M-RuCym. To a suspension of 1-propyl-3-mesityl-imidazolium iodide functionnalized material having a passivated surface (250 mg), **M-PrMesIm**, in THF (5 mL), 0.17 mL of a 0.5 M solution of KHMDS in toluene was added dropwise. After 30 min, a mixture of 25 mg of $[RuCl_2(p\text{-cymene})]_2$ in 15 mL THF was added, and the resulting suspension stirred for 3 h. The solid was filtered, and successively washed three times with 15 mL THF and twice with 10 mL diethyl ether. Drying under high vacuum (10^{-5} mbar) for 1 h afforded an orange powder, **M-RuCym**. ^{1}H MAS solid-state NMR (500 MHz,): 0.2, 2.3, 7.1. ^{13}C CPMAS solid-state NMR (125.7 MHz,): 129, 80, 68, 52, 31, 26, 18, 9, 0. CP/MAS ^{29}Si NMR: -61 (T2), -68 (T3), -101 (Q3), -111 (Q4).

Preparation of the carbon-13 labelled M-RuCym*. This material was synthesized using the same procedure as described for **M-RuCym**, using a ^{13}C-labelled imidazolium material. ^{1}H MAS solid-state NMR (500 MHz) : 0.2, 2.3, 7.1. ^{13}C CPMAS solid-state NMR (125.7 MHz, p15 = 5ms, 100000 scans): 173, 135, 68, 65, 52, 31, 26, 18, 9, 0.

Preparation of M-RuPMe$_3$. To 150mg of **M-RuCym** in a 10 mL Schlenk equipped with Teflon valve (Young) was added by distillation PMe_3 so as to obtain a wet solid. After 1 h, the material was then dried under high vacuum for 8 h to yield **M-RuPMe$_3$** as a light yellow powder. ^{1}H MAS solid-state NMR (500 MHz): 0.1, 1.5, 6.9. ^{13}C CPMAS solid-state NMR (125.7 MHz): 128, 52, 30, 18, 9, 0.

Preparation of material M-RuPMe$_3$*. This material was prepared as described for **M-RuP**, using the ^{13}C-labelled material **M-RuCym*** in place of **M-RuCym**.^{1}H MAS solid-state NMR with spinning at 10kHz (500Mhz): 0.1, 1.5, 6.9, ^{13}C CPMAS solid-state NMR with spinning at 10kHz (125.7 Mhz): 172, 135, 68, 65, 52, 31, 26, 18, 9, 0.

Preparation of M-Rudppe. To 200mg of **M-RuCym** in a double-schlenk was added a solution of dppe (20 eq) in 5 mL of THF and the suspension was heated up to 40℃ for 3 hours. It was then filtered and washed three times with 5mL THF and once with 5 mL Et_2O. It was then dried dried under high vacuum for 1 h to yield **M-Rudppe** as a light yellow powder. ^{1}H MAS solid-state NMR (500 MHz): 0.0, 2.0, 7.0. ^{31}P CPMAS solid-state NMR : 134,116, 81, 64, 28, -17.

Catalytic tests for the hydrogenation of CO_2 in the presence of pyrrolidine. Hydrogenation of CO_2 to 1-formylpyrrolidine. Representative procedure. A 300mL-autoclave was loaded with 3.6 µmol of catalyst and 6.0 mL pyrrolidine under an inert atmosphere. The autoclave was then pressurized at room temperature with 50 bar CO_2 and 50 bar H_2, before being heated up to 100℃. After 5 h, the apparatus was cooled down to around -50 ℃ (cold bath of ethanol and liquid nitrogen) and depressurized before analysing the liquid residue by gas chromatography.

Catalytic tests for the Kharrasch addition of CCl_4 on styrene. A 10 mL Schlenck-tube was charged with 8.5 µmol of catalyst, 1.5 mL of toluene, 3.7 mmol of CCl_4, 2.5 mmol of Styrene and 0.1 mL of undecane as an internal standard. The reaction mixture was heated to 90℃ for 24 hours. The reaction was followed by gas chromatography on a HP5 column.

Calibration data of pyrrolidine and 1-formylpyrrolidine by Gas chromatography.

All GC measurement were performed on a HP6890 equipped with a 30 m HP5-Ultrainert column. Both pyrrolidine and 1-formylpyrrolidine were calibrated with respect to undecane which was used as an internal standard.

Temperature program: 80℃ for 3 min, followed by a temperature ramp of 15℃/min up to 200℃ and 12 min at 200℃.

Retention times: Pyrrolidine : 5.12 min, 1-Formylpyrrolidine : 9.04 min, Undecane : 9.12 min

Quantification of the metal leaching

The quantification of ruthenium leached in solution was performed by ICP-AES on a Jobin-Yvon JY 38+. For a typical analysis, the residue after reaction was filtered, around 1 g was taken as sample and all volatiles were removed in vacuo. The residue was then dissolved in 10 mL of a 5% solution of HNO_3. The apparatus was calibrated with standard ruthenium solutions (0, 1, 2, 5 and 10 mg/L) before analysis.

II-8 References

[1] *IPCC, 2007: Climate Change 2007: Synthesis Report. Contribution of Working Groups I, II and III to the Fourth Assessment Report of the Intergovernmental Panel on Climate Change [Core Writing Team, Pachauri, R.K and Reisinger, A. (eds.)]. IPCC, Geneva, Switzerland, 104 pp.*

[2] G. A. Olah; A. Goeppert; G. K. S. Prakash *Beyond Oil and Gas: The Methanol Economy*; Wiley-VCH, 2009.

[3] P. Haynes; L. H. Slaugh; J. F. Kohnle *Tetrahedron Lett.* **1970**, 365-368.

[4] Y. Inoue; H. Izumida; Y. Sasaki; H. Hashimoto *Chem. Lett.* **1976**, 863-864.

[5] P. G. Jessop; T. Ikariya; R. Noyori *Nature* **1994**, *368*, 231-233.

[6] P. G. Jessop; Y. Hsiao; T. Ikariya; R. Noyori *J. Am. Chem. Soc.* **1994**, *116*, 8851-8852.

[7] P. G. Jessop; Y. Hsiao; T. Ikariya; R. Noyori *J. Chem. Soc.-Chem. Commun.* **1995**, 707-708.

[8] O. Krocher; R. A. Koppel; A. Baiker *Chem. Commun.* **1997**, 453-454.

[9] R. Tanaka; M. Yamashita; K. Nozaki *J. Am. Chem. Soc.* **2009**, *131*, 14168-14169.

[10] Y. P. Zhang; J. H. Fei; Y. M. Yu; X. M. Zheng *Catal. Commun.* **2004**, *5*, 643-646.

[11] L. Schmid; O. Krocher; R. A. Koppel; A. Baiker *Microp. Mesop. Mat.* **2000**, *35-6*, 181-193.

[12] M. Rohr; M. Gunther; F. Jutz; J. D. Grunwaldt; H. Emerich; W. van Beek; A. Baiker *Appl. Catal. A-Gen.* **2005**, *296*, 238-250.

[13] I. Karame; M. Boualleg; J. M. Camus; T. K. Maishal; J. Alauzun; J. M. Basset; C. Coperet; R. J. P. Corriu; E. Jeanneau; A. Mehdi; C. Reye; L. Veyre; C. Thieuleux *Chem.-Eur. J.* **2009**, *15*, 11820-11823.

[14] T. K. Maishal; J. M. Basset; M. Boualleg; C. Coperet; L. Veyre; C. Thieuleux *Dalton Trans.* **2009**, 6956-6959.

[15] A. Richel; S. Delfosse; C. Cremasco; L. Delaude; A. Demonceau; A. F. Noels *Tetrahedron Lett.* **2003**, *44*, 6011-6015.

[16] J. Alauzun; A. Mehdi; C. Reye; R. Corriu *New J. Chem.* **2007**, *31*, 911-915.

[17] J. Sommer; Y. Yang; D. Rambow; J. Blümel *Inorg. Chem.* **2004**, *43*, 7561-7563.

[18] M. A. Bennett; A. K. Smith *J. Chem. Soc. Dalton Trans.* **1974**, 233-241.

II-9 Appendix

Characterization of Ru-NHC complexes and materials

Ru_{Cym}:

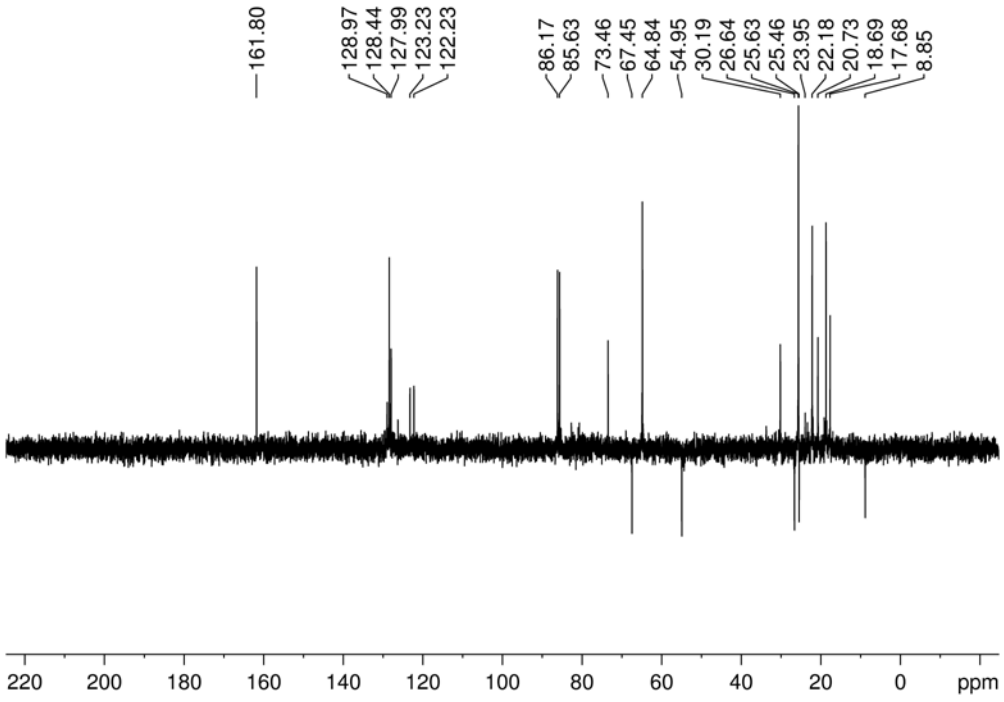

Figure A1. DEPT NMR spectrum of **RuCym**

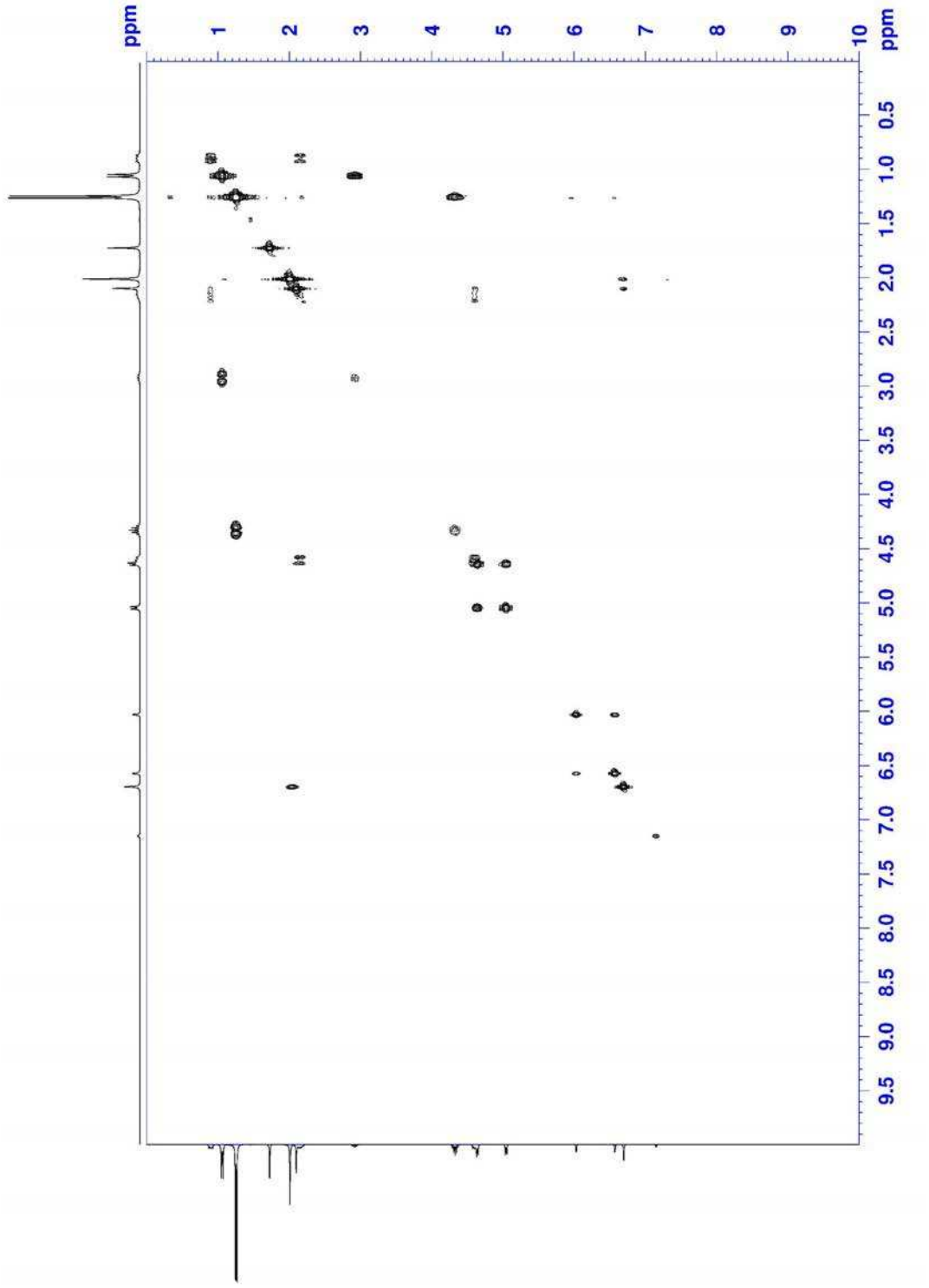

Figure A2. COSY NMR spectrum of **RuCym**

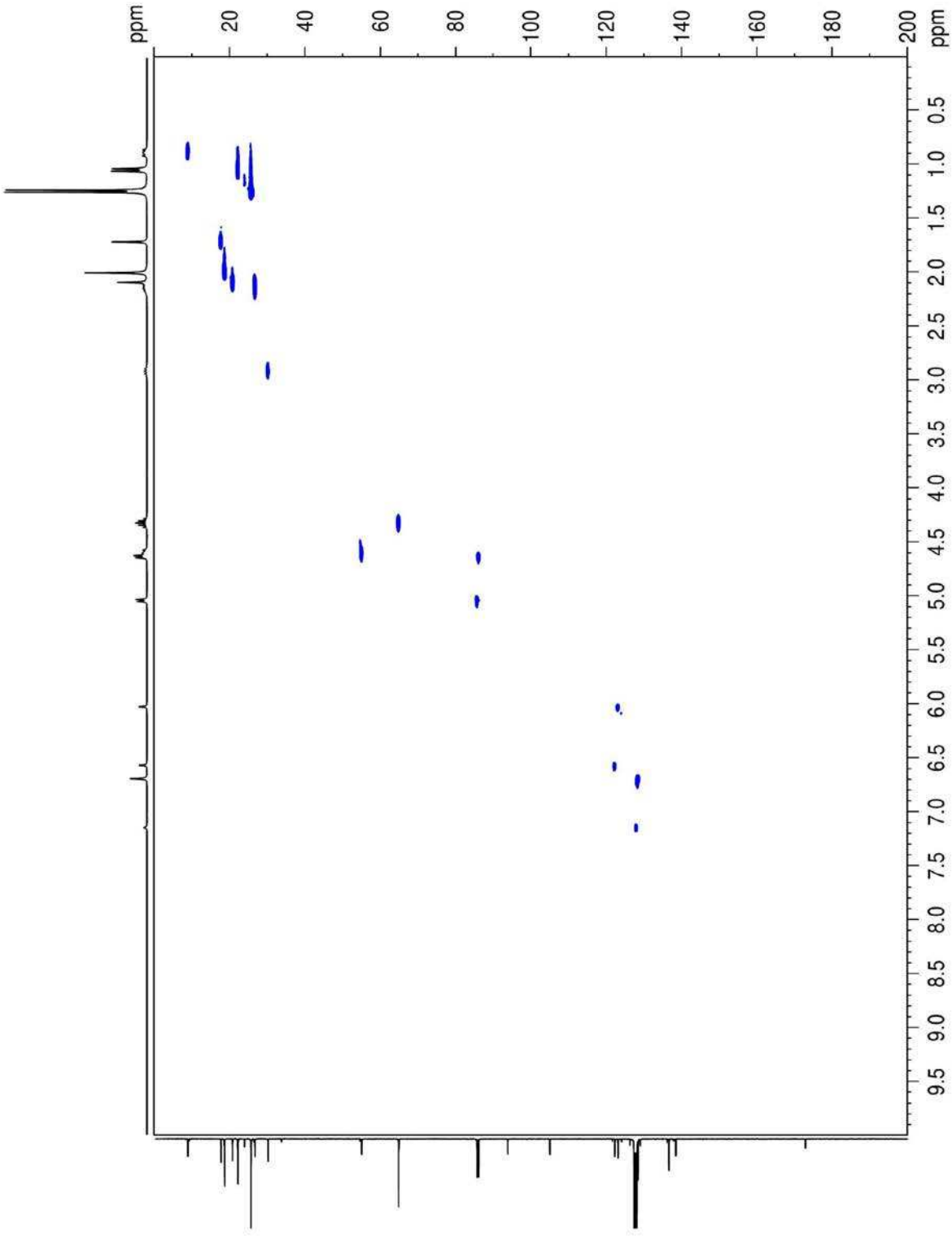

Figure A3. ^{1}H-^{13}C HSQC NMR spectrum of **RuCym**

RuCymP

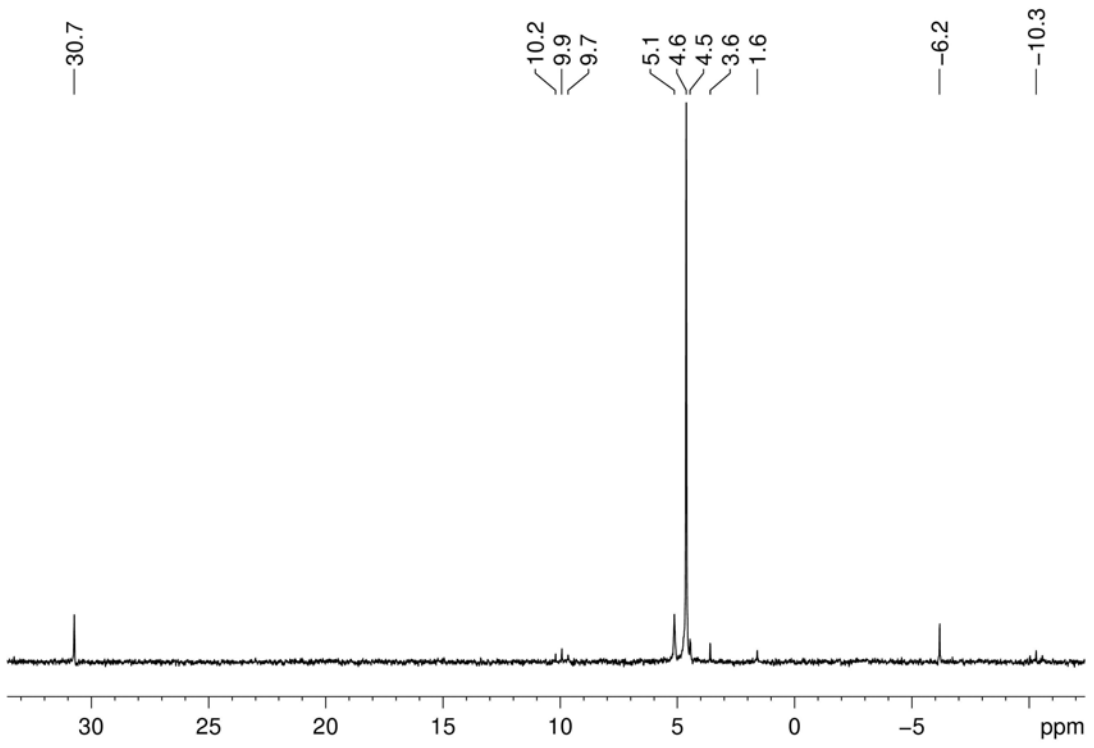

Figure A4. ^{31}P NMR spectrum of **RuCymP**

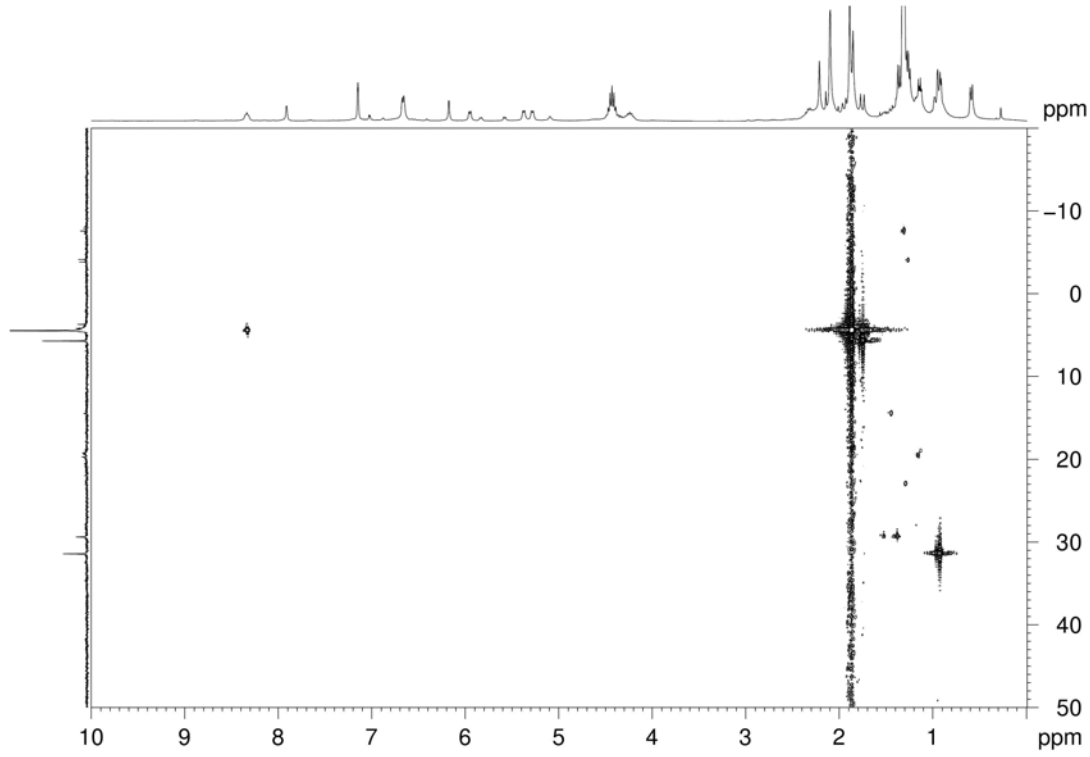

Figure A5. ^{1}H-^{31}P HSQC NMR spectrum of **RuCymP**

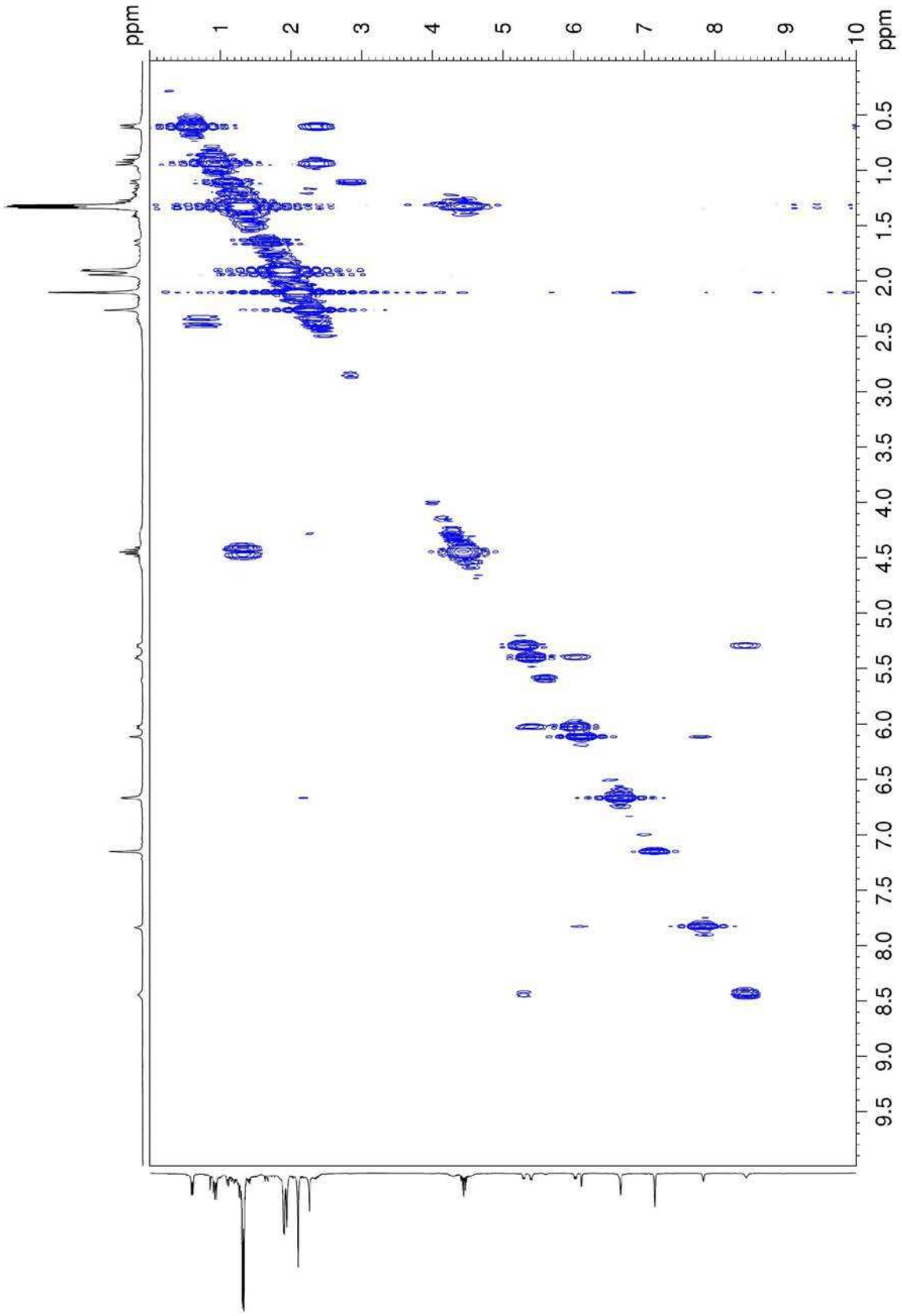

Figure A6. COSY NMR spectrum of **RuCymP**

M-Ru$_{Cym}$

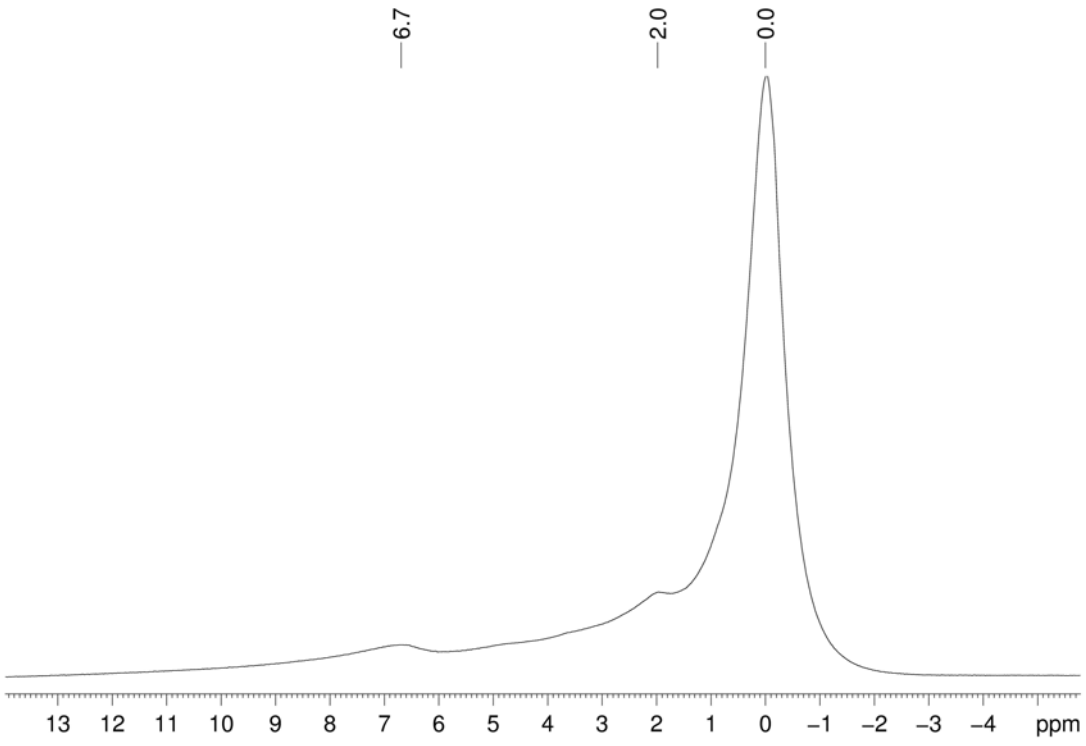

Figure A7. ^{1}H NMR spectrum of **M-RuCym**

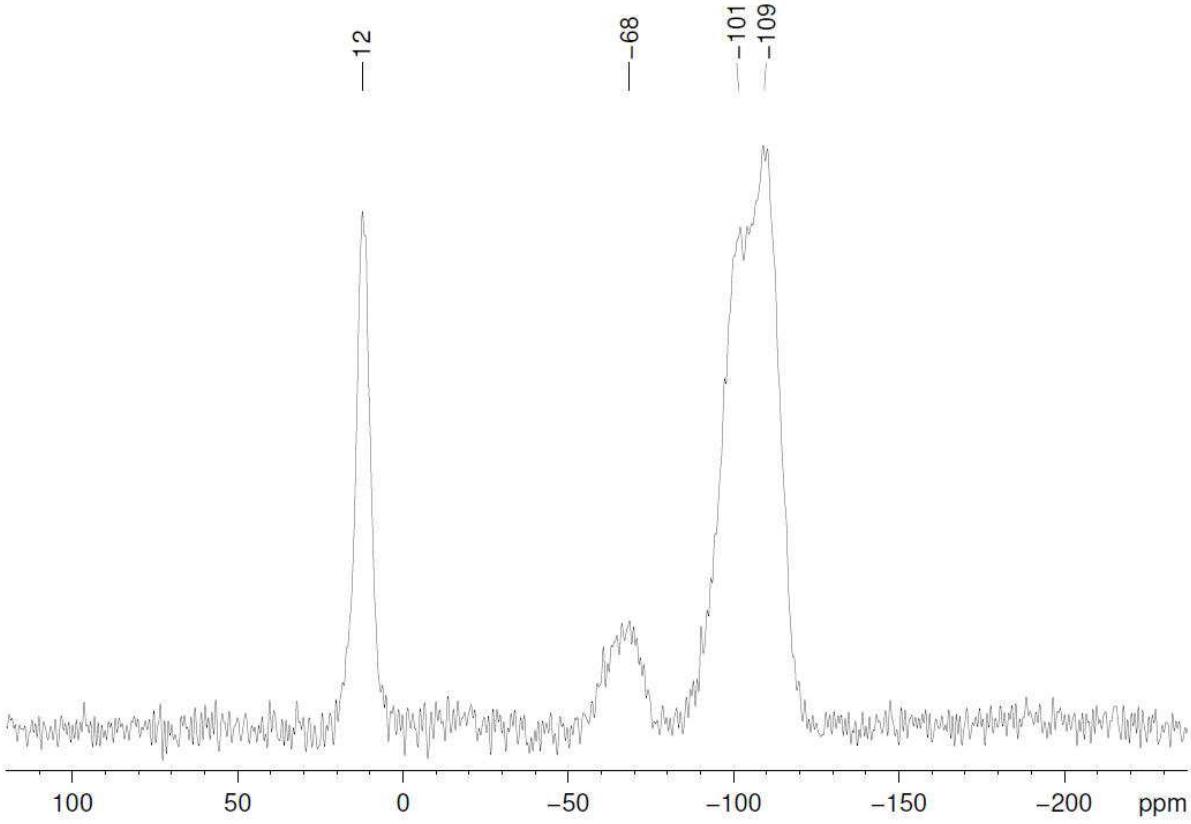

Figure A8. ^{29}Si CPMAS NMR spectrum of **M-RuCym**

M-RuP

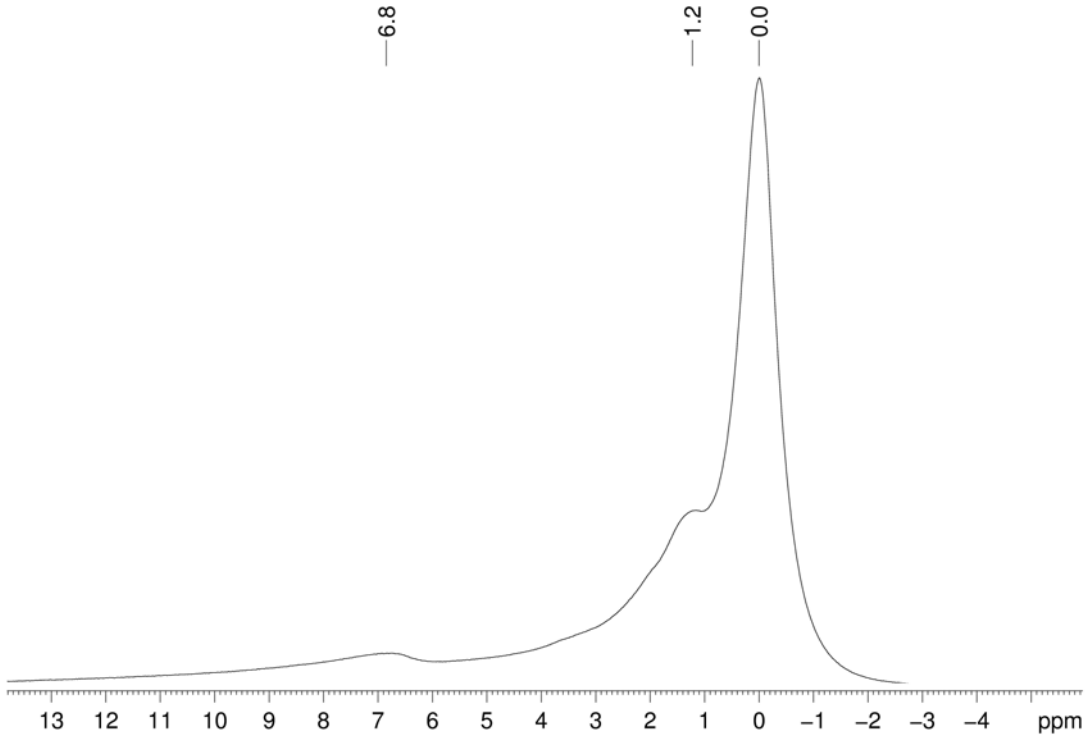

Figure A9. ^{1}H NMR spectrum of **M-RuP**

M-RuP*

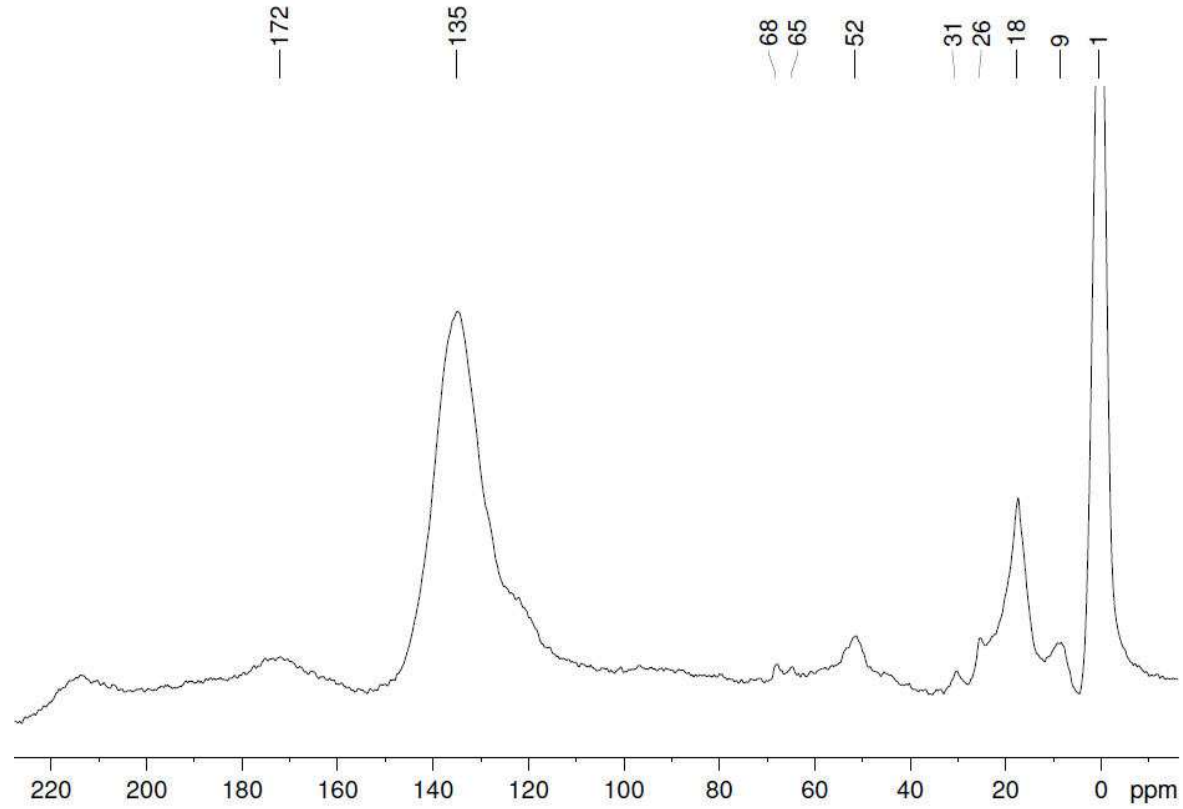

Figure A10. ^{13}C CPMAS NMR spectrum of material **M-RuP***

M-Rudppe

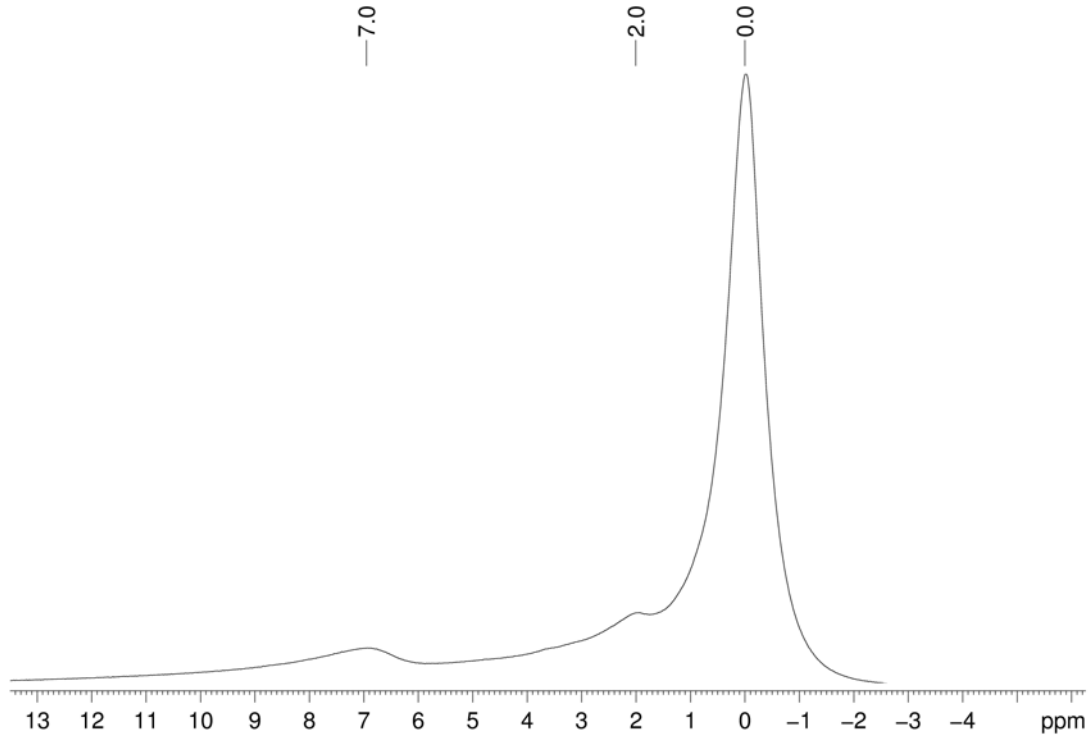

Figure A11. ^{1}H NMR spectrum of **M-Rudppe**

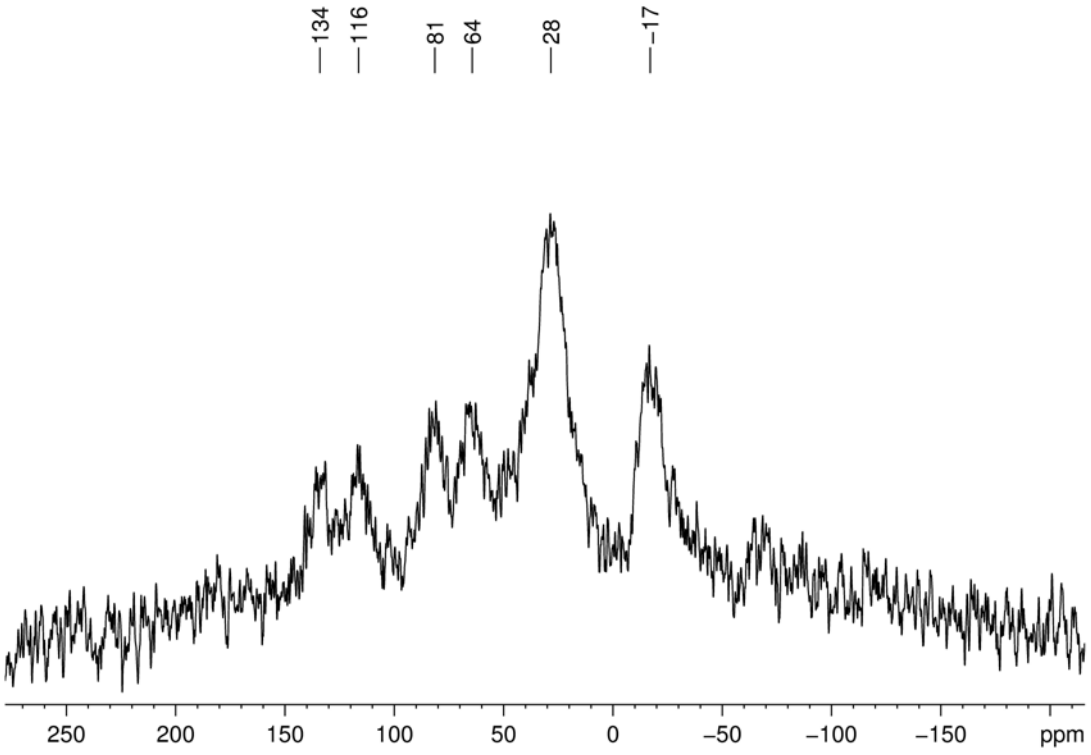

Figure A12. ^{31}P NMR spectrum of **M-Rudppe**

Reactions of exchange with THF and THF-d_8

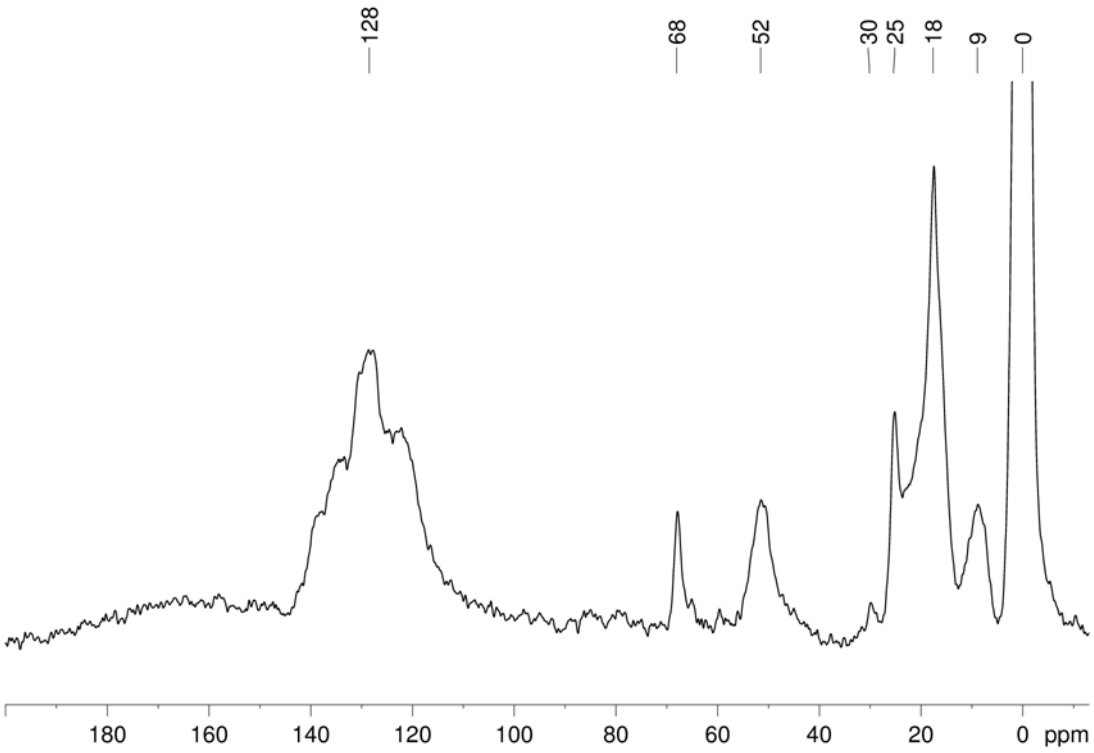

Figure A13. ^{13}C CPMAS NMR spectrum of material **M-RuCym** after reaction with THF

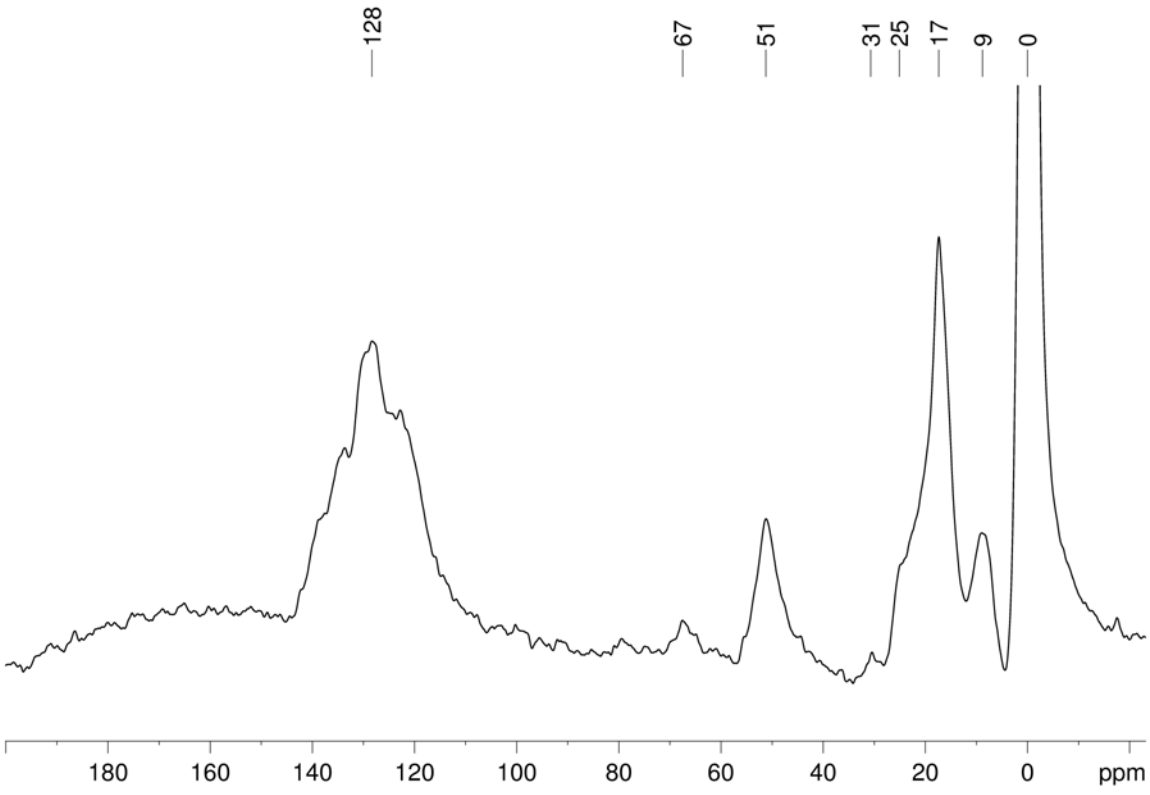

Figure A14. ^{13}C CPMAS NMR spectrum of **M-RuCym** after reaction with THF-d_8

Chapter 3

Hybrid mesoporous silica bearing accessible amine functionalities: selective formation of amide and imidazolium units through post-functionalisation.

TABLE OF CONTENT

LIST OF FIGURES

LIST OF SCHEMES

LIST OF FIGURES IN APPENDIX

III-1. Introduction

One of the main topics of the laboratory is to develop heterogeneous catalysts by SOMC on oxide functional materials. In order to be able to develop a wide range of supported organometallic complexes, it is necessary to develop specific supports offering diverse possibilities in term of surface modifications. Furthermore, being able to fully control the concentration of functional groups is another issue and this also needs to be taken into account in the development of new materials. Having all these criteria in mind, our study will focus on the formation of amine-functionalized materials. Indeed, an amine is a simple and yet reactive functional group that allows a wide range of reactions, like amide formations, nucleophilic substitutions, formation of N-heterocycles, etc.

The first part of this work will consist in describing methodologies to develop amine-functionalized materials. In 1996, Macquarrie *et al.* reported the synthesis of MCM-type materials bearing aminopropyl functionalities,[1] but these materials have small pore sizes which make them difficult to use in catalysis. More recently, the group of Prof. Corriu described large pore SBA-type amino-based materials, using 3-tert-butyloxycarbonylaminopropyl functional groups as precursors to primary amine units[2] or 3-iodopropyl-functionalized materials for substitution reactions, including the formation of secondary and tertiary amines.[3] These syntheses were attempted, but some reproducibility problems were faced under our conditions, in particular when targeting high density of functional groups. As a consequence, a new methodology to prepare well-structured aminopropyl-functionalized materials via the use of azidopropyl-based parent materials will be described hereafter.

In a second part, the further functionalisation of all these amine-based materials will be discussed. Primary and secondary amine materials will be first used for the selective and quantitative formation of amide groups, but a particular attention will be directed to their transformation into diverse imidazolium units. In the 1990s, Arduengo and co-workers developed a convenient synthesis of imidazole and imidazolium species, typically from

glyoxal, formaldehyde, a primary amine and ammonium acetate to get the desired substituted imidazole, or only glyoxal, formaldehyde and two equivalents of the amine to get to the symmetrical bis-substituted imidazolium (see Scheme 1).[4]

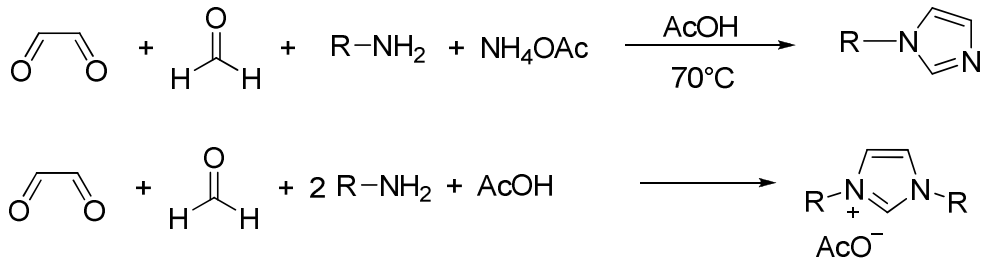

Scheme 1. Formation of imidazoles and imidazoliums[4]

However, this synthesis is not selective for the formation of unsymmetrical imidazolium units. Indeed, the use of a mixture of two amines leads to the formation of a mixture of both symmetrical and unsymmetrical imidazolium units but it is not a viable way to form unsymmetrical compounds. The only clean procedure is thus carried out in two steps and presents some restrictions because it goes through the formation of a mono-substituted imidazole and reaction with an halogenated alkyl derivative bearing the other desired substituent. The aim of this study is to benefit from the solid phase containing amino groups to form *in situ* unsymmetrical imidazolium units in one step as inspired from peptidic synthesis processes.

III-2. Formation of amine-functionalised materials

2.1. Formation of highly ordered mesoporous materials bearing diluted amine functionalities

2.1.1. Synthesis of a primary amine-functionalised material

2.1.1.1. Synthesis of the NHBoc-based material

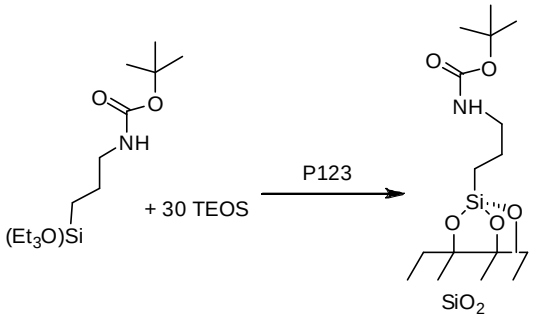

M-NHBoc

The synthesis of aminopropyl-functionalised materials was performed by co-hydrolysis and co-condensation of TEOS and 3-tert-butyloxycarbonylaminopropyl triethoxysilane with further thermal or acidic treatments to form the targeted primary amine. This material was reported by the group of Prof. Corriu,[2] with a SBA-type structure and 600m²/g surface area. As problems were faced to reproduce the exact synthesis reported (poor structuration), some modifications were achieved in the synthesis and we reproduced the experiments using a reaction temperature of 45°C instead of the reported 60°C. The synthesis was carried out with two different concentrations of organic functionalities, with a organosilane/TEOS ratio of 1/19 and 1/30. The 1/19 diluted material was characterized by N_2 adsorption isotherm at 77K and showed a bimodal distribution of pore sizes, meaning that the high concentration of organic part impacts the surfactant mesophase. In the case of the 1/30 dilution, N_2 adsorption-desorption analyses exhibited a type IV isotherm characteristic of mesoporous materials, with a high surface area of 830 m²/g, a narrow pore size distribution centred on 9.1 nm (BJH at the adsorption branch) and a high pore volume of 1.6 cm^3/g. The porous structure of the material was confirmed using small angles X-Ray diffraction and TEM. The X-Ray diffraction pattern shows an intense and broad peak at 1.0°, proving the

periodic arrangement of the pores (see Figure A1). The TEM confirms worm-like structure of the material as suggested by the broad signal in X-ray diffraction, confirming the difficulty to introduce high content of organic functionality using the mentioned starting silane precursor. (see Figure A2) The DRIFT spectrum shows an intense ν(C=O) signal at 1697 cm^{-1}, which proves the presence of the Boc group (see Figure A3). Solid-state NMR was performed to prove the incorporation of the organic part in the material: the CPMAS ^{13}C spectrum shows peaks at 8, 15, 22, 26, 42, 58 and 156 ppm (see Figure 1). The peaks at 15 and 58 ppm correspond to surface ethoxy groups. The peaks at 42, 22 and 8 ppm can be attributed to the three carbons of the propyl chain, in position α, β and γ to the nitrogen atom respectively. The signal at 26 ppm corresponds to the methyl groups of the isopropyl functionality and the carbonyl group gives a signal at 156 ppm. These results are fully consistent with the formation of a periodic mesoporous material incorporating tert-butyloxycarbonylaminopropyl functionalities, **M-NHBoc.**

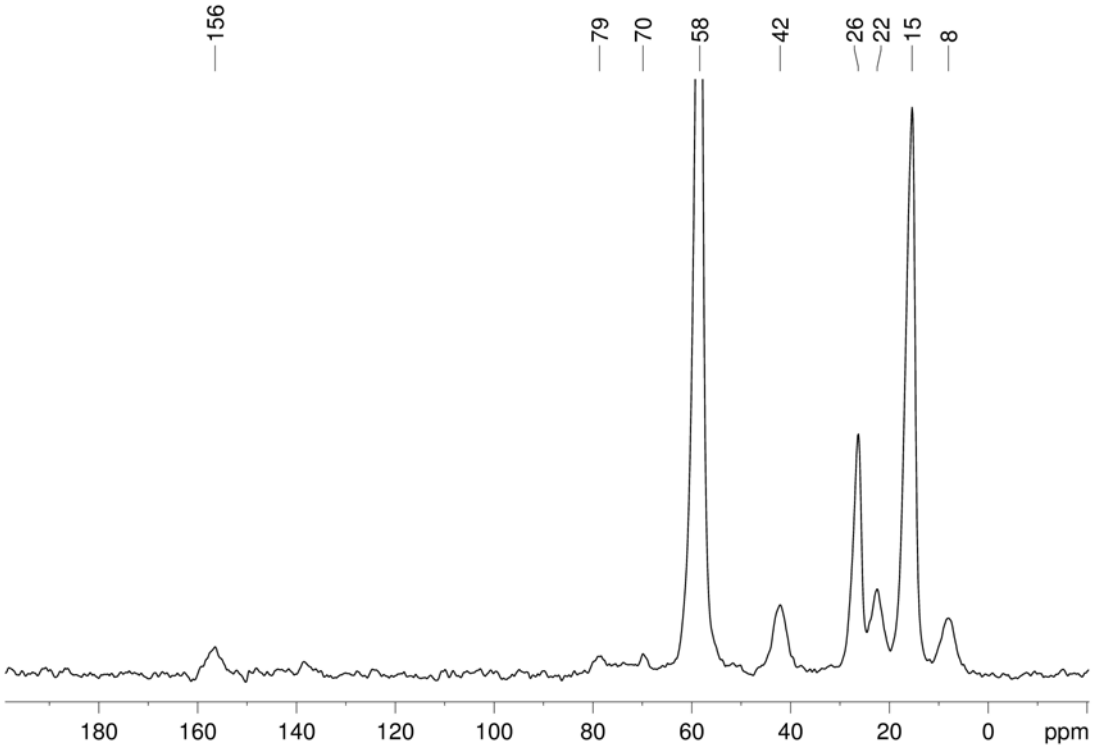

Figure 1. ^{13}C-CPMAS solid-state NMR spectrum of **M-NHBoc**

2.1.1.2. Deprotection of the amine

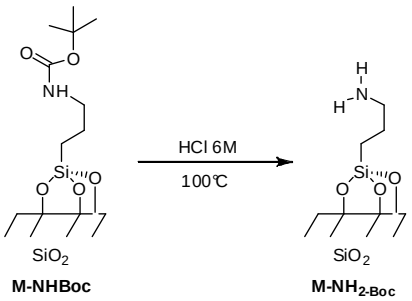

M-NHBoc **M-NH$_{2\text{-Boc}}$**

The deprotection of the Boc group was tested under two different conditions: a thermal treatment and an acidic hydrolysis. The first method was found to be less efficient and we therefore chose the hydrolysis under acidic conditions afterwards. In this case, the DRIFT spectrum shows a complete disappearance of the intense band at 1697 cm^{-1} and the appearance of two weaker bands at 1669 and 1596 cm^{-1}, corresponding to δ(N-H) vibrations of the amide (see Figure A3). The CPMAS ^{13}C spectrum shows signals at 8, 15, 24, 42 and 58 ppm (see Figure 2). The peaks at 15 and 58 ppm correspond to ethoxy surface groups. The three peaks at 42, 24 and 8 ppm can be attributed to the three carbons of the propyl chain in α, β and γ position of the NH_2. These results are coherent with the full deprotection of the Boc group and the formation of an aminopropyl-functionalised material, **M-NH$_{2\text{-boc}}$**.

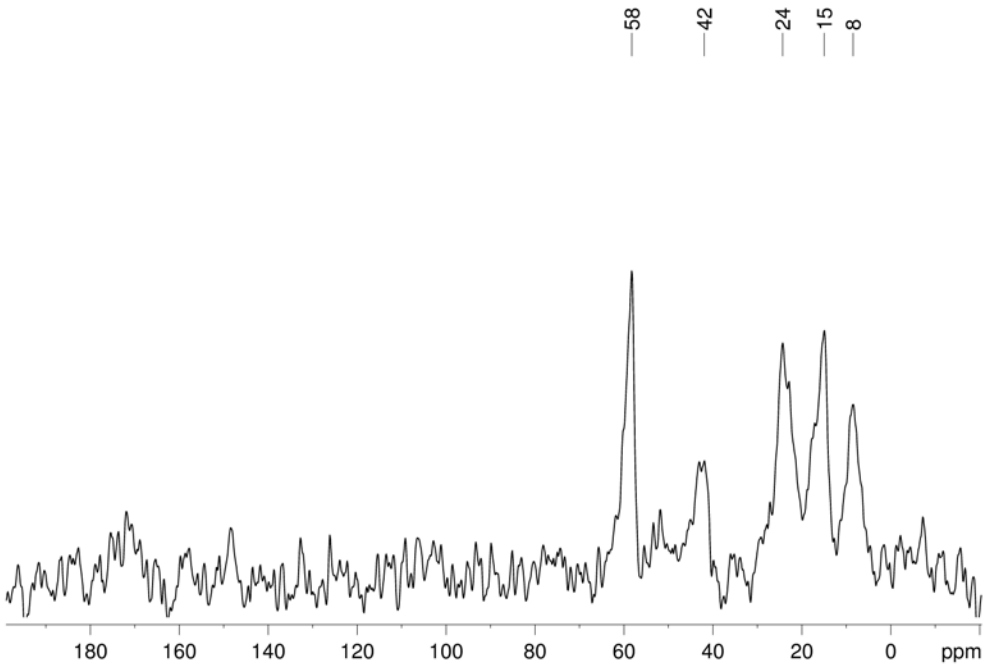

Figure 2. ^{13}C-CPMAS solid-state NMR spectrum of **M-NH$_{2\text{-boc}}$**

2.1.2. Synthesis of a secondary amine functionalised material

2.1.2.1. Synthesis of an iodopropyl-based material

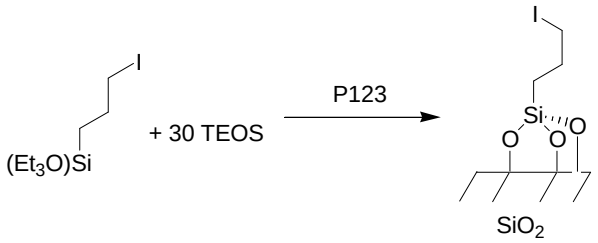

The use of iodopropyl-functionalised materials for the formation of secondary amine as already proved to be an interesting strategy.[3] The synthesis has been performed using similar procedures, with a dilution of the organic functionality of 1/30. The nitrogen adsorption-desorption isotherms are of type IV, with a specific surface area of 900 m^2/g and a narrow pore size distribution centred on 7.6 nm (BJH, adsorption branch of the isotherm). The structure of the material was confirmed to be 2D hexagonal by Transmission Electron Microscopy (TEM) and by small-angle X-Ray diffraction. The ^{29}Si cross-polarization magic-angle-spinning (CPMAS) solid-state NMR confirmed the presence of Si-C bond and thus the incorporation of organosilane in the material, as attested by the presence of the peaks at -66 and -58 ppm, characteristic of the T_3 and T_2 substructures. The major organic species contain T_3 substructures, confirming the high chemical condensation of the material. By ^{13}C CPMAS solid-state NMR, we could confirm the structure of the organic groups present. The three signals at 5, 12 and 27 ppm are characteristic of the three carbons of the iodopropyl unit.

2.1.2.2. Reaction of the iodopropyl material with benzyl amine

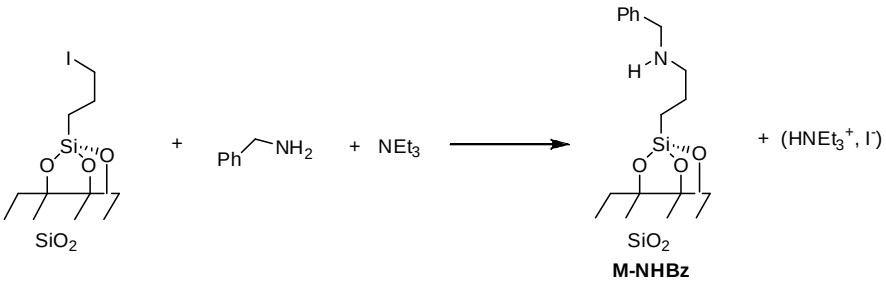

The reaction of benzylamine with iodopropyl materials led to the formation of material **M-NHBz**. The ^{1}H MAS solid-state NMR spectrum showed the presence of an aromatic signal at 7.1 ppm, attributed to the aromatic protons of the benzyl functionality (See Figure A4). The ^{13}C CPMAS solid-state NMR spectrum exhibited signals at 7, 21, 53, 128 and 139 ppm. (see Figure A5) The signals at 7 and 21 ppm correspond to carbon atoms of the propyl chain in α and β position to the silicon atom respectively. The signal at 53 ppm corresponds to the two carbon atoms linked to the nitrogen atom which have close chemical shifts. The presence of aromatic carbon atoms is confirmed by signals at 139 ppm for the quaternary carbon and 128 ppm for the other ones. Elemental analysis gives a nitrogen content of 0.46 mmol/g which is very close to the expected 0.43 mmol/g, confirming the full conversion of the iodopropyl groups into amine. Finally, all these results are in agreement with the quantitative transformation of iodopropyl-functionalised materials into secondary amine containing materials without damaging the physical properties of the material.

2.2. Synthesis of highly concentrated amine materials by selective reduction of an azide

As the method described before to synthesise aminopropyl-based materials could not allow to obtain high concentrations, we thus developed azidopropyl-based materials taking advantage of the hydrophobicity of the azidopropyl group to incorporate high loadings of organic functionalities.[5] The further reduction of the azide into amine should therefore allow to obtain highly concentrated aminopropyl materials.

2.2.1. Formation of azidopropyl materials in different dilutions

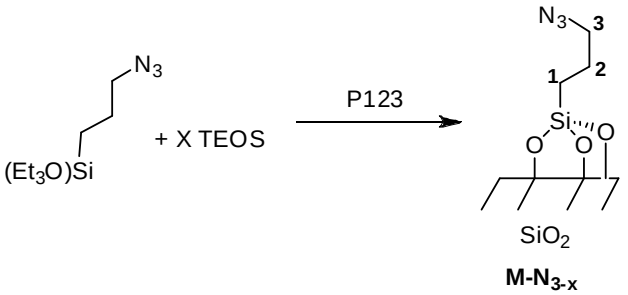

M-N$_{3-x}$

Three different materials with dilutions of 1/30, 1/19 and 1/12, labelled **M-N$_{3-30}$**, **M-N$_{3-19}$** and **M-N$_{3-12}$** respectively were synthesised. These materials were obtained by co-hydrolysis and co-condensation of TEOS and 3-azidopropyltriethoxysilane in an aqueous HCl solution in presence of P123 as template and catalyzed by NaF. In all cases, the materials obtained were characterized by N_2 adsorption-desorption at 77K and a type IV isotherm was obtained (see Figures A6 and A7), a narrow pore size distribution and a high specific surface area were also observed (see Table 1). When increasing the organic content, the specific surface area is almost unchanged but the average pore size decreases and the distribution becomes broader. In our conditions, the 1/12 dilution was the limit dilution for keeping high

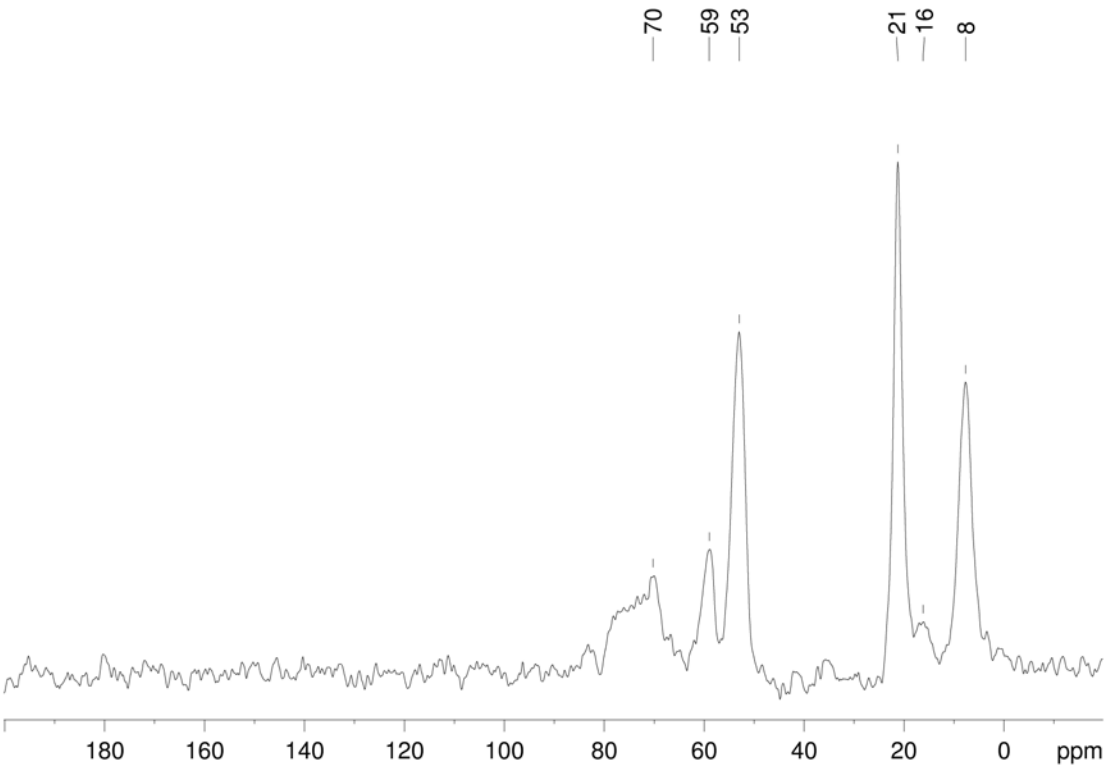

Figure 3. ^{13}C CPMAS solid-state NMR spectrum of **M-N$_{3-19}$**

mesoporosity. The mesostructuration of the materials was confirmed by TEM with the presence of 2D hexagonal arrangement of the channels even in a 1/12 dilution (see Figure A8). An increase in the organic content to a 1/9 ratio led to the formation of small mesopores and broad pore size distribution of the material. Solid-state ^{13}C CPMAS spectrum shows the incorporation of the organic fragments with the three signals at 8, 21 and 53 ppm corresponding to the three carbon atoms of the propyl tether in positions 1, 2 and 3 respectively (see Figure 3). The DRIFT analysis shows a strong signal at 2114 cm^{-1}, characteristic of the $\nu(N_3)$ vibration (see Figure A9). Our method to synthesize azidopropyl-based materials was therefore highly effective for the formation of materials with 1/30 to 1/12 dilution ratio.

Table 1. N_2 adsorption data of azide-based materials.

Material	Surface (m^2/g)	Pore size (nm)	Pore volume (cm^3/g)
M-N_{3-30}	930	9.5	1.35
M-N_{3-19}	740	6.6	0.66
M-N_{3-12}	860	6.4	0.83
M-N_{3-9}	900[a]	4.7	0.70

[a] For this material, pore size distribution is quite broad, with a large quantity of small mesopores.

2.2.2. Conversion of azide to amino functionalities with the Staudinger Reaction

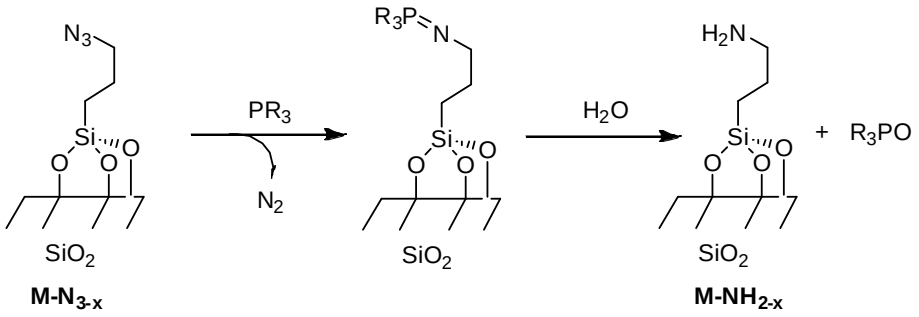

The reduction of azido-group to amino-unit is known as the Staudinger reaction.[6] It involves the formation of an intermediate iminophosphorane species, which can then be hydrolyzed to an amino group and phosphine oxide. For effective surface modification, the reaction is

carried out with a perfectly dry azide material and dry THF as solvent for the formation of the iminophosphorane. The reduction was tested with two different phosphines: triphenylphosphine and dimethylphenylphosphine. The reaction was monitored by DRIFT spectroscopy, as the azido group is easily characterised by a very intense signal at 2114 cm^{-1}. After reduction with both phosphines, the DRIFT spectrum shows the significant reduction of the azide band and appearance of two δ(N-H) bands at 1594 and 1667 cm^{-1}. (see Figure A11) The reduction was more effective in the case of dimethylphenylphosphine, which can be easily explained by its more electron-rich character. Indeed, from DRIFT analysis the conversion of N_3 to NH_2 was 97% quantitative with PMe_2Ph and only 85% with PPh_3. Solid-state ^{13}C CPMAS NMR spectrum presents a new band at 43 ppm and a significant decrease of the peak at 52 ppm (see Figure 4). As previously observed for the material **M-$NH_{2\text{-boc}}$,** the peak at 43 ppm can be attributed to a carbon in α-position to a NH_2 group. Finally, the reduction of the azide materials **M-$N_{3\text{-x}}$** with dimethylphenylphosphine allows the formation of aminopropyl functionalities in a selective and quantitative way (more than 90% conversion) to form material **M-$NH_{2\text{-x}}$**.

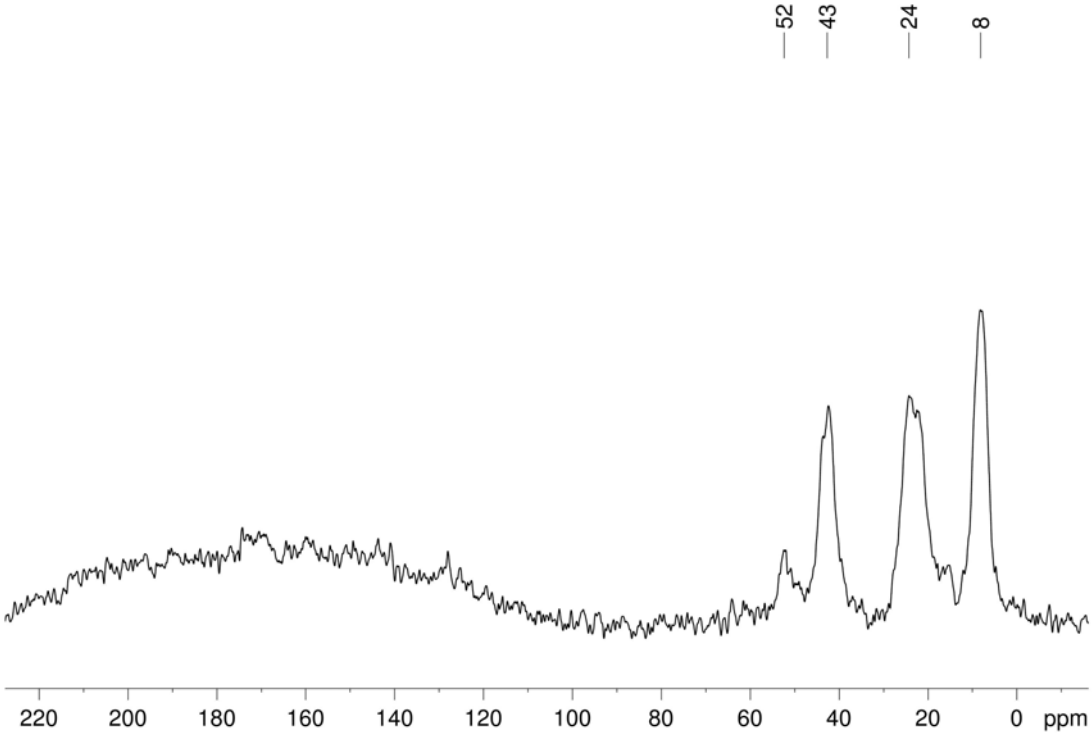

Figure 4. ^{13}C CPMAS solid-state NMR spectrum of **M-$NH_{2\text{-12}}$**

III-3. Accessibility and surface modification

3.1. Selective amide formation

In order to test the accessibility of the amine functional groups on the surface, we carried out an amidation reaction, in presence of an effective organic catalyst, namely the 2-hydroxypyridine.[7]

3.1.1. Reaction of the aminopropyl material with ethyl hydrocinnamate

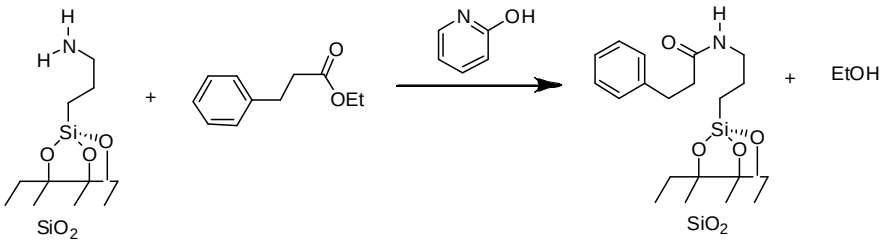

M-NH$_{2\text{-Boc}}$ **M-NHAm**

The amidation reaction on material **M-NH$_{2\text{-boc}}$** was carried out with ethyl hydrocinnamate in the presence of 2-hydroxypyridine, in meta-xylene at reflux.[7] The ^{13}C CPMAS solid-state NMR shows signals at 8, 15, 22, 31, 37, 41, 58, 124, 128, 140 and 173 ppm. (See Figure 5) The peaks at 15 and 58 ppm come from surface ethoxy groups. By comparison with the starting material (peaks at 8, 24 and 42 ppm), the signals at 8, 22 and 41 ppm can be attributed to carbon 1, 2 and 3 respectively. The signals at 31 and 37 ppm can then be attributed to carbons 6 and 5 respectively. Aromatic carbon atoms show three different signals at 124, 128 and 140 ppm. If we compare with ethyl hydrocinnamate ^{13}C NMR spectrum, carbon 8 and 9 present similar chemical shift around 128 ppm, whereas carbon 7 and 10 are characterized by signals at 140 and 124 respectively. The carbonyl group 4 is also present and shows a signal at 173 ppm. In the DRIFT spectrum, the ν(C=O) region shows two sets of signals. (see Figure A13) The first set of two signals at 1650 and 1605 cm^{-1} corresponds to vibrations of physisorbed 2-hydroxypyridine, as confirmed by a blank experiment with only 2-hydroxypyridine. The second set corresponds to the signal at 1629 cm^{-1} which is characteristic of an amide ν(C=O) vibration. Thus, the results are in agreement

with the selective and quantitative formation of an amide by reaction of the NH_2 groups with ethyl hydrocinnamate to generate material **M-NHAm**. However, the full extraction of 2-hydroxypyridine was not successful at this point, and the extraction method using Pyridine/HCl solutions could be a way for quantitative extraction.[8]

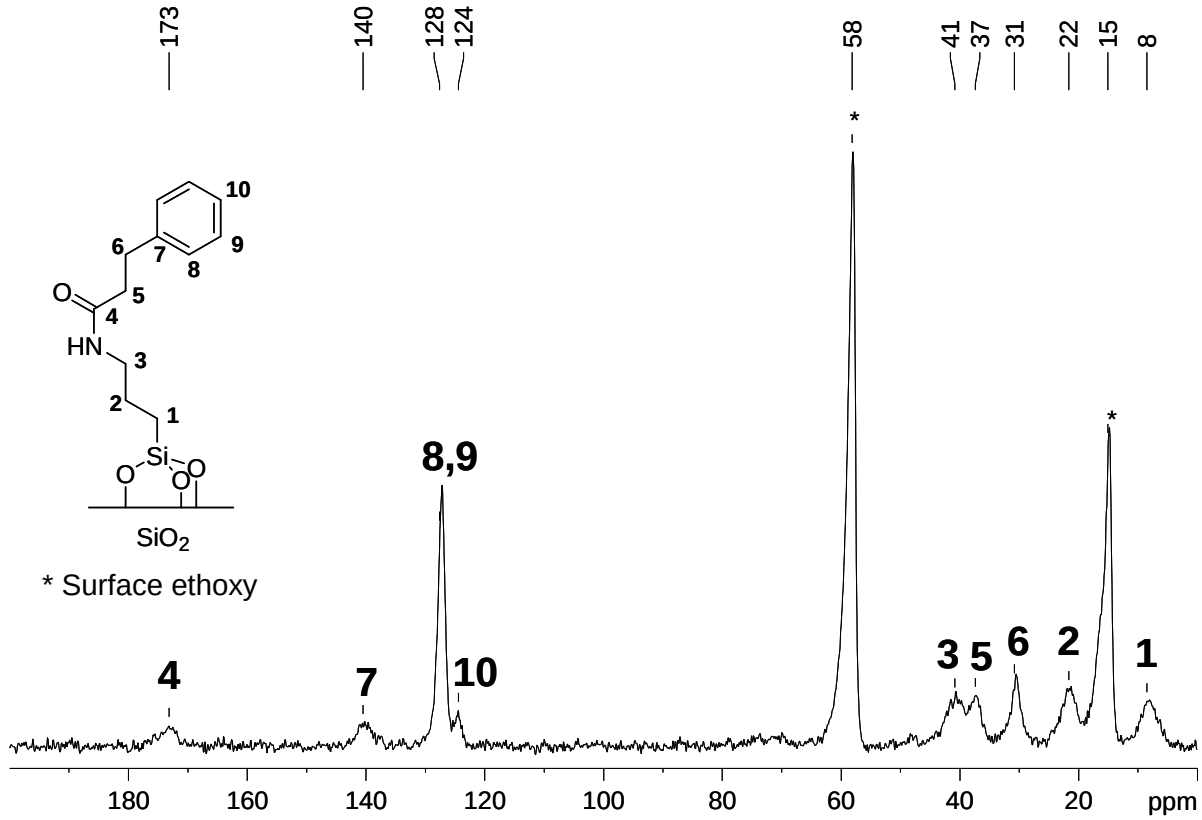

Figure 5. ^{13}C CPMAS NMR spectrum of **M-NHAm**

3.1.2. Reaction of the propylbenzylamine-based material with ethyl hydrocinnamate

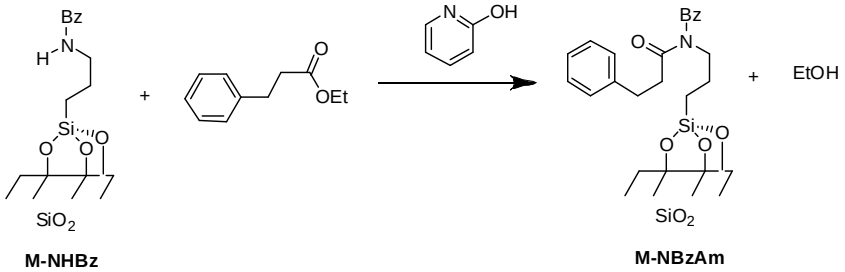

The accessibility and reactivity of secondary amine functionalities was tested by the amidation reaction between material **M-NHBz** and ethyl hydrocinnamate to yield material **M-NBzAm**. The ^{13}C CPMAS solid-state NMR shows signals at 7, 16, 20, 30, 34, 50, 58, 127

and 138 ppm. (See Figure 6) As for the previous material, all the spectrum signals could be easily attributed compared to ethyl hydrocinnamate and **M-NHBz**: signals at 7 and 20 ppm were attributed to carbon 1 and 2. The two CH carbon in α to nitrogen display a broad signal at 50 ppm. The two CH_2 5 and 6 are observed at 34 and 30 ppm respectively. All the aromatic CH carbon atoms give a signal around 127 ppm and the two quaternary carbons show a single signal at 138 ppm. By DRIFT analysis, the same set of bands is observed as in material **M-NHAm** with two bands for 2-hydroxypyridine at 1657 and 1609 cm^{-1} and band at 1629 cm^{-1} for an amide ν(C=O), proving the presence of the amide bond. (see Figure A15) These results confirm the formation of the amide to give material **M-NBzAm**.

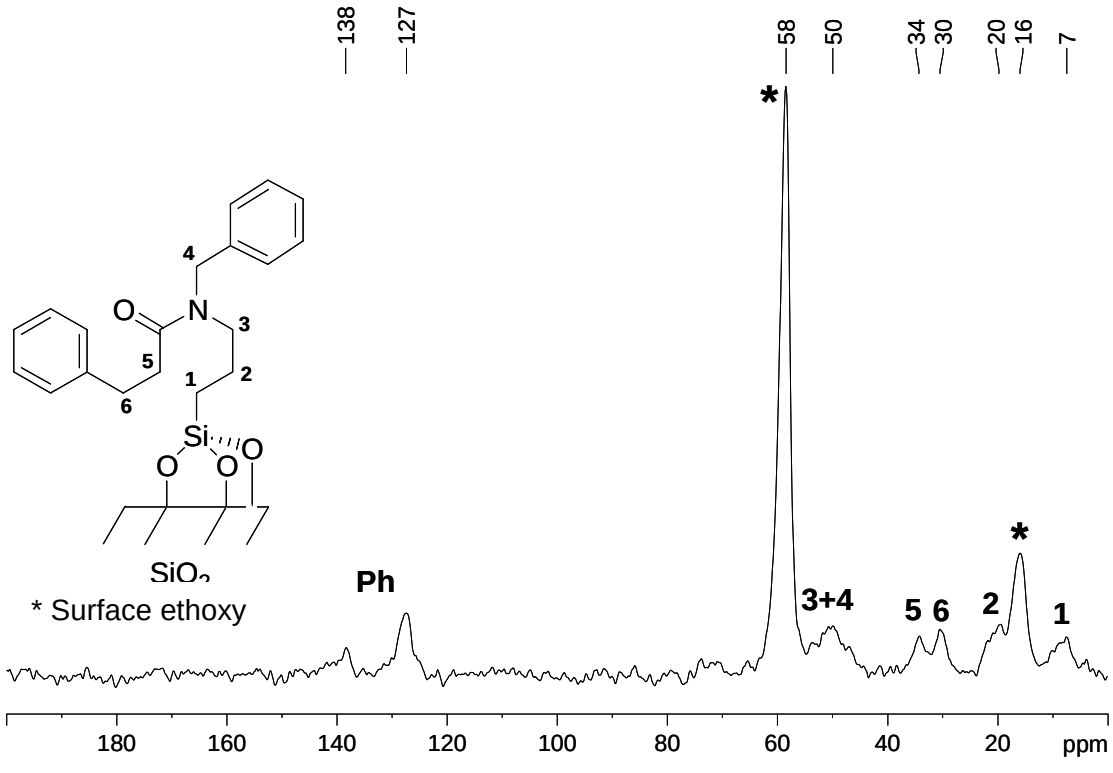

Figure 6. ^{13}C CPMAS NMR spectrum of **M-NBzAm**

3.2. In-situ formation of imidazole rings from an aminopropyl material.

3.2.1. Formation of propyl imidazole groups

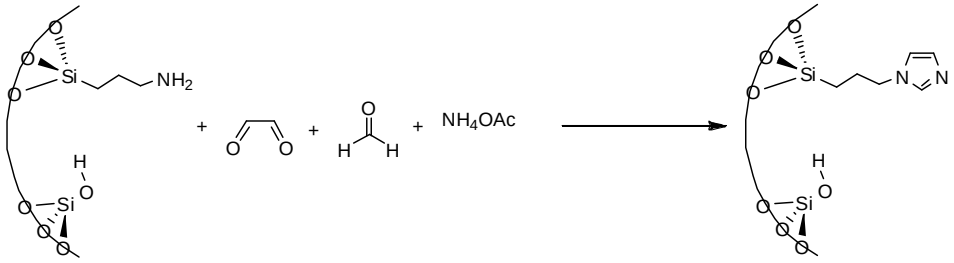

M-PrIm$_{12}$

Using a derived procedure from Arduengo's imidazole and imidazolium synthesis, we studied the reactivity of aminopropyl-functionalised material **M-NH$_{2\text{-}12}$** in presence of glyoxal, formaldehyde and ammonium acetate in presence of acetic acid to yield material **M-PrIm$_{12}$**. The solid-state ^{13}C CPMAS spectrum shows the quasi-quantitative disappearance of the band at 43 ppm associated with aminopropyl functionalities and four new peaks at 48, 117, 126 and 136 ppm (see Figure 7). These chemical shifts are in agreement with an alkyl imidazole unit, if comparing with the spectrum of 1-ethylimidazole for instance (signals at 136, 129, 118, 41 and 16 ppm).

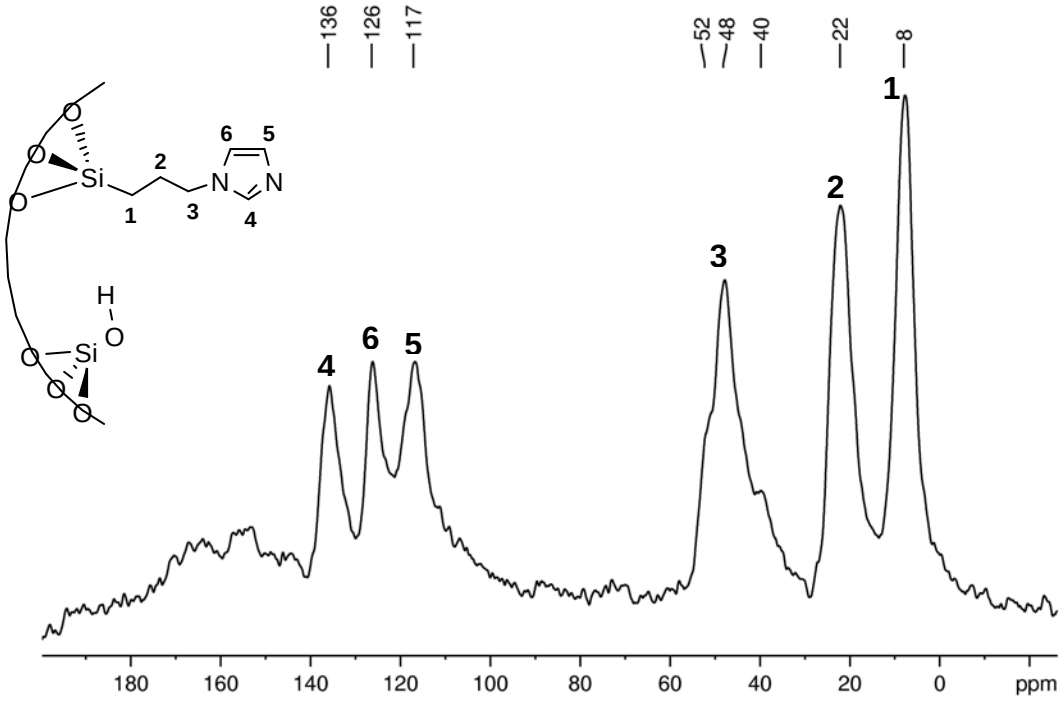

Figure 7. ^{13}C CPMAS solid-state NMR spectrum of **M-PrIm$_{12}$**

The solid was also analyzed by DRIFT spectroscopy to confirm the presence of the imidazole ring. Imidazole rings show, in infrared spectroscopy, some characteristic bands. Among others, they show one sharp band around 1520 cm^{-1} corresponding to a planar vibration of the imidazole ring and another broad one around 1650 cm^{-1} being a combination of C-C and C-H vibrations. In the Csp^2-H region, the C-H vibrations of the imidazole C=C bond are observable around 3150 cm^{-1}. The DRIFT spectrum of material **M-PrIm$_{12}$** shows new bands at 1516, 1641, 1712 and 3150 cm^{-1} (see Figure 8) and the bands corresponding to NH_2 are not visible any longer. The bands at 1516, 1641 and 3150 cm^{-1} correspond to known characteristic bands of imidazole rings. The band at 1712 cm^{-1} is certainly due to the presence of some unwashed aldehyde species from the synthesis or unidentified aldehyde surface species. This is also confirmed by the presence of a broad signal in the ^{13}C NMR spectrum between 150 and 170 ppm. These results are consistent with the formation of imidazole functionalities within the pores, yielding material **M-PrIm$_{12}$**.

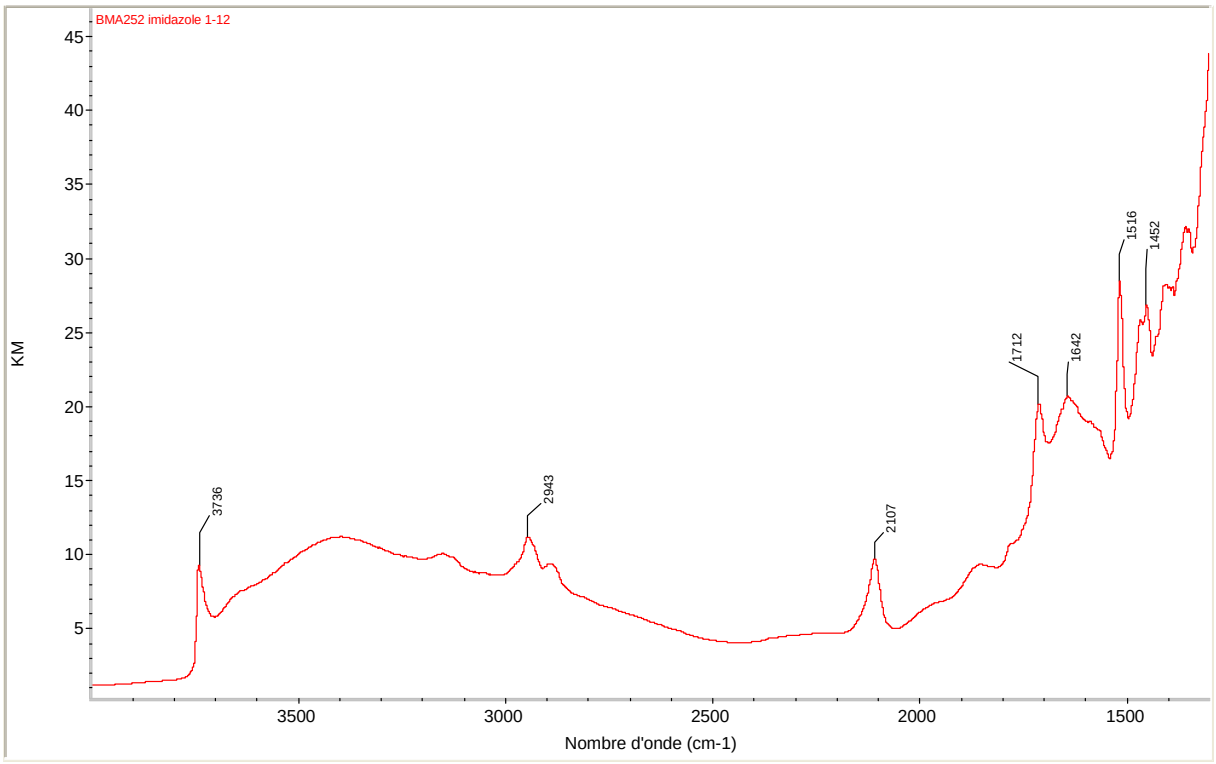

Figure 8. DRIFT spectrum of **M-PrIm$_{12}$**

3.2.2. Formation of substituted imidazolium rings

There are two different strategies to prepare imidazolium units: from the reaction between an imidazole unit and an alkyl or aryl chloride, or directly by reaction of the primary amine-functionalised material with Arduengo's conditions in presence of a primary amine instead of ammonium acetate.

3.2.2.1. Propyl-benzyl-imidazolium from imidazole-material

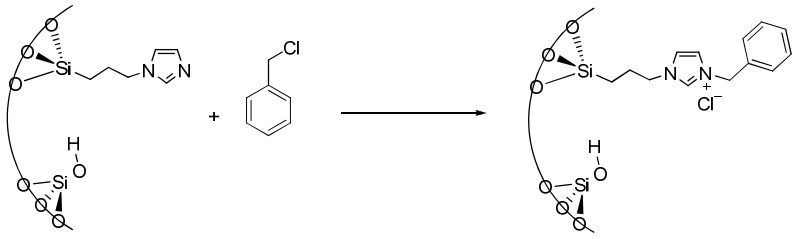

M-PrIm$_{12}$ **M-PrBzIm$_{12}$**

The reaction of imidazole material with benzylchloride in toluene under reflux for 18 hours affords material **M-PrBzIm$_{12}$**. The solid-state ^{13}C CPMAS spectrum shows signals at 8, 21, 40, 51, 120, 128 and 134 ppm (see Figure A19). The peaks at 8 and 21 ppm correspond to CH_2 in α and β position to the silicon atom respectively. Unreacted NH_2 units are still present as attested by the presence of the small peak at 40 ppm. The peak at 51 ppm corresponds to the two carbon atoms in α to the imidazolium ring. Finally, aromatic carbon atoms of imidazolium are present at 120 ppm, CH of the benzyl unit is observed at 128 ppm and the quaternary carbon signal is visible at 134 ppm. All these data are consistent with the formation of a 1-propyl-3-benzyl imidazolium unit within the pores and the formation of material **M-PrBzIm$_{12}$**.

3.2.2.2. One-step formation of propyl-benzyl-imidazolium

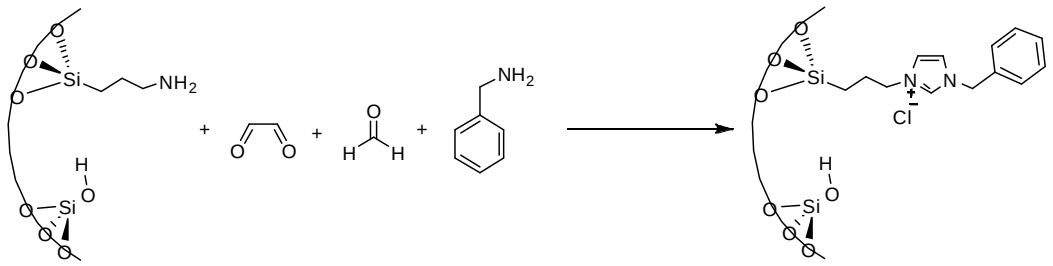

M'-PrBzIm$_{12}$

Similarly to what was done for the synthesis of material **M-PrIm**$_{12}$, the reaction of **M-NH$_{2\text{-}12}$** in presence of 20 equivalents of glyoxal, formaldehyde and benzyl amine in the presence of acetic acid affords material **M'-PrBzIm$_{12}$**, which is subsequently treated by a HCl solution to hydrolyse the surface of the material and exchange the imidazolium anion. The obtained surface species is identical to that obtained by the two-steps reactions, as confirmed by ^{13}C CPMAS solid-state NMR (see Figure 9). These experimental conditions are usually used for the synthesis of symmetrical imidazolium species.[4] Indeed, it is not possible to synthesize selectively unsymmetrical imidazolium species in homogenenous conditions by adding two different amines, because the reaction would result in a mixture of three

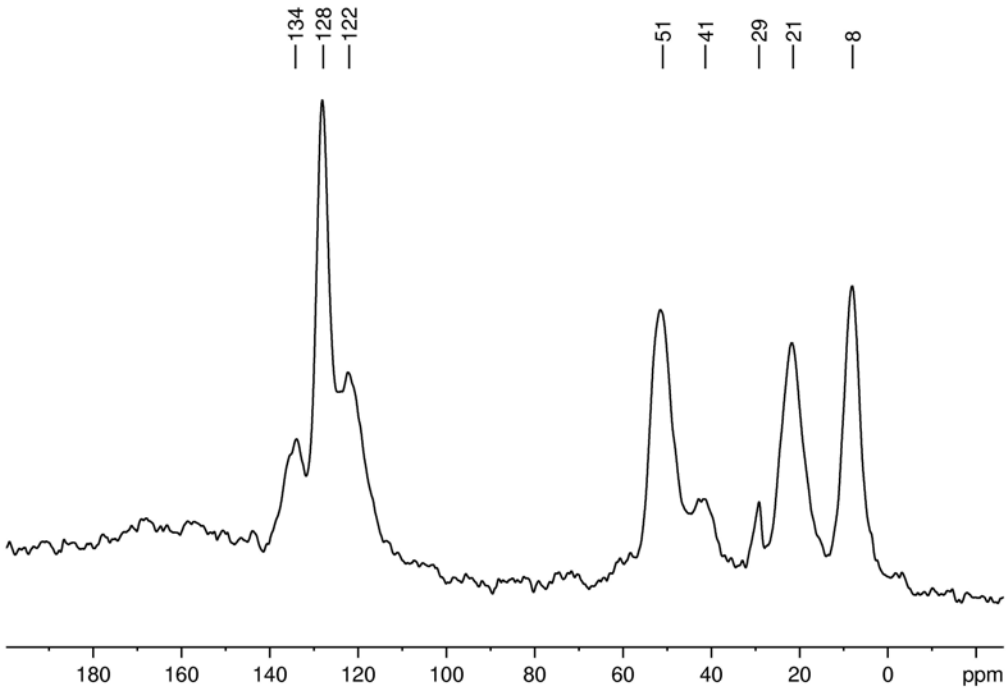

Figure 9. ^{13}C CPMAS solid-state NMR spectrum of **M'-PrBzIm$_{12}$**

compounds being the two symmetrical imidazolium species and the unsymmetrical

imidazolium. But by taking advantage of the presence of an amine-containing solid phase, only one unsymmetrical imidazolium surface compound is obtained. There is still the possibility to form bis-benzylimidazolium species in solution; however, if formed, this compound is washed away after. These interfacial reactions should therefore allow to in situ generate any type of imidazolium.

3.2.2.3. One-step formation of propyl-mesityl-imidazolium

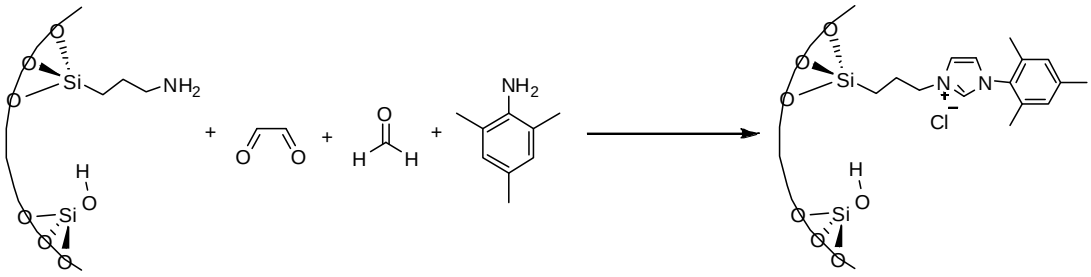

M-PrMesIm$_{12}$

The synthesis of propyl-mesityl-imidazolium material was more difficult, due to the fact that mesityl amine is a more sensitive amine, which has a tendency to decompose to form diazo compounds and other highly dark molecules. When using twenty equivalents of reagents as in the previous synthesis, the material obtained is almost black, and we therefore tried different conditions to avoid this coloration. In our hands, the best conditions where obtained when using a slight excess of reactants (3 equivalents), and by treating the obtained material which HCl/Pyridine solutions, leading to a light beige material, **M-PrMesIm$_{12}$**. In ^{13}C CPMAS solid-state NMR, there are three signals at 8,20 and 52 ppm corresponding to aliphatic carbon atoms and three other signals in the aromatic region at 122, 130 and 140 ppm (see Figure 10). The peaks at 8 and 52 ppm can unambiguously be attributed to the carbon atoms 1 and 3 of the propyl chain respectively, whereas the peak at 20 ppm is a superposition of the signal of carbon 2 of the propyl tether, and the CH_3 carbon atoms of the mesityl group. The aromatic signal at 130 ppm corresponds to the CH carbon atoms of the mesityl group and the two peeks at 122 and 140 ppm correspond to the carbon atoms of the imidazolium ring. Interestingly, with these conditions the conversion of NH_2 groups to imidazolium is much better, as attested by the very weak intensity of the peak at 42 ppm characteristic of a carbon in α-position to a NH_2 functionality. Indeed, the use of a less important quantity of glyoxal and

formaldehyde in aqueous solution limits the quantity of water in the reaction mixture and therefore limits the parallel hydrolysis reactions of the water-sensitive diimine intermediates. The DRIFT spectroscopy confirms also the formation of the imidazolium ring, with the presence of the two characteristic signals at 1563 and 3146 cm^{-1} (see Figure A23). All spectroscopic evidences are in agreement with the formation of a material having 1-propyl-3-mesityl-imidazolium units, **M-PrMesIm$_{12}$**.

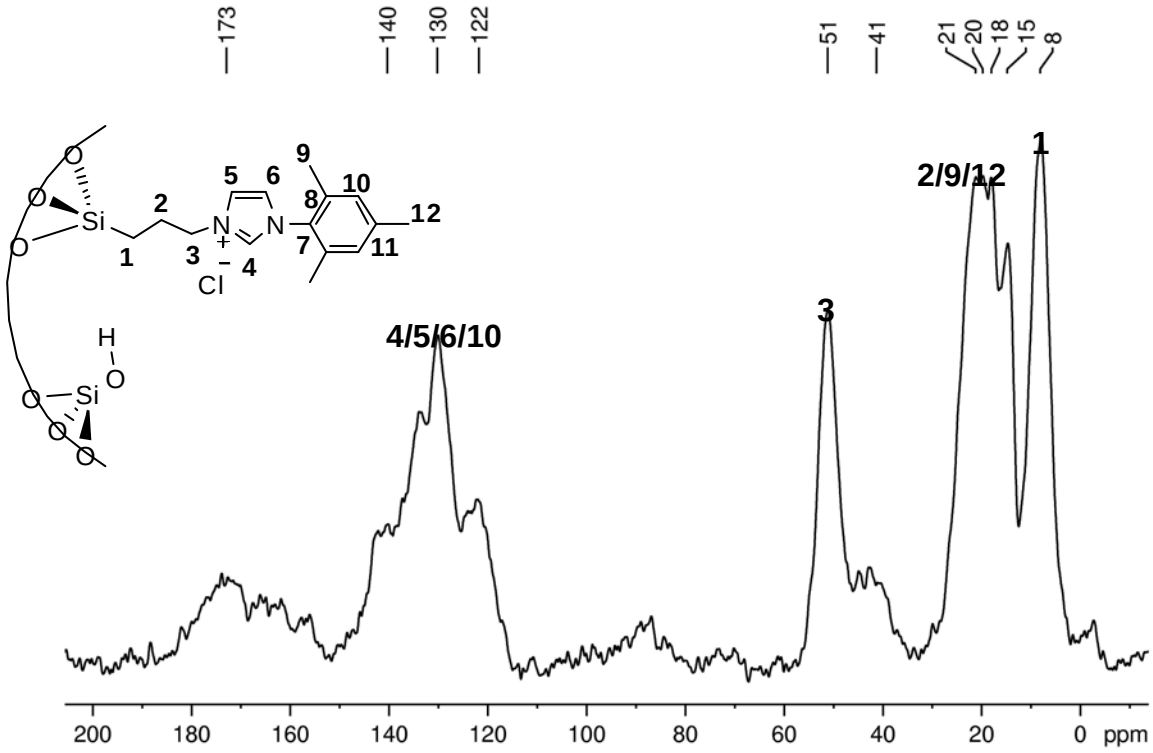

Figure 10. ^{13}C CPMAS solid-state NMR spectrum of **M-PrMesIm$_{12}$**

3.2.3. Quantification of the different sites

In order to truly quantify the yield of each synthetic step, elemental analyses were performed on a series of samples : **M-N$_{3\text{-}30}$**, **M-NH$_{2\text{-}30}$** and **M-PrIm$_{30}$**. (see Table 2)

Table 2. Elemental analysis of azido, amino and imidazole materials in 1/30 dilution

Sample	Nitrogen (w%)	Silicium (w%)
M-N$_{3\text{-}30}$	1.97	39.9
M-NH$_{2\text{-}30}$	0.97	39.3
M-PrIm$_{30}$	1.29	38.7

The yields can then be easily calculated for each step, thanks to the different number of nitrogen atoms in each functionality (3 nitrogen in the azido, 1 nitrogen in the amino and 2

nitrogen in the imidazole). The yield of the reduction of the N_3 group to NH_2 is of 75% and the conversion of NH_2 to imidazole is 70%. In total, we therefore form 53% of imidazole groups (0.185 mmol/g) considering all the starting azido functionalities, leaving around 25% unreacted azido groups and 22% unreacted NH_2 groups. For further calculations, it will be assumed that the yields of reactions on materials in 1/30 and 1/12 concentrations are approximately the same.

3.3. Generalising the method to the formation of bis-imidazolium units

3.3.1. Strategy

Our strategy to prepare bis-imidazolium units is to take advantage of the heterogeneous phase and the impossibility of two adjancent organic sites to interact with each other if the material is diluted enough. The idea is then to form step by step the two (or even more) NHC units, as it would be done in biochemistry to synthesize peptides from a step by step addition of amino acids. We have shown that we can form in situ imidazolium units from an aminopropyl material and another molecular amine in presence of glyoxal and formaldehyde. In order to form bis-imidazolium units, we would then need to use a diamine. (see Scheme 2) In this particular case, we chose to use 1/30 diluted materials to avoid any interaction between two adjacent sites which would make the reaction more difficult.

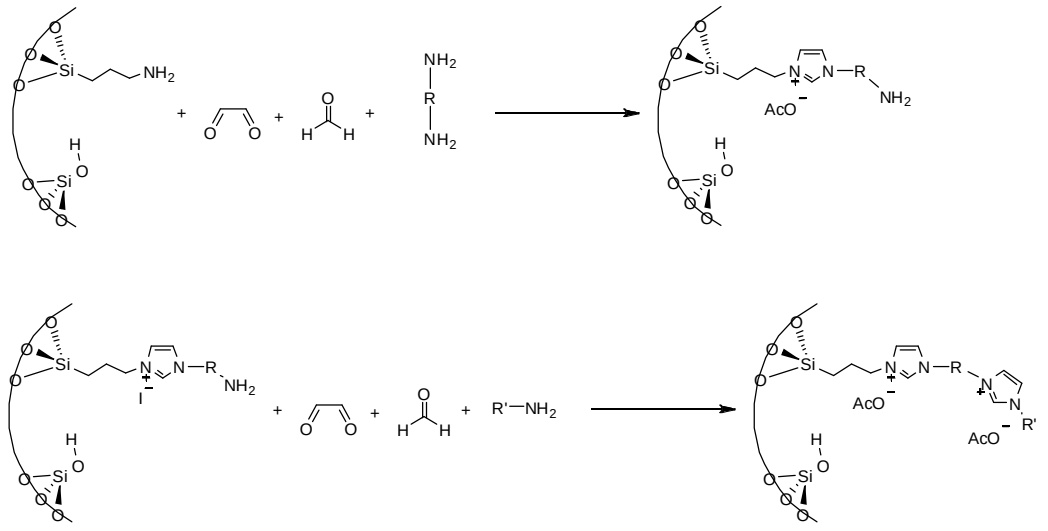

Scheme 2. Strategy for the formation of bis-imidazolium units

3.3.2. Formation of bis-imidazolium units with an ethyl linker

3.3.2.1. Reaction of material M-NH_{2-30} with ethylenediamine, formaldehyde and glyoxal

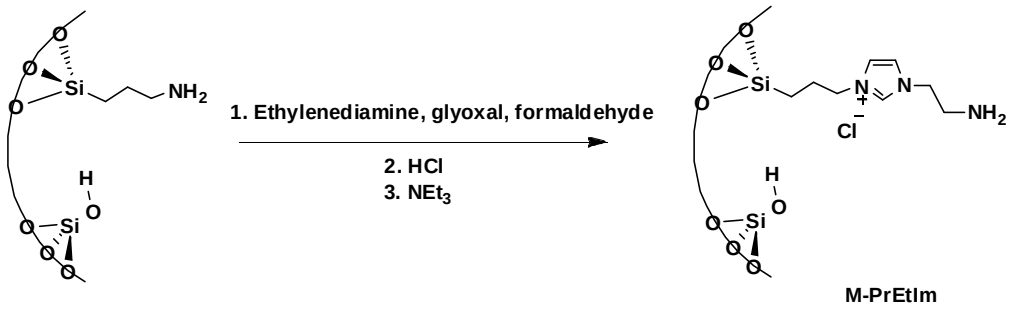

The material **M-NH_{2-30}** was contacted with 1.0 equiv. of 1,2-ethylenediamine, and 2 equiv. of glyoxal and formaldehyde to form material **M-PrEtIm**. This material was characterized by ^{13}C CPMAS solid-state NMR and the spectrum shows signals at 9, 23, 52, 125 and 140 ppm (See Figure 11). The peaks at 9 and 23 ppm correspond to the carbon atoms of the propyl tether in α and β position to the silicon atom respectively, and the two peaks at 125 and 140

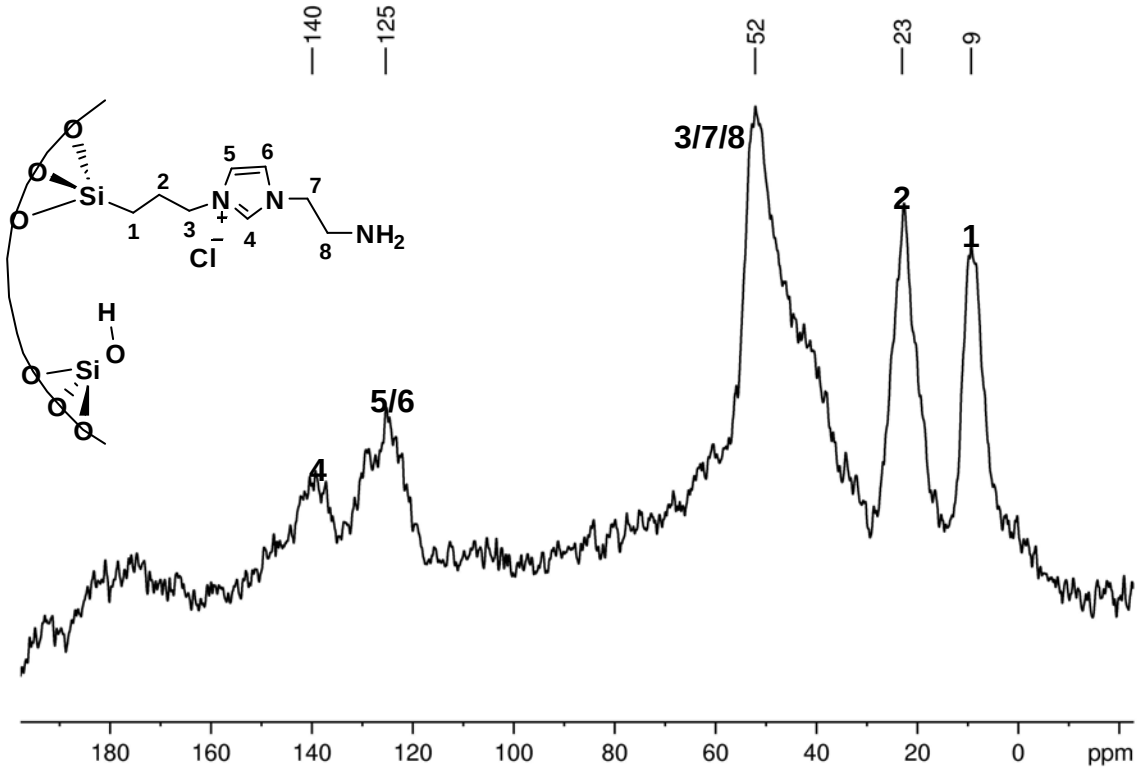

Figure 11. ^{13}C CPMAS solid-state NMR spectrum of **M-PrEtIm**

ppm are characteristic of the imidazolium unit, the first one corresponding to the two carbon atoms in position 5 and 6, whereas the latter corresponds to the carbon in position 4. The peak at 52 ppm, which shows a shoulder around 43 ppm, is including different signals, being mainly the three carbon atoms linked to nitrogen: two of them are directly bonded to the imidazolium unit , which should give a signal around 50 ppm and the third one is bonded to the NH_2 of the ethylenediamine group and would give a signal between 40 and 45 ppm. There are also probably some unreacted surface aminopropyl functionalities which would give a characteristic signal at 43 ppm, but the important intensity of the new peaks tells us that the conversion is almost quantitative. This method was therefore an efficient way to generate imidazolium units with a pendant amino group.

3.3.2.2. Reaction of material M-PrEtIm with mesityl amine, formaldehyde and glyoxal

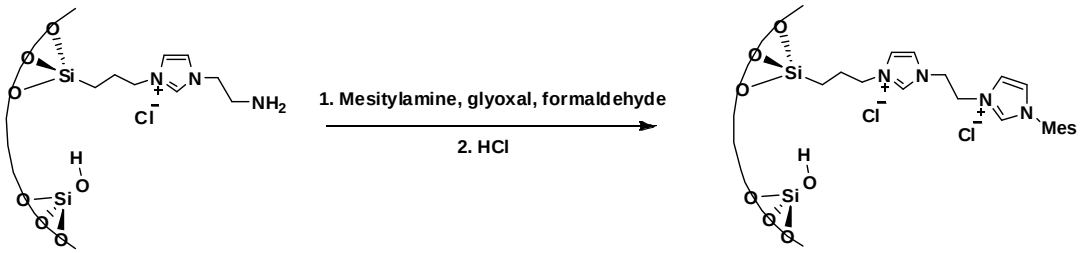

The reaction of material **M-PrEtIm** with 3 equivalents of mesityl amine, glyoxal and formaldehyde gives material **M-PrEtMesIm$_2$**. The ^{13}C CPMAS analysis gives signals at 10, 24, 53, 125, 130, 139 and 174 ppm (see Figure 12). The presence of the small signal at 174 ppm is probably due to the presence of oligomers or polymers of formaldehyde which can be formed during the synthesis, and which were not extracted from the material. The extraction procedure with pyridine/HCl[8] might be useful in this case to remove these impurities, but it was not investigated yet. The presence of a new peak at 130 ppm is characteristic of the presence of the mesityl group (CH of the aromatic ring) as well as the broadening of the peak at 24 ppm (CH_3 of mesityl). These signals can only be due to the reactivity of the NH_2 group from the ethyl linker to form a second imidazolium unit bearing a mesityl substituent. In DRIFT spectroscopy, an intense band appears at 1642 cm^{-1}, also consistent with the

formation of the imidazolium rings (see Figure A26). If we consider the yields of reactions obtained previously from elemental analyses (75% for the N_3 reduction and 70% for the imidazolium formation), there are 37% of the total functional groups bearing a bis-imidazolium unit (0.14 mmol/g) and 16% residual mono-imidazolium(0.045 mmol/g).

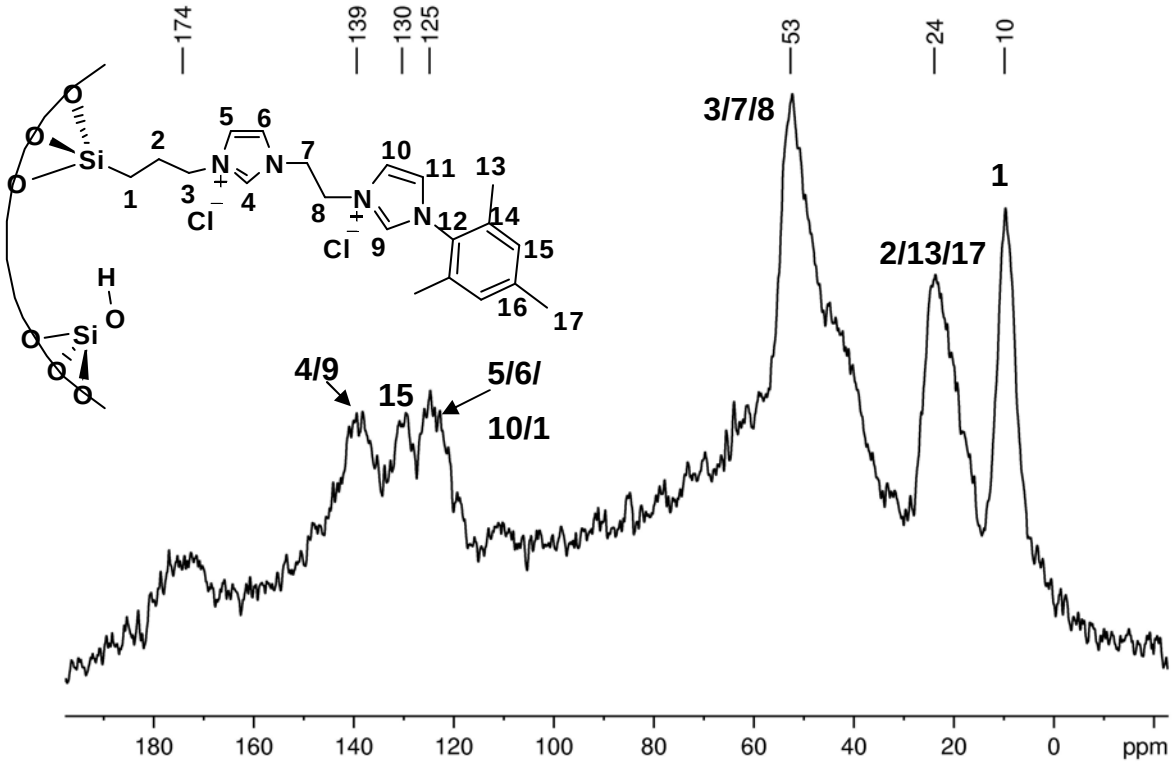

Figure 12. ^{13}C CPMAS solid-state NMR spectrum of **M-PrEtMesIm$_2$**

3.3.3. Formation of bis-imidazolium units having a pyridine linker

3.3.3.1. Reaction of material M-NH$_{2\text{-}30}$ with 2,6-diaminopyridine, formaldehyde and glyoxal

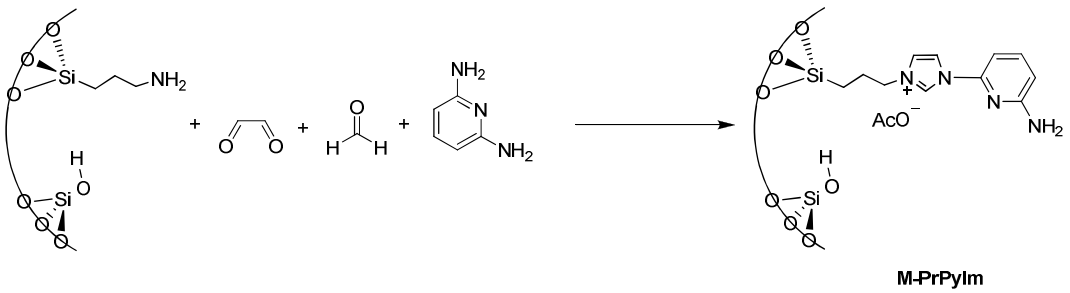

The reaction of material **M-NH$_{2\text{-}30}$** with 1.0 equiv. of 2,6-diaminopyridine, and 2 equiv. of glyoxal and formaldehyde allowed the formation of material **M-PrPyIm**. By ^{13}C CPMAS solid-state NMR, peaks at 7, 21, 50, 106, 121, 137, 155 and 174 ppm are observed (see

Figure 13). The peaks at 7, 21 and 50 ppm correspond to the three carbon atoms of the propyl tether. The absence of any signal at 43 ppm is already a proof that most NH_2 groups have reacted. The signals of the CH groups of the imidazolium ring are present at 121 and 137 ppm. We can thus attribute the three remaining signals at 106, 155 and 174 ppm to the carbon atoms of the pyridine ring in meta, para and ortho positions respectively. It is also important to notice that all aromatic signals are very broad and this can be explained by the fact that pyridine could interact with the silica surface and especially with the silanol surface groups. This interaction reduces dramatically the mobility and thus increases the chemical shift anisotropy of the corresponding carbon atoms, therefore leading to a broadening of the signals. By DRIFT spectroscopy, a broad signal is present at 1611 cm^{-1}, which corresponds to both aromatic signals of the pyridine, and planar vibration of the imidazolium unit (see Figure A28). Both DRIFT and NMR spectroscopy are therefore in agreement with the formation of the desired imidazolium unit.

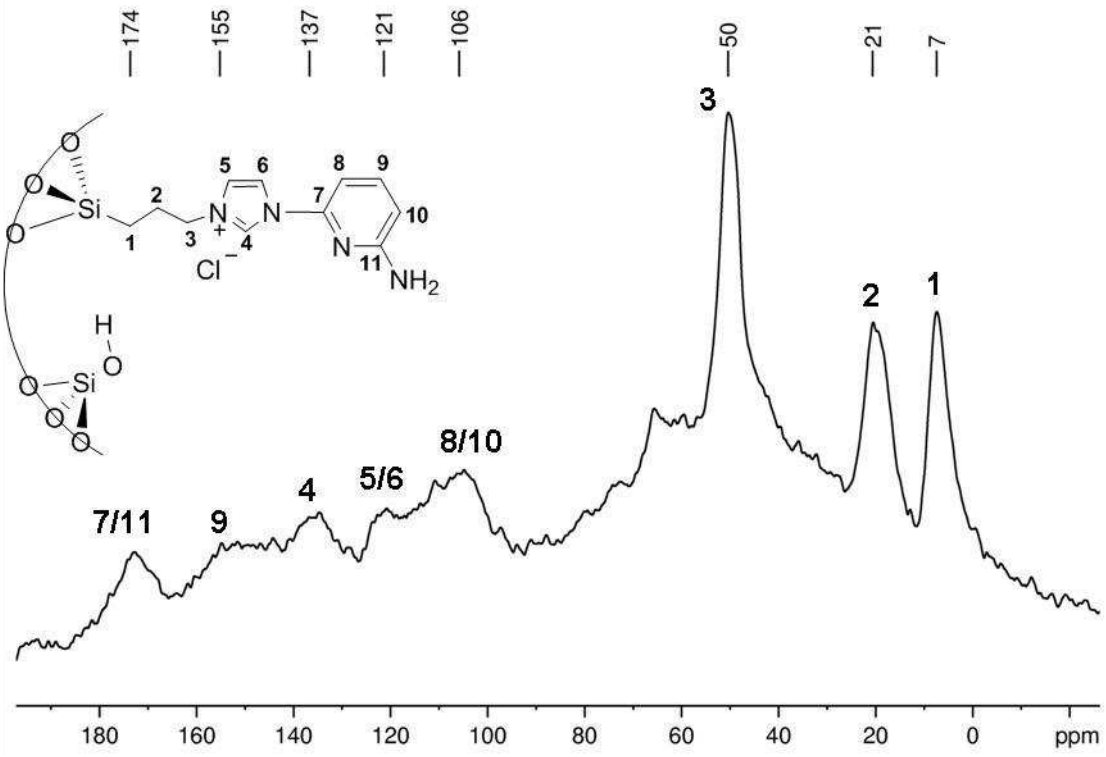

Figure 13. ^{13}C CPMAS solid-state NMR spectrum of **M-PrPyrIm**

3.3.3.2. Reaction of material M-PrPyIm with mesityl amine, formaldehyde and glyoxal

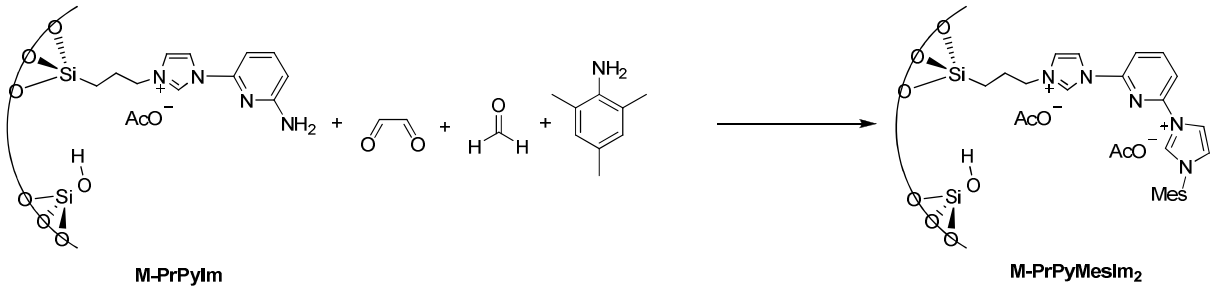

After reaction of material **M-PrPyIm** with mesityl-amine, glyoxal and formaldehyde, the ^{13}C CPMAS solid-state spectrum presents some modifications with that of the parent material (see Figure 14). In the aliphatic region, the peak at 50 ppm (corresponding to carbon 3) has decreased significantly but is still present, and there is a new peak at 45 ppm and the peak at 21 ppm is broader, probably because of the presence a new peak. In the aromatic

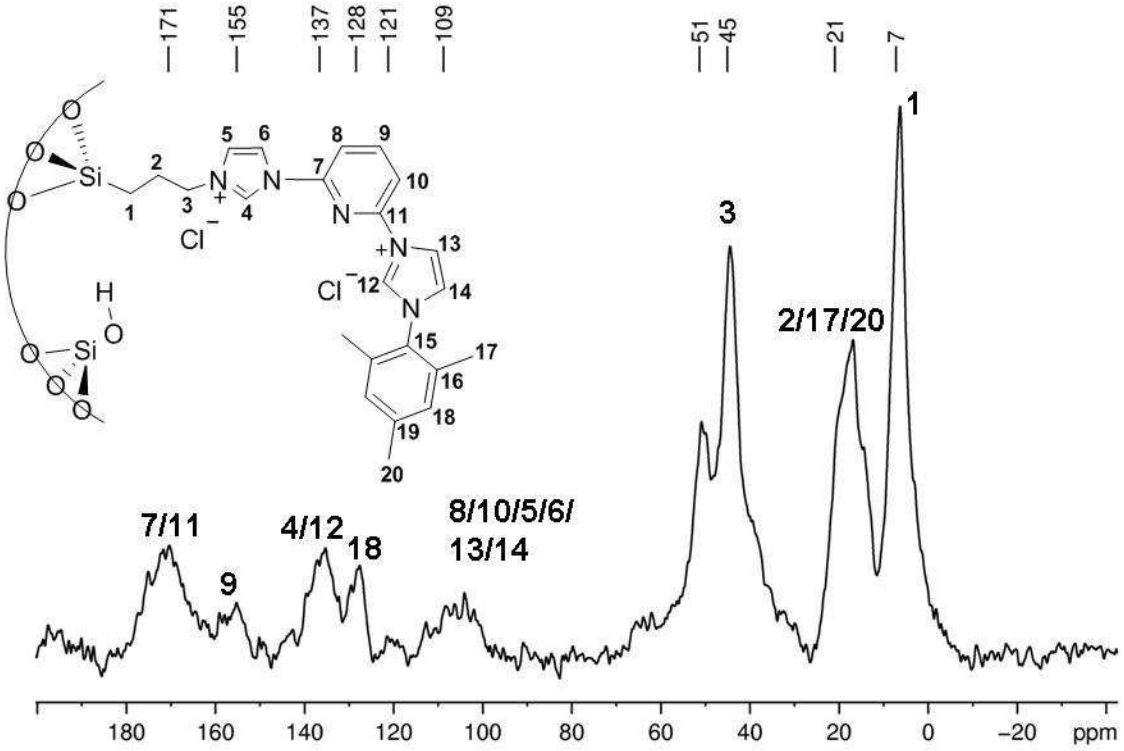

Figure 14. ^{13}C CPMAS solid-state NMR spectrum of **M-PrPyrMesIm$_2$**

region, most of the peaks remain unchanged, but there is a new peak at 128 ppm. The peak at 128 ppm can be attributed to aromatic CH of the mesityl ring, which is confirmed by the presence of a new peak around 21 ppm, corresponding to CH_3 of the mesityl group. The formation of the second imidazolium unit is confirmed undirectly by the change of chemical shift of the carbon 3 of the propyl chain, from 50 ppm to 45 ppm. However, this reaction is not complete, as we still see a significant quantity of the mono-imidazolium unit. In DRIFT spectroscopy, the formation of a new imidazolium unit is confirmed by an increase of the peak at 1617 cm^{-1} (see Figure A30). These results are in agreement with the partial formation of a propyl-pyridine-mesityl bis-imidazolium unit. The reaction needs to be optimized, as the presence of unreacted mono-imidazolium unit leads to two different possible coordination sites for the organometallic ruthenium precursor. As for the previous case, if we consider the yields of reactions obtained from elemental analyses (75% for the N_3 reduction and 70% for the imidazolium formation), we would have 37% of the total functional groups bearing a bis-imidazolium units (0.14 mmol/g) and 16% residual mono-imidazolium (0.045 mmol/g).

III-4. Conclusion

In this chapter, the formation of different amine-functionalized mesostructured materials was described. By using 3-tert-butyloxycarbonylaminopropyl and iodopropyl groups, it is possible under our reaction conditions to obtain hybrid materials with 1/30 dilution ratios with respect to TEOS, leading to primary amines and secondary amines respectively. However, as these two methods did not allow us to prepare more concentrated materials, another method was developed starting from an azidopropyl-functionalised material. This material could be obtained in a range of dilution from 1/30 to 1/12. The primary amine can then be quantitatively formed with a Staudinger reaction using dimethylphenylphosphine as the reactant. Using appropriate conditions, it is therefore possible to get amine-functionalised materials with concentrations up to 1.2 mmol/g.

The accessibility of all organic groups was evidenced by an amidation reaction on both primary and secondary amine-based materials, using an ester as reagent and catalyzed by 2-hydroxypyridine. The quantitative formation of the amide bond was proved by both ^{13}C NMR and DRIFT spectroscopy. In addition, aminopropyl-based materials obtained from azide proved to be very useful supports for the synthesis of imidazole- and imidazolium-functionalized hybrid mesoporous materials in different concentrations up to ca. 0.6 mmol/g. Typically, propyl-benzyl imidazolium, propyl-mesityl-imidazolium and propylimidazole were quantitatively formed *in situ*, using glyoxal, formaldehyde and either a primary amine or ammonium acetate. It was then possible to form bis-imidazolium units by the use of similar reaction conditions, via the subsequent formation of two imidazolium units. Here was described the formation of two bis-imidazolium groups having either an ethyl or a pyridine linker. Although these syntheses need to be optimised to get 100% of the desired surface bis-imidazolium units, these results are very promising for the formation of supported bis-NHC metal complexes. Overall, the amine materials open the way to a large diversity of new hybrid materials.

III-5. Experimental Part

General procedure. All experiments related to surface-modifications were carried out under an inert atmosphere of argon. 3-tert-Butyloxycarbonylaminopropyltriethoxysilane,[2] 3-iodopropyltriethoxysilane[3] and 3-azidopropyltriethoxysilane[5] were synthesized according to literature procedures. Dimethylphenylphosphine, glyoxal solution, formaldehyde solution, mesityl amine, benzyl amine, ethylenediamine and 2,6-diaminopyridine were purchased from Aldrich. ^{1}H and ^{13}C, solid state NMR spectra were recorded on a Bruker Avance 500 (500MHz) and a Bruker DSX 300 (300MHz). ^{1}H solid state spectra were recorded using Magic Angle Spinning (MAS) at 10 kHz. ^{13}C solid state spectra were recorded using Cross Polarization with D1 of 2s, p15 of 2 ms, around 30000 scans and MAS at 10 kHz . Elemental analysis were performed at the "Mikroanalytisches Labor Pascher", Remagen, Germany. Nitrogen adsorption-desorption experiments at 77K were performed on an ASAP 2020 Micromeritics system. DRIFT spectra were recorded on a Thermo Scientific Nicolet 6700 FT-IR spectrometer.

Preparation of M-NHBoc. 4.1 g of P123 dissolved in an aqueous HCl solution (164 mL, pH ≈ 1.5) was added in a mixture of TEOS (8.62 g, 41.38 mmol) and 3-tert-Butyloxycarbonylaminopropyltriethoxysilane (0.44 g, 1.38 mmol) at room temperature. The reaction mixture was stirred for 90 min giving rise to a micro-emulsion (transparent mixture). To the reaction mixture heated at 45 °C, a small amount of NaF (77 mg, 1.83 mmol) was added under stirring (composition of the mixture: 0.04 F^- : 1 TEOS: 0.033 of 3-tert-Butyloxycarbonylaminopropyltriethoxysilane: 0.016 P123: 0.12 HCl: 220 H_2O). The mixture was left at 45°C under stirring for 72 h. The resulting solid was filtered and washed three times with 100 mL water and three times with 100 mL acetone. The surfactant was removed by an extraction with ethanol using a Soxhlet during 48 h. After filtration and drying at 135 °C under vacuum (10^{-5} mbar), **M-NHBoc$_{-30}$** was obtained as a white solid. ^{1}H solid state NMR (500 MHz): 1.1, 3.7 ^{13}C CP-MAS solid state NMR: 15, 22, 26, 42, 58 and 156 ppm.

Preparation of M-NH_2. 2 g of **M-NHBoc** is put in a 100 mL round-bottom flask with 40 mL of a 6M HCl solution and the suspension is heated up to 100℃ and stirred for 17 hours. The resulting material is filtered and washed several times with water. The resulting material is put in suspension in a solution containing 5 mL triethylamine and 25 mL dichloromethane for one hour. After filtration, it is washed three times with 70 mL ethanol, and three times with 70 mL diethylether. After drying under high vacuum (10^{-5} mbar) at 135℃ for 17 hours, **M-$NH_{2\text{-}30}$** is obtained as a white solid. ^{1}H solid state NMR (500 MHz): 1.0, 1.7, 3.7 ppm. ^{13}C CP-MAS solid state NMR: 8, 15, 24, 42 and 58 ppm.

Preparation of M-IPr. 4.24 g of P123 dissolved in an aqueous HI solution (170 mL, pH ≈ 1.5) was added in a mixture of TEOS (8.91 g, 42.79 mmol) and 3-iodopropyltriethoxysilane (0.47 g, 1.43 mmol) at room temperature. The reaction mixture was stirred for 90 min giving rise to a micro-emulsion (transparent mixture). To the reaction mixture heated at 45 ℃, a small amount of NaF (80 mg, 1.90 mmol) was added under stirring (composition of the mixture: 0.04 F^- : 1 TEOS: 0.033 of 3-iodopropyltriethoxysilane: 0.016 P123: 0.12 HI: 220 H_2O). The mixture was left at 45℃ under stirring for 72 h. T he resulting solid was filtered and washed three times with 100 mL water and three times with 100 mL acetone. The surfactant was removed by an extraction with ethanol using a Soxhlet during 48 h. After filtration and drying at 135 ℃ under vacuum (10^{-5} mbar), **M-IPr$_{\text{-}30}$** was obtained as a white solid.

Preparation of M-NHBz. A mixture of 1g **M-IPr**, 1g benzylamine and 0.5g of triethylamine in 20 mL of toluene is heated to reflux for 24h. After filtration, the material is washed two times with hot toluene to remove triethylammoniumiodide. It is then washed two times with 100 mL acetone and two times with 100 mL diethylether. After drying at 135℃ under vacuum (10^{-5} mbar), **M-NHBz** is obtained as a white powder. ^{1}H solid state NMR (500 MHz): 0.1, 1.3, 1.7, 3.2, 7.1 ppm. ^{13}C CP-MAS solid state NMR: 0, 7, 16, 21, 26, 52, 70, 128, 139 ppm.

Preparation of material M-$N_{3\text{-}12}$. 3.80 g of P123 dissolved in an aqueous HCl solution (152 mL, pH ≈ 1.5) was added in a mixture of TEOS (8.30 g, 39.86 mmol) and 3-azidopropyltriethoxysilane (1.10 g, 4.43 mmol) at room temperature. The reaction mixture was stirred for 3 h giving rise to a micro-emulsion (transparent mixture). To the reaction mixture heated at 45 °C, a small amount of NaF (74 mg, 1.77 mmol) was added under stirring (composition of the mixture: 0.04 F^- : 1 TEOS: 0.111 of 3-azidopropyltriethoxysilane: 0.016 P123: 0.12 HCl: 220 H_2O). The mixture was left at 45°C under stirring for 72 h. The resulting solid was filtered and washed three times with 100 mL water and three times with 100 mL acetone. The surfactant was removed by an extraction with ethanol using a Soxhlet during 48 h. After filtration and drying at 135 °C under vacuum (10^{-5} mbar), **M-$N_{3\text{-}12}$** was obtained as a white solid. ^{1}H solid state NMR (500 MHz): 1.0, 1.7, 3.1, 3.7 ppm. ^{13}C CP-MAS solid state NMR: 8, 16, 21, 53, 53 ppm.

Preparation of material M-$NH_{2\text{-}12}$. 1mL of PMe_2Ph in solution in 10 mL of dry THF is added to 1g of material **M-$N_{3\text{-}12}$** and the suspension is stirred for 24 h at room temperature. It is then filtered, and the product washed with THF. The resulting material is put in suspension in a mixture of 1mL water and 10mL THF and stirred for an additional 17 h. It is then filtered, washed 3 times with 100 mL acetone and three times with 100 mL methanol. The remaining phosphine oxide was removed by an extraction with methanol using a Soxhlet during 48 h. After filtration and drying at 135 °C under vacuum (10^{-5} mbar), **M-$NH_{2\text{-}12}$** was obtained as a white solid. ^{1}H solid state NMR (500 MHz): 1.4, 1.9, 2.9 ppm. ^{13}C CP-MAS solid state NMR: 8, 24, 43, 52 ppm.

Preparation of material M-NHAm. To a suspension of 300mg **M-NH_2** in 10 mL m-xylene is added 1g ethylhydrocinnamate and 145 mg of 2-hydroxypyridine. The round-bottom flask is equipped with a Dean Stark to separate ethanol formed. It is then heated to reflux, and stirred for 24 h. After filtration, the material is washed 4 times with 100 mL acetone and once

with 100 mL ethanol. After drying at 135°C under vacuum (10-5 mbar), **M-NHAm** is obtained as a white powder. ^{1}H solid state NMR (500 MHz): 1.7, 4.4, 7.8 ppm. ^{13}C CP-MAS solid state NMR: 8, 15, 22, 31, 37, 41, 58, 124, 128, 140, 173 ppm.

Preparation of material M-NBzAm$_{-30}$. The procedure is the same as for material **M-NHAm**, using **M-NHBz$_{-30}$** instead of **M-NH$_2$**. **M-NBzAm** is obtained as a white powder. ^{1}H solid state NMR (500 MHz): 1.0, 3.7, 7.0 ppm. ^{13}C CP-MAS solid state NMR: 7, 16, 20, 34, 50, 127, 138 ppm.

Preparation of material M-PrIm$_{12}$. In a round-bottom flask, 1g of material **M-NH$_{2-12}$** is put in suspension in 10 mL acetic acid, and then is added 1.8 g ammonium acetate, 0.7 mL water, 3.4g of glyoxal solution (40% in water) and 1.9g formaldehyde solution (37% in water). The suspension is heated up to 70°C and stirred overnight (18 hours). The product was filtered, washed with water (3 x 100 mL) and methanol (3 x 100 mL). It was subsequently treated overnight with pyridine/HCl solution at 70°C. It was then washed with water (3 x 100 mL), triethylamine (5mL in 25mL of CH_2Cl_2, to deprotonate the imidazole), acetone (2 x 100 mL) and diethyl ether (2 x 100 mL). After drying at 135°C under vacuum (10^{-5} mbar), **M-PrIm$_{-12}$** is obtained as a light orange powder. ^{1}H solid state NMR (500 MHz): 1.2, 1.8, 3.4, 6.9, 7.5 ppm. ^{13}C CP-MAS solid state NMR: 136, 126, 117, 48, 22, 8 ppm.

Preparation of material M-PrBzIm$_{-12}$ via M-PrIm$_{-12}$. In a schlenck charged with 500 mg of material M-PrIm-12 is added 10 mL dry toluene and 1.5 g benzyl chloride. It is then heated to reflux at 110°C and stirred overnight (18 hours) under a flow of argon. The product is filtered, washed with toluene (2 x 50 mL) and acetone (2 x 50 mL). It was subsequently treated with 2M HCl solution at 45°C for 2 hours. After filtration, it was washed with water (3 x 100 mL), acetone (2 x 100 mL) and diethyl ether (2 x 100 mL). After drying at 135°C under vacuum (10^{-5} mbar), **M-PrBzIm$_{-12}$** is obtained as a light orange powder. ^{1}H solid state NMR (500 MHz): 1.9, 7.5 ppm. ^{13}C CP-MAS solid state NMR: 134, 128, 120, 51, 21, 8 ppm.

Preparation of material M'-PrBzIm$_{-12}$ directly from M-NH$_{2-12}$. In a schlenck, 1g of material M-NH$_{2-12}$ is put in suspension in a degassed solution with 10 mL acetic acid, 3.4g of glyoxal solution (40% in water) and 1.9g formaldehyde solution (37% in water). Then benzyl amine is added (2.5 mL). The suspension is heated up to 70°C and stirred overnight (18 hours). The product was filtered, washed with water (3 x 100 mL) and methanol (3 x 100 mL). It was subsequently treated with 2M HCl solution at 45°C for 2 hours. It was then washed with water (3 x 100 mL), acetone (2 x 100 mL) and diethyl ether (2 x 100 mL). After drying at 135°C under vacuum (10^{-5} mbar), **M'-PrIm$_{-12}$** is obtained as a light orange powder. ^{1}H solid state NMR (500 MHz): 1.9, 2.3, 7.4 ppm.^{13}C CP-MAS solid state NMR: 134, 128, 122, 51, 41, 21, 8 ppm.

Preparation of material M-PrMesIm$_{-12}$. In a schlenck, 1g of material M-NH$_{2-12}$ is put in suspension in 10 mL degassed acetic acid. Then are added 0.50 mL of glyoxal solution (40% in water), 0.67 mL mesitylamine and 0.28 mL formaldehyde solution (37% in water). The suspension is heated up to 70°C and stirred overnight (18 hours). The product was filtered (hot filtration is better), washed with water (3 x 100 mL) and methanol (3 x 100 mL). The coloured by-products were removed in the majority by an extraction with methanol using a Soxhlet during 8 hours and a subsequent overnight treatment with a Pyridine/HCl solution at 70°C. It was then washed with water (3 x 100 mL), acetone (2 x 100 mL) and diethyl ether (2 x 100 mL). After drying at 135°C under vacuum (10^{-5} mbar), **M-PrMesIm$_{-12}$** is obtained as a light beige powder. ^{1}H solid state NMR (500 MHz): 1.7, 7.1 ppm. ^{13}C CP-MAS solid state NMR: 140, 130, 122, 51, 41, 20, 15, 8 ppm.

Preparation of material M-PrEtIm$_{-30}$. In a schlenck, 1g of material **M-NH$_{2-30}$** is put in suspension in 10 mL degassed acetic acid. Then are added 0.15 mL of glyoxal solution (40% in water), 34.5 µL ethylenediamine (1.0 eq) and 0.08 mL formaldehyde solution (37% in

water). The suspension is heated up to 70°C and stirred overnight (18 hours). The product was filtered (hot filtration is better), washed with water (3 x 100 mL) and methanol (3 x 100 mL). The coloured by-products were removed in the majority by an extraction with methanol using a Soxhlet during 8 hours and a subsequent overnight treatment with a Pyridine/HCl solution at 70°C. It was then washed with water (3 x 100 mL), acetone (2 x 100 mL) and diethyl ether (2 x 100 mL). After drying at 135°C under vacuum (10^{-5} mbar), **M-PrPyIm$_{-30}$** is obtained as a light beige powder. ^{1}H solid state NMR (500 MHz): 1.7, 3.5, 6.9 ppm. ^{13}C CP-MAS solid state NMR: 140, 125, 52, 23, 9 ppm.

Preparation of material M-PrEtMesIm$_{2-30}$. In a schlenck, 1g of material **M-PrEtIm$_{-30}$** is put in suspension in 10 mL degassed acetic acid. Then are added 0.50 mL of glyoxal solution (40% in water), 0.67 mL mesitylamine and 0.28 mL formaldehyde solution (37% in water). The suspension is heated up to 70°C and stirred overnight (18 hours). The product was filtered (hot filtration is better), washed with water (3 x 100 mL) and methanol (3 x 100 mL). The coloured by-products were removed in the majority by an extraction with methanol using a Soxhlet during 8 hours and a subsequent overnight treatment with a Pyridine/HCl solution at 70°C. It was then washed with water (3 x 100 mL), acetone (2 x 100 mL) and diethyl ether (2 x 100 mL). After drying at 135°C under vacuum (10^{-5} mbar), **M-PrEtMesIm$_{2-30}$** is obtained as a light orange powder. ^{1}H solid state NMR (500 MHz): 1.7, 3.5, 6.8 ppm. ^{13}C CP-MAS solid state NMR: 139, 130, 125, 53, 24, 10 ppm.

Preparation of material M-PrPyIm$_{-30}$. In a schlenck, 1g of material **M-NH$_{2-30}$** is put in suspension in 10 mL degassed acetic acid. Then are added 0.15 mL of glyoxal solution (40% in water), 56 mg 2,6-diaminopyridine (1.0 eq) and 0.08 mL formaldehyde solution (37% in water). The suspension is heated up to 70°C and stirred overnight (18 hours). The product was filtered (hot filtration is better), washed with water (3 x 100 mL) and methanol (3 x 100 mL). The coloured by-products were removed in the majority by an extraction with methanol

using a Soxhlet during 8 hours and a subsequent overnight treatment with a Pyridine/HCl solution at 70°C. It was then washed with water (3 x 100 mL), acetone (2 x 100 mL) and diethyl ether (2 x 100 mL). After drying at 135°C under vacuum (10^{-5} mbar), **M-PrPyIm$_{-30}$** is obtained as a light orange powder. ^{1}H solid state NMR (500 MHz): 0, 1.8 ppm. ^{13}C CP-MAS solid state NMR: 7, 21, 50, 106, 121, 137, 155, 174 ppm.

Preparation of material M-PrPyMesIm$_{2-30}$. In a schlenck, 1g of material **M-PrPyIm$_{-30}$** is put in suspension in 10 mL degassed acetic acid. Then are added 0.50 mL of glyoxal solution (40% in water), 0.67 mL mesitylamine and 0.28 mL formaldehyde solution (37% in water). The suspension is heated up to 70°C and stirred overnight (18 hours). The product was filtered (hot filtration is better), washed with water (3 x 100 mL) and methanol (3 x 100 mL). The coloured by-products were removed in the majority by an extraction with methanol using a Soxhlet during 8 hours and a subsequent overnight treatment with a Pyridine/HCl solution at 70°C. It was then washed with water (3 x 100 mL), acetone (2 x 100 mL) and diethyl ether (2 x 100 mL). After drying at 135°C under vacuum (10^{-5} mbar), **M-PrPyMesIm$_{2-30}$** is obtained as a light orange powder. ^{1}H solid state NMR (500 MHz): 1.2, 1.7, 2.9, 7.0 ppm. ^{13}C CP-MAS solid state NMR: 171, 155, 137, 128, 121, 109, 51, 45, 21, 7 ppm.

III-6. References

[1] D. J. Macquarrie *Chem. Commun.* **1996**, 1961-1962.
[2] A. Mehdi; C. Reye; S. Brandes; R. Guilard; R. J. P. Corriu *New J. Chem.* **2005**, *29*, 965-968.
[3] J. Alauzun; A. Mehdi; C. Reye; R. Corriu *New J. Chem.* **2007**, *31*, 911-915.
[4] A. J. Arduengo, US Patent 5077414, **1991**.

[5] J. Nakazawa; T. D. P. Stack *J. Am. Chem. Soc.* **2008**, *130*, 14360-14361.
[6] H. Staudinger; E. Hauser *Helvetica Chimica Acta* **1921**, *4*, 861-886.
[7] H. T. Openshaw; N. Whittaker *Journal of the Chemical Society C: Organic* **1969**, 89-91.

III-7. Appendix

M-NHBoc

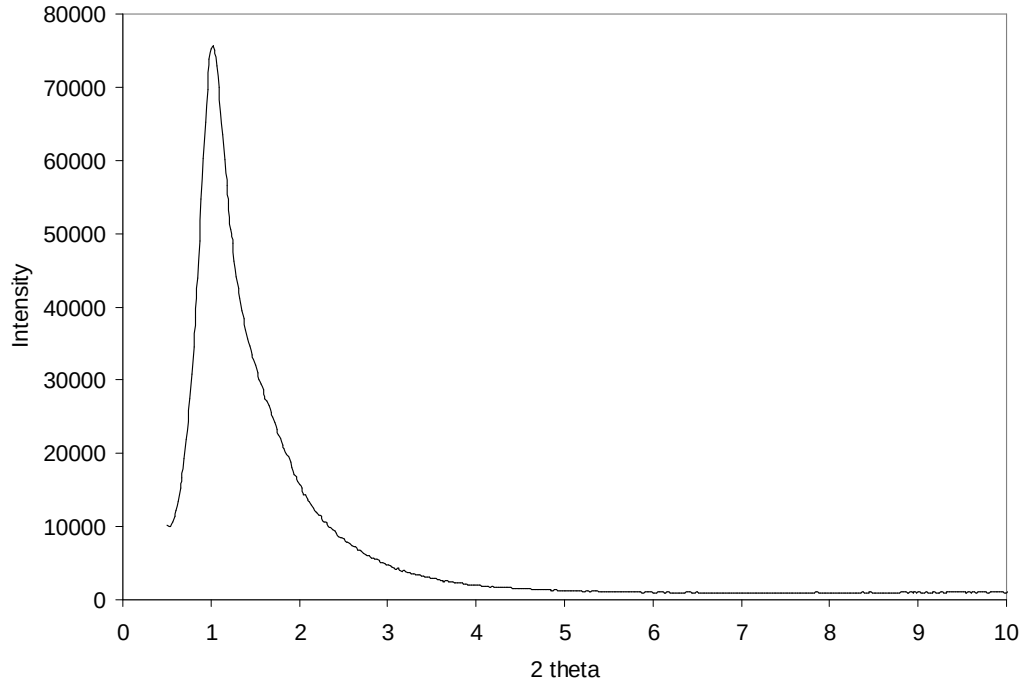

Figure A1. Low angle X-Ray diffraction on material **M-NHBoc**

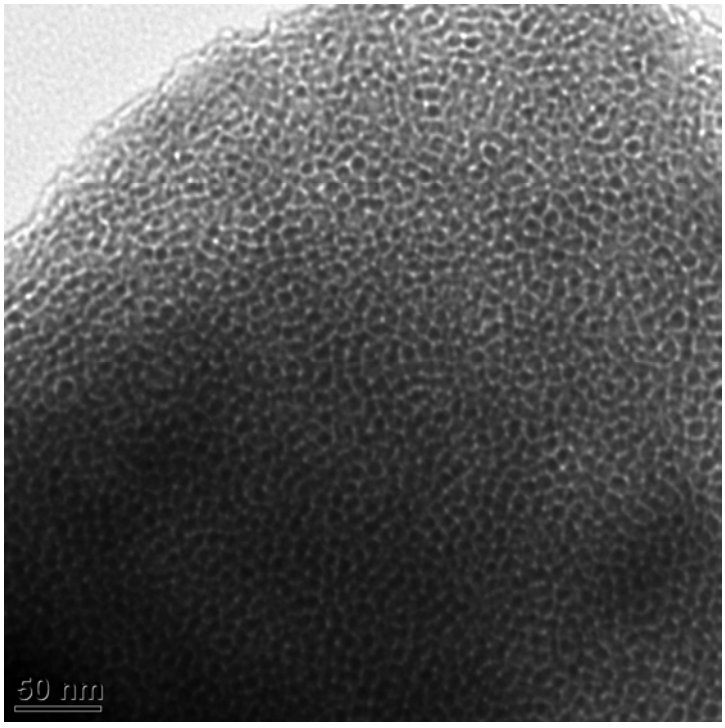

Figure A2. TEM picture of material **M-NHBoc**

M-NH$_2$ and **M-NHBoc**

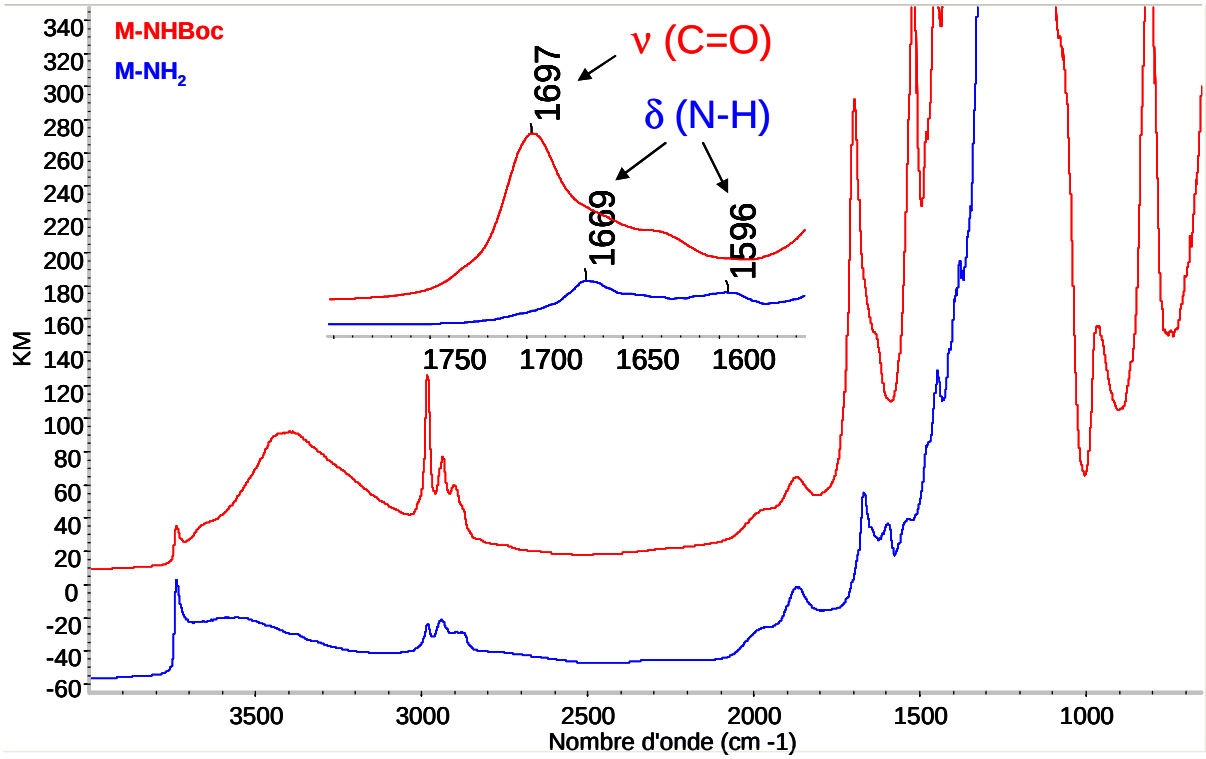

Figure A3. DRIFT spectra of materials **M-NHBoc** (red) and **M-NH$_2$** (blue)

M-NHBz

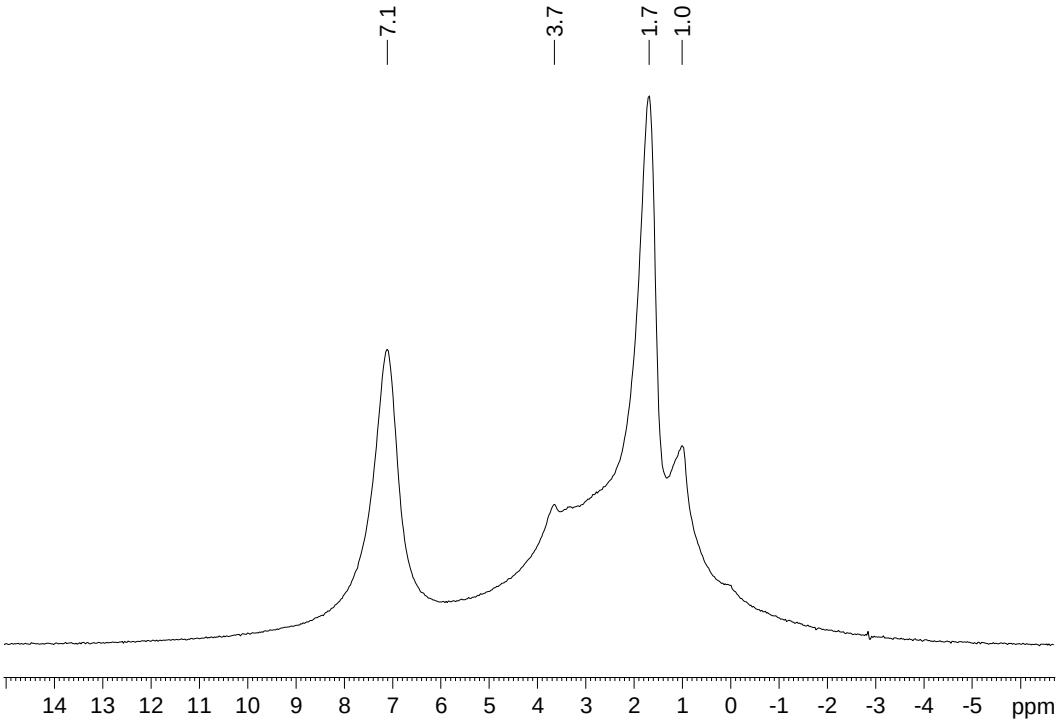

Figure A4. ^{1}H MAS solid-state NMR of **M-NHBz**

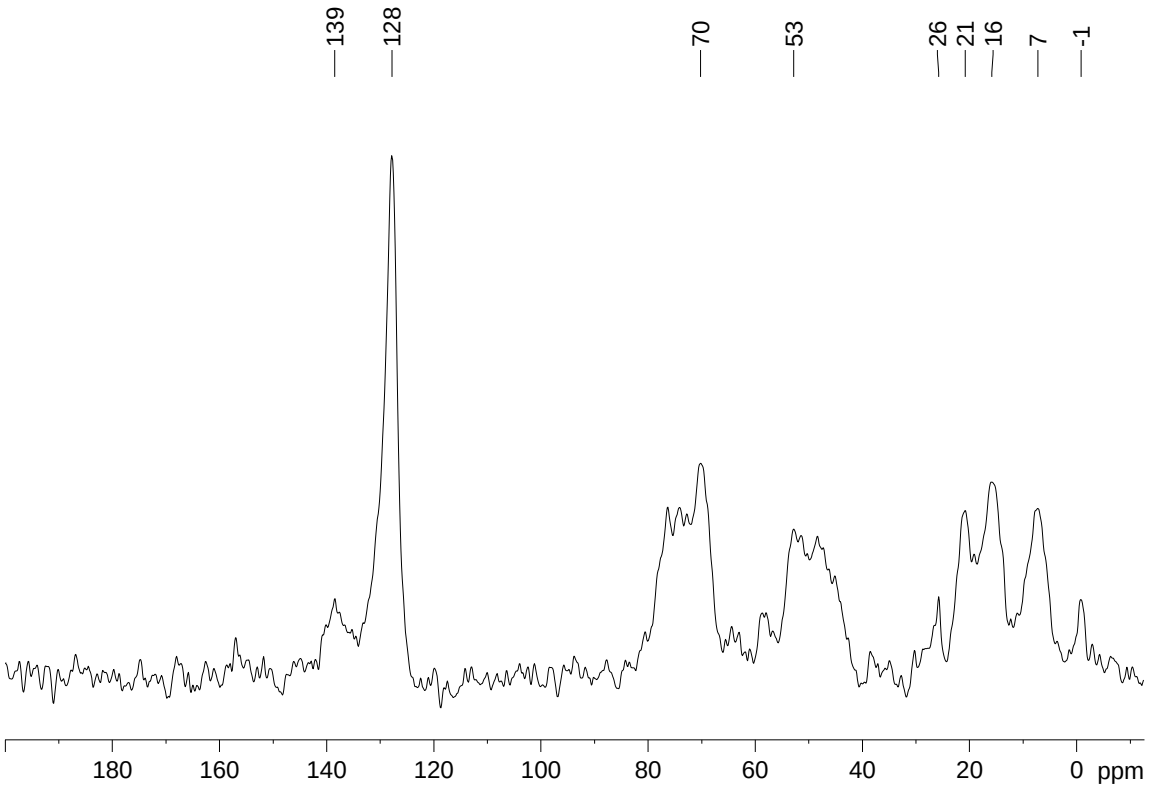

Figure A5. ^{13}C CPMAS NMR spectrum of **M-NHBz**

M-N_{3-x}

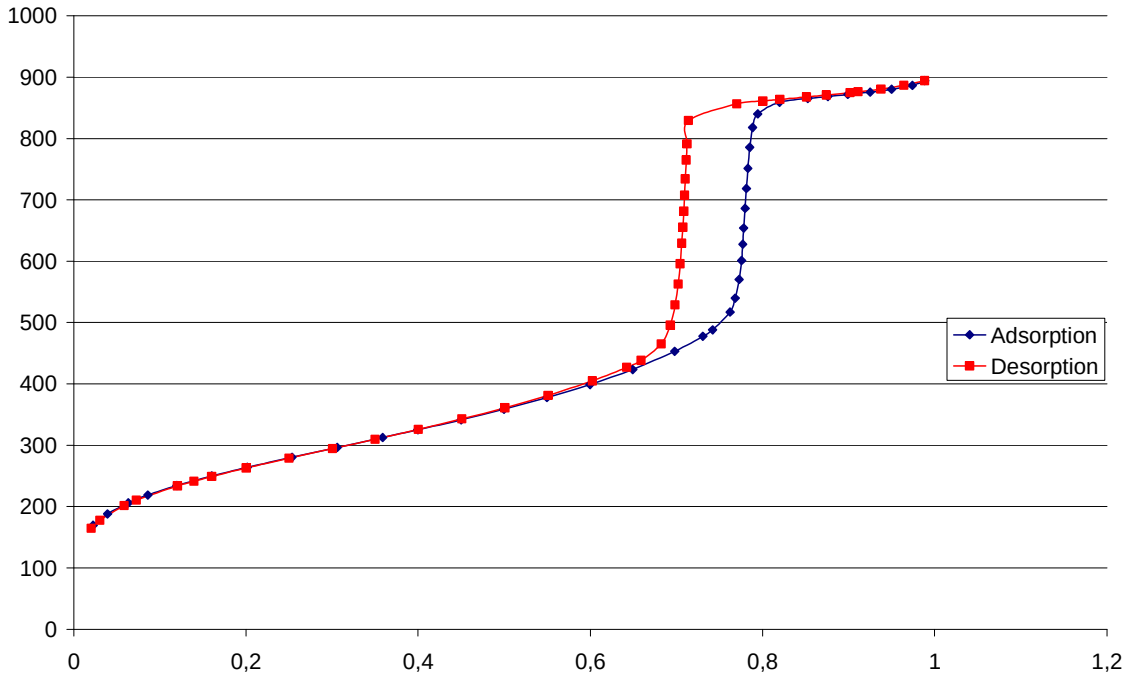

Figure A6. N_2 adsorption-desorption isotherm at 77K of **M-N_{3-30}**

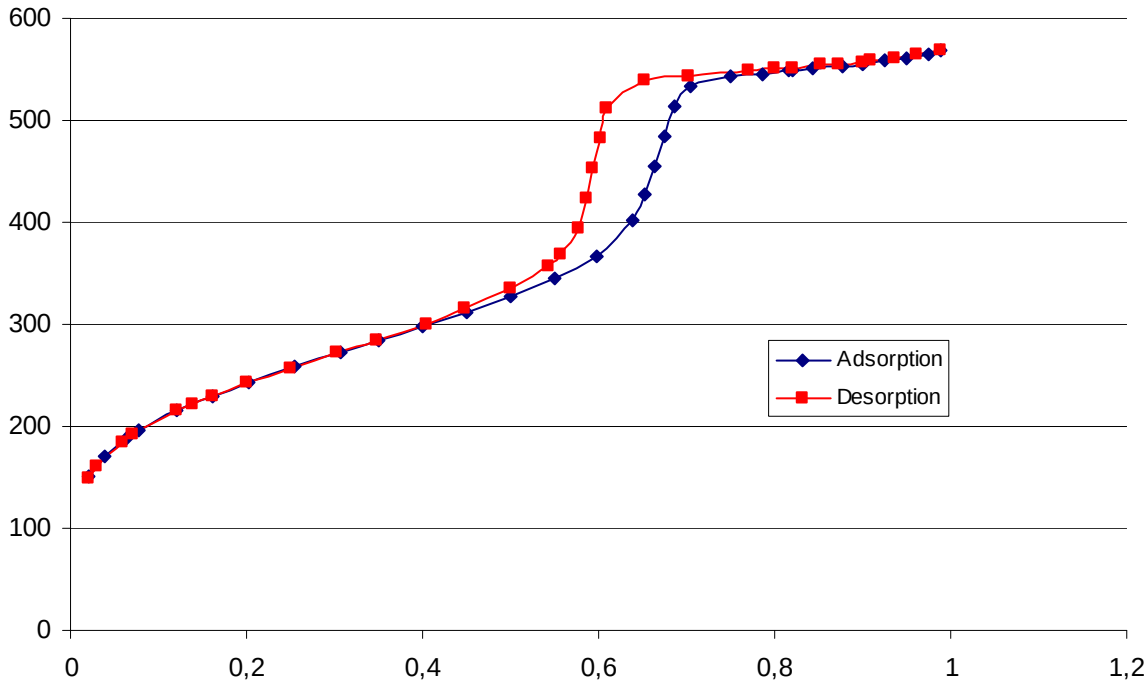

Figure A7. N_2 adsorption-desorption isotherm at 77K of **M-N_{3-12}**

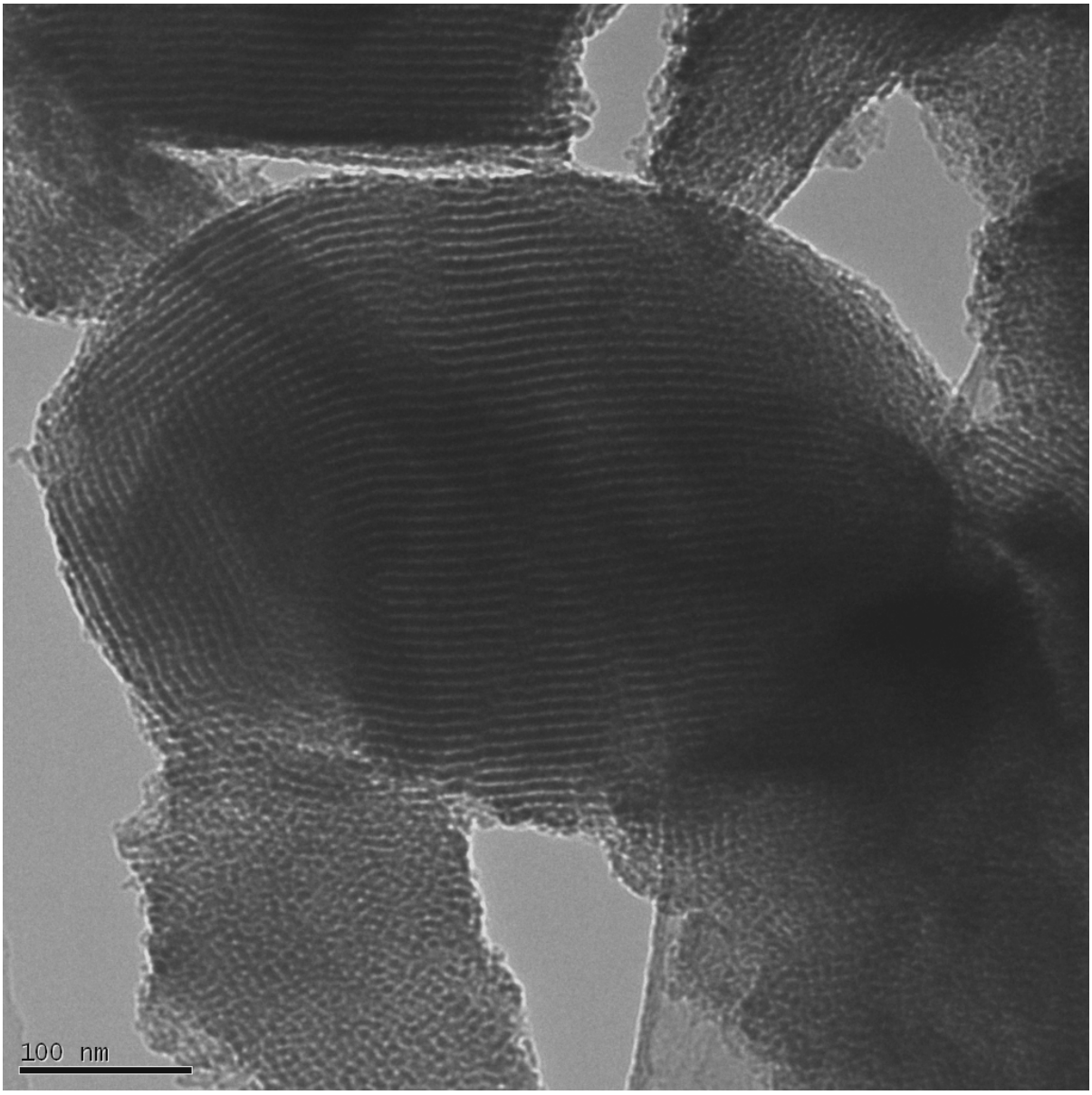

Figure A8. TEM picture of **M-N$_{3\text{-}12}$**

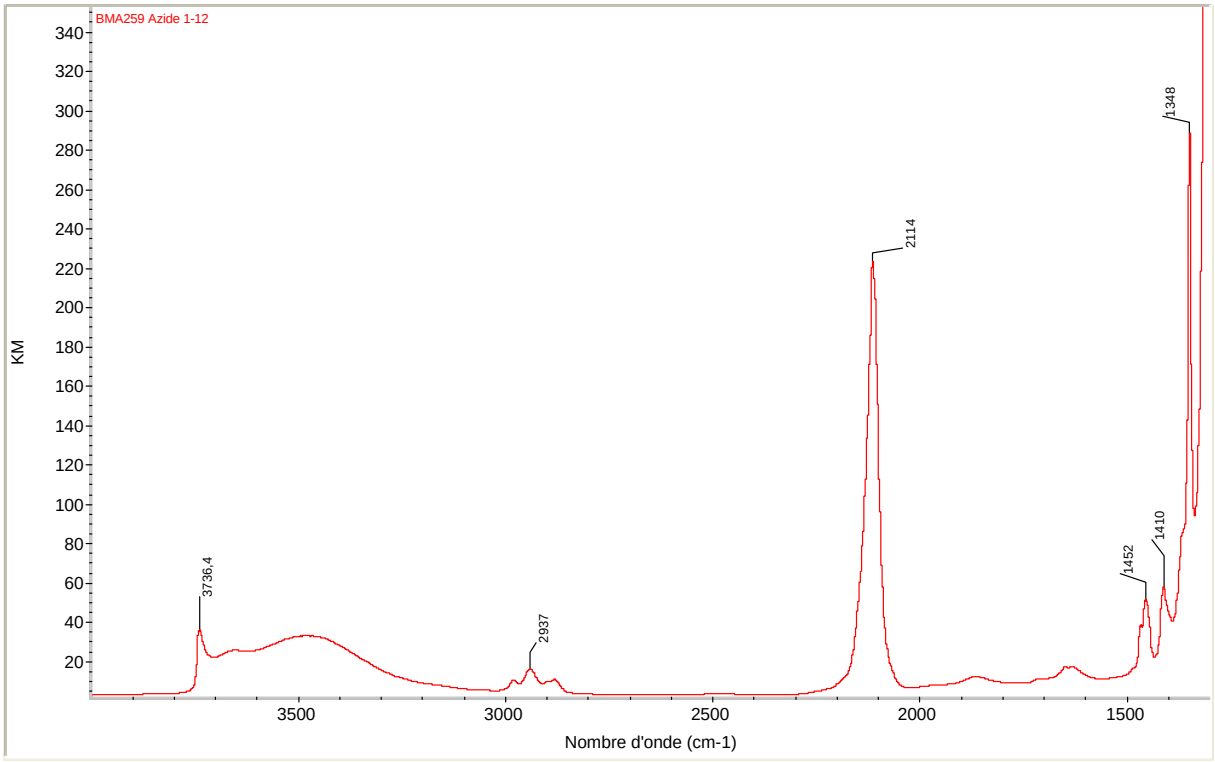

Figure A9. DRIFT spectrum of **M-N_{3-12}**

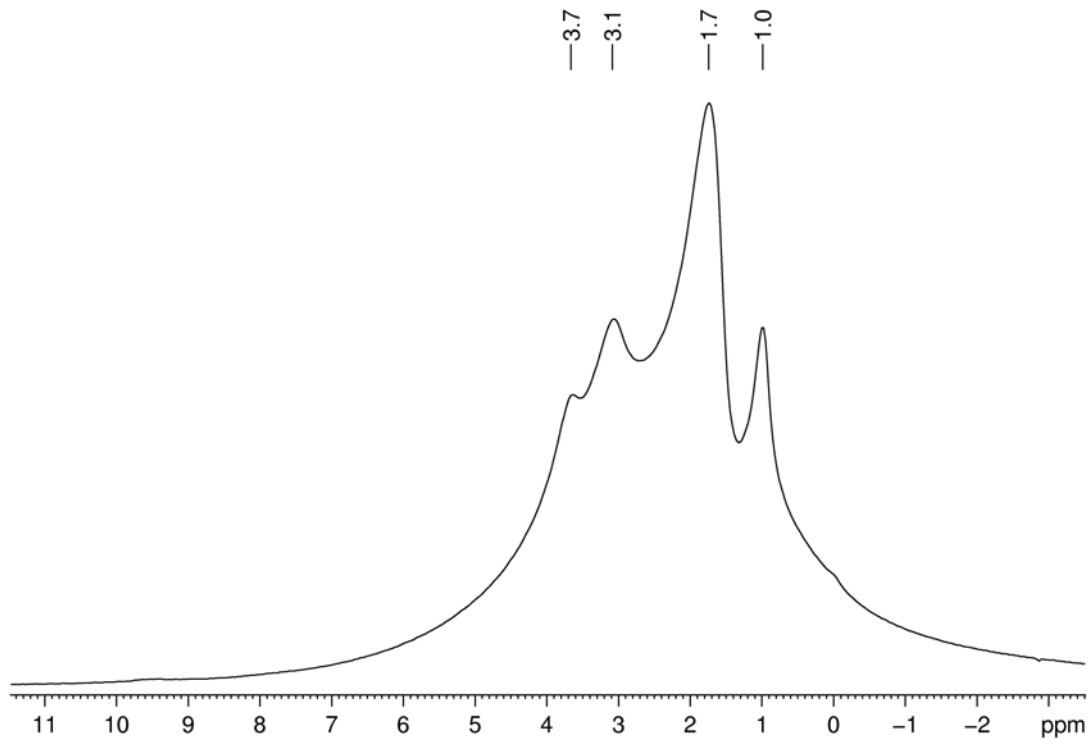

Figure A10. ^{1}H MAS solid-state NMR of **M-N_{3-12}**

M-NH$_{2\text{-}12}$

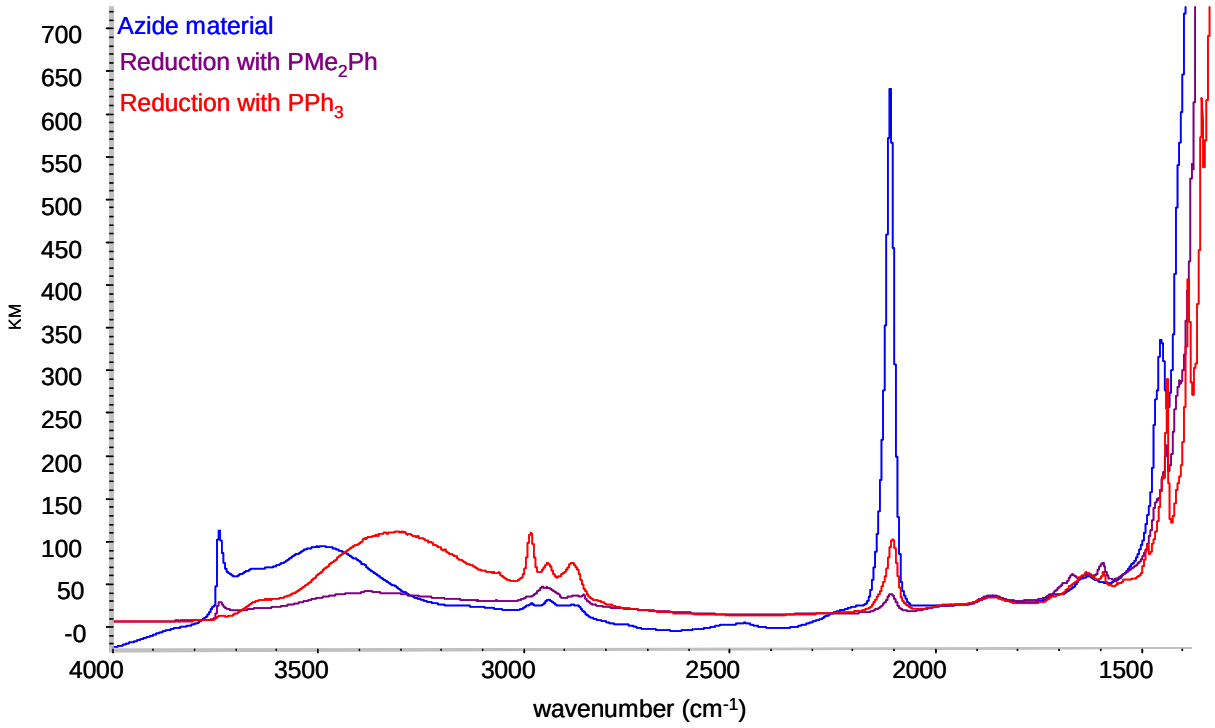

Figure A11. DRIFT spectrum of **M-NH$_{2\text{-}19}$**

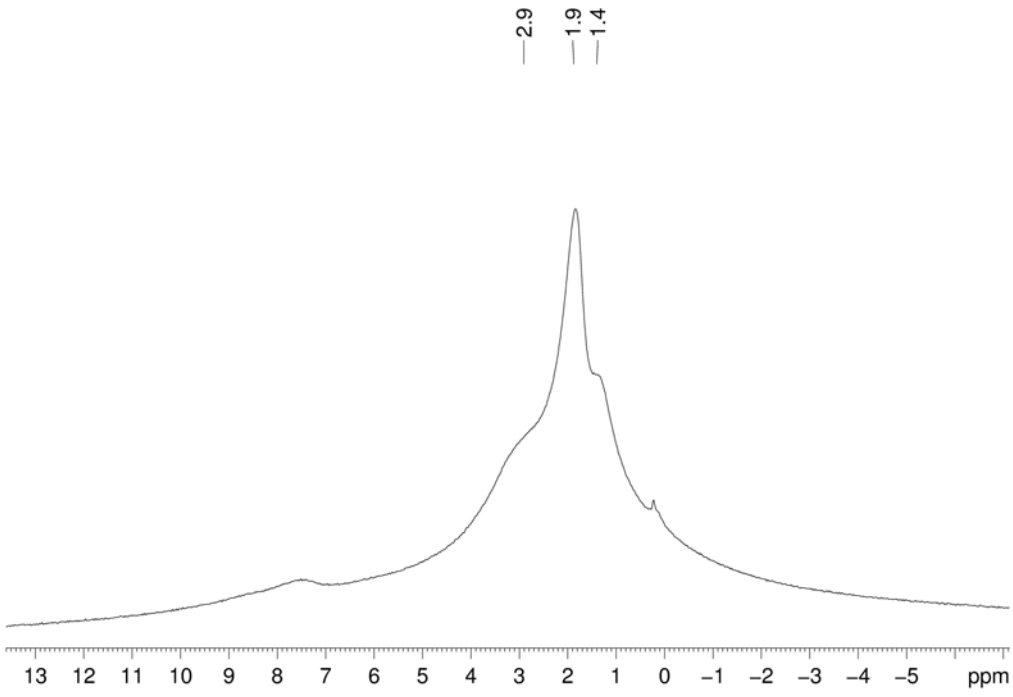

Figure A12. 1H MAS solid-state NMR of **M-NH$_{2\text{-}12}$**

M-NHAm

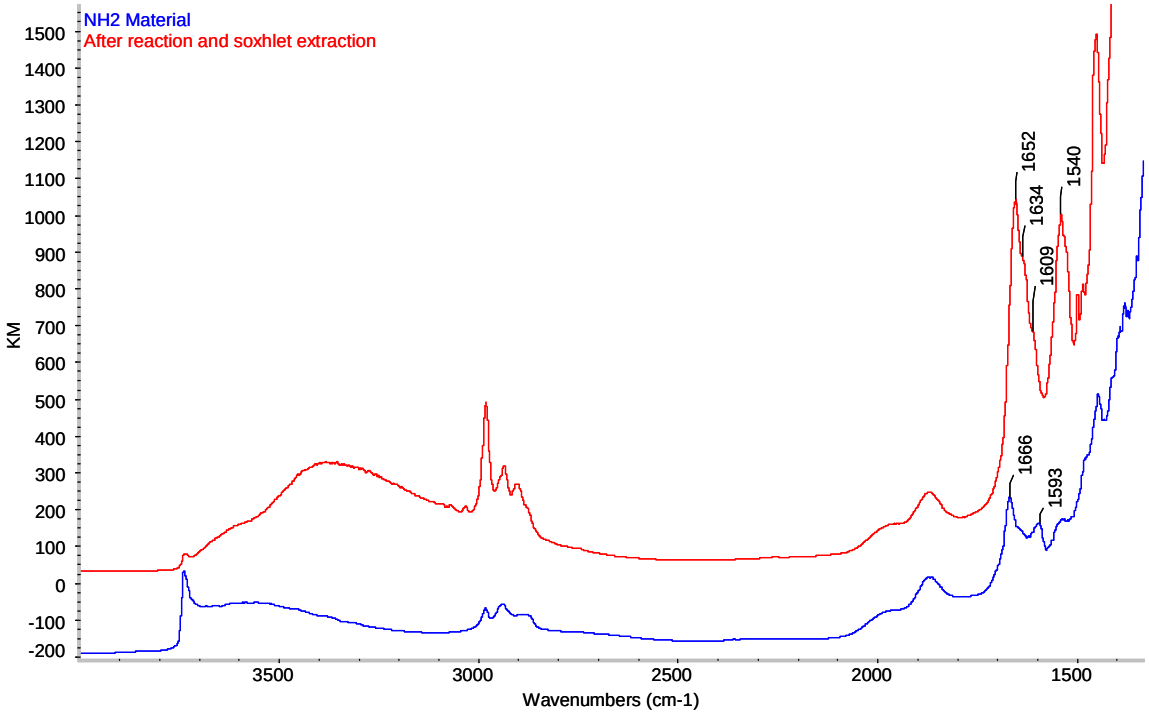

Figure A13. DRIFT spectrum of **M-NHAm** and **M-NH$_2$**

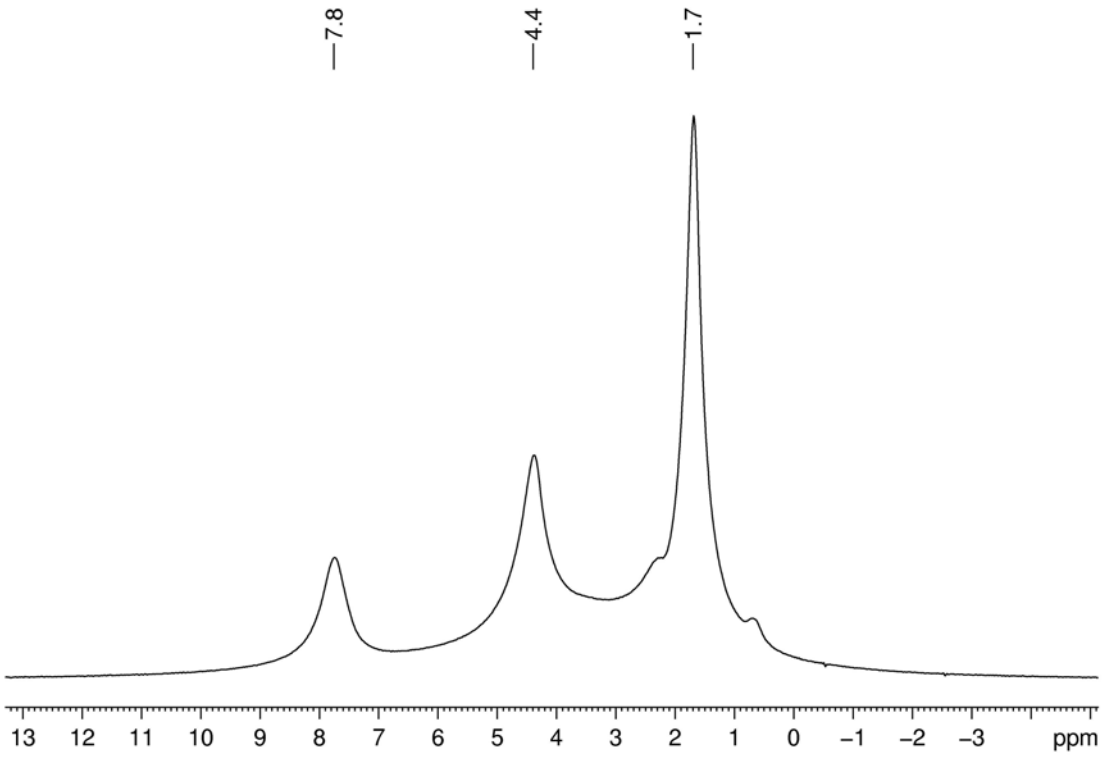

Figure A14. ^{1}H MAS solid-state NMR of **M-NHAm**

M-NBzAm

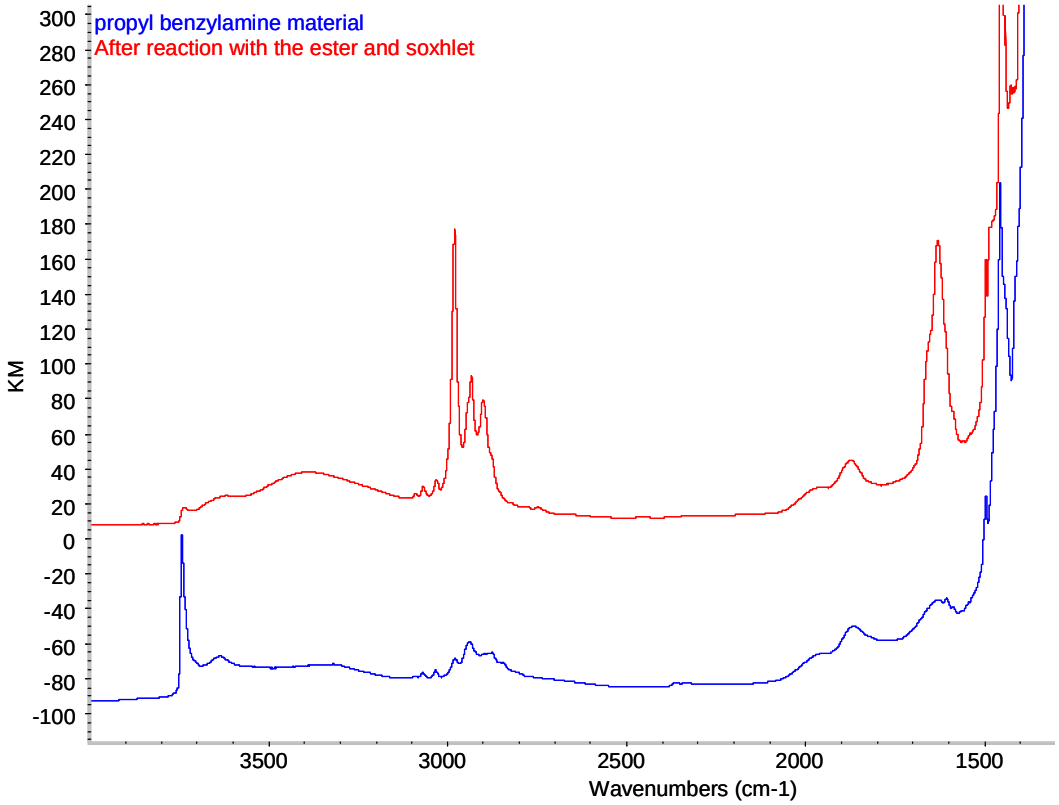

Figure A15. DRIFT spectrum of **M-NBzAm** and **M-NH$_2$**

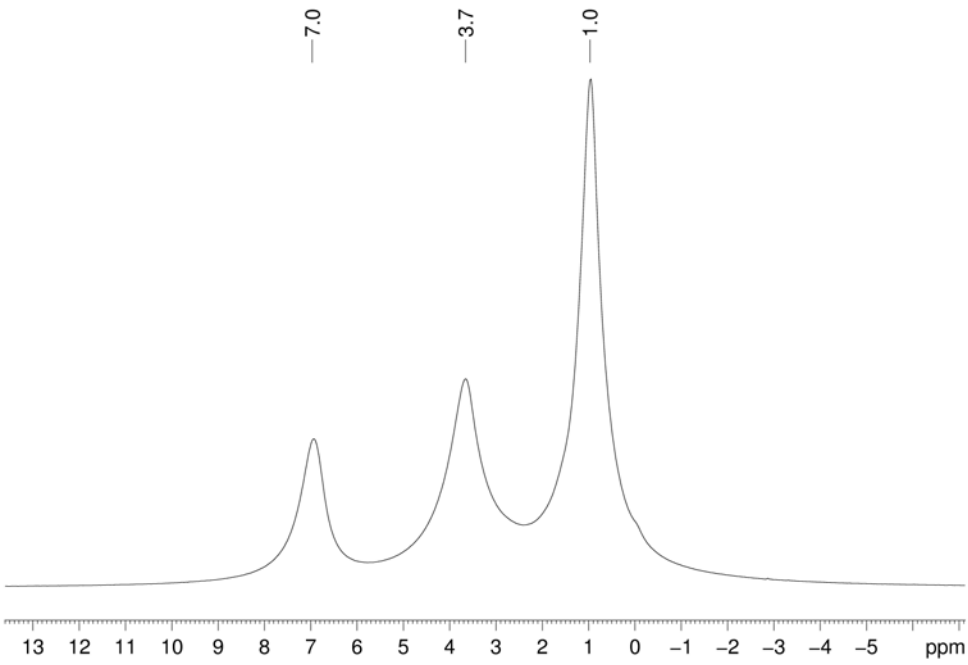

Figure A16. ^{1}H MAS solid-state NMR of **M-NBzAm**

M-PrIm$_{12}$

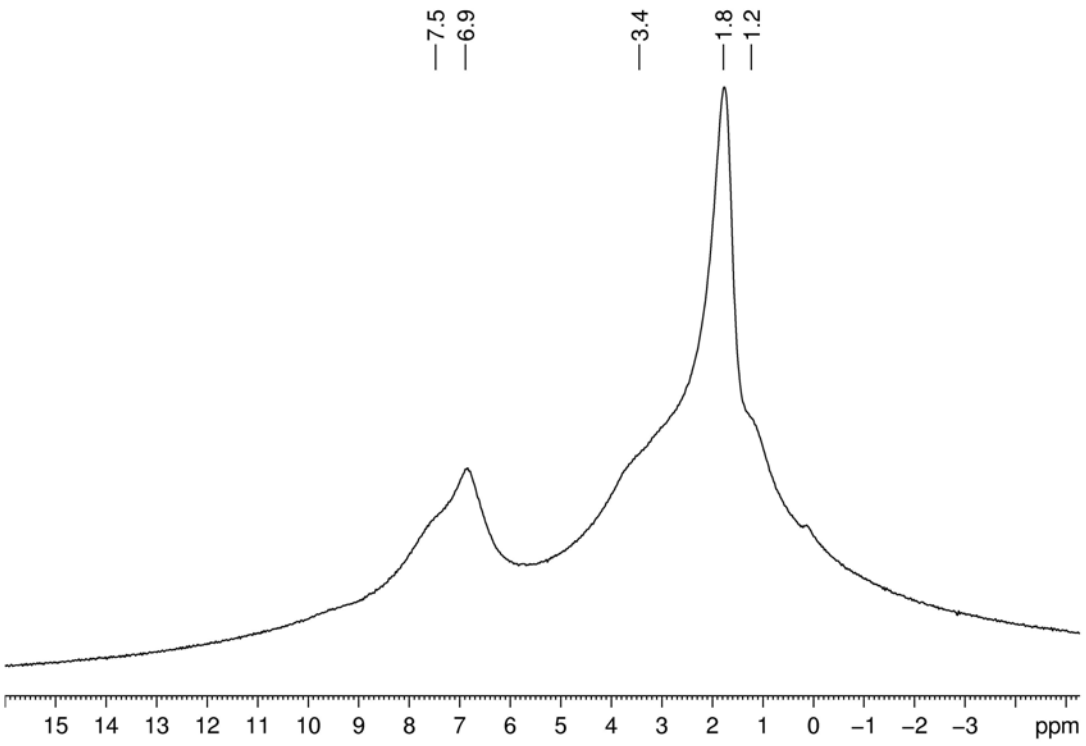

Figure A17. ^{1}H MAS NMR spectrum of **M-PrIm$_{12}$**

M-PrBzIm$_{-12}$

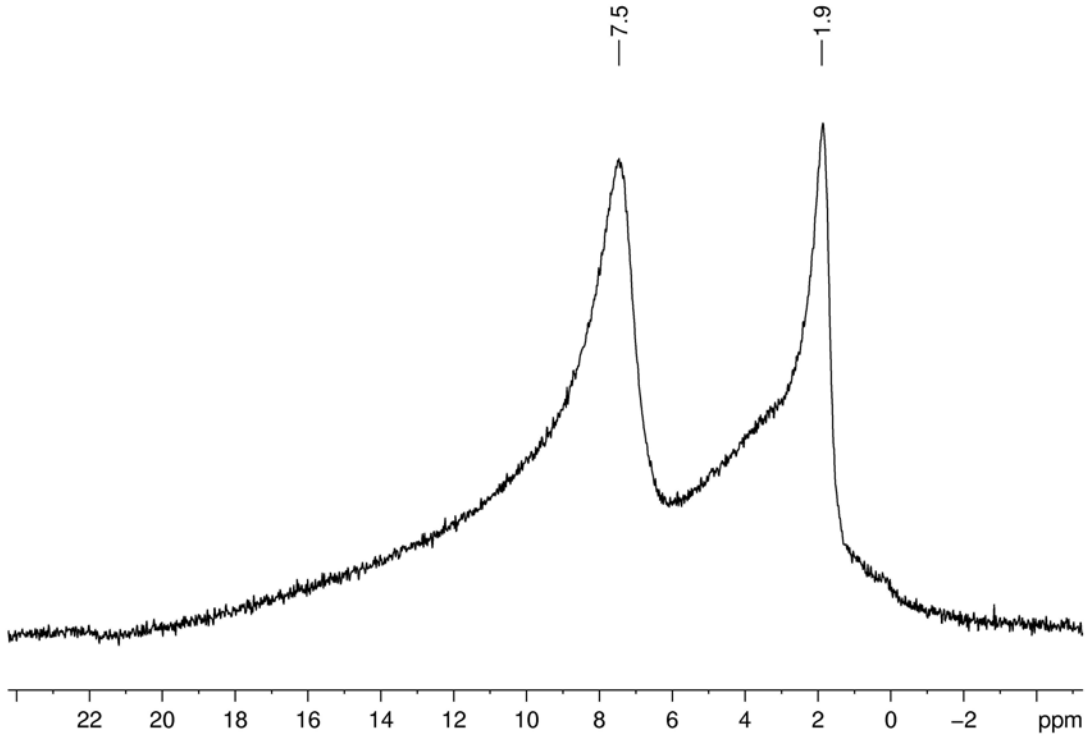

Figure A18. ^{1}H MAS NMR spectrum of **M-PrBzIm$_{12}$**

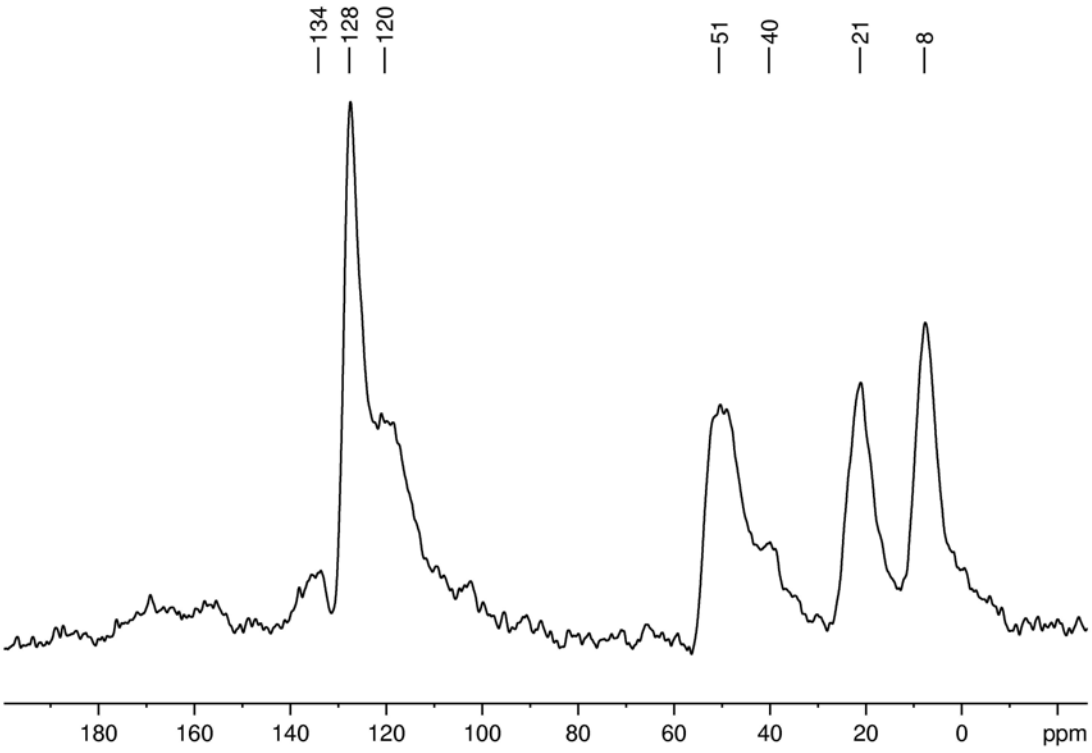

Figure A19. ^{13}C CPMAS NMR spectrum of **M-PrBzIm$_{12}$**

M'-PrBzIm$_{12}$

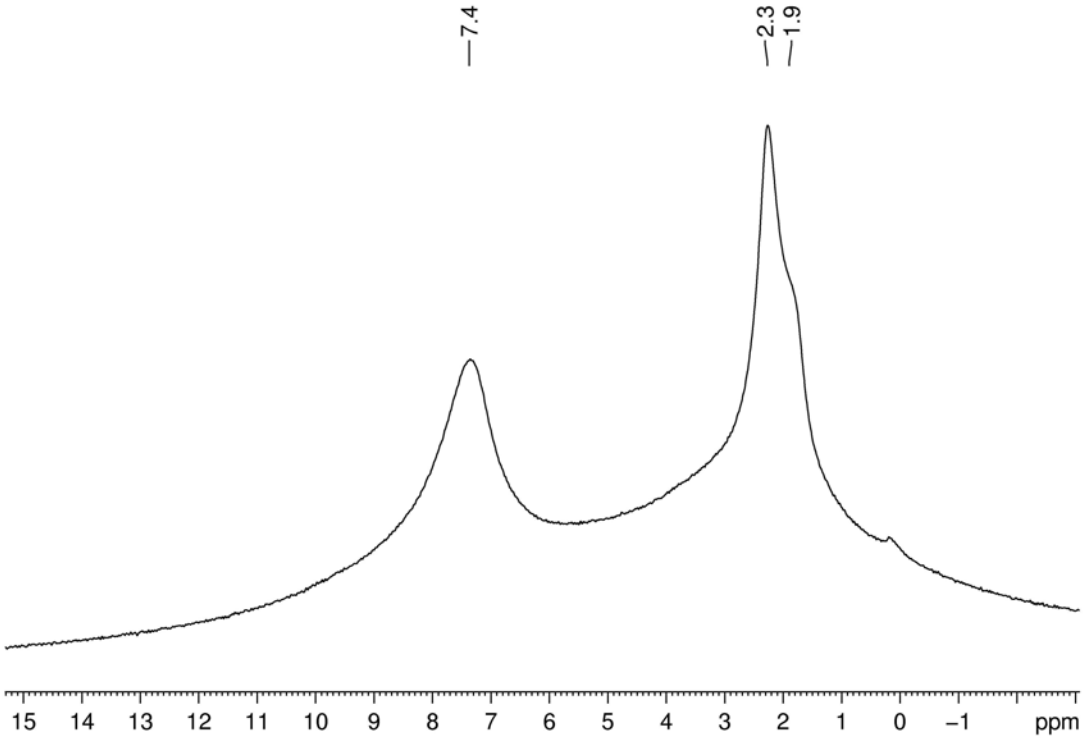

Figure A20. ^{1}H MAS NMR spectrum of **M'-PrBzIm$_{12}$**

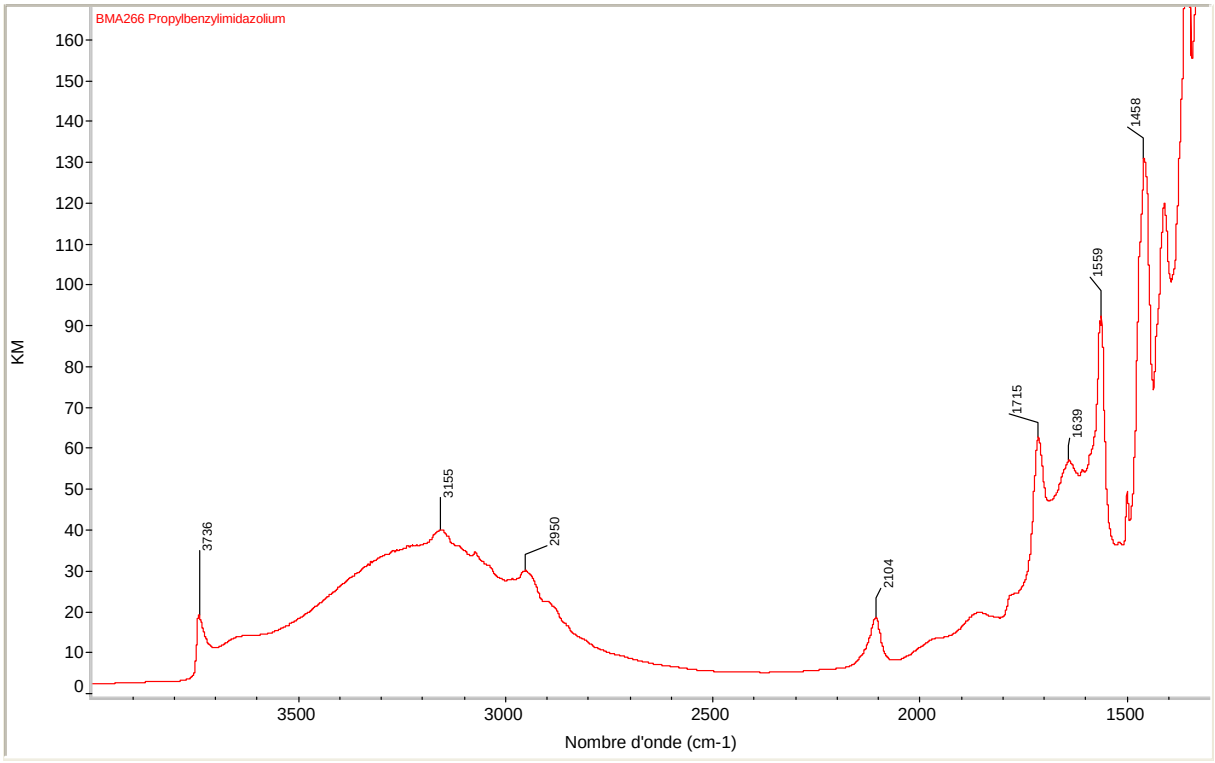

Figure A21. DRIFT spectrum of **M'-PrBzIm$_{12}$**

M-PrMesIm$_{-12}$

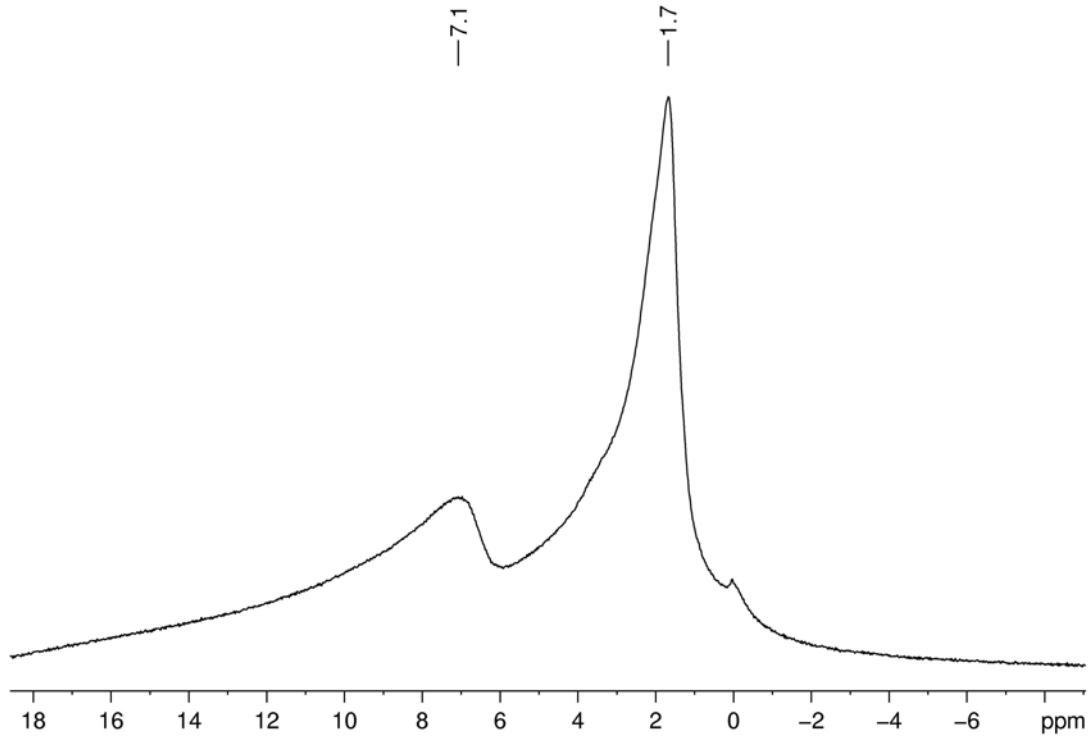

Figure A22. ^{1}H MAS NMR spectrum of **M-PrMesIm$_{12}$**

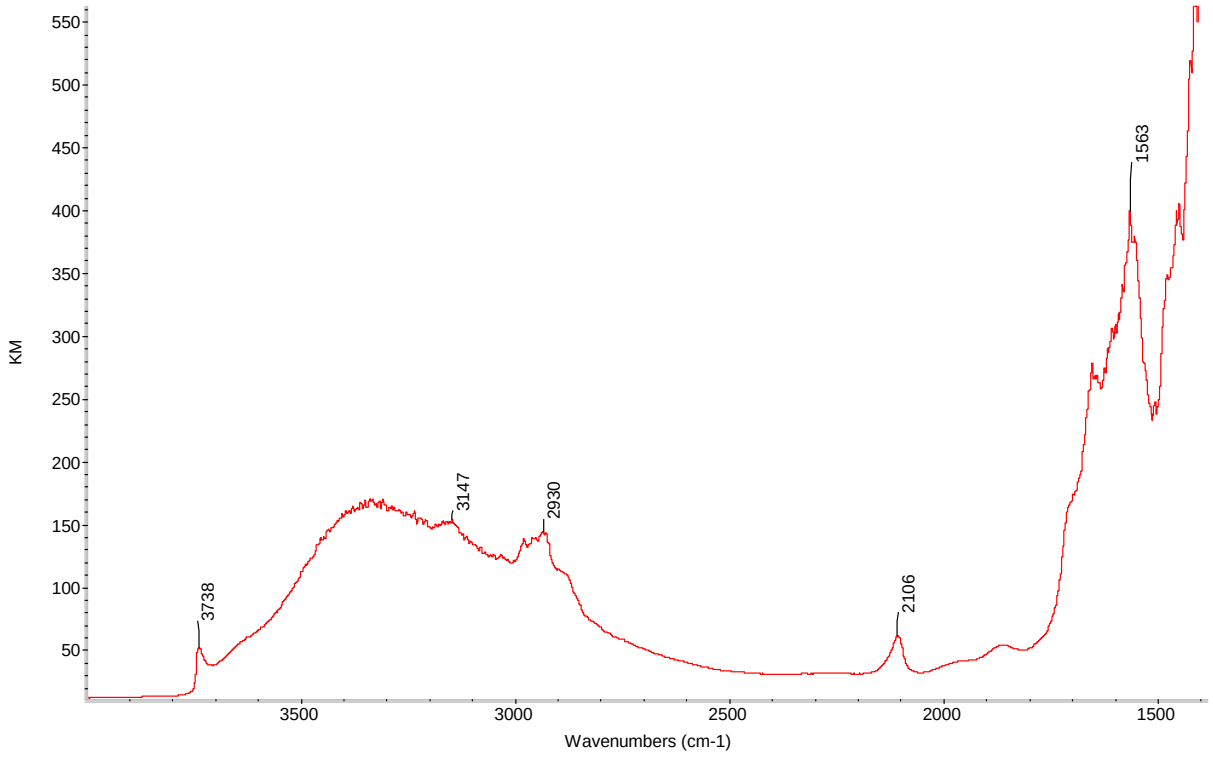

Figure A23. DRIFT spectrum of **M-PrMesIm$_{12}$**

M-PrEtIm

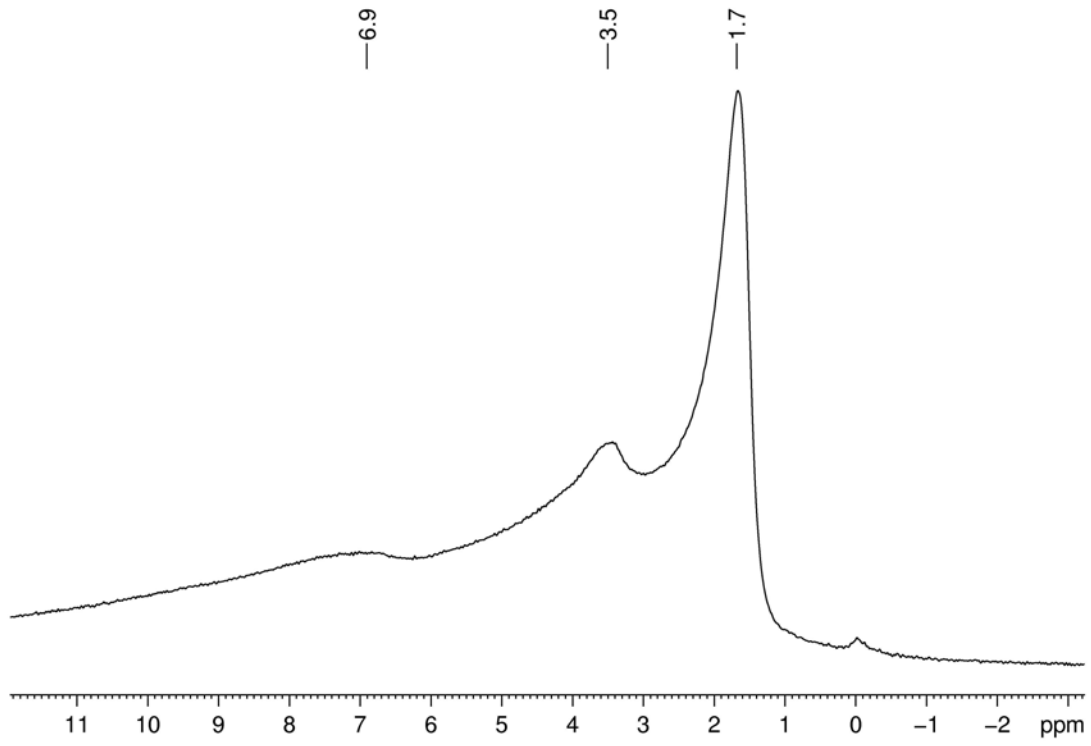

Figure A24. ^{1}H MAS NMR spectrum of **M-PrEtIm**

M-PrEtMesIm$_2$

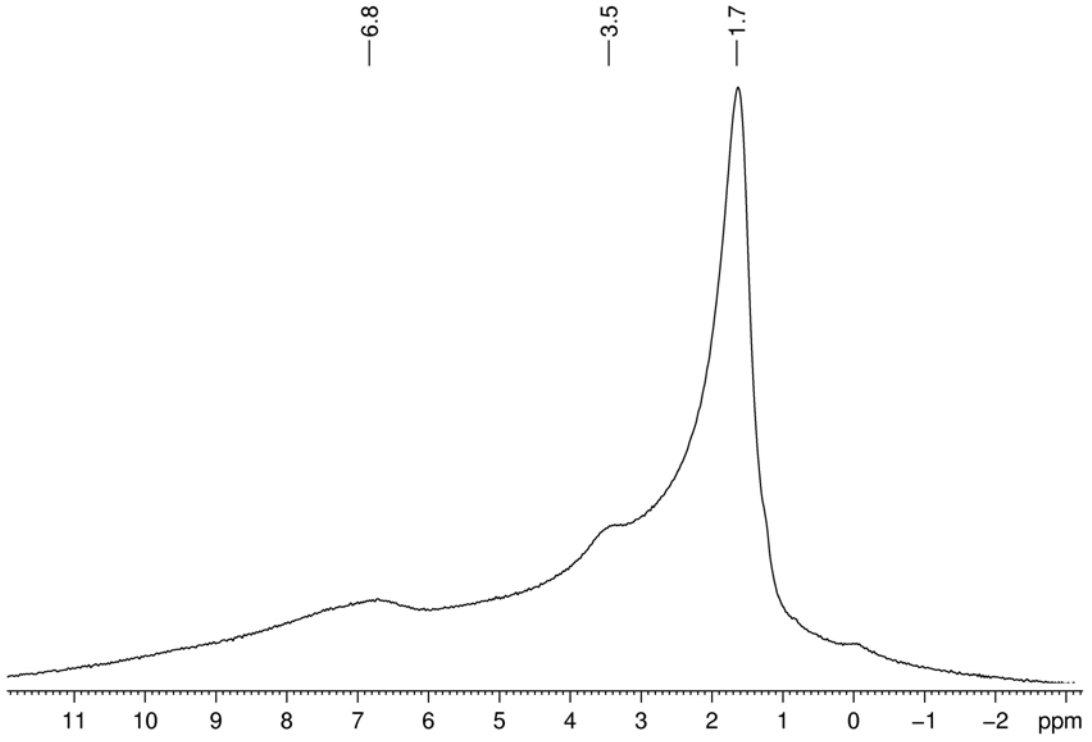

Figure A25. ^{1}H MAS NMR spectrum of **M-PrEtMesIm$_2$**

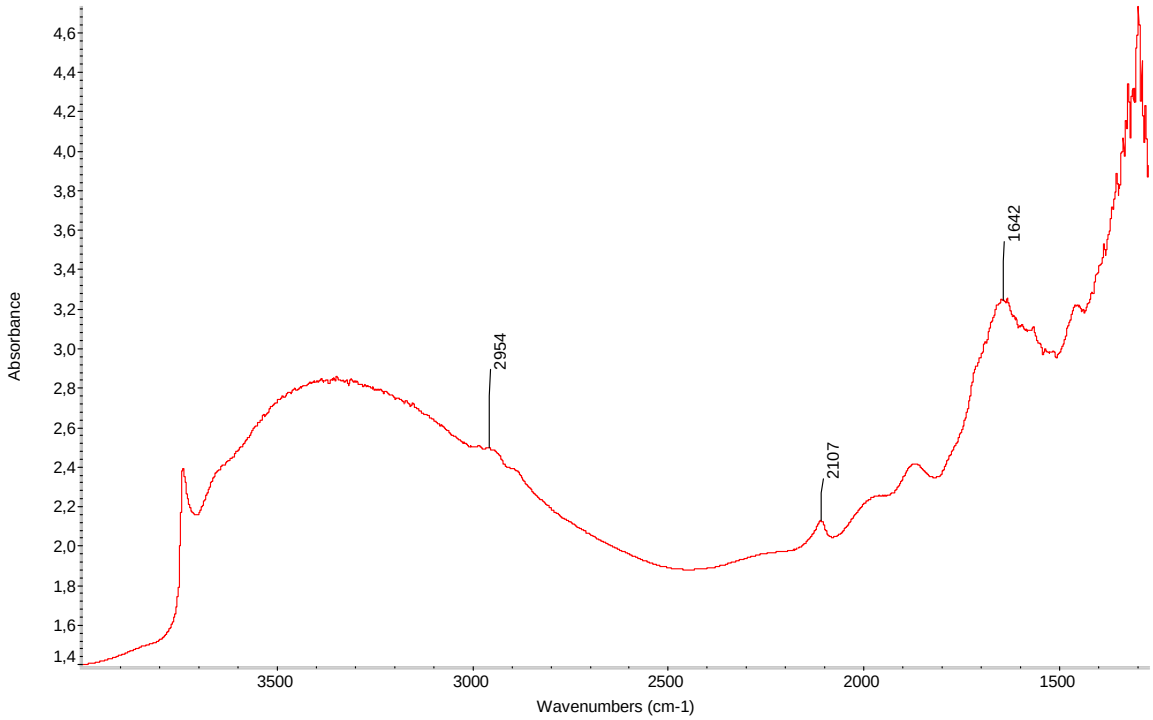

Figure A26. DRIFT spectrum of **M-PrEtMesIm$_2$**

M-PrPyIm

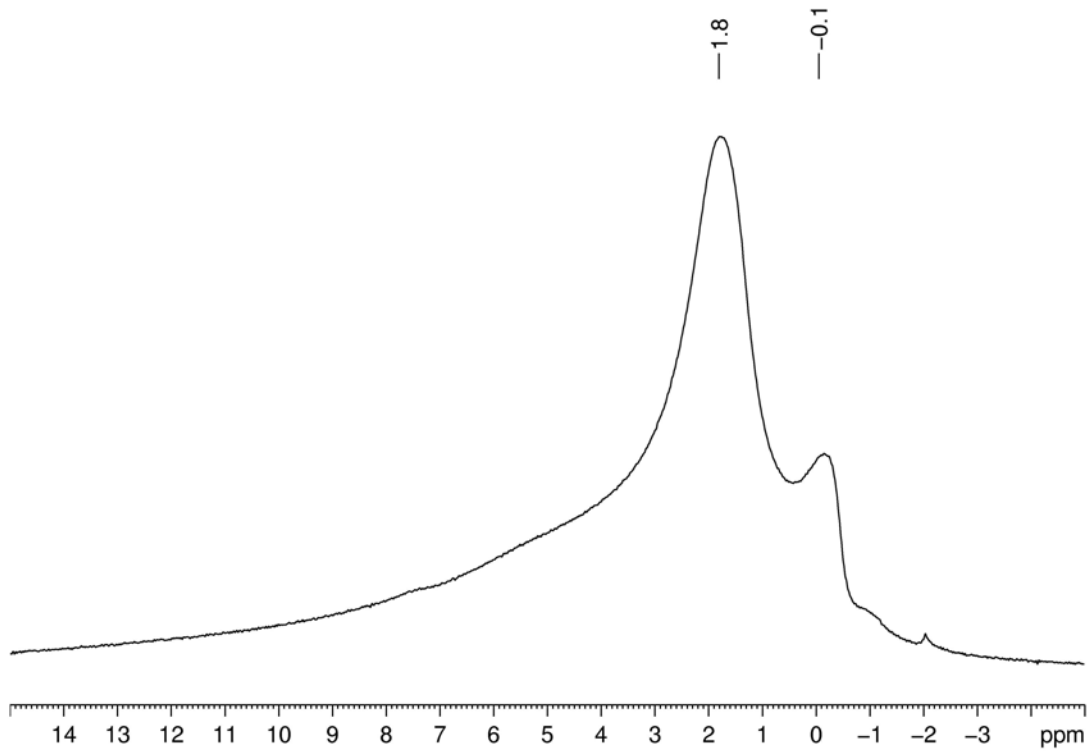

Figure A27. ^{1}H MAS NMR spectrum of **M-PrPyIm**

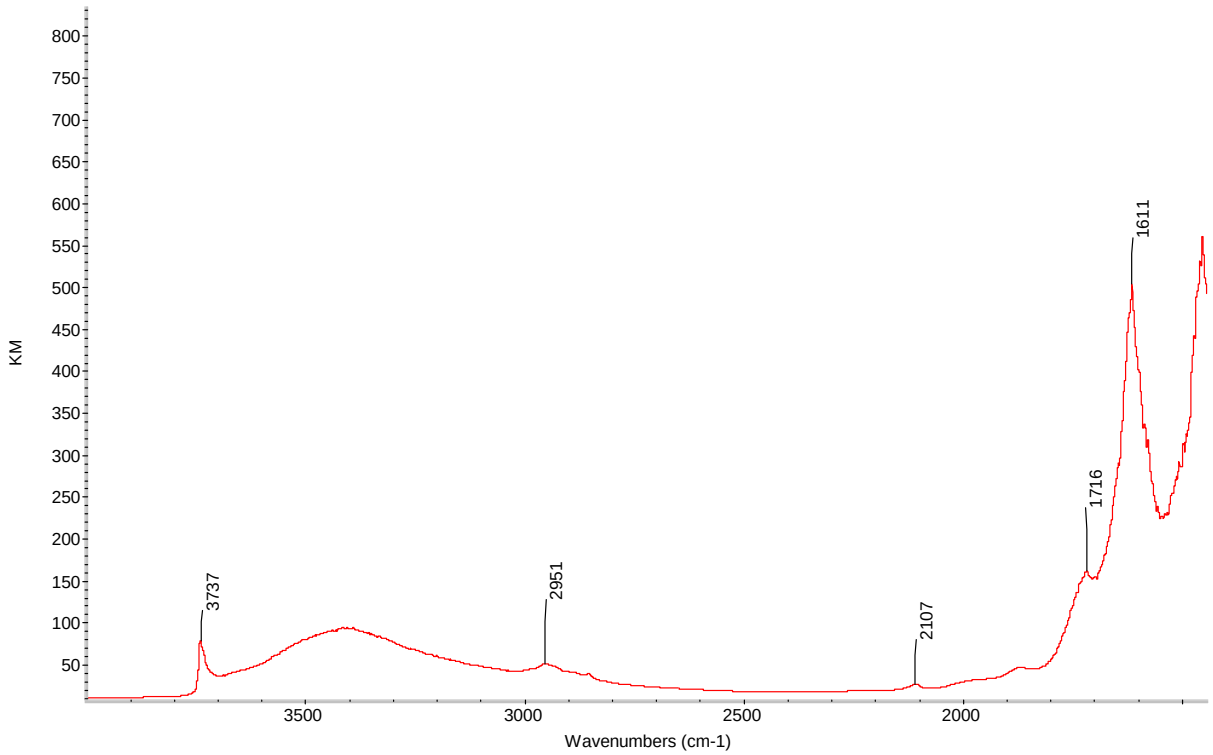

Figure A28. DRIFT spectrum of **M-PrPyIm**

M-PrPyMesIm$_2$

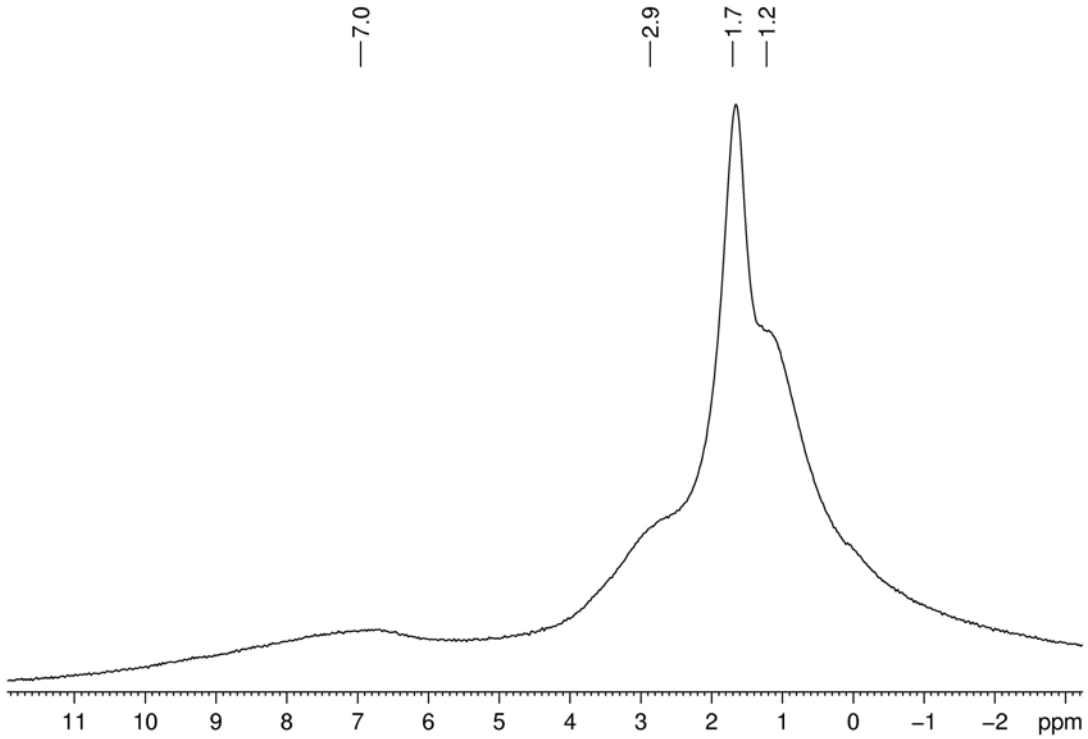

Figure A29. ^{1}H MAS NMR spectrum of **M-PrPyMesIm$_2$**

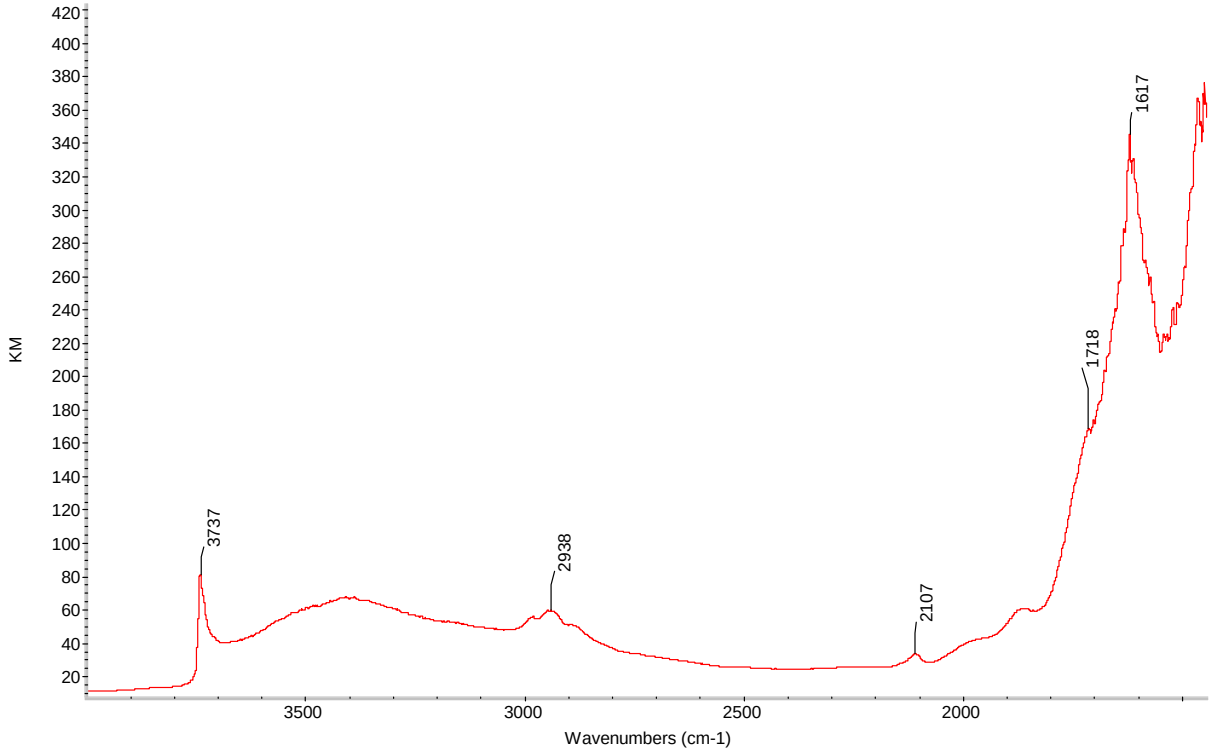

Figure A30. DRIFT spectrum of **M-PrPyMesIm$_2$**

Chapter 4

Formation of Ru-NHC and bis-NHC catalytic materials and their use in the hydrogenation of CO_2.

TABLE OF CONTENT

LIST OF FIGURES

LIST OF SCHEMES

LIST OF FIGURES IN APPENDIX

LIST OF TABLES

IV-1. Introduction

Recent works of Peris et al. described the use of bis-NHC complexes of ruthenium and iridium in the hydrogenation of CO_2 to formates in KOH solutions,[1,2] and they showed that these complexes are much more active than mono-NHC complexes, and moreover they are stable at elevated temperatures, up to 200°C. However, such complexes still suffer from solubility problems, and the use of water-soluble NHC ligands is necessary to get high TON values.[3] We therefore aimed at developing supported bis-NHC ruthenium complexes designed towards the hydrogenation of carbon dioxide. Our strategy to form Ru(bis-NHC) materials was based on two possible pathways, using imidazolium and bis-imidazolium-based hybrid materials developed in chapter 3.

The first pathway (Strategy 1, Scheme 1) was to use the highly concentrated 1/12 diluted imidazolium-based materials to favour the formation of bis-NHC Ru-species. Indeed, it was previously shown that acac-based materials can coordinate heavy transition metals by the interaction of two adjacent acac groups with a single metal atom.[4] However, this is only observed when the materials used reached a critical concentration.

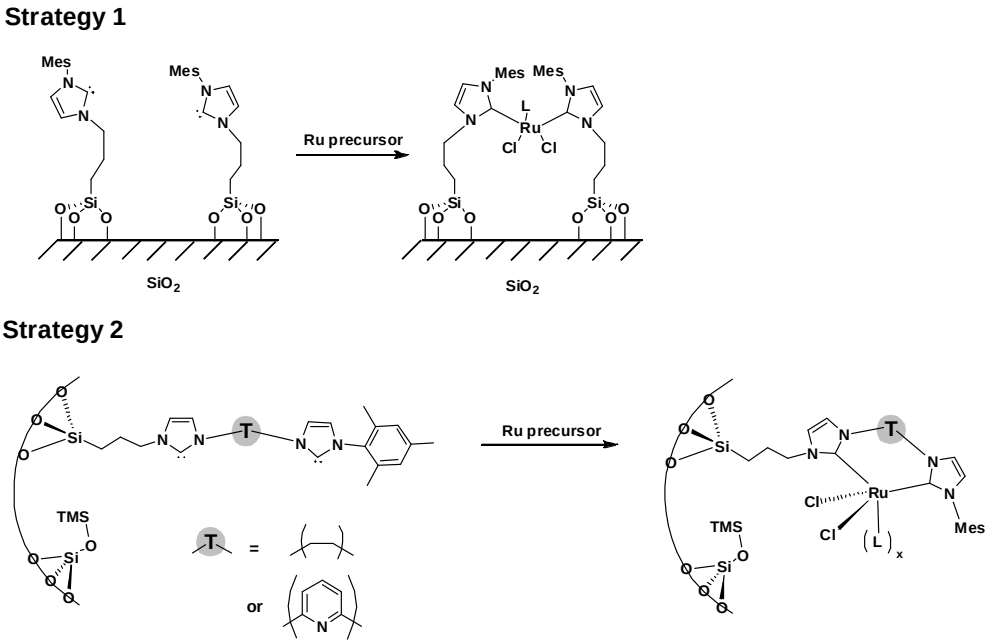

Scheme 1. Two strategies for the formation of Ru(bis-NHC) catalytic materials

Indeed, increasing the concentration lowers the average distance between two functional groups and will at some point enable the formation of bipodal metal complexes. If our imidazolium materials in 1/12 dilution have a sufficient concentration, we could then form bipodal bis-NHC complexes.

The second option (Strategy 2, Scheme 1) is to directly use organic functionalities bearing two imidazolium units (bis-imidazolium), which will allow the formation of a bidentate bis-NHC ligand. As discussed in chapter 1, these bis-NHC ligands were reported to form chelate bis-NHC complexes with ruthenium[5,6] and other metals.[7,8] In some cases, which were rarely observed, there can also be formation of a dinuclear bis-NHC complex.[1]

The aim of this chapter will be first to obtain different Ru(bis-NHC) complexes via these two strategies and then to evaluate their performances and stability in the hydrogenation of CO_2 in presence of pyrrolidine.

IV-2. Formation of Ru-NHC catalytic materials

2.1. Reaction of $[RuCl_2(p\text{-cymene})]_2$ on material M_P-PrMesIm-$_{12}$

2.1.1. Reaction in toluene with an excess of $[RuCl_2(p\text{-cymene})]_2$

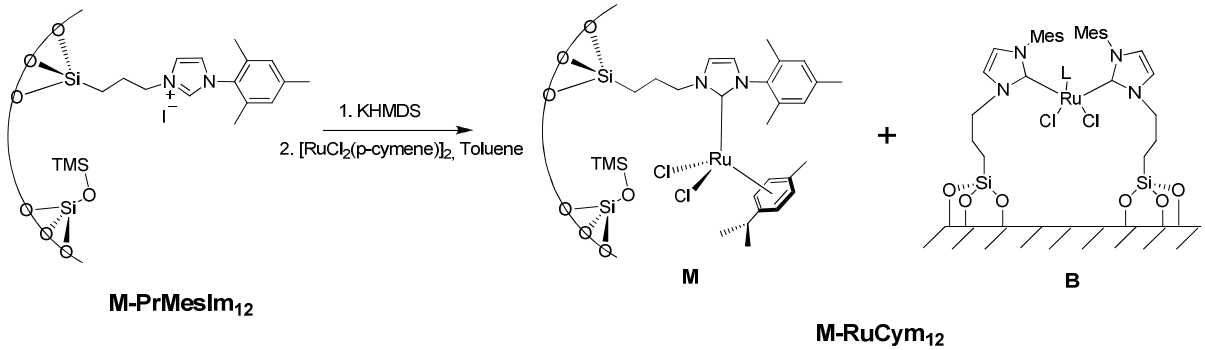

M-PrMesIm$_{12}$ **M** **B**

M-RuCym$_{12}$

In order to understand the reactivity of $[RuCl_2(p\text{-cymene})]_2$ with the concentrated **M$_p$-PrMesIm$_{12}$** material†, the reaction was first studied in toluene at room temperature in presence of an excess of the ruthenium precursor with respect to NHC functionalities to form material **M-RuCym$_{12}$**. Elemental analyzes give ruthenium and nitrogen loading of 3.42%$_{wt}$ and 1.62%$_{wt}$, respectively. This would roughly correspond to 0.34 mmol Ru and 0.30 mmol

† **M$_P$-PrMesIm$_{12}$** is formed by passivation of material **M-PrMesIm$_{12}$** with TMSBr in toluene and in the presence of triethylamine

of NHC units per g in a 1/12 diluted materials (see 3.2.3 in chapter 3), and thus ca. 1.1 Ru per NHC unit, that is a Ru/NHC ratio close to 1, consistent with the formation of mono-NHC species (**M**) as major species and not bipodal ones (**B**) as targeted. The ^{13}C CPMAS solid-state NMR spectrum is obtained with a very good signal-to-noise ratio, because of the high loading of functionalities inside the material, with signals at 0, 8, 18, 30, 51, 81, 123, 128 and 136 ppm as obtained in Chapter 2 for more diluted materials: the p-cymene ligand displays signals at 30 ppm (CH of the isopropyl) and 81 ppm (CH of the aromatics) and also part of the large signal at 18 ppm. All other signals correspond to the NHC ligand like the peaks at 8 and 51 ppm (C_1 and C_3 of the propyl chain), 18 ppm (CH_3 of the mesityl group and C_2 of the propyl chain) and the three peaks at 123, 128 and 136 ppm (all aromatic CH mainly). Finally, this sample was analyzed by TEM in order to control if any evolution of the mesostructure occurs during all steps from **M-N$_{3\text{-}12}$** to **M-RuCym$_{12}$.** It showed the conservation of the 2D-hexagonal structure in **M-RuCym$_{12}$** (see Figure A1). These results are in agreement with the formation of $RuCl_2$(NHC)(p-cymene) surface species and the formation of material **M-RuCym$_{12}$**.

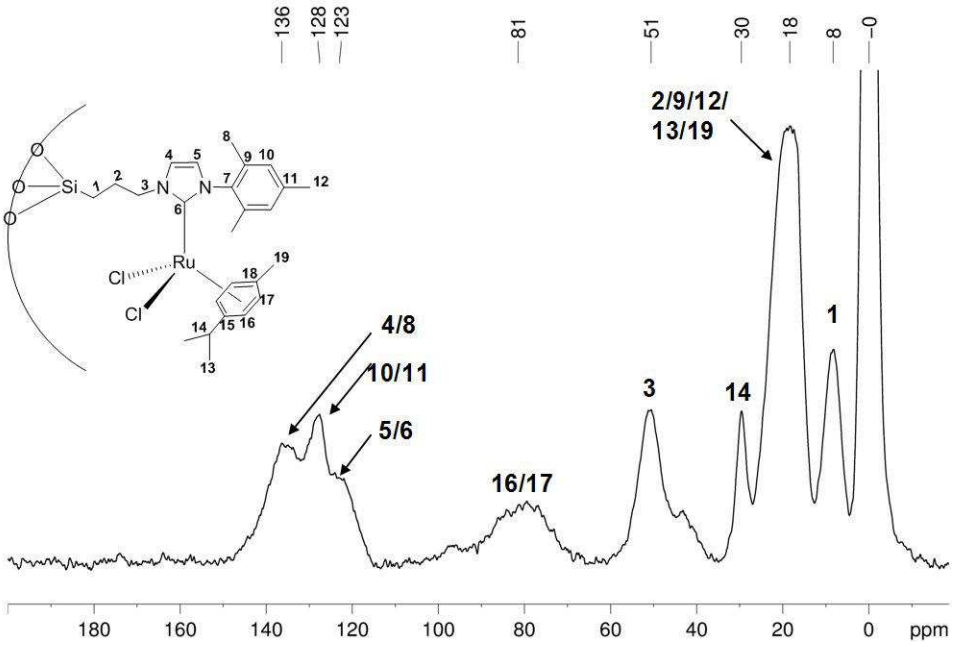

Figure 1. ^{13}C CPMAS NMR spectrum of **M-RuCym$_{\text{-}12}$**

2.1.2. Reaction in warm THF with 0.5 equiv. of ruthenium

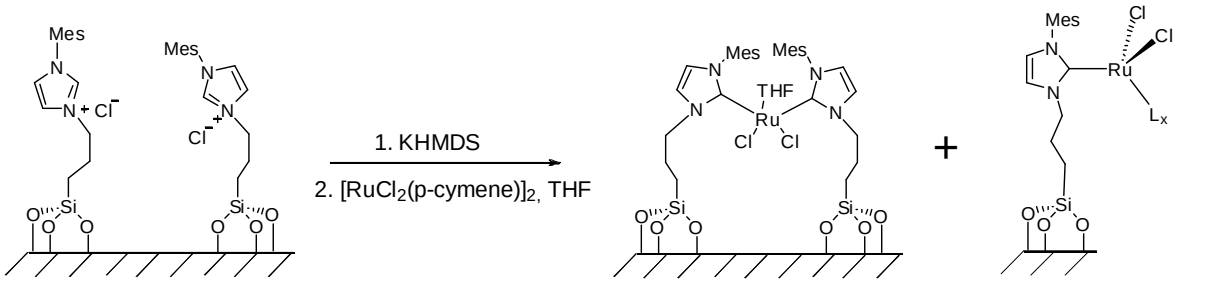

M_p-PrMesIm$_{12}$ **B** **M** **M-RuIm$_2$THF$_{12}$**

In order to favour bis-NHC systems, the reaction of $[RuCl_2(p\text{-cymene})]_2$ on **M_p-PrMesIm$_{12}$** materials was studied in different conditions: THF in place of toluene (allowing the exchange of the p-cymene ligand) and 0.5 equiv. of Ru (to favour the reaction with two adjacent NHC ligands).

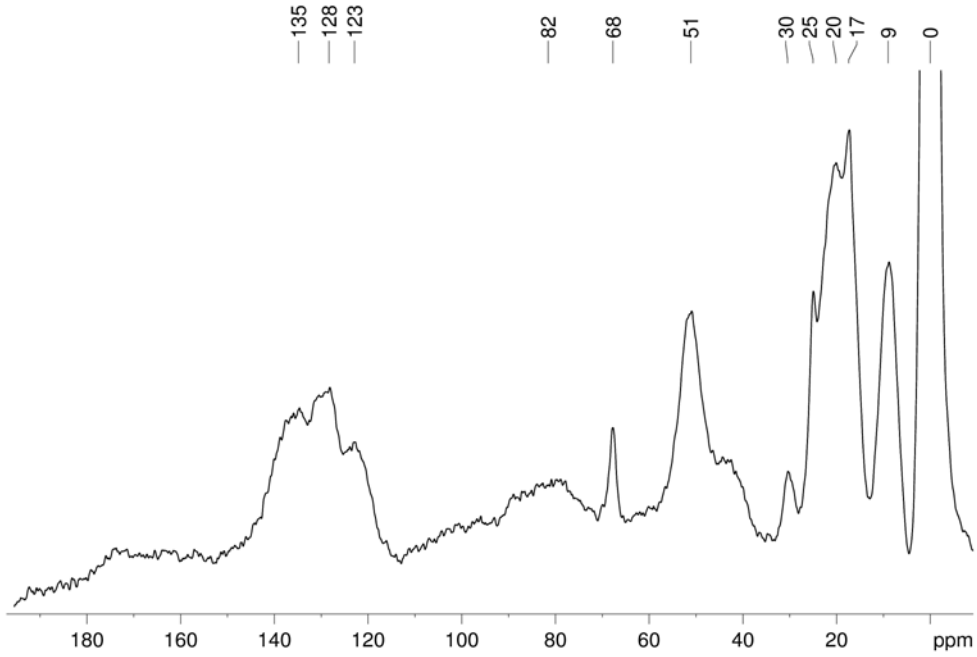

Figure 2. ^{13}C CPMAS NMR spectrum of **M-RuIm$_2$THF$_{12}$**

The targeted complex would bear THF ligands and two NHC ligands with 18 electrons when two THF are present (the Ru(p-cymene)(bis-NHC) system could also be obtained, but only if we form a 18 electron cationic complex). The reaction of a deprotonated **M_P-PrMesIm$_{12}$** material with $[RuCl_2(p\text{-cymene})]_2$ in THF at 45°C for 3h30, with 0.5 equiv. ruthenium per accessible NHC unit leads to material **M-RuIm$_2$THF$_{12}$**. Elemental analyses give a ruthenium

content of 1.43%$_{wt}$ and 1.75%$_{wt}$ nitrogen. This corresponds to 0.141 mmol Ru and 0.33 mmol NHC units per g of materials, and therefore to a Ru/NHC ratio of 0.43, which is slightly lower than the maximum possible amount of ruthenium considering the quantity introduced in the reaction mixture. The ^{13}C CPMAS solid-state NMR spectrum shows both THF signals (25 and 68 ppm) and p-cymene signals (30 ppm and 82 ppm), in agreement with a partial exchange between THF and p-cymene ligands, but at this point it is difficult to know whether any bridging bis-NHC species (**B**) have been formed or not. However, the intensity of the signals of THF compared to p-cymene is consistent with the presence of THF on a majority of ruthenium centres.

2.2. Formation of Ru(NHC)(PMe$_3$) complexes

2.2.1. Reaction of material M-RuCym$_{12}$ with PMe$_3$

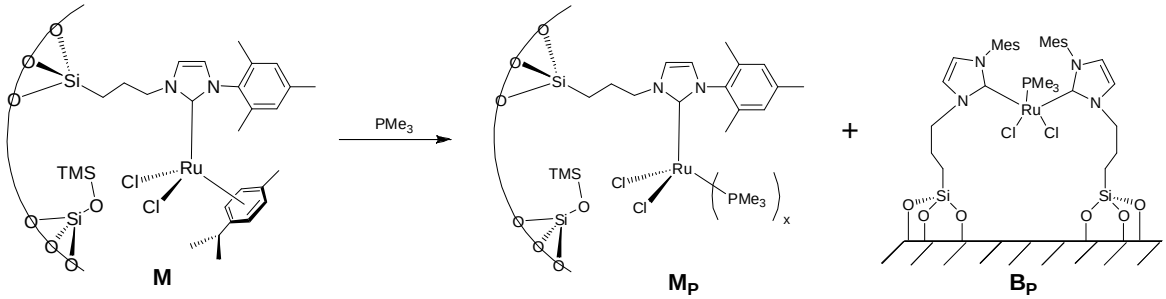

M **M$_P$** **B$_P$**

M-RuCym$_{12}$ **M-RuPMe$_{3\text{-}12}$**

Material **M-RuCym$_{12}$** was contacted with PMe$_3$, and after 1h of stirring at room temperature, all volatiles were removed in vacuo (8h at 10^{-5} mbar). The so-obtained material **M-RuPMe$_{3\text{-}12}$** was characterized by ^{31}P HPDEC solid-state NMR, which gave two signals at 1 and -9 ppm (see Figure 3). The spectrum is very similar to what was obtained on material **M-RuPMe$_3$** which had lower density of functional groups (See Chapter 2), which is consistent with the fact that the grafting performed in toluene from a 1/12 diluted material, probably leads to the same surface species, a mono-NHC ruthenium complex (**M$_P$**). In ^{13}C CPMAS solid-state NMR, the signals at 30 and 80 ppm corresponding to the p-cymene ligand have been reduced significantly, and there is an increase of the signal at 16 ppm, due to the coordination of PMe$_3$ (see Figure A2).

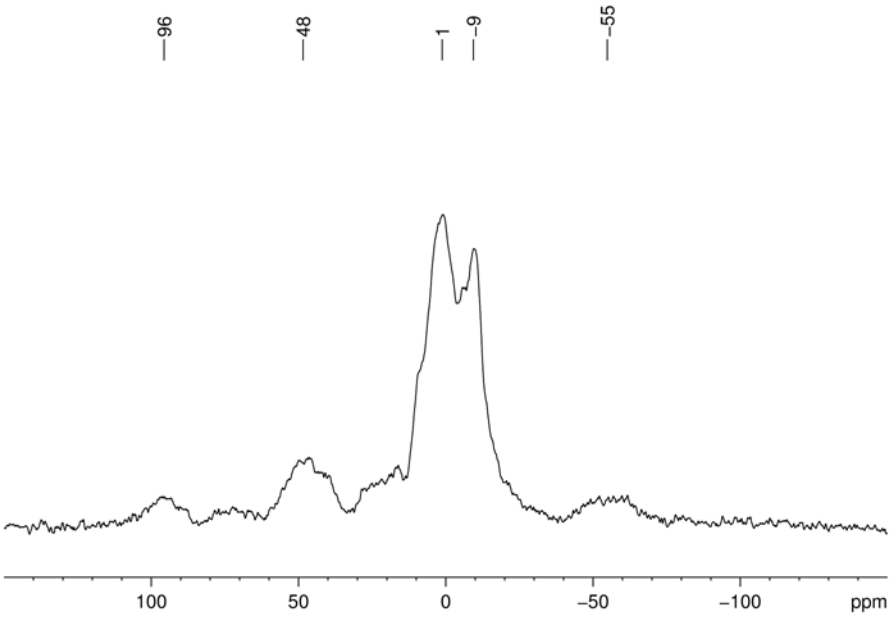

Figure 3. ^{31}P HPDEC NMR spectrum of **M-RuPMe$_3$**

2.2.2. Reaction of material M-RuIm$_2$THF$_{12}$ with PMe$_3$

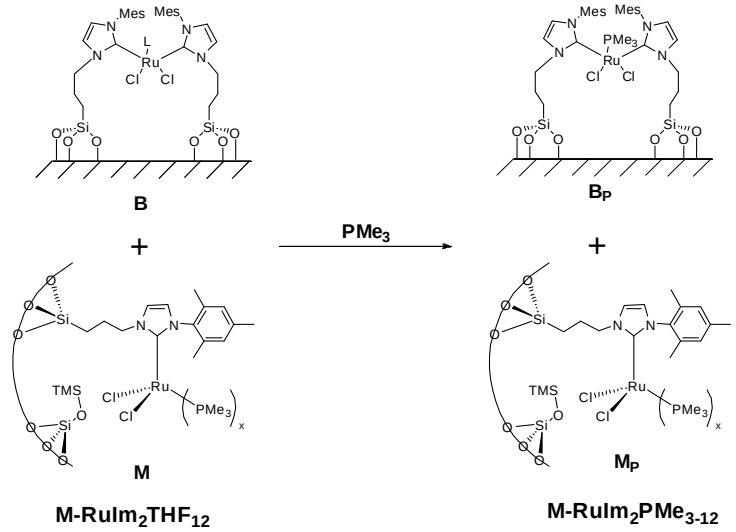

The reaction of **M-RuIm$_2$THF$_{12}$** with PMe$_3$ leads to **M-RuIm$_2$PMe$_{3\text{-}12}$**. In ^{13}C CPMAS solid-state NMR, there is an increase of the intensity of the peak at 17 ppm, due to the coordination of PMe$_3$ ligands, and all peaks corresponding to THF (25 and 68 ppm) and to p-cymene (30 and 80 ppm) have disappeared (see Figure A3). We therefore have a quantitative exchange of both THF and p-cymene ligands with PMe$_3$. The ^{31}P HPDEC NMR spectrum shows two main signals at 18 and -3 ppm and a smaller one at -10 ppm. The peaks at -3 and -10 ppm are very close to those observed at 1 and -9 ppm in material **M-RuPMe$_{3\text{-}12}$**, and are believed to correspond to **M$_p$** as previously discussed. However, the presence of a peak at 18 ppm, which is completely absent in the spectrum of **M-RuPMe$_{3\text{-}12}$**,

is consistent with the formation of a new surface species. The reaction of $[RuCl_2(p\text{-cymene})]_2$ with bis-imidazolium species in the presence of a base is known to form almost exclusively cationic bidentate species, by substitution of one of the chlorine ligands in the coordination sphere of ruthenium.[2-4] Therefore, if Ru(bis-NHC) species are formed in our systems, they will most probably be cationic species. This would be consistent with the downfield shift observed in ^{31}P NMR, which would be attributed to PMe_3 coordinated to a cationic Ru(bis-NHC) surface complex $\mathbf{B_P^+}$ (Figure 4) and not to a neutral Ru(mono-NHC) complex ($\mathbf{M_P}$ or $\mathbf{B_P}$). However, this signal is of lower intensity than this at -3 ppm associated with neutral species, so that such bis-NHC species is only a minor species. This is not completely surprising, as in the work reported by the group of Prof. Corriu, the coordination of Eu ions on all acac sites is only observed for materials of concentration of 1/6.

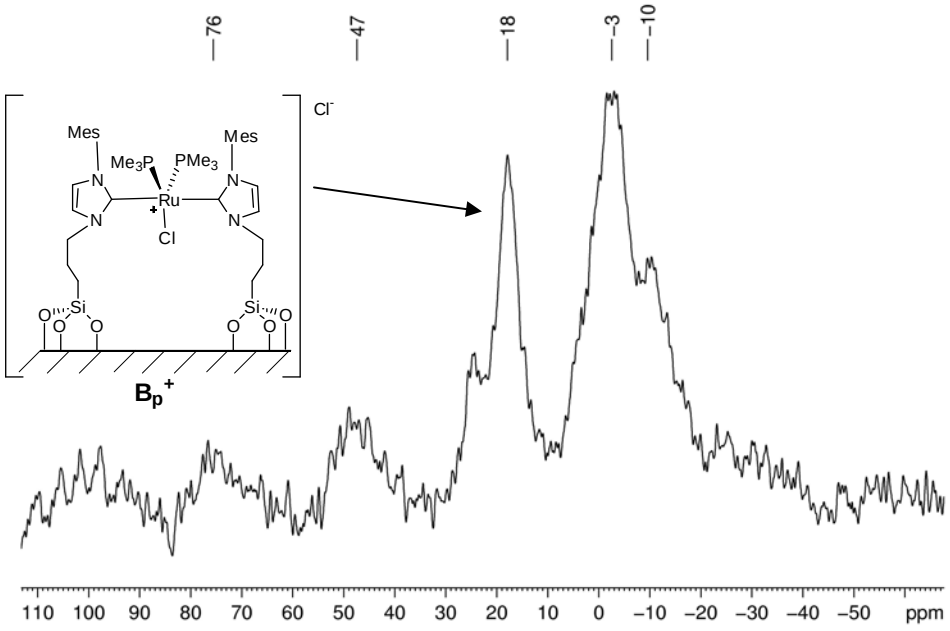

Figure 4. ^{31}P HPDEC NMR spectrum of **M-RuIm$_2$PMe$_{3\text{-}12}$**

IV-3. Formation of Ru(bis-NHC) catalytic materials

The formation of Metal(bis-NHC) complexes is generally a more difficult process, in particular when trying to form the rather geometrically constrained chelate complexes. For these reasons, the reactions were performed in different conditions than what was used typically for the formation of Ru(NHC) species, and higher reaction temperatures were used.

3.1. Formation of Ru(bis-NHC) complexes from M-PrEtIm$_2$ material.

3.1.1. Reaction of [RuCl$_2$(p-cymene)]$_2$ on M$_p$-PrEtMesIm$_2$

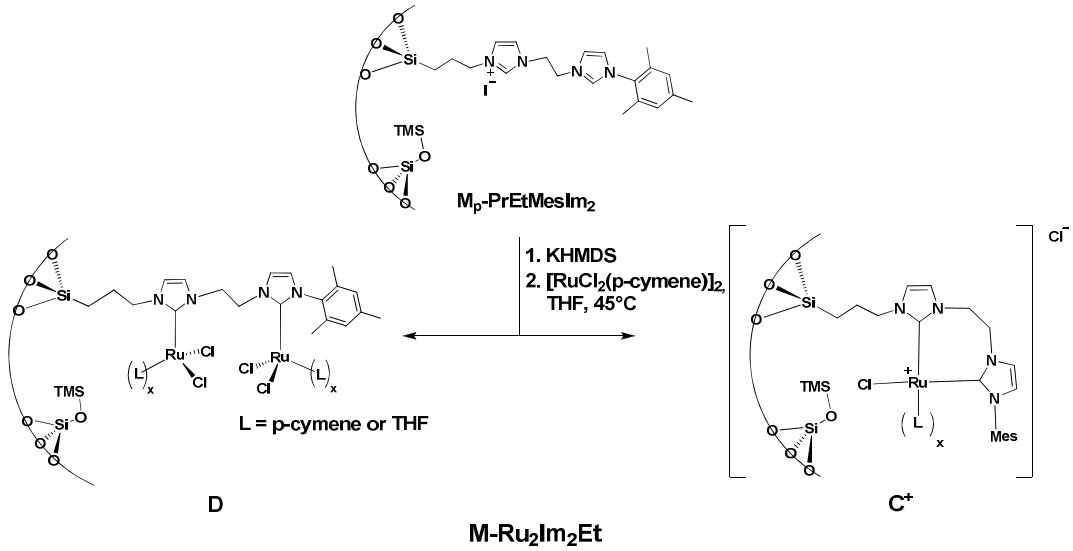

The reaction of [RuCl$_2$(p-cymene)]$_2$ on the passivated material **M$_p$-PrEtMesIm$_2$** after deprotonation with 2.4 equiv. of KHMDS was carried out in THF at 45°C, in order to allow exchange of p-cymene for THF ligands. Elemental analyses showed a Ru and N loadings of 2.86%$_{wt}$ and 1.38%$_{wt}$ respectively. With 0.13 mmol of bis-imidazolium units and around 0.057 mmol mono-imidazolium per gram of material and 0.283 mmol/g ruthenium, there is a minimum ratio of 1.7 ruthenium per bis-NHC unit considering a maximum ratio of 1 Ru/(mono-NHC). This result is consistent with the formation of dinuclear ruthenium bis-imidazolium complexes (**D**), but the presence of the targeted bidentate Ru(bis-NHC) complexes cannot be excluded.

The formation of dinuclear complexes have already been reported for metals of group 9 (rhodium)[10,11] and group 10 (nickel)[5] and has been reported very recently with ruthenium.[6]

Depending on the reaction conditions and of the bis-imidazolium which is used, $[RhBr(COD)]_2$ can either form neutral dinuclear bis-NHC complexes, neutral mono-nuclear chelating bis-NHC complexes or cationic mono-nuclear chelating bis-NHC complexes. In the case of ruthenium, there are several reports of the reaction of bis-imidazoliums with $[RuCl_2(p\text{-cymene})]_2$, and the formation of cationic mono-nuclear bis-NHC complexes was observed in most cases;[2-4] however, the formation of a dinuclear bis-NHC complex was only recently reported for the first time. Based on these reports, the further discussions in this chapter will be focused on two main types of Ru(bis-NHC) species which we consider to be the most probable ones: a neutral dinuclear Ru(bis-NHC) species (**D**) and a cationic mono-nuclear Ru(bis-NHC) species ($\mathbf{C^+}$) (vide infra).

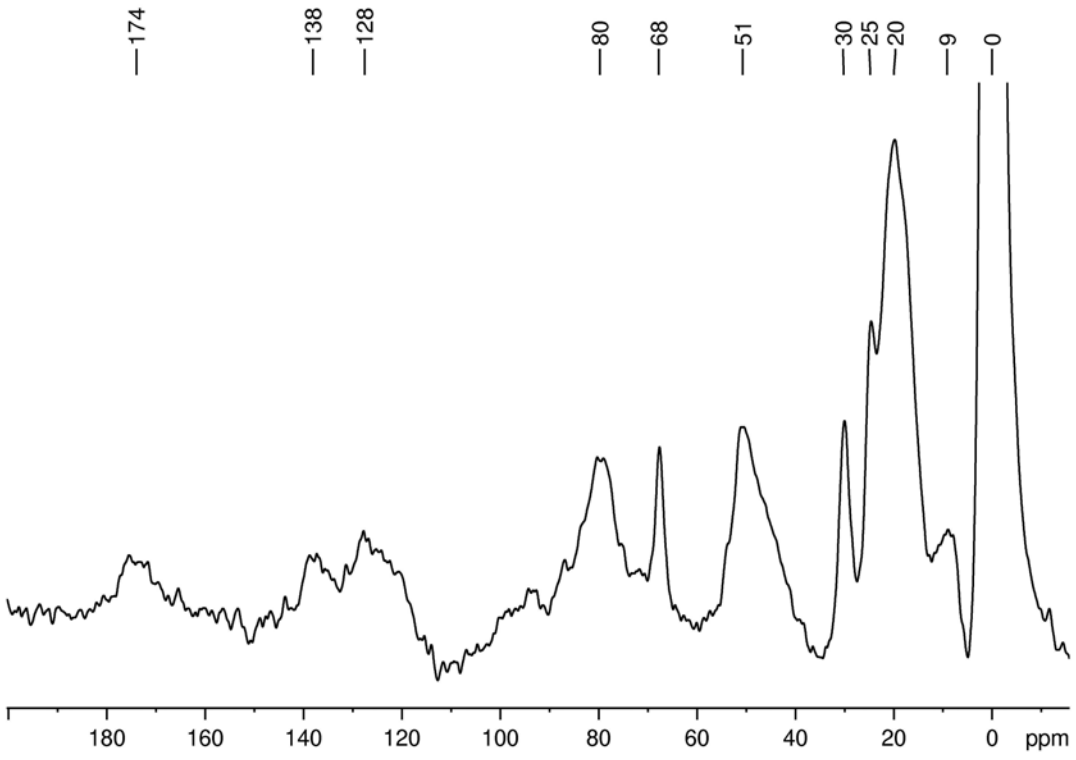

Figure 5. ^{13}C CPMAS NMR spectrum of **M-RuIm$_2$Et**

The product, **M-Ru$_2$Im$_2$Et**, shows signals in ^{13}C CPMAS NMR at 9, 20, 25, 30, 51, 68, 80, 128, 138 and 174 ppm (see Figure 5). It appears very clearly that we have signals from both p-cymene ligands (aromatic CH at 80 ppm, CH of the isopropyl at 30 ppm and CH_3 at 20 ppm) and THF ligands (signals at 25 and 68 ppm). This exchange between p-cymene and THF ligands was already discussed previously. However, in this case with 4 hours at

45℃, while a total displacement of the p-cymene ligands was expected, only a very partial exchange took place. Indeed, in the same conditions with the mono-NHC derivatives, all p-cymene ligands were exchanged with THF. This is an evidence of the very different reactivity of such bis-NHC derivatives compared to the single-NHC ones. This different reactivity might be due to a strong Ru-Ru interaction or the presence of μ^2-coordinated ligands.

3.1.2. Reaction of M-RuIm$_2$Et with trimethylphosphine

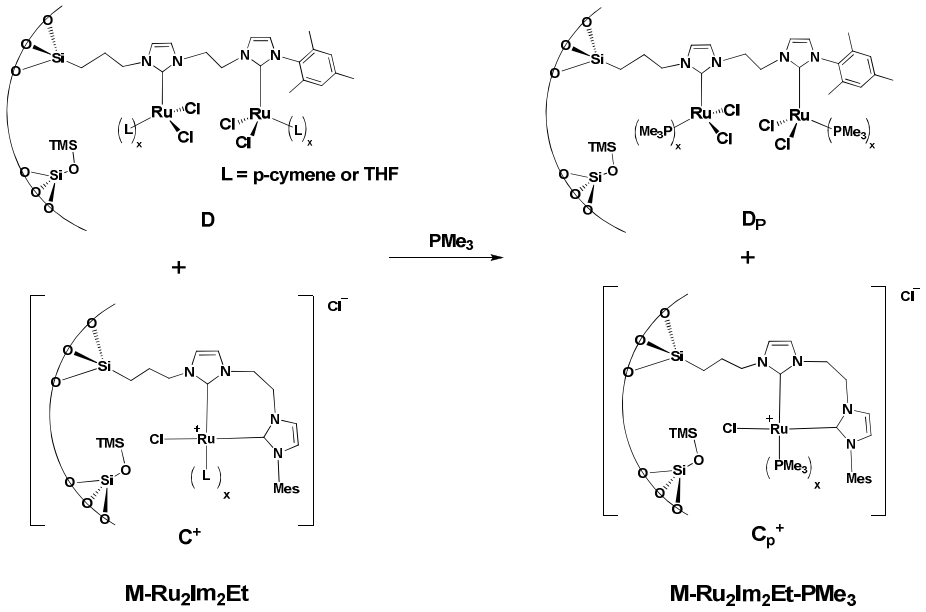

The reaction of **M-Ru$_2$Im$_2$Et** with PMe_3 to form **M-Ru$_2$Im$_2$Et-PMe$_3$** was monitored by ^{31}P HPDEC solid-state NMR, and it shows three main signals at -2, 1 and 19 ppm (see Figure 6). The two signals at -2 and 19 ppm were already observed in material **M-Ru$_2$Im$_2$PMe$_{3\text{-}12}$** in which the formation of cationic bis-NHC complexes was evidenced, whereas the peak at 1 ppm was only present in the mono-NHC derivatives, namely **M-RuPMe$_3$** and **M-RuPMe$_{3\text{-}12}$**. The peaks at -2 and 1 ppm are very close, and they probably correspond to ruthenium neutral complexes bonded to only one NHC unit, with similar structures. These peaks could therefore correspond to the **D$_P$** species, as the chemical shift of PMe_3 coordinated to a neutral dinuclear complex is thought to be very similar to the mono-NHC derivatives. However, the presence of a peak at 19 ppm probably corresponds to a cationic Ru(bis-NHC) complex (**C$_P^+$**), as previously discussed for material **M-Ru$_2$Im$_2$PMe$_{3\text{-}12}$**. In order to have more

information on these complexes, it will be necessary to develop similar chemistry on molecular complexes.

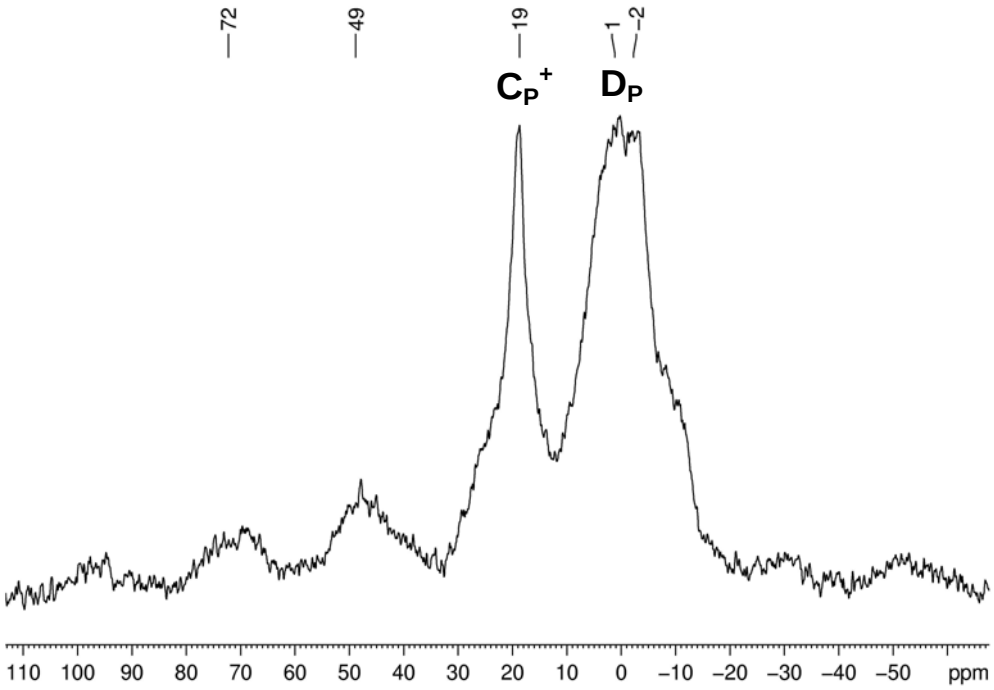

Figure 6. ^{31}P HPDEC NMR spectrum of **M-Ru$_2$Im$_2$Et-PMe$_3$**

3.2. Formation of Ru(bis-NHC) complexes from M-PrPyIm$_2$ material.

3.2.1. Reaction of [RuCl$_2$(p-cymene)]$_2$ on M$_p$-PrPyMesIm$_2$

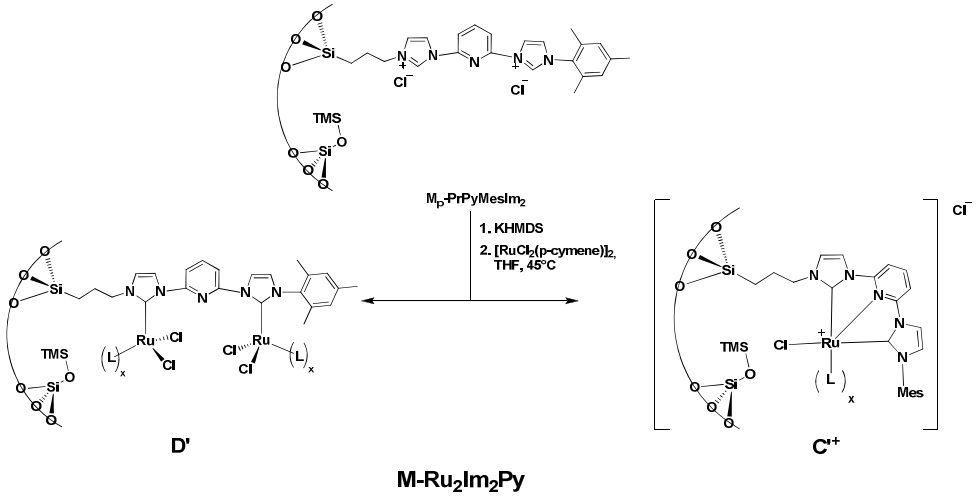

The reaction of [RuCl$_2$(p-cymene)]$_2$ on the passivated material **M$_p$-PrPyMesIm$_2$,** which was previously reacted with 2.4 equiv. of KHMDS, was performed in THF at 45℃ to obtain material **M-Ru$_2$Im$_2$Py**. The elemental analyses gave ruthenium and nitrogen contents of 2.81%$_{wt}$ and 2.01%$_{wt}$, respectively. This is consistent with the presence of 0.07 mmol/g

mono-imidazolium species and 0.16 mmol/g of bis-imidazolium species as well as 0.278 mmol/g ruthenium.

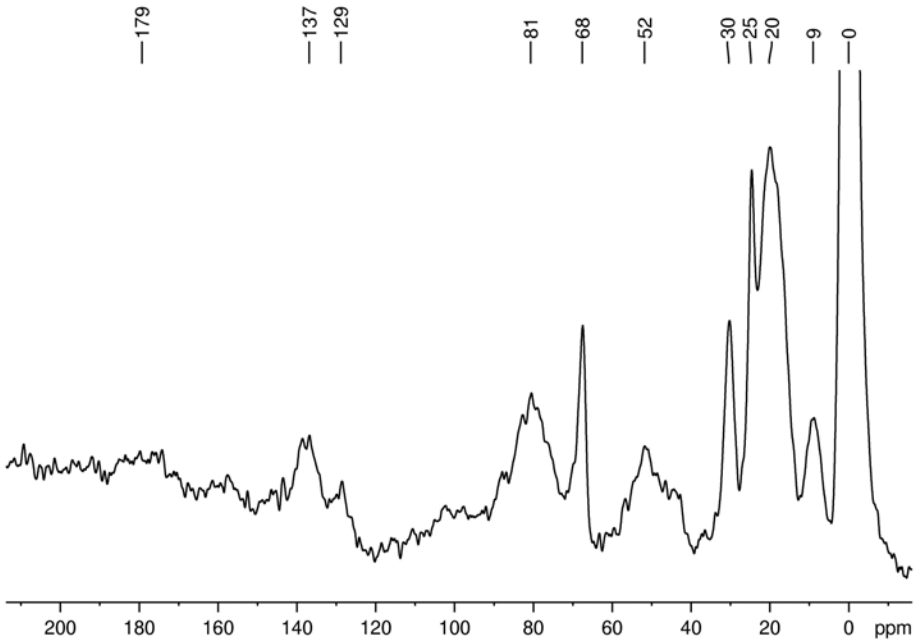

Figure 7. ^{13}C CPMAS NMR spectrum of **M-Ru$_2$Im$_2$Py**

Considering a maximum Ru/(mono-NHC) ratio of 1, there is a minimum Ru/(bis-NHC) ratio of 1.3. This is also consistent with the presence of dinuclear Ru(bis-NHC) complexes (**D'**), but the Ru/(bis-NHC) ratio cannot exclude the presence of the cationic bidentate Ru(bis-NHC) complexes (**C'$^+$**). In ^{13}C CPMAS solid-state NMR, we observe peaks at 0, 9, 20, 25, 30, 52, 68, 81, 129, 137 and 179 ppm (see Figure 7). The peaks at 30 and 80 ppm are consistent with the presence of p-cymene coordinated to Ru(NHC) species. As seen in previous reactions, there is a partial exchange of THF with p-cymene, explaining the two peaks at 25 and 68 ppm corresponding to THF. These results are consistent with the formation of ruthenium bis-NHC complexes having either p-cymene or THF as ligands.

3.2.2. Reaction of M-RuIm$_2$Py with trimethylphosphine

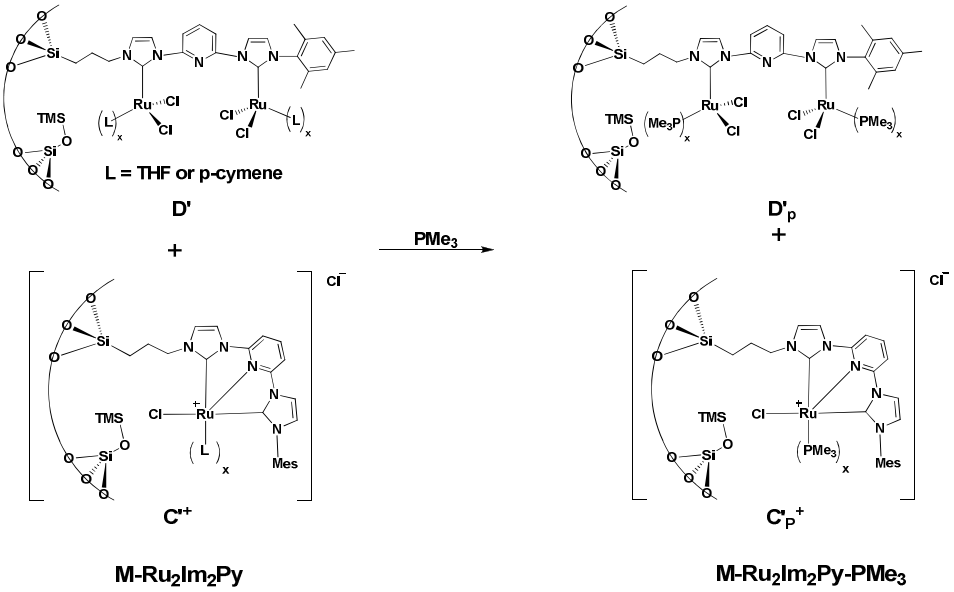

The reaction of **M-Ru$_2$Im$_2$Py** with an excess of PMe_3 and further evacuation under high vacuum gives **M-RuIm$_2$Py-PMe$_3$**. The ^{31}P HPDEC solid-state NMR shows three main signals at -2, 2 and 19 ppm. The relative intensities of the peaks at 2 and -2 ppm are almost unchanged compared to **M-Ru$_2$Im$_2$Et-PMe$_3$** and are thought to correspond to the neutral dinuclear bis-NHC (**D'$_P$**) species. The peak at 19 ppm is attributed to the cationic chelate bis-NHC species (**C'$_P^+$**), and is less intense than in material **M-Ru$_2$Im$_2$Et-PMe$_3$**, meaning that the formation of the cationic Ru(bis-NHC) species is less favoured in this case. In order to fully understand the spectra, we will need to study these reactions with molecular complexes.

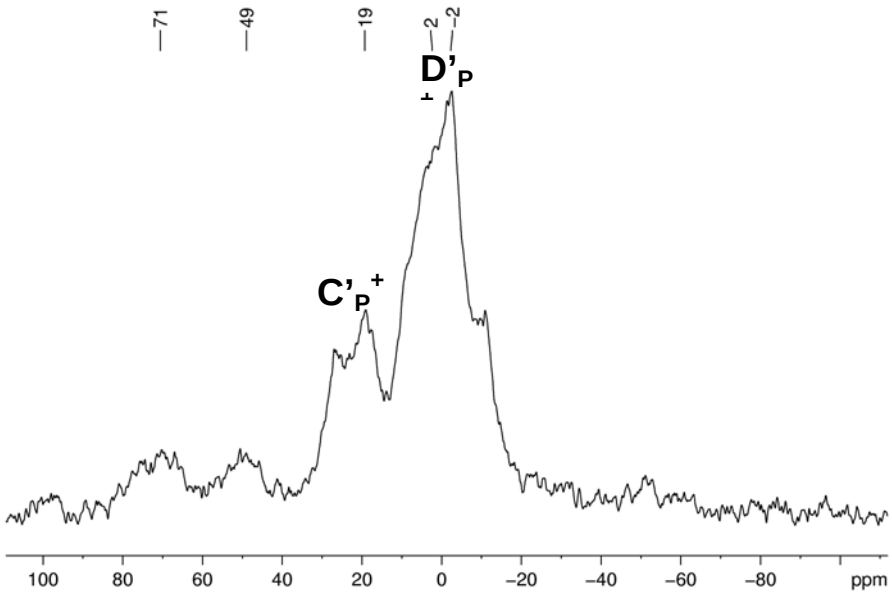

Figure 8. ^{31}P HPDEC NMR spectrum of **M-Ru$_2$Im$_2$Py-PMe$_3$**

IV-4. Catalytic performances

The performances of our new Ru-NHC catalytic materials were evaluated in the hydrogenation of CO_2 in presence of pyrrolidine (the reaction conditions are identical to chapter 2). It would first be interesting to compare all catalysts based on the propyl-mesityl-imidazolium ligand, in order to see if there is any influence of the concentration of active sites. When comparing materials in a 1/30 dilution prepared from an iodopropyl-based material (catalysts **M-RuCym** and **M-RuPMe$_3$**) and materials in a 1/12 dilution prepared from an azidopropyl-based material (catalysts **M-RuCym$_{-12}$** and **M-RuPMe$_{3-12}$** and **M-RuIm$_2$-PMe$_{3-12}$**), **M-RuCym** and **M-RuCym$_{12}$** (150 and 140 TON respectively), as **M-RuPMe$_3$** and **M-RuPMe$_{3-12}$** (2770 and 2780 respectively) show similar catalytic performances. (See Table 1) This is consistent with the presence of the same active sites in both cases, which is in agreement with the formation of mono-NHC complexes in **M-RuCym$_{12}$**. The catalyst **M-RuIm$_2$-PMe$_{3-12}$**, in which cationic bipodal bis-NHC complexes are present, shows a slight increase in activity with 2970 TON. This increase compared to **M-RuPMe$_{3-12}$** is not very important, but it could be consistent with the presence of bis-NHC species. In comparison, $RuCl_2(PMe_3)_4$ shows 5300 TON and $RuCl_2(dppe)_2$ 12100 TON, both at 100°C.

Table 1. Catalytic hydrogenation of CO_2 in presence of pyrrolidine

Entry	Catalyst	Substrate/Ru ratio	T(°C)	t(h)	TON
1	$RuCl_2(PMe_3)_4$	20000	100	5	5300
2	$RuCl_2(dppe)_2$	20000	100	5	12100
3	$RuCl_2(dppe)_2$	20000	200	5	13200
4	**M-RuPMe$_{3-12}$**	20000	100	5	2780
5	**M-RuPMe$_3$**	20000	100	5	2770
6	**M-RuCym**	20000	100	5	150
7	**M-RuCym$_{12}$**	20000	100	5	140
9	**M-RuIm$_2$-PMe$_{3-12}$**	20000	100	5	2970
10	**M-Ru$_2$Im$_2$Et-PMe$_3$**	13000	100	5	2220
11	**M-Ru$_2$Im$_2$Py**	13000	100	5	70
12	**M-Ru$_2$Im$_2$Py**	13000	200	5	1020
13	**M-Ru$_2$Im$_2$Py-PMe$_3$**	13000	100	5	3500
14	**M-Ru$_2$Im$_2$Py-PMe$_3$**	13000	200	5	8780

All catalysts generated from the propyl-mesityl imidazolium-based materials are therefore poorly active compared to the best homogeneous systems.

When **M-Ru$_2$Im$_2$Py** catalyst having no phosphine ligand is tested in the standard conditions at 100°C, it shows a very poor activity with a TON of 70. However, a dramatic effect of temperature is observed, and a TON of 1020 is obtained when performing the reaction at 200°C.[‡] This corresponds to an increase in activity of one order of magnitude between 100°C and 200°C, which was also observed with the bis-NHC systems of Peris *et al.* for the hydrogenation of CO_2 to formic acid.[7] These results are therefore also consistent with the presence of the dinuclear bis-NHC ruthenium complexes as active sites in our systems.

With **M-Ru$_2$Im$_2$Et-PMe$_3$** at 100°C, TON increased to 2500, which is in the range of mono-NHC systems, but **M-Ru$_2$Im$_2$Py-PMe$_3$** shows a TON of 3500 which is already better than all the mono-imidazolium systems. This difference between the two catalysts could be related with the fact that more dinuclear species (**D**) are observed in **M-Ru$_2$Im$_2$Py-PMe$_3$** than in **M-Ru$_2$Im$_2$Et-PMe$_3$**, consistent with a better activity and stability of these active sites. Finally, the best catalytic performances are obtained when using the same catalyst **M-Ru$_2$Im$_2$Py-PMe$_3$** at 200 °C, for which a TON of 8780 is obtained. In the same conditions, $RuCl_2(dppe)_2$, gave a TON of 13200 which is very close from its activity at 100°C (12100 TON). The bis-NHC catalyst **M-Ru$_2$Im$_2$Py-PMe$_3$** therefore shows very close performances with respect to the best reported catalyst $RuCl_2(dppe)_2$.

Furthermore, these uncommon dinuclear bis-NHC complexes have a strong advantage compared to the mono-NHC systems: an ICP analysis was carried out on the liquid phase after catalysis with material **M-Ru$_2$Im$_2$Py-PMe$_3$** at 200°C, and it showed that only 20% of the ruthenium had leached in solution, compared to 50% at 100°C with the mono-NHC systems. This very important gain in stability is, as the characterization and the catalytic performances, fully consistent with the formation of the dinuclear bis-NHC species. Indeed, dinuclear bis-

[‡] We confirmed that this increase in activity was effectively due to the activity of the catalyst by performing a blank reaction without catalyst at 200°C, and it showed no conversion of pyrrolidine.

NHC catalysts of rhodium were described as highly stable species and showed very high activities when they were used at high temperatures for the hydroformylation of terminal alkenes.[1,8] This very good stability at high temperatures and under harsh reaction conditions, that are present during the hydrogenation of CO_2, is very encouraging for the further development of bis-NHC-based supported catalysts.

IV-5. Conclusion

In conclusion, this study describes the use of new imidazolium and bis-imidazolium materials for the formation of a new class of ruthenium NHC heterogeneous catalysts. The use of more concentrated propyl-mesityl-imidazolium materials led to the formation of heterogeneous catalysts bearing the same active sites and having the same activities than the materials described in chapter 1, but with a much more important metal loading. Favouring the formation of bis-NHC (bis-podal) system with the same material led to the formation of bis-NHC cationic surface specie upon contacting PMe_3, and this system showed overall very similar – yet slightly improved activities – than the neutral species. More importantly, the use of the bis-imidazolium materials with either ethylene or pyridine linker allowed the formation of dinuclear ruthenium bis-imidazolium complexes, which showed greatly improved catalytic activity and stability in the hydrogenation of CO_2 in presence of pyrrolidine. For example, material **M-Ru$_2$Im$_2$Py** based on a bis-imidazolium unit having a pyridine linker showed a very strong dependence of the catalytic activity with respect to temperature, with an activity changing by a factor of 50 when changing reaction temperature from 100 to 200°C, going from 70 to 1000 TON in 5 hours. Under our conditions (130 bar, 1/1 CO_2/H_2 mixture), the catalyst **M-Ru$_2$Im$_2$Py-PMe$_3$**, obtained by addition of trimethylphosphine on **M-Ru$_2$Im$_2$Py**, showed the best performances, with activities of 3500 and 8780 TON at 100°C and 200°C respectively after 5 hours with little metal leaching. Considering that conditions involving supercritical CO_2 typically allow much better performances, it is clear that it would be worth investigating such supported ruthenium bis-NHC systems under such optimal conditions. Overall, we have reported here the most active and stable heterogeneous catalysts developed so far for the catalytic hydrogenation of CO_2. This stability probably arises from the nature of the active species and the presence of dinuclear Ru bis-NHC complexes. The detailed level of molecular understanding, while still preliminary, already shows that better catalytic materials would probably results from the selective formation of dinuclear Ru(bis-NHC) complexes, which will also be studied as homogeneous catalysts.

IV-6. Experimental Part

General procedure. All experiments were carried out using either Schlenck techniques, vacuum line or a glovebox, with freshly distilled, degassed solvents. $[RuCl_2(p\text{-cymene})]_2$,[9] $RuCl_2(PMe_3)_4$[10] and $RuCl_2(dppe)_2$[11] were synthesized according to literature procedures. Trimethylphosphine was purchased from Strem. KHMDS solution was purchased from Aldrich. ^1H and ^{13}C solution spectra were recorded on a Bruker Avance DRX 300 (300MHz). ^1H, ^{13}C and ^{31}P solid state NMR spectra were recorded on a Bruker Avance 500 (500MHz) and a Bruker DSX 300 (300MHz). ^1H solid state spectra were recorded using Magic Angle Spinning (MAS) at 10 kHz. ^{13}C solid state spectra were recorded using Cross Polarization with D1 of 2s, p15 of 2 ms, around 30000 scans and MAS at 10 kHz . ^{31}P solid state spectra were recorded with HPDEC direct detection experiments, D1 of 30s and MAS at 10 kHz. ^{29}Si solid state spectra were recorded using both Cross Polarization and MAS at 5 kHz. Elemental analysis were performed at the "Mikroanalytisches Labor Pascher", Remagen, Germany.

Preparation of material M_p-PrMesIm$_{-12}$. In a schlenck, 1g of material **M-PrMesIm$_{-12}$** is put in suspension in 70 mL toluene. Then are added 13.4 mL of triethylamine and 6.4 mL trimethylsilyl bromide. The suspension is stirred overnight (18 hours). The product was filtered, washed with toluene (2 x 20 mL) and dichloromethane (4 x 20 mL). After drying at 135℃ under vacuum (10^{-5} mbar), **M_p-PrMesIm$_{-12}$** is obtained as a light beige powder.

Preparation of M-RuCym$_{-12}$. To a suspension of 1-propyl-3-mesityl-imidazolium chloride functionnalized material having a passivated surface (250 mg), **M_p-PrMesIm$_{-12}$**, in toluene (5 mL), 0.70 mL of a 0.5M solution of KHMDS in toluene was added dropwise. After 15 min, a solution of 98 mg of $[RuCl_2(p\text{-cymene})]_2$ in 40 mL Toluene was added, and the resulting suspension stirred for 3 h. The solid was filtered, and successively washed three times with 30 mL Toluene and twice with 10 mL diethyl ether. Drying under high vacuum (10^{-5} mbar) for 1 h afforded an orange powder, **M-RuCym$_{-12}$**. ^{13}C CPMAS solid-state NMR (125.7 MHz): 136, 128, 123, 81, 51, 30, 18, 8, 0.

Representative procedure for the preparation of M-RuPMe$_{3\text{-}12}$. To 150mg of **M-RuCym$_{12}$** in a 10 mL Schlenk equipped with Teflon valve (Young) was added by distillation PMe_3 so as to obtain a wet solid. After 1 h, the material was then dried under high vacuum for 8 h to yield **M-RuPMe$_{3\text{-}12}$** as a light yellow powder. ^{13}C CPMAS solid-state NMR (125.7 MHz): 133, 126, 121, 82, 50, 29, 16, 8, 0. ^{31}P HPDEC solid-state NMR : 96, 48, 1, -9, -55.

Preparation of M-RuIm$_2$THF$_{12}$. To a suspension of 1-propyl-3-mesityl-imidazolium chloride functionnalized material having a passivated surface (250 mg), **M$_p$-PrMesIm$_{.12}$**, in THF (5 mL), 0.70 mL of a 0.5M solution of KHMDS in toluene was added dropwise. After 15 min, a solution of 13 mg of $[RuCl_2(p\text{-cymene})]_2$ in 15 mL THF was added, and the resulting suspension heated up to 45°C and stirred for 3 h30. The solid was filtered, and successively washed three times with 15 mL THF and twice with 10 mL diethyl ether. Drying under high vacuum (10^{-5} mbar) for 1 h afforded an orange powder, **M-RuIm$_2$THF$_{12}$**. ^{13}C CPMAS solid-state NMR (125.7 MHz): 135, 128, 123, 82, 68, 51, 30, 25, 20, 17, 9, 0.

Preparation of M-RuIm$_2$PMe$_{3\text{-}12}$. This material was synthesized using the same procedure as described for **M-RuPMe$_{3\text{-}12}$**, using **M-RuIm$_2$THF$_{12}$**, to yield **M-RuIm$_2$PMe$_{3\text{-}12}$** as a yellow powder. ^{13}C CPMAS solid-state NMR (125.7 MHz): 129, 51, 17, 9, 0. ^{31}P HPDEC solid-state NMR : 76, 47, 18, -3, -10.

Preparation of M-RuIm$_2$Et. To a suspension of material **M$_p$-PrEtMesIm$_2$** having a passivated surface (250 mg), in THF (5 mL), 0.34 mL of a 0.5M solution of KHMDS in toluene was added dropwise. After 15 min, a mixture of 25 mg of $[RuCl_2(p\text{-cymene})]_2$ in 15 mL THF was added, and the resulting suspension was heated up to 45°C and stirred for 4h. The solid was filtered, and successively washed three times with 15 mL THF and twice with 10 mL diethyl ether. Drying under high vacuum (10^{-5} mbar) for 1 h afforded a brown powder, **M-RuIm$_2$Et**. ^{13}C CPMAS solid-state NMR (125.7 MHz): 174, 138, 128, 80, 68, 51, 30, 25, 20, 9, 0.

Preparation of M-Ru$_2$Im$_2$Et-PMe$_3$. This material was synthesized using the same procedure as described for **M-RuPMe$_{3\text{-}12}$**, using **M-RuIm$_2$Et**, to yield **M-Ru$_2$Im$_2$Et-PMe$_3$** as a

brown powder. ^{13}C CPMAS solid-state NMR (125.7 MHz): 172, 137, 127, 81, 68, 50, 30, 17, 9, 0. ^{31}P HPDEC solid-state NMR : 72, 49, 19, 1, -2.

Preparation of M-RuIm$_2$Py. To a suspension of material **M$_p$-PrPyMesIm$_2$** having a passivated surface (250 mg), in THF (5 mL), 0.34 mL of a 0.5M solution of KHMDS in toluene was added dropwise. After 15 min, a mixture of 25 mg of [RuCl$_2$(p-cymene)]$_2$ in 15 mL THF was added, and the resulting suspension was heated up to 45℃ and stirred for 4h. The solid was filtered, and successively washed three times with 15 mL THF and twice with 10 mL diethyl ether. Drying under high vacuum (10^{-5} mbar) for 1 h afforded a brown powder, **M-RuIm$_2$Py**. ^{13}C CPMAS solid-state NMR (125.7 MHz): 179, 137, 129, 81, 68, 52, 30, 25, 20, 9, 0.

Preparation of M-Ru$_2$Im$_2$Py-PMe$_3$. This material was synthesized using the same procedure as described for **M-RuPMe$_{3\text{-}12}$**, using **M-RuIm$_2$Py**, to yield **M-Ru$_2$Im$_2$Py-PMe$_3$** as a brown powder. ^{13}C CPMAS solid-state NMR (125.7 MHz): 171, 137, 129, 81, 68, 51, 45, 31, 18, 10, 0. ^{31}P HPDEC solid-state NMR : 71, 49, 19, 2, -2.

IV-7. References

[1] M. Poyatos; P. Uriz; J. A. Mata; C. Claver; E. Fernandez; E. Peris *Organometallics* **2002**, *22*, 440-444.
[2] M. Poyatos; E. Mas-Marza; M. Sanau; E. Peris *Inorg. Chem.* **2004**, *43*, 1793-1798.
[3] C. Gandolfi; M. Heckenroth; A. Neels; G. Laurenczy; M. Albrecht *Organometallics* **2009**, *28*, 5112-5121.
[4] S. Sanz; A. Azua; E. Peris *Dalton Trans.* **2010**, *39*, 6339-6343.
[5] A. Mrutu; K. I. Goldberg; R. A. Kemp *Inorg. Chimi. Acta* **2010**, *364*, 115-119.
[6] G. Su; X.-K. Huo; G.-X. Jin *J. Organomet. Chem.* **2011**, *696*, 533-538.
[7] S. Sanz; A. Azua; E. Peris *Dalton Trans.* **2010**
39, 6339-6343.
[8] M. Poyatos; P. Uriz; J. A. Mata; C. Claver; E. Fernandez; E. Peris *Organometallics* **2003**, *22*, 440-444.
[9] M. A. Bennett; A. K. Smith *J. Chem. Soc., Dalton Trans.* **1974**, 233-241.
[10] R. A. Jones; F. M. Real; G. Wilkinson; A. M. R. Galas; M. B. Hursthouse; K. M. A. Malik *J. Chem. Soc., Dalton Trans.* **1980**, 511-518.
[11] R. Mason; D. W. Meek; G. R. Scollary *Inorg. Chimi. Acta* **1976**, *16*, L11-L12.

IV-8. Appendix

M-RuCym$_{12}$

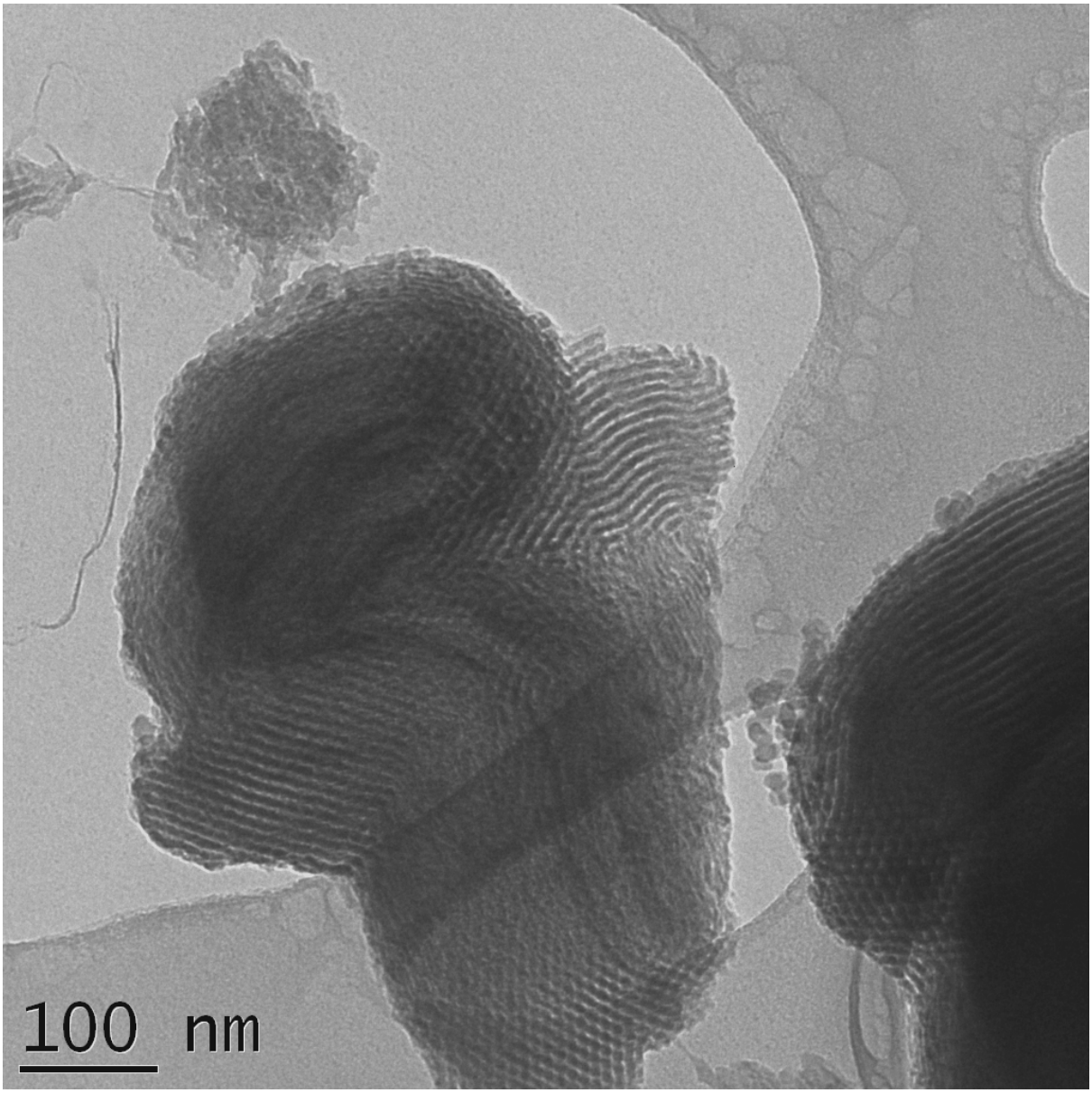

Figure A1. TEM picture of **M-RuCym$_{12}$**

M-RuPMe$_{3\text{-}12}$

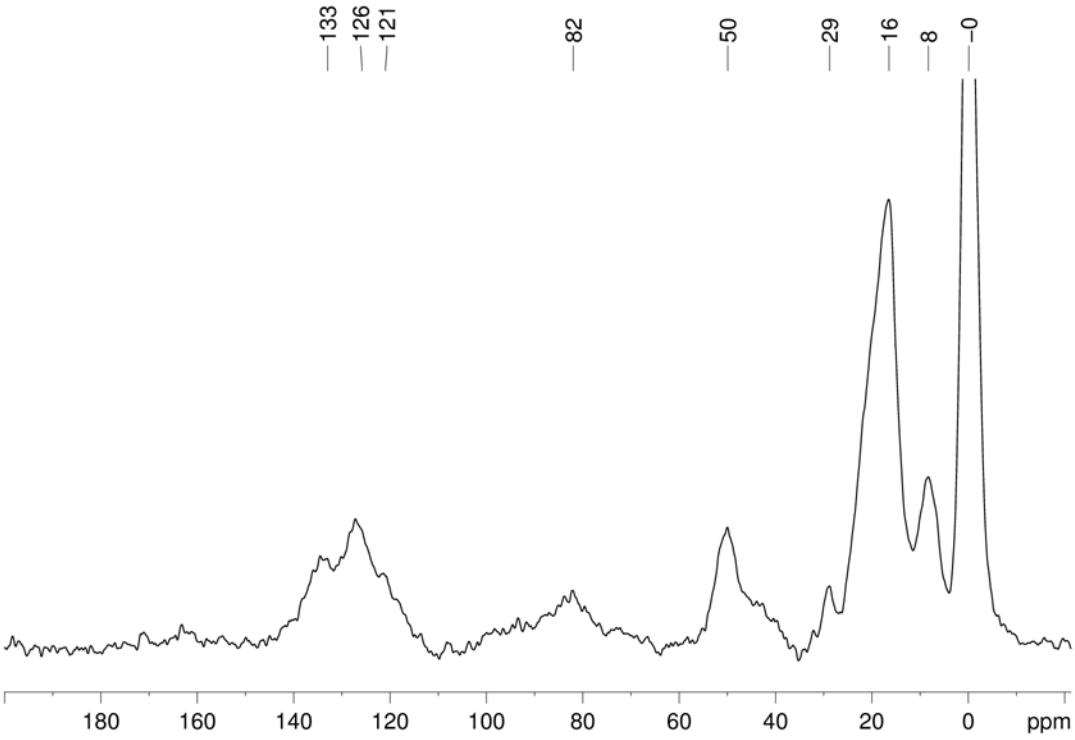

Figure A2. ^{13}C CPMAS solid-state NMR of **M-RuPMe$_{3\text{-}12}$**

M-RuIm$_2$PMe$_{3\text{-}12}$

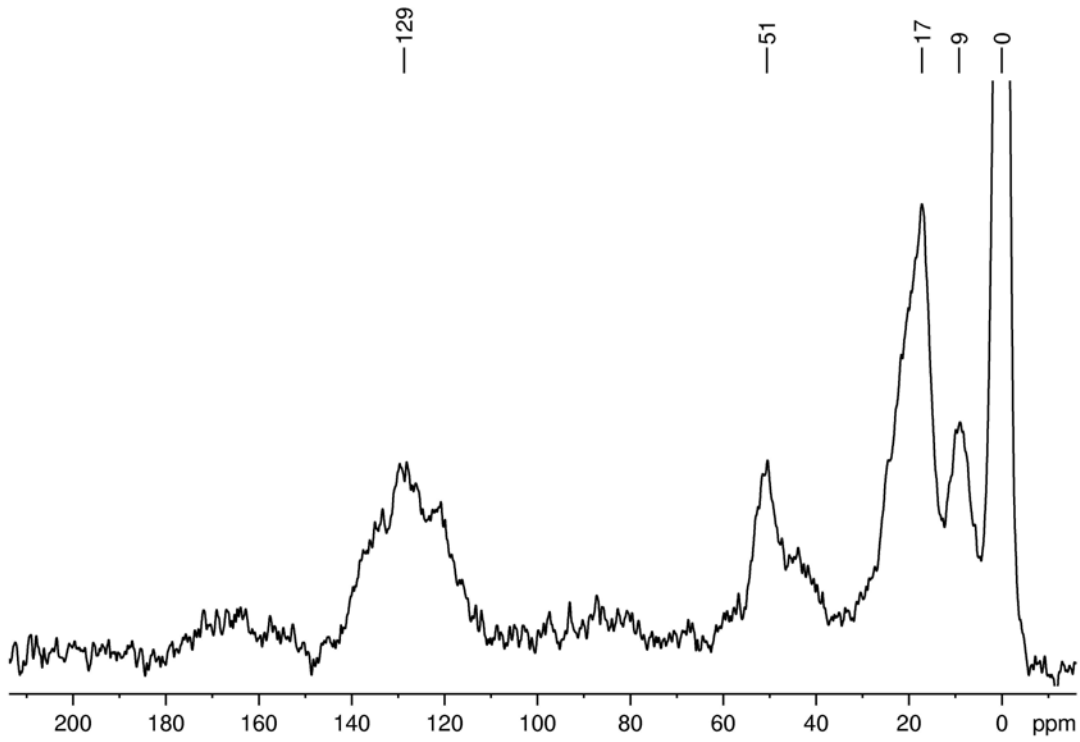

Figure A3. ^{13}C CPMAS solid-state NMR of **M-Ru$_2$Im$_2$PMe$_{3\text{-}12}$**

M-Ru_2Im_2Et-PMe_3

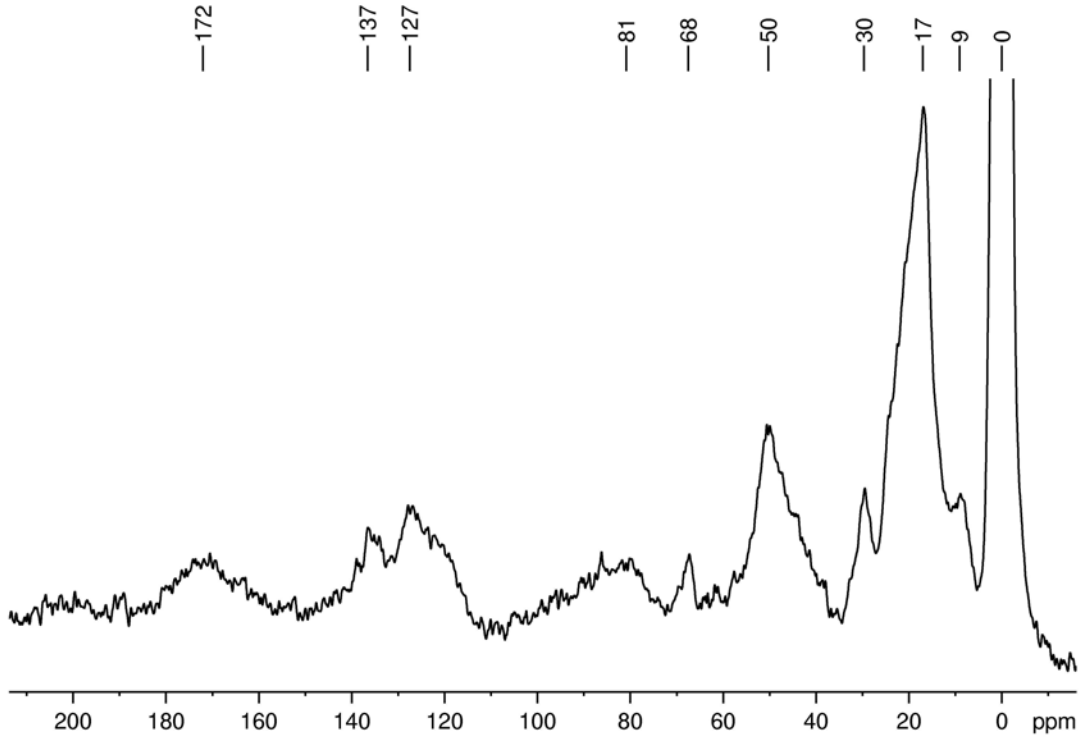

Figure A4. ^{13}C CPMAS solid-state NMR of **M-Ru_2Im_2Et-PMe_3**

M-Ru_2Im_2Py-PMe_3

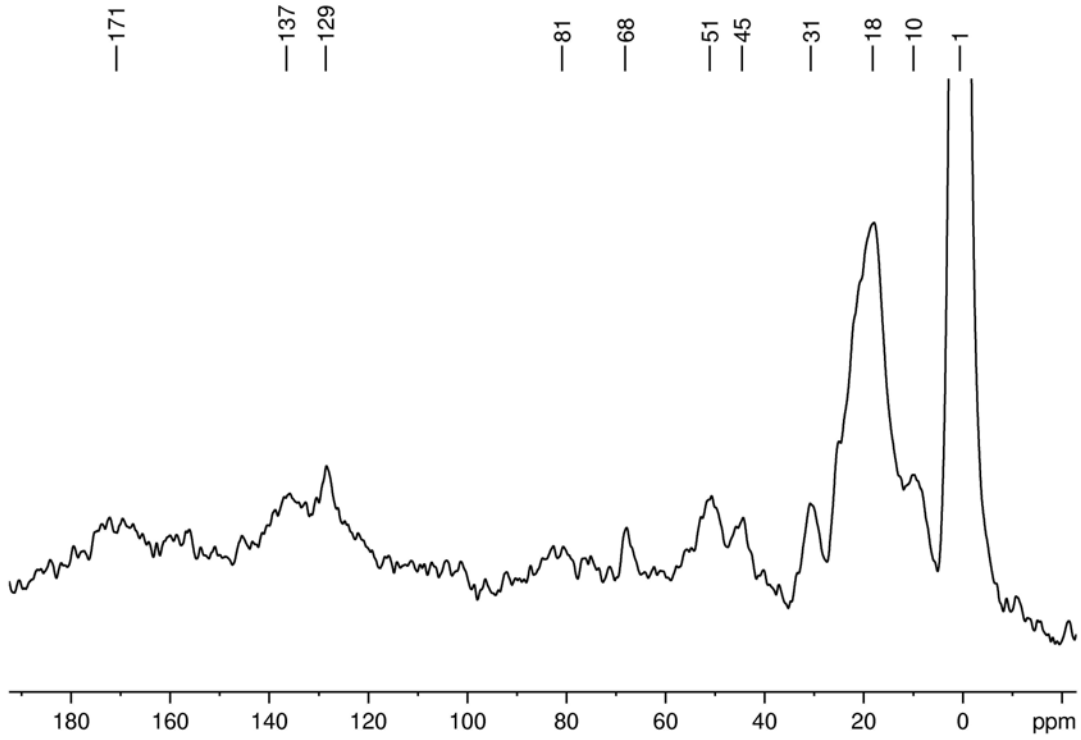

Figure A5. ^{13}C CPMAS solid-state NMR of **M-Ru_2Im_2Py-PMe_3**

Chapter 5

Conclusion and Prospects

Conclusion and Prospects

The objective of this study was to develop NHC-Ru-based heterogeneous catalysts for the hydrogenation of CO_2, obtained via a controlled grafting of a ruthenium precursor on imidazolium-based hybrid mesoporous organic-inorganic materials obtained from a direct synthesis approach.

First, using the already developed propyl-mesityl-imidazolium materials in a 1/30 dilution, the reaction of **M-PrMesIm** with $[RuCl_2(p\text{-cymene})]_2$ in THF after deprotonation led to the formation of material **M-RuCym**. The use of a ^{13}C-enriched material at the carbenic position allowed having a direct insight at the Ru-C bond, with a characteristic signal at 173 ppm, in agreement with what was observed for the corresponding molecular complex **RuCym**. Moreover, characterization by ^{13}C CPMAS NMR showed that a partial exchange between THF and p-cymene ligands occurred during the grafting step, leading to two different surface species. This could be confirmed by studying the further exchange with THF and THF-d_8. The elemental analysis confirmed the presence of ruthenium on 60% of the NHC units, which is particularly interesting, as previous attempts to graft ruthenium metathesis catalysts on the same supports led to only 20% of grafting.

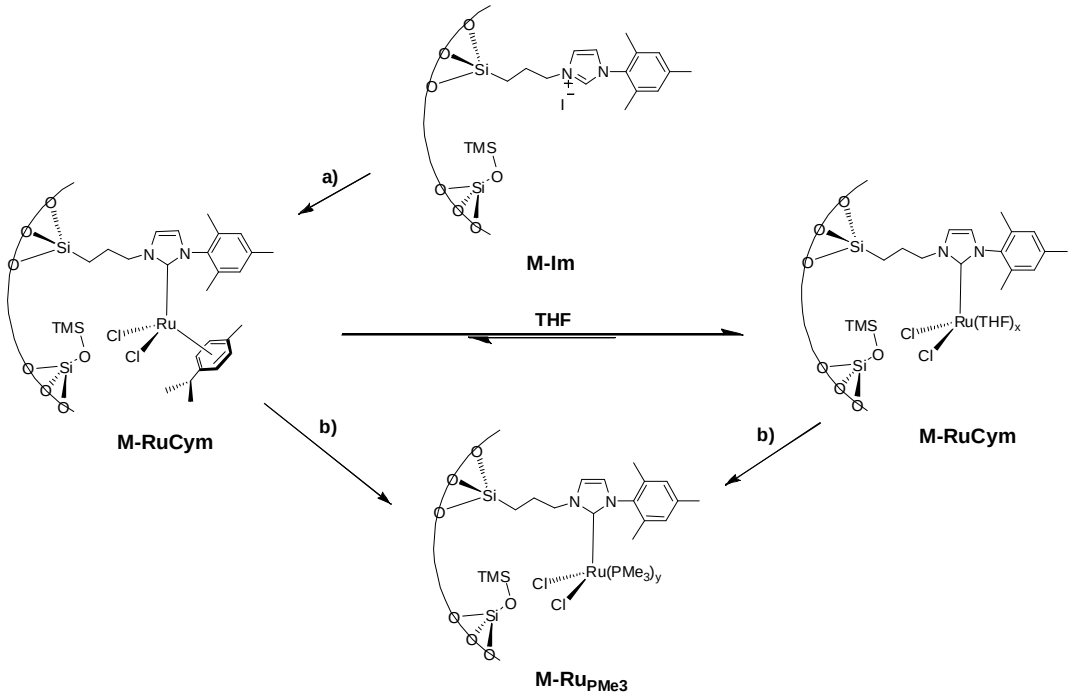

Scheme 1. Preparation of materials **M-Ru$_{Cym}$** and **M-Ru$_{PMe3}$** : a) KHMDS (1.2 equivalent), followed by $[RuCl_2(p\text{-cymene})]_2$ in THF ; b) impregnation of pure degassed PMe_3.

Then, further reaction of **M-RuCym** with either PMe_3 or dppe ligands led to a partial displacement of the p-cymene and THF ligands by the desired phosphine ligand and the formation of materials **M-RuPMe$_3$** and **M-Rudppe** respectively. The solid-state ^{31}P NMR spectra are consistent with the presence of PMe_3 complexes, whose exact structures could not be fully identified.

All these catalysts were used in the hydrogenation of CO_2 in presence of pyrrolidine in a batch reactor at 130 bar and 100°C to form 1-formylpyrrolidine, and their catalytic performances were compared with these of two of the best homogeneous catalysts, namely $RuCl_2(PMe_3)_4$ and $RuCl_2(dppe)_2$. Although the non-phosphine containing **M-RuCym** catalyst showed only poor activity (150 TON), the addition of phosphine ligands led to an important increase of the activity with 2770 and 5110 TON for **M-RuPMe$_3$** and **M-Rudppe**, respectively, which is close to activities obtained for best homogeneous catalysts $RuCl_2(PMe_3)_4$ (5300 TON) and $RuCl_2(dppe)_2$ (12100 TON), when run under identical conditions. While it is noteworthy that the activities of the heterogeneous and homogeneous catalysts are of the same order of magnitude, the main drawback of the supported Ru(NHC) catalysts is their unstability under the reaction conditions as evidenced by large amount of metal leaching (50% according to ICP-AES). This family of catalyst based on mono-NHC-Ru complexes is thus not well adapted to these harsh reaction conditions, and we have thus developed in the second part of this PhD thesis a strategy to develop bis-NHC-Ru complexes because they are known to be much more stable complexes.

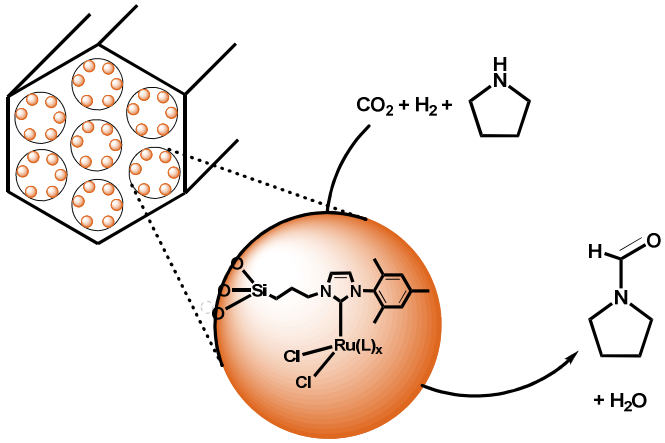

Scheme 2. Catalytic hydrogenation of CO_2 in presence of pyrrolidine.

Conclusion and Prospects

The stability of such complex as a function of reaction conditions was further illustrated in the use of these well-defined **M-RuCym** catalyst for the Kharasch addition of CCl_4 onto styrene. In this case, similar catalytic performances were obtained for homogeneous and heterogeneous catalysts, but here no metal leaching could be detected, thus showing that the stability of the NHC-Ru bond highly depends on the reaction conditions. Another prospect for these **M-RuCym** materials could be their transformation into metathesis catalysts since it is known that ruthenium(p-cymene) precursors can form in situ Grubbs catalysts when appropriate activators are used.[1,2]

Second, in order to circumvent the stability problem of NHC-Ru systems, we have developed strategies to generate bis-NHC Ru complexes incorporated into materials: the first ones consisted in increasing the density of imidazolium units inside the materials with the hope to generate bis-NHC Ru-complexes and the second ones was based on the development of functionalities already containing bis-imidazolium units.

With the first strategy, it involved the development of methods to increase the concentration of functionalities. Here we chose the *in situ* formation of imidazolium units from amino groups. Of the different methods investigated, the best solution turned out to be the incorporation of azidopropyl-functionalities into silica-materials followed by their conversion into aminopropyl groups via the Staudinger reaction and then their conversion to imidazolium units (Scheme 3). This approach allowed obtaining concentration from 1/30 to 1/12.

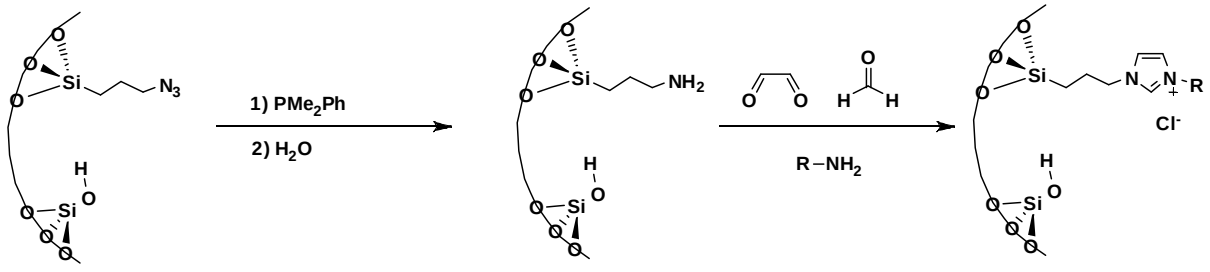

Scheme 3. Two-step formation of an imidazolium-based material from an azido-based material

Conclusion and Prospects

The reaction of the 1/12 concentrated **M-PrMesIm$_{12}$** material with [RuCl$_2$(p-cymene)]$_2$ was studied with different stoichiometries, and the products were further contacted with PMe$_3$. Using an excess of [RuCl$_2$(p-cymene)]$_2$ led to the formation of **M-RuCym$_{12}$ and M-RuPMe$_{3\text{-}12}$** in which the formation of mono-NHC complexes was evidenced. The reaction with 0.5 equiv. of ruthenium per NHC led to materials **M-RuIm$_2$-PMe$_{3\text{-}12}$ and M-RuIm$_2$-PMe$_{3\text{-}12}$**. The presence of a new peak at 19 ppm in ^{31}P solid-state NMR was attributed to the presence of cationic Ru(bis-NHC) bipodal species.

The evaluation of the catalytic performances of materials **M-RuCym$_{12}$** and **M-RuPMe$_{3\text{-}12}$** showed similar activities with **M-RuCym** and **M-RuPMe$_3$** with 140 and 2780 TON respectively, confirming the formation of mono-NHC species. **M-RuIm$_2$-PMe$_{3\text{-}12}$**, showed a slight increase of the performance compared to **M-RuPMe$_{3\text{-}12}$**, with 2970 TON, probably due to the presence of the bipodal bis-NHC complexes. However, this formation of bipodal bis-NHC complexes is not quantitative, probably because the density of functional groups at the surface of the material is not high enough to form quantitatively such species. It would thus be necessary to develop even-more concentrated materials (up to a 1/6 dilution probably) in order to be able to form bipodal species in a very selective and quantitative way (see Scheme 4).

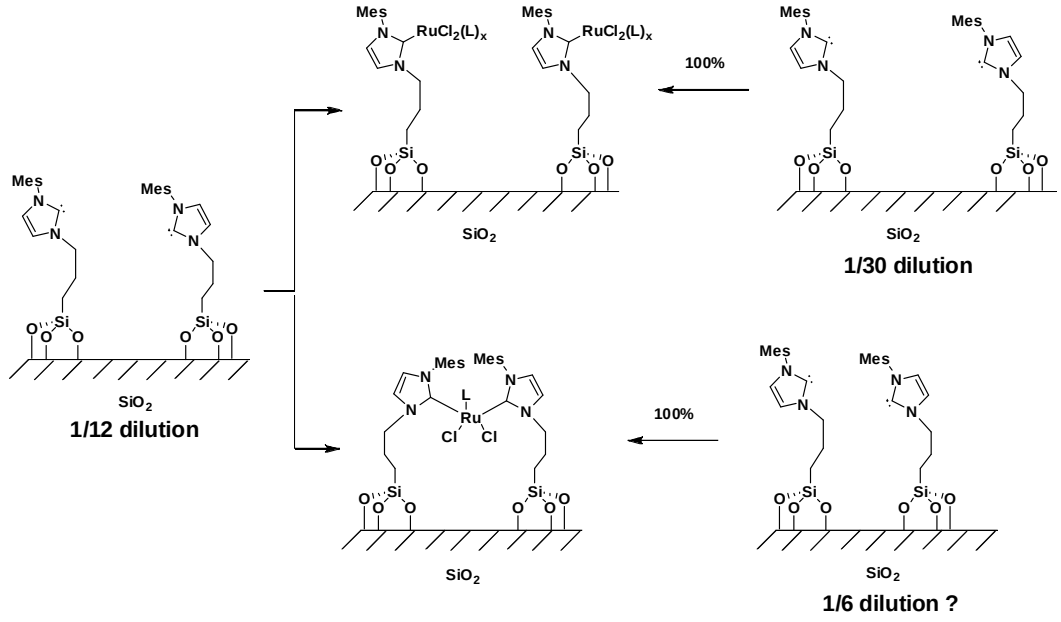

Scheme 4. Influence of the concentration of the material on the nature of the grafted species

Conclusion and Prospects

Two bis-imidazolium functionalized materials were developed, having either a pyridine linker (material **M-PrPyMesIm$_2$**) or an ethyl linker (material **M-PrEtMesIm$_2$**). The reaction of [RuCl$_2$(p-cymene)]$_2$ on these two materials was performed in THF at 45°C to obtain materials **M-Ru$_2$Im$_2$Py** and **M-Ru$_2$Im$_2$Et** respectively. Elemental analyses were consistent with the presence of binuclear bis-NHC complexes in each material. The further reaction with PMe$_3$ led to **M-Ru$_2$Im$_2$Et-PMe$_3$** and **M-Ru$_2$Im$_2$Py-PMe$_3$**, which analysis by ^{31}P NMR also evidenced the presence of cationic Ru(bis-NHC) complexes (see Scheme 5).

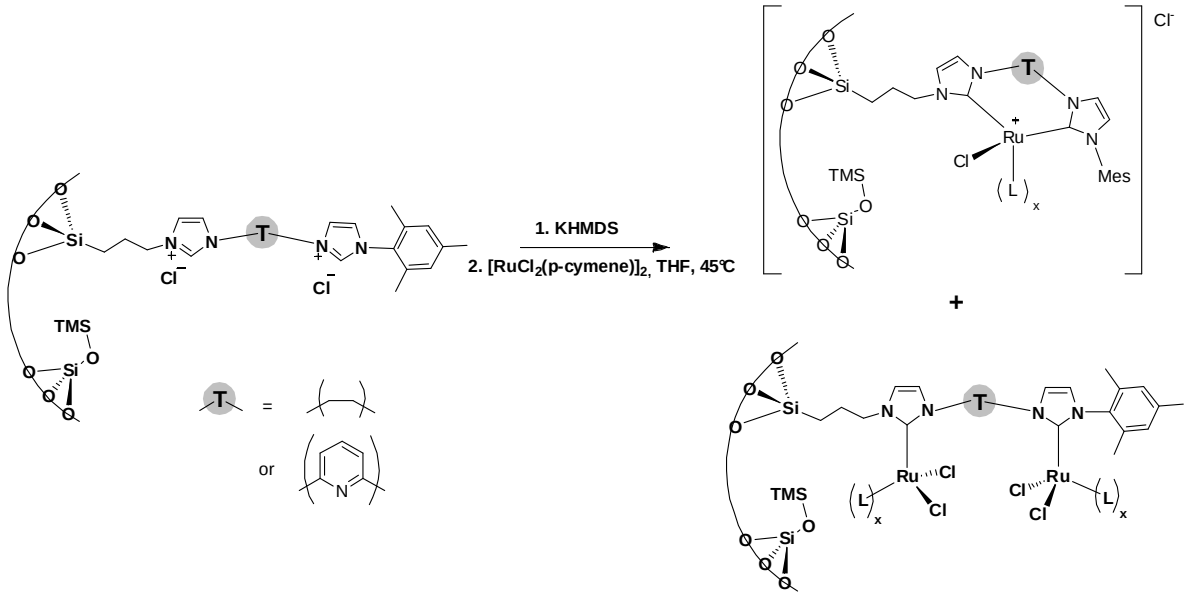

Scheme 5. Formation of ruthenium(bis-NHC) complexes from the bis-imidazolium units

In catalytic hydrogenation of CO_2, the catalyst **M-Ru$_2$Im$_2$Py-PMe$_3$** showed the best performances with 3500 TON at 100°C after 5h and 8780 TON at 200°C. In the same conditions, the best reported catalyst RuCl$_2$(dppe)$_2$ gives 13200 TON. Moreover, an ICP analysis of the filtrate of the reaction mixture after catalysis with **M-Ru$_2$Im$_2$Py-PMe$_3$** showed a leaching of only 20% of ruthenium at 200°C, whereas catalyst **M-RuPMe$_3$** led to 50% leaching at only 100°C. In addition to a better activity, the bis-NHC systems are also much more stable catalysts.

Conclusion and Prospects

Overall, this study has shown that it is possible to design supported catalysts in the same way homogenous catalysts are conceived, so that when problems, e.g. leaching or more generally speaking unstability of Metal-Ligand bonds, occurs, one can propose strategies to improve such systems. This allowed to find heterogeneous catalysts with unprecedented performances for the targeted reactions, and further improvements are clearly visible. In parallel to this work using the same strategy, we also developed Pd-based NHC systems, which also show promising and unprecedented catalytic performances for the partial hydrogenation of alkynes to alkenes (see Appendix).

One must recognize that the selective *in situ* formation of a targeted complex on a hybrid organic-inorganic material is indeed a challenge, because the surface is not innocent and can bring paramount complexity. It is thus required to adapt molecular chemistry, including for “pure organic reactions” to surface chemistry. However, the surface can also bring big advantages, allowing reactions not possible in a homogeneous phase. The one-step *in situ* formation of unsymmetrical imidazolium units is an example of such a reaction which fully took advantage of the heterogeneous phase brought by site isolation on surfaces. However, this requires to conduct a true molecular approach to surface chemistry, and thus to characterise surface species at every step of material synthesis or post-functionalisation. It is thus clear that one of the main limitations is the requirement of advanced characterization techniques, in particular solid-state NMR spectroscopy, which is one of the most powerful tools to obtain structures and dynamics of surface species.[3] Recent developments such as Surface Enhanced NMR spectroscopy,[4,5] clearly show that such goals can now be reached and that understanding surface chemistry including for reaction intermediates and surface species in catalytic cycles will be possible and that true molecular design and development will be possible in the near future.

References

[1] D. Sémeril; C. Bruneau; P. H. Dixneuf *Adv. Synth. Catal.* **2002**, *344*, 585-595.
[2] M. Ahr; C. Thieuleux; C. Copéret; B. Fenet; J.-M. Basset *Adv. Synth. Catal.* **2007**, *349*, 1587-1591.
[3] F. Blanc; C. Coperet; A. Lesage; L. Emsley *Chem. Soc. Rev.* **2008**, *37*, 518-526.
[4] A. Lesage; M. Lelli; D. Gajan; M. A. Caporini; V. Vitzthum; P. Mieville; J. Alauzun; A. Roussey; C. Thieuleux; A. Mehdi; G. Bodenhausen; C. Coperet; L. Emsley *J. Am. Chem. Soc.*, *132*, 15459-15461.
[5] M. Lelli; D. Gajan; A. Lesage; M. A. Caporini; V. Vitzthum; P. Mieville; F. Heroguel; F. Rascon; A. Roussey; C. Thieuleux; M. Boualleg; L. Veyre; G. Bodenhausen; C. Coperet; L. Emsley *J. Am. Chem. Soc.*, *133*, 2104-2107.

Appendix

A-1. Formation of supported Pd(NHC) derivatives and their catalytic performances

1.1. Reaction of Pd(DAB$_{tBu}$)(MA) with M$_p$-PrMesIm in presence of maelic anhydride.

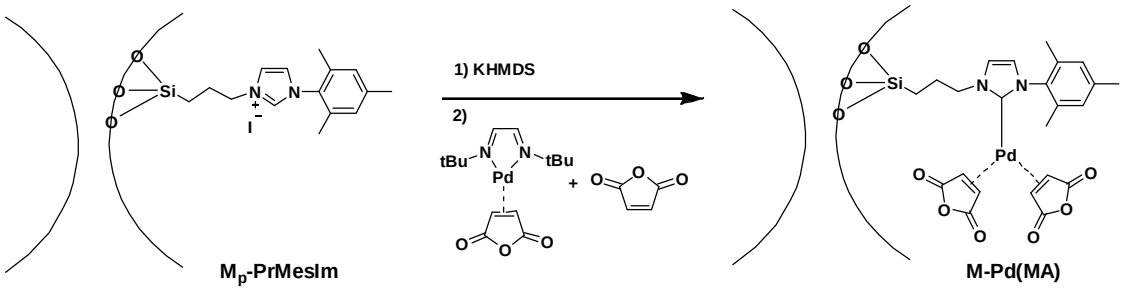

As previously reported, the reaction of a NHC ligand on the Pd(DAB)(MA) complex will lead to displacement of the DAB(Diazabutadiene) ligand,[1] and a second stabilizing ligand is needed, we therefore chose to add extra maleic anhydride (MA). The Pd(DAB)(MA) complex dissolved in THF was added to a deprotonated **M$_p$-PrMesIm** material in presence of 1 equivalent of MA and the mixture was stirred for 3 hours to obtain after washing and drying the red material **M-Pd(MA)**. The color itself is already an evidence of the formation of Pd(NHC) species, as the starting Pd(DAB)(MA) complex is pale yellow and reported Pd(NHC)(MA) complexes are red. The elemental analyses gave a palladium content of 0.5% and a nitrogen content of 1.03%. Despite the very strong color of the material, there is thus only 13% of the NHC ligands which have reacted with palladium.

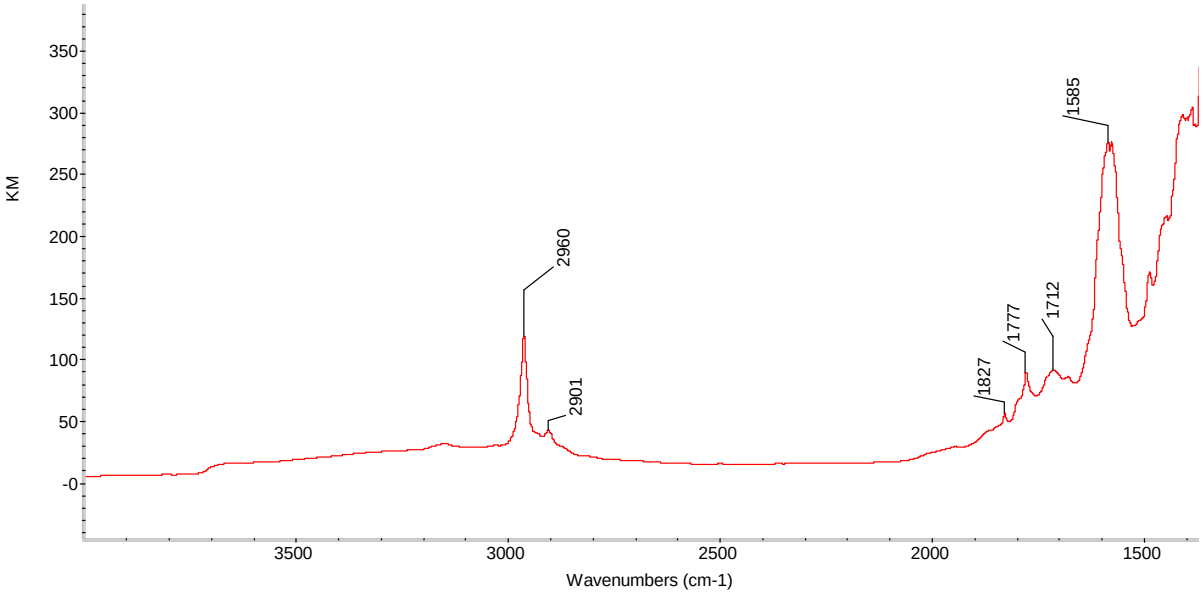

Figure 1. DRIFT Spectrum of material **M-Pd(MA)**

The reaction was monitored by DRIFT spectroscopy, and it shows the appearance of a strong band at 1585 cm^{-1} corresponding to a ν(C=O) signal, consistent with the presence of grafted Pd(NHC)(MA) derivatives. (see Figure 1) By ^{13}C CPMAS solid-state NMR, there are signals at 0, 10, 18, 25, 52, 68, 123, 128, 135 and 171 ppm. The peaks at 0, 10, 18, 52, 123, 128 and 135 are all coming from the starting material and correspond to the NHC ligand, except for the peak at 0 ppm which corresponds to the TMS passivation of the surface. The peaks at 25 and 68 ppm are characteristic signals of THF and therefore corresponds to THF coordinated to the $Pd^{(0)}$ center, as drying under high vacuum for one hour excludes any presence of physisorbed THF. The peak at 171 ppm, as well as a shoulder at around 67 ppm are consistent with the presence of coordinated maleic anhydride.[1] However, in order to truly see the maleic anhydride signal at 67 ppm, the use of another solvent or a subsequent displacement of THF with maleic anhydride would be necessary. These results are consistent with the formation of Pd(NHC) species having either MA or THF ligands.

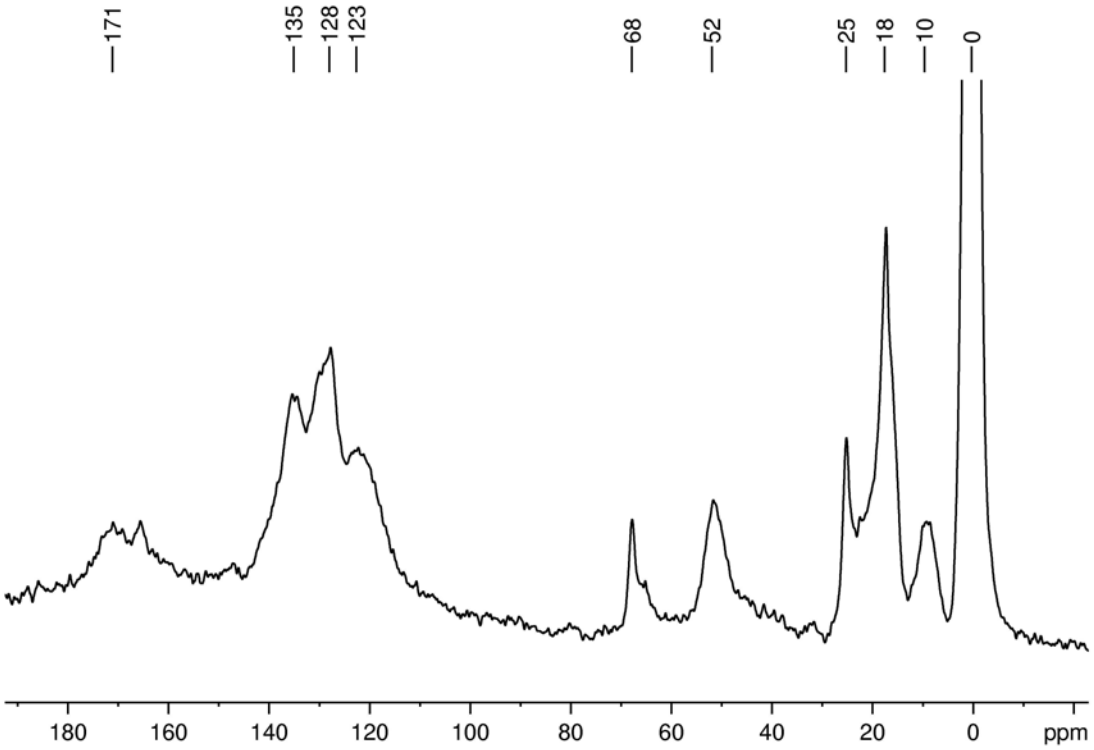

Figure 2. ^{13}C CPMAS solid-state NMR of material **M-Pd(MA)**

1.2. Reaction of [Pd(allyl)Cl]$_2$ with M$_p$-PrMesIm

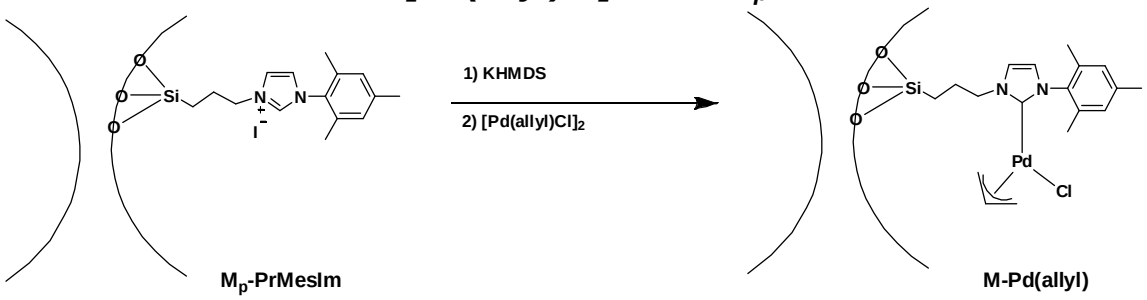

The reaction of [Pd(allyl)Cl]$_2$ is already reported and known to form selectively Pd(NHC)(allyl) complexes.[2] The Pd(allyl)(Cl) complex dissolved in THF was added to a deprotonated **M$_p$-PrMesIm** material and the mixture was stirred for 3 hours. After several washings and drying under high vacuum, **M-Pd(allyl)** was obtained as a pale solid. Elemental analyses gave a palladium content of 2.03 % and a nitrogen content of 1.03 %, which is consistent with the grafting of Pd on 52% of the NHC species. By ^{13}C CPMAS solid-state NMR, new peaks are observed at 25, 68 and 112 ppm. The peaks at 25 and 68 ppm are consistent with the presence of THF coordinated on the palladium center. The peak at 112 ppm is consistent with the presence of allyl ligands. The three peaks of the allyl are expected around 115, 70 and 50 ppm.[2] Unfortunately, the presence of peaks at 68 and 52 ppm do not allow to see any extra signal in these regions.

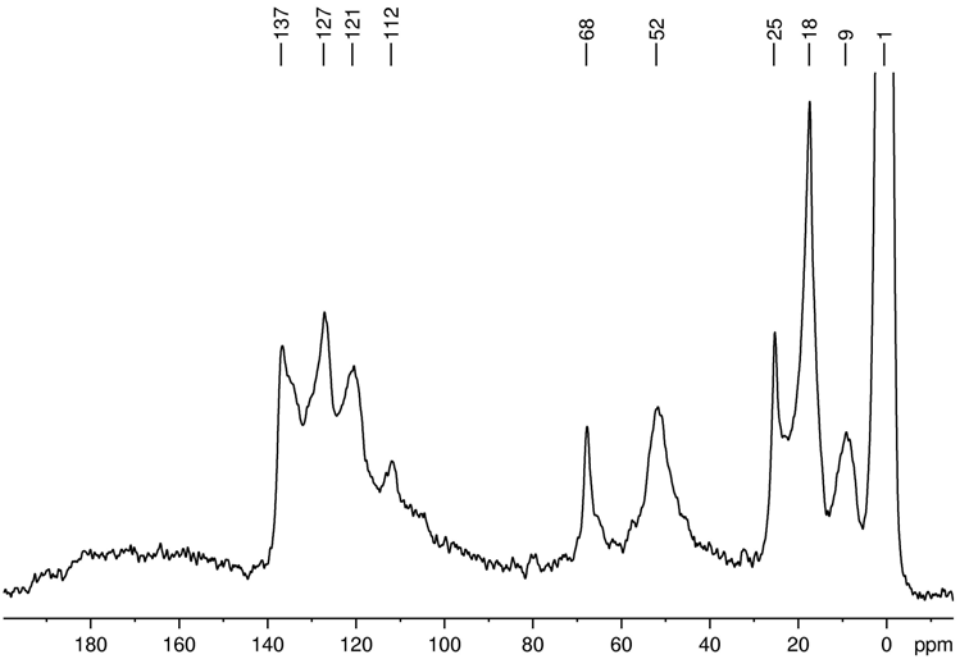

Figure 3. ^{13}C CPMAS solid-state NMR of material **M-Pd(allyl)**

1.3. Reaction of Pd(DAB$_{tBu}$)(MA) with the more concentrated M$_p$-PrMesIm$_{12}$ in presence of maelic anhydride.

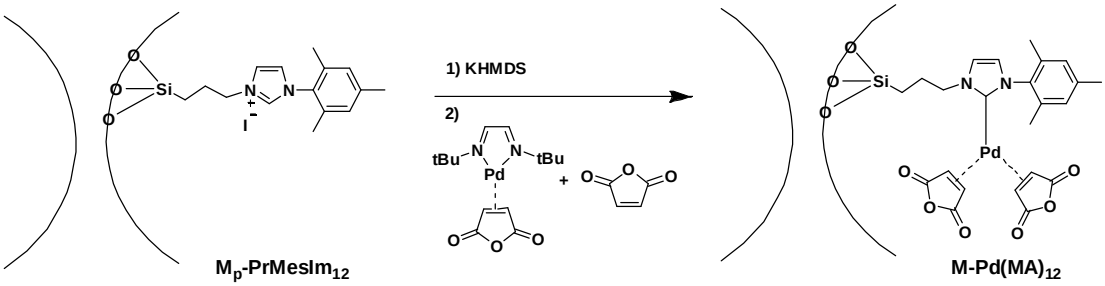

After deprotonation of **M$_p$-PrMesIm$_{12}$** (see Chapter 3) with KHMDS, Pd(DAB)(MA) was grafted using a THF solution, to obtain the purple material **M-Pd(MA)$_{12}$**. Analyzing the solid by ^{13}C CPMAS solid-state NMR showed the appearance of new bands at 25, 50, 68 and 173 ppm, compared to the starting material. The peaks at 25 and 68 are weak and can be attributed to coordinated THF. The peaks at 173 ppm obviously corresponds to carbonyl groups of maleic anhydride. The peak at 49 ppm, overlapping with the signal of the CH2 in a-position to the nitrogen of imidazole ring at 51 ppm, is very broad and its chemical shift is in the range of a maleic anhydride ligand coordinated to Pd. The very weak signal

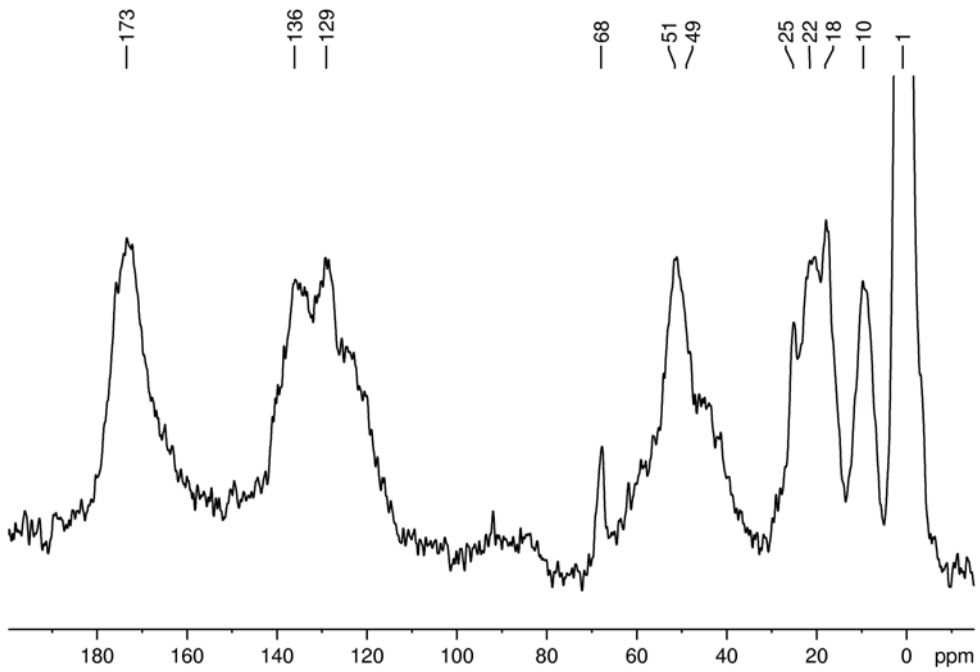

Figure 4. ^{13}C CPMAS solid-state NMR of material **M-Pd(MA)$_{12}$**

corresponding to THF would suggest that the vacant coordination sites were almost fully replaced by MA instead of THF, contrarily to what was observed in material **M-Pd(MA)**. This would be in agreement with the formation of a surface complex of general structure $Pd(NHC)(MA)_2$.

1.4. Catalytic performances[†]

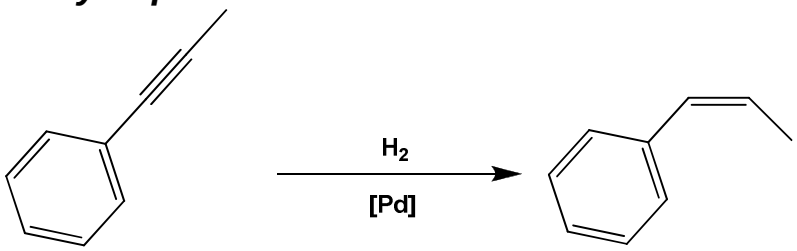

The Pd(NHC) heterogeneous catalyst were tested in the partial hydrogenation of Phenylpropyne to the cis-alkene. Both catalysts **M-Pd(MA)** and **M-Pd(allyl)** show a very good selectivity (93 %) in the formation of the cis-alkene. In terms of stability, catalyst M-Pd(MA) is much more stable and leads to 85% conversion, whereas **M-Pd(allyl)** deactivates after 5% conversion. These very good observed selectivities are completely in agreement with the formation of the Pd(NHC) derivatives, as the starting complexes have no particular selectivity in this reaction.

[†] All catalytic tests were performed by Ruben Drost at the laboratory of Molecular Inorganic Chemistry at the University of Amsterdam.

A-2. Experimental section

Preparation of M-Pd(MA). To a suspension of 1-propyl-3-mesityl-imidazolium iodide functionnalized material prepared in a 1/30 dilution having a passivated surface (200 mg), **M_p-PrMesIm**, in THF (5 mL), 0.15 mL of a 0.5M solution of KHMDS in toluene was added dropwise. After 30 min, a mixture of 27 mg of Pd(DAB_{tBu})(MA) and 8 mg maleic anhydride in 10 mL THF was added, and the resulting suspension stirred for 3 h. The solid was filtered, and successively washed three times with 10 mL THF and twice with 10 mL diethyl ether. Drying under high vacuum (10^{-5} mbar) for 1 h afforded an intensely coloured red-orange powder, **M-Pd(MA)**. ^{13}C CPMAS solid-state NMR (125.7 MHz,): 171, 135, 128, 123, 68, 52, 25, 18, 10, 0.

Preparation of M-Pd(allyl). To a suspension of 1-propyl-3-mesityl-imidazolium iodide functionnalized material prepared in a 1/30 dilution having a passivated surface (200 mg), **M_p-PrMesIm**, in THF (5 mL), 0.15 mL of a 0.5M solution of KHMDS in toluene wa,s added dropwise. After 30 min, a solution of 15 mg of $[Pd(allyl)Cl]_2$ in 10 mL THF was added, and the resulting suspension stirred for 3 h. The solid was filtered, and successively washed three times with 10 mL THF and twice with 10 mL diethyl ether. Drying under high vacuum (10^{-5} mbar) for 1 h afforded an off-white powder, **M-Pd(allyl)**. ^{13}C CPMAS solid-state NMR (125.7 MHz,): 137, 127, 121, 112, 68, 52, 25, 18, 9, 1.

Preparation of M-Pd$(MA)_{12}$. To a suspension of 1-propyl-3-mesityl-imidazolium iodide functionnalized material prepared in a 1/12 dilution having a passivated surface (150 mg), **M_p-PrMesIm$_{12}$**, in THF (3 mL), 0.42 mL of a 0.5M solution of KHMDS in toluene was added dropwise. After 30 min, a mixture of 78 mg of Pd(DAB_{tBu})(MA) and 20 mg maleic anhydride in 20 mL THF was added, and the resulting suspension stirred for 3 h. The solid was filtered, and successively washed three times with 10 mL THF and twice with 10 mL diethyl ether. Drying under high vacuum (10^{-5} mbar) for 1 h afforded a deep purple powder, **M-Pd$(MA)_{12}$**. ^{13}C CPMAS solid-state NMR (125.7 MHz,): 173, 136, 129, 68, 51, 25, 22, 18, 10, 1.

A-3. References

[1] P. Hauwert; G. Maestri; J. W. Sprengers; M. Catellani; C. J. Elsevier *Angewandte Chemie International Edition* **2008**, *47*, 3223-3226.

[2] S. Warsink; R. M. Drost; M. Lutz; A. L. Spek; C. J. Elsevier *Organometallics* **2010**, *29*, 3109-3116.